Optimising head and neck radiotherapy treatment using adaptive radiotherapy

Dr Brian Yune Ng Cheng Hin

The Institute of Cancer Research

and

The Royal Marsden Hospital

Thesis submitted for the degree of Doctor of Medicine

to

The University of London

Declaration

I declare as the sole author of this thesis that the data presented here represent my personal work conducted as a Clinical Research Fellow at Royal Marsden Hospital between September 2017 and March 2020. Data produced in collaboration with other colleagues are fully acknowledged in the text.

Brian Ng Cheng Hin

Abstract

Radiotherapy delivery in head and neck cancer (HNC) has dramatically improved recently with the introduction of advanced techniques such as intensity-modulated radiation therapy (IMRT) and image-guided radiation therapy (IGRT). The aim of IGRT is to correct for setup errors such as positional shifts without modifying the original treatment plan. Intra-treatment structural and spatial changes are not corrected using IGRT. In contrast, Adaptive radiotherapy (ART) is an exciting concept that aims to modify the radiotherapy treatment plan in response to temporal changes to the anatomy and tumour. In an anatomy-adapted ART, repeat planning is based on intra-treatment structural changes to reduce organs at risk (OARs) planned dose deviations and improve dose homogeneity to preserve target coverage. Treatment can be individualised further by adapting to a changing target volume in a response-adapted ART. Improved soft tissue contrast with magnetic resonance (MR) guidance has made the latter a real possibility.

This thesis lays the groundwork for the introduction of ART at our institution. To assist with the increased clinician workload, I first demonstrate the utility of using deformable image registration (DIR) for contour propagation during repeat planning. This improves delineation efficiency by significantly reducing clinician delineation time. Whilst intra-treatment changes are evident in CT-based studies, there are few magnetic resonance imaging (MRI) studies reporting this. This thesis demonstrates that these intra-treatment changes in target volume and OARs are evident on MR imaging and that MR-guided response-adapted ART leads to OAR dose reduction and improves target volume coverage. The clinical introduction of a hybrid MRI and linear accelerator (MR-Linac) has made daily MR-guided ART possible but this has important practical differences to a conventional linear accelerator. Patient selection

is crucial due to a restricted craniocaudal treatment field length and a longer treatment time. A hyo-sternal neck length <14.6 cm in a neutral neck position can be used to identify suitable patients. The dosimetry in a neutral neck position can be optimised using an oral cavity dose constraint, allaying concerns about increased oral cavity doses. Finally, this thesis reports the first HNC patient to be treated on the MR-Linac using a simple online adapted workflow.

Whilst certain findings in this thesis such as the utility of DIR for contour propagation can be applied to current clinical practice, the response-adapted ART findings remain investigative and lay the groundwork for future randomised controlled studies.

Table of contents

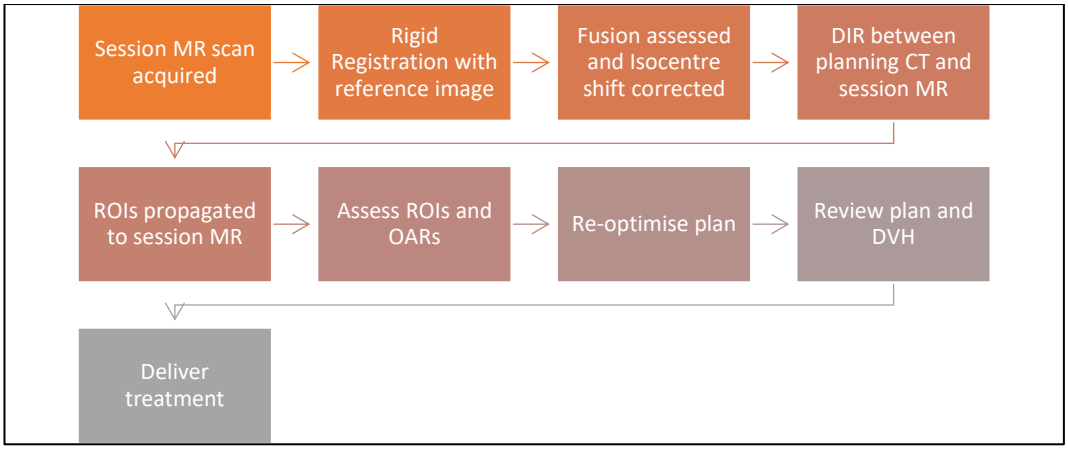

List of figures

List of Tables

Publications arising from thesis

Ng-Cheng-Hin B, Nutting C, Newbold K, Bhide S, McQuaid D, Dunlop A, et al. The impact of restricted length of treatment field and anthropometric factors on selection of head and neck cancer patients for treatment on the MR-Linac. Br J Radiol. 2020 May 21;20200023.

Poster presentations arising from thesis

Ng-Cheng-Hin B, Wong K, McQuaid D, Nutting C, Newbold K, Bhide S, Harrington K. The impact of the MR-Linac field length on head and neck cancers patient selection – Multidisciplinary head and neck cancer symposium - ASTRO February 2020.

Ng-Cheng-Hin B, McQuaid D, Dunlop A, Court S, Petkar I, Nutting C, Harrington K, Newbold K, Bhide S. Structure delineation using a deformable image registration-based contour propagation in Head and Neck cancer – ESTRO 38 April 2019.

Acknowledgements

I would like to thank my supervisors Professor Kevin Harrington, Dr Shreerang Bhide, Dr Kee Wong and Dr Kate Newbold for the opportunity to undertake this exciting project and for their support, advice and guidance over the past few years as their clinical research fellow.

I would like to pay my special regards to the Radiotherapy Physics team without whom the work presented in this thesis would not have been possible. I am grateful to Dr Alex Dunlop, Dr Dualta McQuaid and Dr Steven Court for their patience and their time teaching me radiotherapy planning and for generating scripts required for my thesis. I express my sincere appreciation to Dr Imran Petkar and Dr Derfel ap Dafydd for their time spent reviewing my work. It has been a privilege to contribute to the treatment of the first head and neck cancer patient on the MR-linac in the United Kingdom and I would like to thank the MR-Linac team for making this possible. I would like to acknowledge the support from the Cancer Research Head and Neck grant which provided the funding for this project.

Finally, I would like to thank my family. My parents, grandparents and uncle Harold inspired me at a young age to set and achieve my goals. Last but not least, I am truly grateful for the unwavering support of my wife throughout the highs and lows of this research project.

Abbreviations

AAPM	American Association of Physicists in Medicine
AJCC	American Joint Committee on Cancer
ANACONDA	Anatomically Constrained Deformation Algorithm
ART	Adaptive radiotherapy
ATP	Adapt to position
ATS	Adapt to shape
BOT	Base of tongue
CBCT	Cone beam CT
CC	craniocaudal
cc	cubic centimetre
CCR	Committee for Clinical Research number
COM	centre of mass
CRT	Chemoradiotherapy
CT	Computed tomography
CTV	Clinical target volume
D	Dose
DCE-MRI	Dynamic-contrasting enhanced MRI
DIR	Deformable image registration
DM	Dose mapping
D_{max}	Maximum dose

DRR	Digitally reconstructed radiographs
DSC	Dice similarity coefficient
DVF	Deformation vector field
DVH	Dose-Volume Histogram
DW-MRI	Diffusion-weighted magnetic resonance imaging
$D_{x\%}$	Dose delivered to x% of the volume
E	Energy
ED	Electron densities
EN	Extended neck
EUD	Equivalent uniform dose
FI	Functional imaging
FOV	Field of view
GTV	Gross tumour volume
GTV-p	Gross tumour volume primary
GTV-n	Gross tumour volume node
Gy	Gray
HNC	Head and neck cancer
HNSCC	Head and neck cancer squamous cell carcinoma
HPV	Human papilloma virus
IGRT	Image-guided radiation therapy
IPCM	Inferior pharyngeal constrictor muscle

IMRT	Intensity-modulated radiation therapy
IS-MRI	Intrinsic-susceptibility MRI
IV	Intravenous
LAHNC	Locally advanced head and neck cancer
LUT	Look-up-table
M	Mass
MDA	Mean distance to agreement
MLC	Multi-leaf collimator
MR	Magnetic resonance
MRgRT	Magnetic resonance-guided radiotherapy
MRI	Magnetic resonance imaging
MR-linac	Magnetic resonance linear accelerator
MV	Megavolts
MVCT	Megavoltage computed tomography
NN	Neutral neck
NPC	Nasopharyngeal cancer
NTCP	Normal tissue complication probability
OARs	Organs at risk
OPC	Oropharyngeal cancer
PCM	Pharyngeal constrictor muscle
PEG	Percutaneous endoscopic gastrostomy

PET-CT	Positron emission tomography – computed tomography
PRV	Planning organ at risk volume
PTV	Planning target volume
QoL	Quality-of-life
RMH	Royal Marsden Hospital
ROI	Region of interest
RT	Radiotherapy
SCC	Squamous cell carcinoma
SD	Standard deviation
SMPCM	Superior and middle pharyngeal constrictor muscle
TE	Echo time
TPS	Treatment Planning System
TR	Repetition time
TS	Thermoplastic Shell
T1W	T1-weighted
T2W	T2-weighted
UICC	Union for International Cancer Control
Vx(%)	Percentage volume of the ROI receiving a dose of x Gy
VMAT	Volumetric-modulated arc therapy
2D-RT	Two-dimensional radiotherapy
3D-CRT	Three-dimensional conformal radiation therapy

1 Introduction

1.1 Background

Head and Neck cancer (HNC) consists of a spectrum of diseases with different responses to treatment and prognoses. HNC may arise from the upper aerodigestive tract, paranasal sinus, salivary glands and thyroid gland. In the literature, the term HNC commonly refers to squamous cell carcinoma (SCC) as this accounts for the majority of HNC (90 to 95%). HNC is among the ten most common malignancies in the world with an annual incidence of approximately 530,000 (1) and is predicted to increase to 856,000 annually by 2035 due to changes in demographics (2,3). Declining rates of cigarette smoking has contributed to a decreased incidence of laryngeal and oral cavity HNC (4,5). Conversely, there has been a dramatic increase in the incidence oropharyngeal cancer (OPC) associated with the human papillomavirus (HPV) (5,6).

At least 50% of HNC patients present with locally advanced HNC (LAHNC) i.e. Stage III and above (American Joint Committee on Cancer 7th edition) (7). Many patients in this category will undergo multimodality treatment consisting of a combination of chemotherapy, radiotherapy and surgery. There has been a shift to treating patients with chemoradiotherapy (CRT) as this organ-sparing treatment offers equivalent or even better loco-regional control and disease-free survival to surgery (8,9). However, the 5-year disease-free and overall survival rates remain disappointing at 30-40% in poor prognostic groups despite advances in radiotherapy treatment delivery (7). Intrinsic tumour radio-resistance and limitations of current anatomical imaging to accurately define disease extent may account for these disappointing figures (10,11). Thus, attempts to improve treatment outcomes have

revolved around chemotherapy or radiotherapy dose escalation or improving radiotherapy technique delivery and planning. Escalating cytotoxic chemotherapy and radiotherapy dose has been at the expense of severe acute and morbid late side effects (12–14). Improved target volume definition with multi-modality imaging with MRI and Positron emission tomography – computed tomography (PET-CT) has the potential to increase certainty about the spatial location and extent of tumours and organs at risk thereby avoiding geographical miss and enabling steeper dose gradients. However, this is limited by available resources and the need to scan in the treatment position.

Different prognostic groups exist based on factors such as demographics, staging and pathological variables. Whilst tobacco and alcohol consumption used to be the leading risk factors for developing HNC, there has been an increase in HPV-associated OPC which affects a younger and non-smoking category of HNC patients. HPV-negative OPC and HPV-associated OPC are two separate biological entities with different responses to treatment and prognoses (15). Despite a rising incidence, HPV-associated OPC shows a better response to treatment and prognosis compared to HPV-negative OPC (15,16). A significant proportion of these patients is cured with multi-modality treatment but must live with the long-term radiation-induced side effects which have a negative impact on patient's quality of life. On the other hand, HPV-negative OPC exhibits a more aggressive phenotype with worse prognosis despite current intensive multi-modality treatment (15).

Given the prognostic importance of HPV status, it has been incorporated in the 8th edition of AJCC/Union for International Cancer Control (UICC) staging to reflect the better prognosis of HPV-associated OPC. Despite the prognostic differences, current standard-of-care treatment for both HPV-associated and HPV-negative OPC

remain cisplatin-based CRT. The differing outcomes have led to the development of clinical trials aimed at personalizing treatment according to HPV status. For example, trials are underway to investigate treatment de-intensification for HPV-associated OPC to reduce long-term treatment-related morbidities without compromising oncological outcomes. Such strategies include alterations to the chemotherapy component (omitting or substituting with cetuximab) (17,18) or the radiotherapy component (reduction of dose or target volume modification) (19). De-intensification strategy using cetuximab has been disappointing with both the DeESCALaTE HPV trial (17) and the NRG oncology RTOG 1016 trial (18) reporting a worse overall survival in the cetuximab arm compared with the cisplatin arm. In the DeESCALaTE HPV trial, 334 low-risk HPV-associated oropharyngeal SCC patients were randomised to cisplatin or cetuximab with concurrent radiotherapy. Although there was no significant difference in toxicities between both arms, the 2-year overall survival was significantly worse in the cetuximab arm compared with the cisplatin arm (89.4% vs 97.5%, p=0.0012) (17). Although this was a non-inferiority study, a similar effect on overall survival was reported in the NRG oncology RTOG 1016 trial with a 5-year overall survival of 77.9% and 84.6% in the cetuximab and cisplatin arm, respectively (18). There was an increased risk of 5-year locoregional failure with cetuximab compared to cisplatin (17.3% vs 9.9%) (18). Treatment de-intensification with the omission of concurrent cisplatin was investigated by the NRG-HN-002 study (20). In this study 306 patients were randomised to 60 Gy with accelerated radiation compared with 60 Gy with standard fractionation and concurrent cisplatin. Only the concurrent cisplatin arm met the non-inferiority margin and showed an improved 2-year progression free survival compared to the accelerated radiotherapy arm (90.5% vs 87.6%) (20).

To improve clinical outcomes in the HPV-negative OPC, there has been considerable interest in treatment intensification such as the addition of novel targeted therapies or by escalating radiotherapy dose (21). Sun *et al.* investigated the addition of a novel oral antagonist of inhibitor of apoptosis protein (Debio 1143) as a radiosensitiser to standard cisplatin chemoradiotherapy. In the Debio 1143 arm, there was an improved local control rate at 18 months compared with the placebo arm (54% versus 33%, p=0.026) but at the expense of greater mucositis (31% versus 21%), dysphagia (50% versus 21%), anaemia (35% versus 23%) (22).

1.2 Head and neck cancer radiotherapy

Radiotherapy plan is optimised to deliver a homogeneous tumoricidal dose to the target volume whilst sparing the organs at risk (OARs) as much as possible. This achieves a high probability of local tumour control whilst minimising the risk of normal tissue complications (i.e. therapeutic ratio).

Recent technological advances in imaging and radiotherapy have enabled an improvement in this therapeutic ratio. Radiotherapy delivery has evolved from conventional two-dimensional radiotherapy (2D-RT) to more conformal techniques such as three-dimensional conformal radiation therapy (3D-CRT), intensity-modulated radiation therapy (IMRT), volumetric-modulated arc therapy (VMAT) and image-guided radiation therapy (IGRT).

IMRT and VMAT deliver a precisely sculpted dose to the target volume whilst sharp dose gradients can reduce normal tissue toxicities such as xerostomia (23). This is particularly important in the HNC due to the proximity of the OARs to the target volume. However, the improved radiotherapy dose conformality is at the expense of

increased sensitivity to geometrical errors, which can have a significant impact on the delivered dose.

1.2.1 **Morbidity associated with HNC radiotherapy**

The proximity of the OARs to the target volume means that HNC radiotherapy is still associated with significant long-term morbidities despite the implementation of conformal radiotherapy techniques. Acute- and long-term side-effects include oral mucositis (24), nausea (24), poor voice function (25), swallowing dysfunction (25), xerostomia (26,27), weight loss (25), trismus (28) and osteoradionecrosis (29). All of these can culminate into decreased quality of life (30,31). Xerostomia is an important long-term side effect that may contribute to dysphagia, increased oral bacterial colonization and dental caries (26,27). These long-term morbidities are particularly devastating for the relatively younger HPV-associated OPC patients who have a higher chance of cure.

1.2.2 **Intra-treatment changes and their dosimetric consequences**

At the pre-treatment stage, a radiotherapy plan is created to fulfil a set of target volumes and OARs dose constraints. These planned delivered doses to both target volumes and OARs assume that the patient anatomy and position remain unchanged between the planning scan to the delivered radiotherapy fractions. Although random and systematic patient positioning errors can be adjusted with IGRT, spatial and volumetric changes (such as weight loss, tissue swelling, tumour and normal tissue shrinkage) cannot be corrected using IGRT.

With spatial and volumetric changes consistently reported during HNC treatment (32–34), the doses derived from the planning scan may not be representative of the delivered doses since this represents a single snapshot of the patient's anatomy.

Without accounting these intra-treatment changes, significant deviations from the planned radiotherapy doses can occur, with higher and lower delivered dose to OARs and target volumes, respectively (35).

1.2.2.1 Target Volume

HNCs are radiosensitive and may demonstrate a significant response by the end of treatment, with several CT-based studies reporting a measurable reduction in gross tumour volume (GTV) and clinical target volume (CTV) throughout radiotherapy treatment. (32,36). Overall, target volume reduction (GTV, CTV and planning target volume (PTV)) can be measured as early as within the first 2 weeks of radiotherapy treatment (36), with a median target volume reduction of 3 to 16%, 7 to 48% and 6 to 66% by the end of weeks 2, 4 and 7, respectively (37).

The GTV shrinks by a median volume of 2 to 3% per day (32,36) and by a median volume of up to 70% compared to the initial volume (32). Similarly, the high- and low-dose CTVs demonstrate significant volume changes throughout treatment with the most significant changes occurring at week 2 with volume reduction by 3.2% and 10%, respectively ($p=0.003$ and $p<0.001$, respectively) compared to the initial volume (33). A planning study by Bhide *et al.* reported that if the initial radiotherapy plan was delivered without accounting the CTV change, this led to an increased dose inhomogeneity across the CTV (33). These target volume dose inhomogeneities can translate to poorer local control (38,39). Other studies suggest that these intra-treatment target volume changes led to dosimetric changes to the high-dose target volume only (40), low-dose target volume only (41) or led to no dosimetric consequence (42).

These reported studies show heterogeneity in relation to the timing of the intra-treatment imaging, the imaging modalities (e.g. cone-beam CT (CBCT),

megavoltage CT (MVCT), diagnostic CT imaging) and patient populations (e.g. OPC only, nasopharyngeal cancers, mixed HNC). Thus, it is difficult to draw an overall conclusion on the effects of target volume changes and their dosimetric consequences. Nonetheless, dosimetric changes to the target volume, if present, are small and as a whole appears to be robust during HNC radiotherapy treatment.

1.2.2.2 Organs at risk

Similar to the target volume, OARs have been imaged at different time-points using a variety of imaging modalities such as CBCT, MVCT, helical CT and CT on rails (43–46).

Longitudinal changes to the parotid glands have been of particular interest due to the association of xerostomia with parotid gland mean dose (47–49). Parotid glands have been consistently reported to shrink in volume during radiotherapy. A review article of thirty-eight studies by Brouwer *et al.* reported an overall mean parotid volume loss of 26 ± 11% by the end of treatment (50). The rate of change in parotid gland volume is not linear, with an increased volume loss during the first half of radiotherapy treatment (51). Bhide *et al.* reported that by the end of treatment the parotid volumes reduced by 35% and the most significant parotid gland volume changes occurred at weeks 2 and 4 of treatment, with a reduction of 15% ($p<0.001$) and 31% ($p<0.001$), respectively (33). Increased parotid gland volume loss has been associated with worse complications such as duration of percutaneous endoscopic gastrostomy (PEG) use, saliva reduction and xerostomia scores (50).

In addition to volume loss, the parotid glands can migrate by up to 4 mm medially due to the associated target tumour shrinkage and weight loss (32,33,36). This occurs in a significant number of patients, with an incidence of 74% in a study by Castelli *et al.* (52). The significance of parotid gland medial migration is that the parotid glands

are placed in closer proximity to the high-dose target volume, which may lead to higher than planned parotid gland doses. In a review by Brouwer *et al.*, this translated to a mean dose increase of 2.2 Gy +/- 2.6 Gy compared to the planned dose (50). The mean parotid gland dose deviations can be as large as 10.4 Gy (53). However, not all patients demonstrate a deviation in mean parotid gland dose, with reports estimating an incidence of just under 60% (52). It is likely that significant dosimetric changes only occur in a proportion of patients due to a combination of both volume loss and medial migration.

There are fewer reports on the anatomical changes of other OARs during radiotherapy. Similar to the parotid glands, submandibular glands show a volume reduction ranging between of 15 to 32% and migration superiorly (42,54,55). This can lead to an increased mean dose of up to 1 Gy (42).

In contrast to the parotid and submandibular glands, other critical OARs such as the spinal cord and brainstem do not show significant volumetric changes. However, doses to these OARs can deviate from planned doses, with reported increases in the maximum dose (D_{max}) and dose received by 1 percent of the volume ($D_{1\%}$) (50). The mean increase in dose to spinal cord and brainstem are small (<2%) for the majority of patients, but variations can be large (44). The excess D_{max} can be as high as 2.5 and 5.6 Gy to the brainstem and spinal cord, respectively (56). However, this may apply to a small percentage of patients with Cheng *et al.* reporting that the D_{max} to the brainstem and spinal cord, was exceeded in only 16% and 11% of their patients, respectively (34). The deviation in doses to the spinal cord and brainstem are associated with factors such as overall weight loss (57), patient positional changes (58) and target volume shrinkage (42).

In summary, the anatomic changes observed during radiotherapy lead to cumulative delivered parotid gland doses greater than planned, with magnitude depending on the proximity to the target volumes and volume change. The clinical consequences of the unaccounted larger mean parotid gland dose place the patient at higher risk of xerostomia (52). Dosimetric changes to critical OARs such as the spinal cord and brainstem may also occur in a small number of patients.

1.3 Adaptive radiotherapy

To take into account these aforementioned volume and spatial intra-treatment changes, adaptive radiotherapy (ART) has been developed and investigated. ART is an umbrella term that refers to any online or offline assessments and modifications of the pre-planned radiotherapy parameters in response to a stimulus (e.g. tumour shrinkage or weight loss) or at pre-defined intervals. These can be broadly divided into an anatomy-adapted and a response-adapted workflow that adjusts to a changing anatomy (e.g. correcting target volume and OAR dose deviations (59,60)) or to a treatment response to enable dose escalation (e.g. escalate target volume dose (61)) and de-escalation (e.g. shrink the target volumes according to tumour response (19)), respectively.

1.3.1 ART strategies

ART can be implemented in the treatment workflow at different time-points using different techniques.

ART can be triggered:

- at pre-planned intervals (e.g. weeks 2 and 4) when the risk of dosimetric deviations are felt to be the greatest.
- at any time-point if significant dosimetric deviations occur due to clinical variables.
- following regular treatment response assessments using imaging (such as CBCT, diagnostic CT or MRI scans) or triggered when cumulative dose

delivered to the target volume and OARs deviate from the pre-planned doses.

In the 'online' setting, updated imaging for that session is used to derive and deliver a new treatment plan for that fraction. In contrast, the 'offline' ART workflow is less time-pressured, with a new radiotherapy plan planned for future fractions.

1.3.2 **Dosimetric evidence for ART**

The routine integration of ART in the radiotherapy workflow has financial and workload implications and places a significant burden on an already stretched healthcare system. Thus, the majority studies reporting on the dosimetric benefits of ART in HNC are based on ad-hoc offline correction strategies aimed at reducing plan deviations (41,62,63). These studies use an anatomy-adapted ART to reoptimize treatment parameters to reduce target volume dose inhomogeneities, to improve target volume coverage and to maintain OAR dose to within their constraints. This ensures that delivered doses to the target volume and OARs deviate minimally from the pre-planned parameters and maintain the therapeutic ratio (43,64). The benefits of ART were reported in a study by Surucu *et al.* where fifty-one HNC patients underwent dosimetric assessment half-way through treatment due to clinical reasons with a repeat CT scan (62). Thirty-four patients were deemed to benefit from repeat planning with dosimetric assessments showing a median reduction of 4.5% to the spinal cord D_{max}, 3% to the brainstem D_{max}, 6.2% to the mean ipsilateral parotid and 2.5% to the mean contralateral parotid (62). Importantly, the spinal cord D_{max} exceeded its constraint at 57.1 Gy without adaptation and was corrected with ART for one patient (62). This illustrates the potential benefit of monitoring the OAR dose for treatment adaptation.

Another ART approach is to perform ART at regular intervals where the most significant changes are expected. A study by Zhang *et al.* assessed the most efficient ART replanning strategy to maintain target volume coverage and mean parotid gland dose (63). Sixty-three replanning strategies were assessed for thirteen OPC patients using weekly CT imaging (63). First, the authors reported that no ART led to a mean dose increase of 4 Gy to the parotid glands (63). Second, the authors reported that weekly ART was unnecessary and that two or three repeat plans were the most efficient. ART at weeks 1, 3 and 5 was the optimal ART strategy and this led to a mean parotid gland dose reduction of 3.3 Gy for 94% of the patients. However, two repeat plans at weeks 1 and 5 also improved the mean dose to the parotid glands by 2.9 Gy (63). Similarly, a retrospective planning study of eleven patients by Wu *et al.* evaluated three different ART strategies (single *versus* two *versus* weekly ART). All ART strategies led to an improvement in the mean parotid gland doses, but the most benefit was found in the weekly ART patients. Compared to no ART, one mid-treatment, two mid-treatment and weekly ART led to a reduction in mean parotid gland dose of 3%, 5% and 6%, respectively (41).

1.3.3 **Clinical evidence for ART**

To justify implementing ART into clinical practice, dosimetric improvement should correlate with improved clinical outcomes. However, reports of clinical outcomes following ART are scarce and limited by their non-randomised or retrospective nature. These are summarised in Table 1-1.

In a non-randomised study of 317 HNC patients by Chen *et al.*, 51 patients underwent ART mid-treatment due to clinical reasons, such as tumour shrinkage and weight loss (38). Although the dosimetric benefit of ART was not reported, the ART cohort had a significant improvement in 2-year local control rate compared to the

non-ART cohort (88% versus 79%, respectively; p=0.01). There were no significant differences in overall survival (p=0.55) and in the incidence of acute grade 3 toxicities (p=0.45), acute hospitalisation (p=0.45), late grade 3 toxicities (p=0.71) and gastrostomy tube dependence at 1 year (p>0.05) between the two cohorts. The selection criteria for ART may have contributed to the observed improvement in local-regional improvement in this study due to the selection of tumours with a favourable biology. A similar finding was reported in a non-randomised prospective study of 129 nasopharyngeal cancer patients by Yang *et al.* (65). 86 patients underwent one or two ART plans (pre-planned at fractions 15 or 25 or both), whilst 43 patients formed the control group. ART led to a significant improvement in the quality of life and 2-year locoregional control (97% vs 92%, p=0.04), but did not improve the 2-year overall survival (89.8% versus 82.2%, respectively; p=0.475) compared to no ART. However, the control group consisted of patients who had declined repeat planning CTs as part of ART. Thus, confounding factors may have led to the observed differences between groups.

In a single-arm retrospective study by Kataria *et al.*, radiotherapy treatment was delivered in two phases (66). In phase I, 54 Gy was delivered to both low-dose and high-dose PTV. For phase II, ART was used in week 5 of treatment to an extra 16 Gy to the high-dose PTV. The authors used an anatomy-adapted ART and reported a 2-year disease-free survival and overall survival of 72% and 75%, respectively, which was in keeping with previous data published from their institution (67). The authors acknowledge that a higher proportion of patients with stage IV HNC in their population may explain the lower overall survival and disease-free survival rates compared to other studies. The acute and late toxicities were comparable to other studies. In a prospective, non-randomised study of 22 patients by Schwartz *et al.*,

ART led an excellent 2-year local and regional disease control of 100% and 95%, respectively (43). Most patients underwent a single ART and a second ART if clinically indicated. Both ART strategies led to improved mean parotid gland doses, with the most benefit resulting from two ART plans. One ART reduced the mean dose to the ipsilateral parotid gland by 1.3 Gy (3.9%) (p=0.002) and contralateral parotid gland by 0.6 Gy (2.8 %) (p=0.003). Two ART reduced the mean dose further by 4.1 Gy (9%) (p=0.001) and 0.8 Gy (3.8%) (p=0.026) to the ipsilateral and contralateral parotid glands, respectively.

In contrast, a retrospective case-matched control study by Zhao *et al.* reported that ART did not improve clinical outcomes for patients with nasopharyngeal cancers despite dosimetric benefits to the target volume and OARs (p=0.34) (56). However, patients with locally advanced disease (T stage >2 and N stage >1) benefitted from ART, with an improvement in the 3-year local relapse-free survival and a reduction in late side-effects (mucositis and xerostomia) compared to a matched control group without ART.

Although these studies suggest that ART can improve clinical outcomes, it is important to note that they are limited by their non-randomised nature and potential bias associated with patient selection in the control groups. In the routine clinical practice, ART remains a reactive process to significant weight loss, contour changes, deviations in target volume coverage and OARs dose constraints. Before routine clinical implementation of ART, prospective randomised phase 3 trials are needed to assess most efficient use and clinical benefits of ART.

Table 1-1. Summary of ART studies reporting clinical outcomes.

Study	Design and treatment modalities, primary site	Number of patients			Number of ART	Timing Replans	Follow-up (months)	Clinical outcome
		Total	ART	No ART				
Zhao et al. (56)	Retrospective analysis, case-matched controls. NPC AJCC stage II to IV (7th edition).	99	33	66	1 or 2	**One ART (n = 33):** Fraction 15 (+/- 5) **Two ART (n = 9):** Fraction 15 (+/- 5) Fraction 27 (+/- 4)	Median 38 months (range, 3 to 75 months)	No significant difference in 3-year local relapse-free survival for ART vs no ART (72.7% vs 68.2% (p=0.34)). ART significantly improved 3-year local relapse free survival for patients ≥ T3 (p=0.03).

Study	Design and treatment modalities, primary site	Number of patients			Number of ART	Timing Replans	Follow-up (months)	Clinical outcome
		Total	ART	No ART				
Schwartz et al. (43,60)	Prospective non-randomised trial. OPC Stage III to IVb (7th edition)	22	22	0	1 or 2	**One ART (n = 22):** Fraction 16 (Range, 2 to 28) **Two ART (n = 8):** Fraction 22 (Range, 11 to 25) (n = 8)	Median 31 months (range, 13 to 45 months).	100% 2-year local disease control 95% 2-year regional disease control

Study	Design and treatment modalities, primary site	Number of patients			Number of ART	Timing Replans	Follow-up (months)	Clinical outcome
		Total	ART	No ART				
Yang *et al.* (65)	Prospective non-randomised trial. Nasopharynx (stage I to IV) AJCC 2002.	129	86	43	1 or 2	**One ART (n = 63):** Fraction 15 (n =10) Fraction 25 (n = 53) **Two ART (n =23)** Fractions 15 and 25	Median 29 months (range, 4 to 54 months)	ART significantly improved the 2-year locoregional control compared to no ART (97.2% vs 92.4%, respectively; p=0.04) No significant difference in 2-year overall survival between ART and no ART (89.8% vs 82.2%, respectively; p=0.475)
Chen *et al.* (38)	Non-randomised retrospective study. Oropharynx, oral cavity, larynx, hypopharynx, nasopharynx.	317	51	266	1	At 40 Gy (range, 10 to 58 Gy)	30 months	ART led to significant improvement in 2-year local control rate compared to no ART (88% vs 79%, respectively; p=0.01) No significant difference in 2-year overall survival between ART and no ART (73% vs 79%, respectively; p=0.55)

Study	Design and treatment modalities, primary site	Number of patients			Number of ART	Timing Replans	Follow-up (months)	Clinical outcome
		Total	ART	No ART				
Kataria et al. (66)	Retrospective, non-randomised study. Oropharynx, larynx, hypopharynx	36	36	0	1	Fraction 23	not stated	Median disease-free survival = 17.5 months 2-year disease-free survival = 72% Median overall survival = 23.5 months 2-year overall survival = 75%

Abbreviations: AJCC = American Joint Committee on Cancer; ART = adaptive radiotherapy.

1.3.4 **Patient selection and criteria for ART**

It is widely reported that not all HNC patients benefit from ART, with an estimated 20 to 65% benefiting from ART (58,68). ART may have a greater benefit for LAHNC due to the greater anatomical change observed to the target volume, with a reported improvement in 3-year local disease-free survival in this group of patients (56).

Although studies have investigated baseline and dosimetric factors as predictors for requiring ART, the criteria for selecting patients with the greatest benefit from ART remains unclear (65). In a review of 51 studies, Brouwer *et al.* identified tumour location, age, body mass index, planned parotid gland dose, pre-treatment parotid gland volume and volume overlap between the parotid glands and the target volume as potential predictors (50). The authors concluded from a multivariate analysis that advanced nodal disease (N2), an initial weight of greater than 100 kg, or patients weighing less than 100 kg with large nodes had a 60 to 80% chance of needing a repeat plan (50). Subsequently, Brouwer *et al.* developed and validated a method to select HNC patients at the pre-treatment stage for ART (69). Parotid gland dose deviations greater than 3 Gy from the planned dose was selected as the authors felt that this would be the minimum level of clinical relevance and predicted normal tissue complication probability (NTCP) differences of 3-10% for xerostomia. Multivariable analysis showed that the only significant parameter was the planned mean dose to the parotid gland. A mean parotid dose threshold of ≥ 22.2Gy resulted in a sensitivity of 91%, a specificity of 45%, a negative predictive value of 95% and a low positive predictive value of 29%. In the validation cohort, similar results with a sensitivity of 80%, NPV of 81% and PPV of 19%. This would translate to a sparing of 38% and 24% of patients from the ART procedure in the development and

validation cohorts, respectively. However, the high number of false positives would mean that a high proportion of patients would still undergo unnecessary ART.

1.3.5 **ART conclusion**

Despite positive and promising results from studies suggesting an improved quality of life and local control with ART in HNC, the results are limited by their non-randomised, retrospective nature and the heterogeneous ART protocols and nomenclature. Furthermore, there is a lack of prospective clinical trials to inform the best ART strategies with the largest clinical gain. Implementing ART into routine practice is challenging due to the increased resources required and lack of consensus regarding the time point and threshold required to trigger an adaptive plan (35,36,38,60). Current literature suggests that possible candidates for ART are those who have bulky tumours, early tumour shrinkage or early parotid gland overdose (70–72).

1.4 **MR-guidance in HNC ART.**

Radiotherapy delivery is complex, with systematic and random set-up errors an inherent part of this process. With IGRT, imaging of the patient before treatment delivery enables the verification of the target and patient positions and corrections of these set-up errors to ensure that the planned treatment is delivered. IGRT allows the visualisation of the target and organs at risk and adjustment of the patient position to compensate for gross changes to avoid geographical miss. Thus, IGRT can optimise the accuracy and precision of radiotherapy dose delivery by preventing geographical miss and ensuring that treatment delivery is reproducible, respectively.

This is particularly important with advanced radiotherapy techniques such as IMRT and VMAT where the risk of geographical miss is high. The sculpted dose

distributions created by IMRT plans increase the risk of unintentional increase in dose of spared structures or geographical target miss if organ motion and set-up errors are not taken into account. IGRT can be simple in the form of electronic portal imaging and digitally reconstructed radiographs (DRR) or more complex such as Cone-Beam CT (CBCT). However, these imaging modalities have poor soft tissue contrast and this leads to significant interobserver variability in target volume and OARs definition (73,74). Magnetic resonance-guided radiotherapy (MRgRT) is a form of IGRT that integrates MR imaging to provide direct tumour and OAR visualisation. The superior soft tissue resolution offered by MRI has been reported to reduce inter-observer variability (73,75–77).

Whilst MRI has been increasingly used in the staging and management of HNC, it has not been routinely used for radiotherapy target definition. This is partly due to the difficulty in accurately registering the diagnostic MR and planning CT scans, which are acquired in different patient positions. However, the recent development and availability of MR flat table-tops and MR-compatible immobilisation devices have enabled MRI scans to be acquired in the radiotherapy treatment position. This has led to MRI scans playing a greater role in HNC treatment planning with reports of its use for GTV (78) and CTV (79) delineations.

The non-ionising properties of MRI also make it an attractive prospect for ART workflow, allowing repetitive imaging without any additional radiation. The advantage of using MRI in this setting is the reported reduction in inter-observer delineation variability of the OARs and target volumes (73,75–77). The improved target volume visualisation provides a simple way to assess tumour response by measuring anatomical target volume changes to indicate tumour growth or shrinkage. Thus, enabling dose escalation to non-responding disease or dose de-

escalation to responding disease with the aim of improving tumour control and reducing normal OAR toxicities, respectively. The caveat is that minimal or no measured volume change can occur, which could either represent non-responding tumour or a lag in the observed volume change. In this instance, functional imaging (FI) can provide complementary information to anatomical imaging on the underlying biology (80). In fact, FI can identify response early during treatment before morphological changes are observed (81–83). FI is non-invasive and can characterise spatiotemporal heterogeneity of tumours. MR-based FI can identify and quantify cellularity, vascularity and hypoxia using Diffusion Weighted MRI (DW-MRI), Dynamic-Contrasting Enhanced MRI (DCE-MRI) and Intrinsic-susceptibility MRI (IS-MRI), respectively. Of these, DW-MRI has been increasingly used in the diagnosis and monitoring HNC, with early evidence that DW-MRI can differentiate tumour from radiotherapy changes (84,85). DW-MRI has been investigated as an early predictor to treatment response in HNC and has been reported as an imaging biomarker to differentiate between ultimate responders and non-responders at week 2 of radiotherapy (83). Despite this potential, the use of FI remains an area of research due to limitations such as temporal differences and the lack of standardisation of FI parameters (86). As in-field tumour recurrence remains common in certain sub-groups of HNC (87–89), MRgRT using a combination of anatomical and FI can be used to identify these non-responding patients as candidates for treatment dose escalation.

In contrast, responding patients could be candidates for treatment dose de-escalation by the continuous adaptation and shrinkage of the high-dose CTV to the MR-visible tumour (90,91). Target volume changes can be observed on serial MR scans for HNC undergoing definitive radiotherapy or chemoradiotherapy, but there are limited

published studies reporting this (92–94). A study of 6 HNC patients treated with an integrated MRI-tri-^{60}Co teletherapy device by Raghavan *et al.* (92) quantified and reported similar changes observed by CT-based studies. The GTV and parotid glands demonstrated significant median volume loss of 38.7% and 31.1% over the course of treatment, respectively (92). Kamran *et al.* reported a median volume reduction of 33% for primary GTV (range of 17 to 75%), 22% and 45% for HPV-negative and HPV-associated nodal disease, respectively (93). In a study of 31 HPV-associated OPC by Thiagarajan *et al*., half of their patients demonstrated a complete radiological response on MRI mid-treatment (94). In a prospective feasibility study by Mohamed *et al.*, five HPV-associated LAHNC patients underwent 2-weekly MRI scans during chemoradiotherapy (91). The primary GTV decreased by 44%, 90% and 100% at weeks 2, 4 and 6 whilst the nodal GTV decreased more slowly with an average decrease of 25%, 60% and 80% at weeks 2, 4 and 6, respectively (91). By adapting to the changes in volume, mean parotid doses were reduced by 3.3 Gy which led to a predicted 1% xerostomia reduction at 6 months and an 11% reduction in dysphagia at 6 months using NTCP models. Overall, these studies suggest a higher target volume shrinkage than CT-based studies which may be explained by the improved soft tissue contrast.

1.4.1 **MR-Linac**

Delivery of personalised and real-time MRgRT has been made possible by the development of hybrid MRI scanner and linear accelerators. An example of this is the Elekta Unity magnetic resonance linear accelerator (MR-Linac) which integrates a 1.5 Tesla MR scanner (Philips Healthcare, Best, The Netherlands) with a 6 megavoltage (MV) linear accelerator (linac) (Elekta, AB, Stockholm, Sweden). This revolutionary equipment was installed at the Royal Marsden Hospital (Sutton

Branch) and has been in clinical use since 2018. This is described in more detail in Chapter 6.

1.4.2 **Current challenges with MRgRT and the MR-Linac.**

As with any new technology developed in the era of evidence-based medicine, the routine clinical use of the MR-Linac is currently limited to clinical trials aimed at demonstrating the safety and improving the treatment workflow. This is further limited by a small number of centres world-wide that have access to this technology. Thus, an international research consortium was created to enable international collaboration between different institutions to facilitate the evidence-based introduction of the MR-linac into clinical practice (95).

The treatment of HNC on the MR-Linac is challenging. The MR-linac treatment field is smaller than on a conventional linac which may have an impact on the sub-type of HNC suitable for treatment on the MR-Linac. Another important challenge is the additional time required for online plan adaptation strategies whilst the patient is immobilised in the treatment position. This process is estimated to last around 45 minutes (96). At the Royal Marsden Hospital, radical HNC treatment is delivered over 30 fractions. Daily treatment in a claustrophobic and noisy environment may be difficult for a number of patients. Therefore, improved patient tolerance and careful patient selection are crucial to deliver a successful individualised treatment on the MR-Linac. These issues will be explored in this thesis.

1.5 **The role of deformable image registration in ART.**

A major limitation in adopting ART routinely for HNC is the repeat manual delineation required to adjust the changes in OARs and target volumes which is both time-consuming and labour-intensive, taking an average of between 44 to 56 minutes for Base of Tongue (BOT) and Nasopharyngeal (NPH) cancers respectively (97). Automatic contour propagation using Deformable Image Registration (DIR) may be used to facilitate this delineation process (98). Another useful application of DIR is dose mapping, whereby dose accumulation can be calculated.

DIR is based on the concept of image registration, which defines the spatial correspondence between two images. Image registration can be broadly divided into rigid and deformable (non-rigid) registrations with the key difference residing on the flexibility of the voxel-to-voxel relationships during spatial mapping. During rigid image registration, the voxels move and rotate uniformly whilst maintaining a constant voxel-to-voxel relationship before and after mapping. The key difference with DIR is that voxel-to-voxel relationship can change and thus, allows for a more elastic deformation compared to rigid registration. The DIR algorithm allows the spatial transformation from a 'moving' (target) image to a 'fixed' (reference) image (Figure 1-1A and B). This spatial transformation can be represented by a deformation vector field (DVF) (Figure 1-1C), which describes the displacement between each voxel in the 'fixed' image and each corresponding voxel in the 'moving' image thus, creating a one-to-one mapping between corresponding voxels or spatial correspondence in the two images.

Figure 1-1. An example of a deformable image registration (DIR). A 'fixed' (reference) image and a 'moving' (target) image are shown in panels A and B, respectively. DIR can deform the four rounded corners of the 'moving' image to the sharp corners of the 'fixed' image (C). DIR's ability to change the voxel-to-voxel relationship is illustrated by the deformation vector field (DVF) in panel C, where the direction and size of the arrows represent the direction and magnitude of the deformation. Panel D shows the deformed image. Adapted from Oh et al. (99).

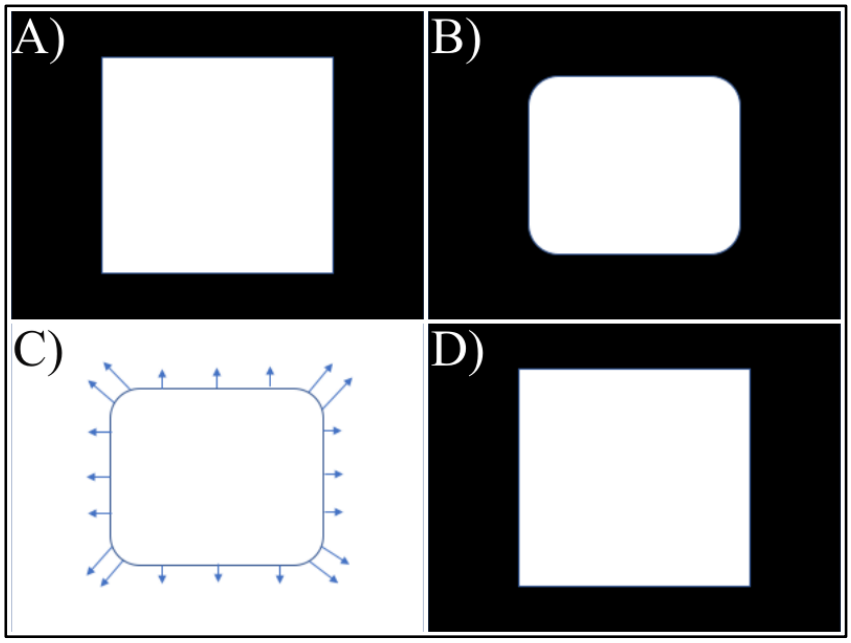

The DIR algorithm is complex and detailed explanation is beyond the scope of this introduction. Briefly, the DIR algorithm is driven by similarity metrics between the two images, which can be based on image intensities (100,101), feature-based (102) or a combination of both metrics (103,104). The intensity-based DIR algorithm matches individual voxels or images patches using a mathematical or statistical criterion, whilst the feature-based approach uses known anatomical landmarks (such as surfaces, points or curves) in both image sets to define the DVF. However, each algorithm is inherently limited by restrictions of the similarity metrics. For example, a reasonable DVF cannot be guaranteed in areas of low contrast and image artefacts, and in areas with no selected landmarks in the intensity-based algorithm and feature-based algorithm, respectively. The feature-based algorithm requires delineation of anatomic landmarks or contours in both images prior to defining a DVF. These can be manually delineated, which is time-consuming and not practical (105), but can be

facilitated by contour propagation or automatic contouring (54). Hybrid algorithms integrating both image-intensities and feature-based algorithms have been developed to overcome these limitations (103,104).

1.5.1 **DIR validation**

Contour propagation must be validated prior to clinical implementation and the simplest way is to measure the geometric agreement between the DIR-propagated contours and the manual contours which act as the ground truth. In this thesis, overlap-based and surface-based geometrics were used. The Dice similarity coefficient (DSC) quantifies the amount of volume overlap between the two structures (Figure 1-2A).

$$DSC(A,B) = 2(A \cap B) / (A + B)$$

where A and B represent the volumes of the 2 structures.

The mean distance to agreement (MDA) between 2 structures is the mean distance that each point on one structure would have to move to overlap with the corresponding point on the other structure (Figure 1-2B).

Figure 1-2. A) The dice similarity coefficient assesses the volume overlap between volumes A and B. B) The mean distance to agreement is the mean surface distance between the surfaces of volumes A and B. A single corresponding point is shown in this example.

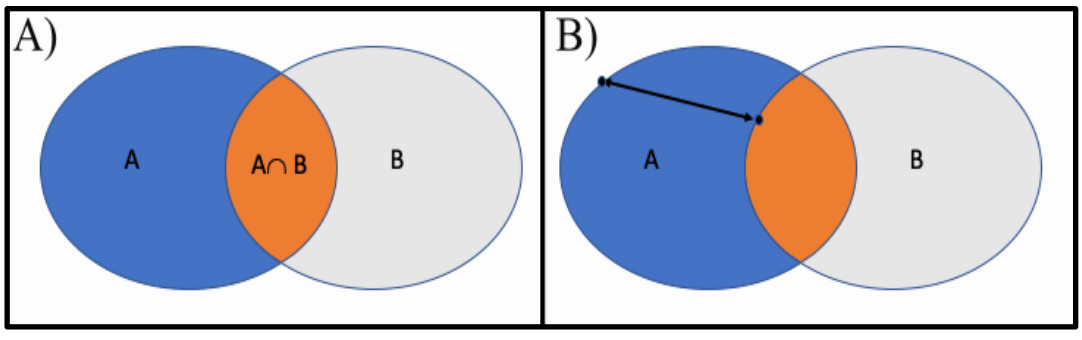

Independent of the type of DIR algorithm, the generated DVF can be applied to contour propagation and radiotherapy dose accumulation, which are of relevance to

the ART chapters explored in this thesis. To implement an efficient ART workflow, regular dosimetric assessment of the planned radiotherapy doses should be calculated on updated anatomy. If deviations are clinically relevant, a new plan is then generated using this updated anatomy. Manual delineation is not feasible and DIR contour propagation from planning CT to CBCTs has been used to assess dose deviations in HNC (105–107).

1.5.2 **Dose accumulation**

For dose accumulation, the generated DVF is used to deform the radiotherapy dose to each voxel and accumulated on a reference image (usually the planning scan) in a process termed as dose mapping (DM). Thus, the planned radiotherapy dose can be first applied to the repeated imaging (weekly or per fraction) to calculate a delivered dosimetry based on updated anatomy at different time-points. Subsequently, the dose cubes from each time-point can be deformed and accumulated to the planning CT and an estimate of the actual delivered dose can be calculated (108–111). This enables the assessment of deviations between planned and delivered doses and justify modification of the treatment plan using ART. It is important to note that accurate dose accumulation is dependent on the performance of the DIR on the spatial correspondence of each point at the geometric boundaries and within these. Therefore, geometric or volume-based assessments of surface boundaries and landmarks (such as DICE and MDA) may be used (105), but these do not provide any information regarding the anatomical point-to-point correspondence accuracy.

Another challenge in dose accumulation is to account for the change in tissue mass observed during treatment such as tumour regression and progression. Although this may not be a significant problem for deformation itself, this can lead to difficulties in mapping voxel to voxel radiotherapy doses from different time-points. The deposited

energy on the reference image may not be consistent with the sum of the energy deposited on each calculated image set (112). This concept of dose accumulation and lack of energy conservation is illustrated in Figure 1-3A and is adapted from Zhong *et al.* (113).

At time-point T_1, an OAR receiving 2 Gy has an initial volume and mass of V_1 and M_1, respectively. This OAR undergoes a volume and mass loss so that at time-point T_2, it has undergone a 50% volume and mass reduction, V_2 and M_2, respectively. Therefore, $M_1 = 2 * M_2$.

Assuming that a DVF field ($\boldsymbol{\varphi_1}$) maps all voxels from V_1 to V_2 and a dose of 2 Gy is mapped from V_1 to V_2 by interpolation, the interpolated dose to V_2 will be 2 Gy.

A dose accumulation is calculated as below:

Total dose accumulated by dose mapping (φ_1) on V_2: $D_{DM} = \varphi_1 (2) + 2 = 4$ Gy

The energy deposited is a product of dose multiplied by mass as shown in the following equation:

Energy (E) = Dose (D) x Mass (M) (99).

Total energy accumulated by dose mapping (φ_1) on V_2: $E_{DM} = 4M_2$

This is in contrast with the total energy delivered which is calculated as below:

Total energy delivered (assuming $M_2 = 0.5M_1$): $E = 2*M_1 + 2*M_2 = 3M_1$ or $6M_2$

Therefore, there is a discrepancy in the total energy delivered ($6M_2$) *versus* the total energy accumulated using dose mapping ($4M_2$) with an underestimation of the energy delivered using dose mapping.

In contrast, dose back projection from V_2 to V_1 via deformation (φ_2) leads to an overestimation of the energy delivered using dose mapping compared to energy delivered ($4M_1$ versus $3M_1$, respectively).

Total dose accumulated by dose mapping (φ_2) on V_1: $D_{DM} = \varphi_2(2) + 2 = 4$ Gy

Total energy accumulated by dose mapping (φ_2) on V_1: $E_{DM} = 4M_1$

Total energy delivered (assuming $M_2 = 0.5M_1$): $E = 2*M_1 + 2*M_2 = 3M_1$ or $6M_2$

Figure 1-3. Dose accumulation underestimation in dose forward projection (A) and overestimation in dose back projection (B).

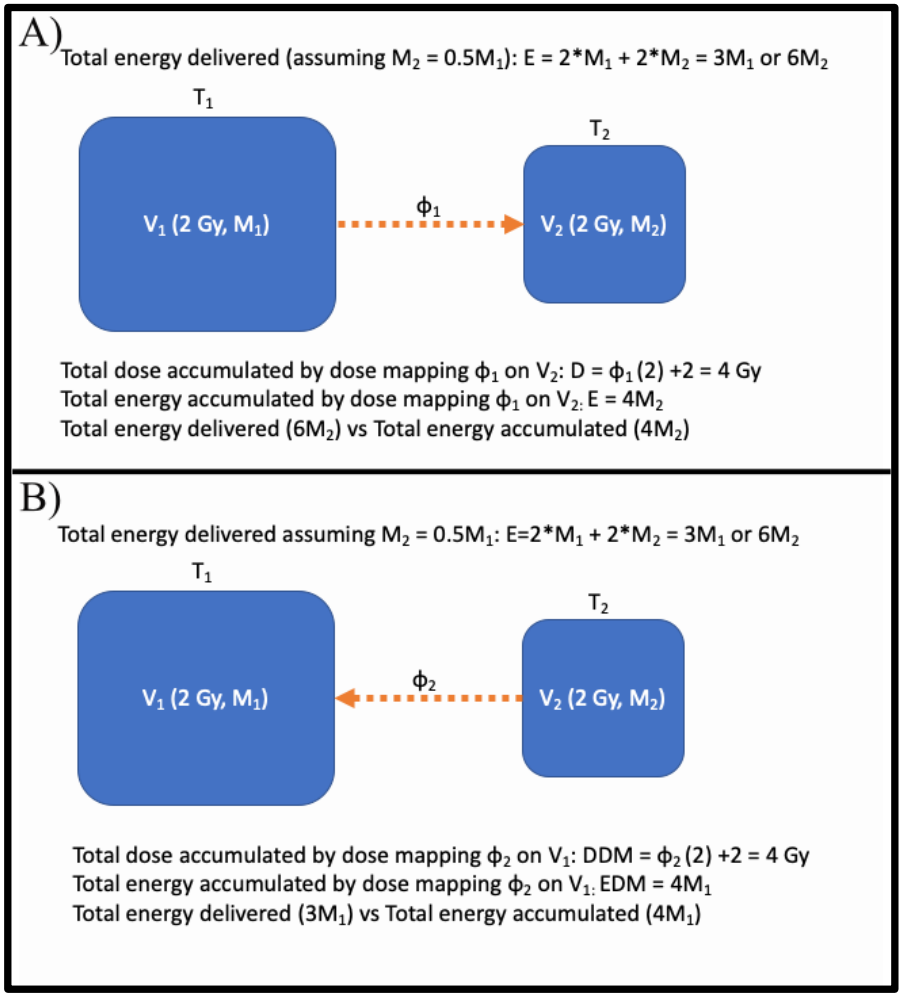

Abbreviations: DDM = Dose using dose mapping; EDM = Energy using dose mapping.

Accurate estimations of the accumulated dose can be given if errors associated with dose mapping will be small and negligible if mass changes are small and the DVF is accurate. In cases where mass changes are large, dose accumulation will be less accurate. One solution is to use DIR models that are less influenced by image intensity changes in the tumour and preserve volume data by including prior knowledge of relational data (113–115).

To this day, there are no rigorous validation methods for dose deformation, but despite these limitations, dose accumulation has the potential to enable treatment plan adaptation (99).

1.5.3 **Clinical validation of DIR**

DIR algorithms should be validated in both the treatment planning system commissioning and routine quality assurance procedure. In HNC ART, few studies have validated DIR for HNC for contour propagation and dose accumulation (116–118). DIR algorithms can achieve acceptable contour propagation results with commercial algorithms demonstrating a low average geometric registration error between 0.5 mm and 3 mm (119). Due to the complex nature of dose accumulation, variation can be profound between different DIR algorithms (119–121). Detailed pre-setting of the DIR algorithm can lead to fewer dosimetric variations, but this is at the expense of manual input in the workflow (121).

1.5.4 **DIR in this thesis**

RayStation (RaySearch Laboratories AB, Stockholm, Sweden) integrates a simple to use hybrid DIR algorithm that uses the ANAtomically CONstrained Deformation Algorithm (ANACONDA) allowing for intensity-based or hybrid registration (intensity plus controlling regions of interest (ROIs)) (103). This algorithm has been validated in thoracic 4DCT data and CT/cone beam CT data and shown to be accurate compared to other algorithms (103).

1.6 **The MR-Linac**

The Elekta Unity magnetic resonance linear accelerator (MR-Linac) is a hybrid system that integrates the imaging capability of a 1.5 Tesla magnetic resonance (MR) scanner (Philips Healthcare, Best, The Netherlands) with a 6 megavoltage (MV) linear accelerator (linac) (Elekta, AB, Stockholm, Sweden) (Figure 1-4).

Figure 1-4. Sketch of the MRI accelerator concept. The 1.5 T MRI is shown in blue (1), the 6 MV accelerator (2) is located in a ring around the MRI. The split gradient coil (3) is shown in yellow and in orange, the superconducting coils (4) are shown. The light blue ring around the MRI indicates the low magnetic field toroid (5) in the fringe field. Figure reproduced from Raaymakers et al. (122).

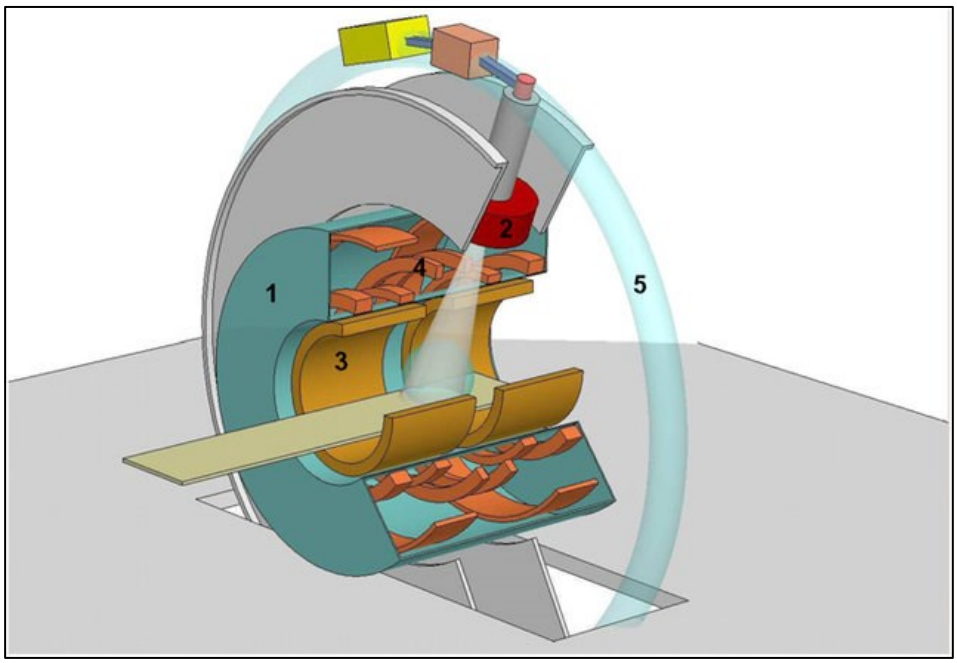

This pioneering machine has the potential to revolutionise radiotherapy delivery. Repetitive MRI scans can be conveniently acquired at the time of radiotherapy treatment delivery without additional exposure to radiation dose, which is associated with other in-room imaging modalities such as cone-beam CT. The superior soft tissue contrast provided by MR imaging paves the way for soft tissue based position verification and real-time assessment of intra- and inter-fraction changes thus, unlocking the potential for daily plan optimisation and real-time adaptive

radiotherapy treatment (123). Serial anatomical and functional MRI scans may also be acquired for the assessment of intra-treatment response (124,125).

1.6.1 Technical differences between the MR-linac and the conventional linac

The integration of a linear accelerator within a strong magnetic field has been a major challenge of modern radiotherapy research. Certain components of the MRI system have been modified (122) to accommodate the linear accelerator and the effects of the magnetic field on the behaviour of charged particles (Lorentz force) need to be accounted for. Thus, the MR-linac bears some important differences to a conventional linac.

- The treatment field size and couch movement of the MR-Linac.

The MR gradient coil is a crucial component located within the MR bore and produces calibrated distortions of the main magnetic field in the *x, y* or *z* axes to enable localisation of the image slices (Figure 1-4). In the MR-linac, this coil is physically split to enable a radiation window which limits the maximum field size at the isocentre to 22 cm and 57 cm in the craniocaudal and lateral directions, respectively (96,126).

Another important difference is that the MR-linac has a static couch and set-up errors are corrected by shifting beam apertures (127). A 1 cm margin in all directions has been suggested for plan adaptation to the daily anatomy and set-up errors (128). This restricts the maximum radiation field to 20 cm in the CC direction and may influence the selection and the absolute number of head and neck cancer (HNC) patients who can be treated on the MR-Linac using a single isocentre technique.

- The electron return effect (ERE) and electron streaming effect (ESE).

As the magnetic field remains active during treatment delivery, scattered secondary electrons can bend back at the air-tissue interfaces (electron return effect) or spiral along the magnetic field (electron streaming effect) (Figure 1-5). Subsequently, these electrons can deposit unwanted radiation in the skin and lung (126), and on surfaces perpendicular to the magnetic field such as the jaw, armpits and arms (129). These must be accounted for at the planning and optimising stages to reduce unwanted radiation dose deposition outside of the treatment field (129,130). For example, the extra dose deposited from the ESE is comparable to the dose of a CBCT based position verification and can be safely reduced using a 1 cm sheet of wax bolus (131).

Figure 1-5. The electron return effect (ERE) in blue and the electron streaming effect (ESE) in green. B_0 field is the main static magnetic field.

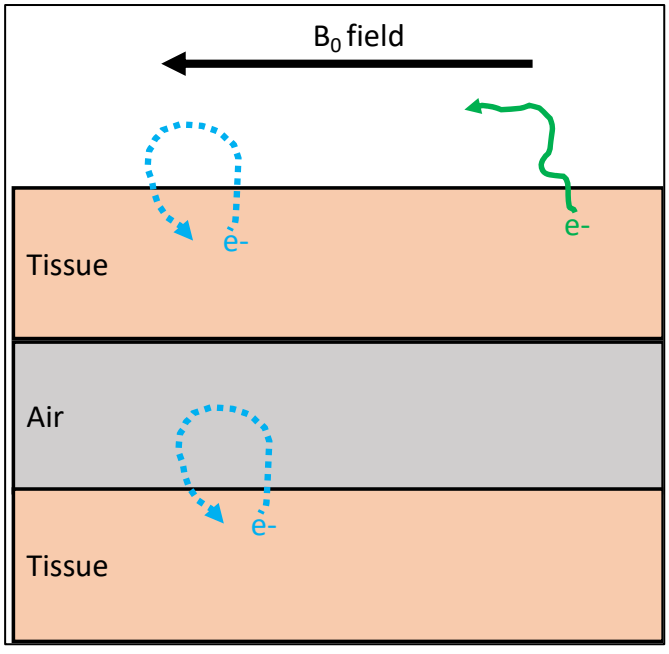

The MR-Linac has evolved from a proof of concept in 2009 (122) to clinical treatment of sites such as oligometastatic lymph nodes in 2018 (132) and prostate cancer (133). Translating this new technology into clinical practice is challenging

and there has been much interest in laying the groundwork for treatment of body sites such as head and neck (128,134), liver (135,136) and pancreas (137).

Chapter 7 first investigates the potential impact of a restricted craniocaudal treatment field on HNC patient selection for the MR-Linac. This is followed by the assessment of the dosimetric difference of delivering radiotherapy in a neutral and extended neck position (Chapter 8). The final section will describe the experience of delivering treatment on the MR-Linac for the first HNC patient (Chapter 9).

1.7 **Hypotheses tested in this thesis**

- DIR-propagation with clinician amendment will be geometrically accurate and this process will be more time-efficient than manual delineation (Chapter 2).
- Sequential MR imaging can measure anatomical changes to the target volume and parotid glands during radical chemoradiotherapy (Chapter 3).
- DIR will enable accurate ROI propagation from the MRI scans and produce contours that are comparable to clinician contours (Chapter 4).
- Radiotherapy plans can be generated from serial MRI scans using an MR-only workflow and dose-adapted radiotherapy will have a dosimetric advantage by reducing doses to the OARs due to a shrinking high-dose target volume (Chapter 5).
- A restricted craniocaudal field length of <20 cm on the MR-Linac will reduce the number of head and neck cancer patients suitable for treatment on the MR-Linac (Chapter 6).
- Radiotherapy treatment in a neutral neck position will lead to increased doses delivered to the oral cavity, parotid glands, posterior fossa and mandible compared to treatment in an extended neck position, irrespective of the nodal irradiation volumes. Optimising the radiotherapy treatment plans with an oral

cavity dose constraint will reduce radiotherapy doses to the ROIs (Chapter 7).

- An online adaptive radiotherapy plan will ensure that the target volume coverage and OARs doses are similar to the reference plan and improve dosimetry compared to a non-adapted plan (Chapter 8).

1.8 **Thesis Chapters**

The hypotheses for this thesis will be tested using a combination of retrospective database of HNC patients treated at the Royal Marsden Hospital (Sutton Branch) and prospective database of HNC patients recruited to the MR-Library (CCR 4477) and PERMIT trials (CCR 4841).

The first data chapter (Chapter 2) investigates the utility of DIR for contour propagation in order to improve ART workflow in a CT-based workflow. This chapter analyses whether DIR-propagation improves delineation efficiency and assesses the geometric and dosimetric differences between DIR-propagated and manual contours.

The subsequent data chapters revolve around the use of MR-guidance for ART. I investigate the intra-treatment anatomical and tumour changes using serial MRI scans (Chapter 3), the use of DIR for contour propagation on MRI scans (Chapter 4) and the feasibility of ART in MR-only workflow (Chapter 5).

The final data chapters describe the Elekta Unity MR-Linac (Chapters 6 to 8). This hybrid system comprises of a 1.5T MRI scanner (Philips, Best, The Netherlands) and a 7 MV linear accelerator (Elekta, Stockholm, Sweden). Due to the modifications required to integrate an MRI scanner with a linear accelerator, the treatment field is restricted in the cranio-caudal direction. Chapter 6 investigates the impact of this

restricted treatment field on the HNC patient selection for treatment on the MR-Linac. With MR-linac treatment time being longer than conventional linac, it is essential to maintain patient comfort whilst immobilised in the treatment position. Chapter 7 investigates the effect on the more comfortable neutral neck position on dosimetry compared to the extended neck position. This culminates in the description of the first HNC undergoing treatment on this machine in the UK in Chapter 8.

1.9 References

1. Siegel RL, Miller KD, Jemal A. Cancer statistics, 2017. CA Cancer J Clin [Internet]. 2017 Jan 1 [cited 2017 Nov 15];67(1):7–30. Available from: http://doi.wiley.com/10.3322/caac.21387

2. Ferlay J, Soerjomataram I, Dikshit R, et al. Cancer incidence and mortality worldwide: Sources, methods and major patterns in GLOBOCAN 2012. Int J Cancer [Internet]. 2015 Mar 1 [cited 2017 Nov 22];136(5):E359–86. Available from: http://www.ncbi.nlm.nih.gov/pubmed/25220842

3. Shield KD, Ferlay J, Jemal A, et al. The global incidence of lip, oral cavity, and pharyngeal cancers by subsite in 2012. CA Cancer J Clin [Internet]. 2017 Jan 1 [cited 2017 Nov 15];67(1):51–64. Available from: http://doi.wiley.com/10.3322/caac.21384

4. Habbous S, Chu KP, Qiu X, et al. The changing incidence of human papillomavirus-associated oropharyngeal cancer using multiple imputation from 2000 to 2010 at a comprehensive cancer centre. Cancer Epidemiol. 2013;

5. Mourad M, Jetmore T, Jategaonkar AA, et al. Epidemiological Trends of Head and Neck Cancer in the United States: A SEER Population Study. J Oral Maxillofac Surg. 2017;

6. Cohen N, Fedewa S, Chen AY. Epidemiology and Demographics of the Head and Neck Cancer Population. Oral and Maxillofacial Surgery Clinics of North America. 2018.

7. Corvò R. Evidence-based radiation oncology in head and neck squamous cell carcinoma. Radiother Oncol [Internet]. 2007 Oct [cited 2017 Nov 7];85(1):156–70. Available from: http://linkinghub.elsevier.com/retrieve/pii/S0167814007001521

8. Lefebvre J AK. Larynx Preservation Clinical Trial Design: Key Issues and Recommendations—A Consensus Panel Summary. Int J Radiat Oncol [Internet].

2009 Apr 1 [cited 2017 Nov 15];73(5):1293–303. Available from: http://www.sciencedirect.com/science/article/pii/S0360301608036936?via%3Dihub

9. Kazi R, Venkitaraman R, Johnson C, Prasad V, Clarke P, Rhys-Evans P, Nutting C HK. Electroglottographic Comparison of Voice Outcomes in Patients With Advanced Laryngopharyngeal Cancer Treated by Chemoradiotherapy or Total Laryngectomy. Int J Radiat Oncol [Internet]. 2008 Feb 1 [cited 2017 Nov 15];70(2):344–52. Available from: http://www.sciencedirect.com/science/article/pii/S0360301607011376?via%3Dihub

10. Brizel DM, Sibley GS, Prosnitz LR, et al. Tumor hypoxia adversely affects the prognosis of carcinoma of the head and neck. Int J Radiat Oncol Biol Phys [Internet]. 1997 May 1 [cited 2017 Nov 10];38(2):285–9. Available from: http://www.ncbi.nlm.nih.gov/pubmed/9226314

11. Janssen HLK, Haustermans KMG, Sprong D, et al. HIF-1A, pimonidazole, and iododeoxyuridine to estimate hypoxia and perfusion in human head-and-neck tumors. Int J Radiat Oncol Biol Phys [Internet]. 2002 Dec 1 [cited 2017 Nov 10];54(5):1537–49. Available from: http://www.ncbi.nlm.nih.gov/pubmed/12459383

12. Harrington KJ, Nutting CM. Interactions between ionizing radiation and drugs in head and neck cancer: how can we maximize the therapeutic index? Curr Opin Investig Drugs [Internet]. 2002 May [cited 2017 Nov 23];3(5):807–11. Available from: http://www.ncbi.nlm.nih.gov/pubmed/12090557

13. Bentzen SM, Trotti A. Evaluation of Early and Late Toxicities in Chemoradiation Trials. J Clin Oncol [Internet]. 2007 Sep 10 [cited 2017 Nov 23];25(26):4096–103. Available from: http://www.ncbi.nlm.nih.gov/pubmed/17827459

14. Hunter KU, Schipper M, Feng FY, et al. Toxicities affecting quality of life after chemo-IMRT of oropharyngeal cancer: prospective study of patient-reported, observer-rated, and objective outcomes. Int J Radiat Oncol Biol Phys [Internet]. 2013

Mar 15 [cited 2017 Nov 23];85(4):935–40. Available from: http://linkinghub.elsevier.com/retrieve/pii/S0360301612034505

15. Dillon MT, Harrington KJ. Human Papillomavirus–Negative Pharyngeal Cancer. J Clin Oncol [Internet]. 2015 Oct 10 [cited 2017 Nov 21];33(29):3251–61. Available from: http://www.ncbi.nlm.nih.gov/pubmed/26351347

16. Bhatia A, Burtness B. Human papillomavirus-associated oropharyngeal cancer: Defining risk groups and clinical trials. J Clin Oncol [Internet]. 2015 Oct 10 [cited 2017 Nov 21];33(29):3243–50. Available from: http://www.ncbi.nlm.nih.gov/pubmed/26351343

17. Mehanna H, Robinson M, Hartley A, et al. Radiotherapy plus cisplatin or cetuximab in low-risk human papillomavirus-positive oropharyngeal cancer (De-ESCALaTE HPV): an open-label randomised controlled phase 3 trial. Lancet. 2019 Jan 5;393(10166):51–60.

18. Gillison ML, Trotti AM, Harris J, et al. Radiotherapy plus cetuximab or cisplatin for human papillomavirus (HPV)-positive oropharyngeal cancer: a randomized, multicenter, non-inferiority clinical trial. Lancet (London, England) [Internet]. 2019 Jan 5 [cited 2021 Aug 25];393(10166):40. Available from: /pmc/articles/PMC6541928/

19. Bahig H, Yuan Y, Mohamed ASR, et al. Magnetic Resonance-based Response Assessment and Dose Adaptation in Human Papilloma Virus Positive Tumors of the Oropharynx treated with Radiotherapy (MR-ADAPTOR): An R-IDEAL stage 2a-2b/Bayesian phase II trial. Clin Transl Radiat Oncol [Internet]. 2018 Aug 24 [cited 2018 Aug 29]; Available from: https://www.sciencedirect.com/science/article/pii/S240563081830048X

20. Yom SS, Torres-Saavedra P, Caudell JJ, et al. NRG-HN002: A Randomized Phase II Trial for Patients With p16-Positive, Non-Smoking-Associated, Locoregionally

Advanced Oropharyngeal Cancer. Int J Radiat Oncol Biol Phys [Internet]. 2019 Nov 1 [cited 2021 Aug 25];105(3):684–5. Available from: http://www.redjournal.org/article/S0360301619336739/fulltext

21. ArChIMEDEs-Op - University of Birmingham [Internet]. [cited 2018 Mar 21]. Available from: https://www.birmingham.ac.uk/research/activity/mds/trials/crctu/trials/arichimedes/index.aspx

22. Sun X-S, Tao Y, Tourneau C Le, et al. Debio 1143 and high-dose cisplatin chemoradiotherapy in high-risk locoregionally advanced squamous cell carcinoma of the head and neck: a double-blind, multicentre, randomised, phase 2 study. Lancet Oncol [Internet]. 2020 Sep 1 [cited 2021 Aug 25];21(9):1173–87. Available from: http://www.thelancet.com/article/S1470204520303272/fulltext

23. Nutting CM, Morden JP, Harrington KJ, et al. Parotid-sparing intensity modulated versus conventional radiotherapy in head and neck cancer (PARSPORT): A phase 3 multicentre randomised controlled trial. Lancet Oncol. 2011 Feb;12(2):127–36.

24. Rosenthal DI, Chambers MS, Fuller CD, et al. Beam Path Toxicities to Non-Target Structures During Intensity-Modulated Radiation Therapy for Head and Neck Cancer. Int J Radiat Oncol [Internet]. 2008 Nov 1 [cited 2019 Jul 11];72(3):747–55. Available from: https://www.sciencedirect.com/science/article/pii/S0360301608000564?via%3Dihub

25. Dornfeld K, Simmons JR, Karnell L, et al. Radiation Doses to Structures Within and Adjacent to the Larynx are Correlated With Long-Term Diet- and Speech-Related Quality of Life. Int J Radiat Oncol [Internet]. 2007 Jul 1 [cited 2019 Jul 11];68(3):750–7. Available from: https://www.sciencedirect.com/science/article/pii/S0360301607001988?via%3Dihub

26. Li Y, Taylor JMG, Ten Haken RK, et al. The impact of dose on parotid salivary

recovery in head and neck cancer patients treated with radiation therapy. Int J Radiat Oncol [Internet]. 2007 Mar 1 [cited 2019 Jul 11];67(3):660–9. Available from: https://www.sciencedirect.com/science/article/pii/S0360301606029889?via%3Dihub

27. Blanco AI, Chao KSC, El Naqa I, et al. Dose–volume modeling of salivary function in patients with head-and-neck cancer receiving radiotherapy. Int J Radiat Oncol [Internet]. 2005 Jul 15 [cited 2019 Jul 11];62(4):1055–69. Available from: https://www.sciencedirect.com/science/article/pii/S0360301605000337?via%3Dihub

28. Dijkstra PU, Kalk WWI, Roodenburg JLN. Trismus in head and neck oncology: A systematic review. Oral Oncol. 2004;

29. Melzner WJ, Lotter M, Sauer R, et al. Quality of interstitial PDR-brachytherapy-implants of head-and-neck-cancers: Predictive factors for local control and late toxicity? Radiother Oncol [Internet]. 2007 Feb 1 [cited 2019 Jul 11];82(2):167–73. Available from: https://www.sciencedirect.com/science/article/pii/S0167814006006633?via%3Dihub

30. Denaro N, Merlano MC, Russi EG. Dysphagia in head and neck cancer patients: Pretreatment evaluation, predictive factors, and assessment during radio-chemotherapy, recommendations. Clinical and Experimental Otorhinolaryngology. 2013.

31. Bhide SA, Newbold KL, Harrington KJ, et al. Clinical evaluation of intensity-modulated radiotherapy for head and neck cancers. Br J Radiol [Internet]. 2012 May [cited 2017 Nov 23];85(1013):487–94. Available from: http://www.ncbi.nlm.nih.gov/pubmed/22556403

32. Barker JL, Garden AS, Ang KK, et al. Quantification of volumetric and geometric changes occurring during fractionated radiotherapy for head-and-neck cancer using an integrated CT/linear accelerator system. Int J Radiat Oncol [Internet]. 2004 Jul 15 [cited 2018 Jan 12];59(4):960–70. Available from:

https://www.sciencedirect.com/science/article/pii/S0360301603024544

33. Bhide SA, Davies M, Burke K, et al. Weekly volume and dosimetric changes during chemoradiotherapy with intensity-modulated radiation therapy for head and neck cancer: a prospective observational study. Int J Radiat Oncol Biol Phys. 2010 Apr;76(5):1360–8.

34. Cheng HCY, Wu VWC, Ngan RKC, et al. A prospective study on volumetric and dosimetric changes during intensity-modulated radiotherapy for nasopharyngeal carcinoma patients. Radiother Oncol [Internet]. 2012 Sep 1 [cited 2018 Feb 12];104(3):317–23. Available from: https://www.sciencedirect.com/science/article/pii/S0167814012001478

35. Hansen EK, Bucci MK, Quivey JM, et al. Repeat CT imaging and replanning during the course of IMRT for head-and-neck cancer. Int J Radiat Oncol [Internet]. 2006 Feb 1 [cited 2018 Sep 11];64(2):355–62. Available from: https://www-sciencedirect-com.ezproxy.icr.ac.uk/science/article/pii/S0360301605021449?via%3Dihub

36. Castadot P, Geets X, Lee JA, et al. Assessment by a deformable registration method of the volumetric and positional changes of target volumes and organs at risk in pharyngo-laryngeal tumors treated with concomitant chemo-radiation. Radiother Oncol [Internet]. 2010 May 1 [cited 2018 Jan 12];95(2):209–17. Available from: https://www.sciencedirect.com/science/article/pii/S0167814010001593

37. Morgan HE, Sher DJ. Adaptive radiotherapy for head and neck cancer. Cancers Head Neck [Internet]. 2020 Dec 9 [cited 2020 Apr 13];5(1):1. Available from: https://cancersheadneck.biomedcentral.com/articles/10.1186/s41199-019-0046-z

38. Chen AM, Daly ME, Cui J, et al. Clinical outcomes among patients with head and neck cancer treated by intensity-modulated radiotherapy with and without adaptive replanning. Head Neck. 2014 Nov;36(11):1541–6.

39. Luo Y, Qin Y, Lang J. Effect of adaptive replanning in patients with locally

advanced nasopharyngeal carcinoma treated by intensity-modulated radiotherapy: a propensity score matched analysis. Clin Transl Oncol. 2017;

40. Nishi T, Nishimura Y, Shibata T, et al. Volume and dosimetric changes and initial clinical experience of a two-step adaptive intensity modulated radiation therapy (IMRT) scheme for head and neck cancer. Radiother Oncol. 2013 Jan;106(1):85–9.

41. Wu Q, Chi Y, Chen PY, et al. Adaptive replanning strategies accounting for shrinkage in head and neck IMRT. Int J Radiat Oncol Biol Phys [Internet]. 2009 Nov 1 [cited 2018 Mar 9];75(3):924–32. Available from: http://linkinghub.elsevier.com/retrieve/pii/S0360301609006233

42. Castadot P, Geets X, Lee JA, et al. Adaptive RT in head and neck cancer Adaptive functional image-guided IMRT in pharyngo-laryngeal squamous cell carcinoma: Is the gain in dose distribution worth the effort? Radiother Oncol [Internet]. 2011 Dec [cited 2019 Jul 10];101(3):343–50. Available from: https://pdf.sciencedirectassets.com/271320/1-s2.0-S0167814011X00154/1-s2.0-S0167814011003227/main.pdf?X-Amz-Security-Token=AgoJb3JpZ2luX2VjEDYaCXVzLWVhc3QtMSJHMEUCIQD0AMpVt3u2sDh%2B2mSjenf4B%2BWWFcclTzC%2FiiCElPMu9QIgFjGTMOvqoQXGwBzwvsev2SNweWQt5El9zrV5rb

43. Schwartz DL, Garden AS, Shah SJ, et al. Adaptive radiotherapy for head and neck cancer—Dosimetric results from a prospective clinical trial. Radiother Oncol [Internet]. 2013 Jan 1 [cited 2018 Mar 9];106(1):80–4. Available from: https://www.sciencedirect.com/science/article/pii/S0167814012004598

44. Robar JL, Day A, Clancey J, et al. Spatial and Dosimetric Variability of Organs at Risk in Head-and-Neck Intensity-Modulated Radiotherapy. Int J Radiat Oncol [Internet]. 2007 Jul 15 [cited 2018 Sep 11];68(4):1121–30. Available from: https://www.sciencedirect.com/science/article/pii/S0360301607001460

45. Jensen AD, Nill S, Huber PE, et al. A clinical concept for interfractional adaptive radiation therapy in the treatment of head and neck cancer. Int J Radiat Oncol Biol Phys. 2012 Feb;82(2):590–6.

46. O'Daniel JC, Garden AS, Schwartz DL, et al. Parotid gland dose in intensity-modulated radiotherapy for head and neck cancer: is what you plan what you get? Int J Radiat Oncol Biol Phys [Internet]. 2007 Nov 15 [cited 2018 Sep 11];69(4):1290–6. Available from: http://linkinghub.elsevier.com/retrieve/pii/S0360301607036814

47. Beetz I, Schilstra C, van der Schaaf A, et al. NTCP models for patient-rated xerostomia and sticky saliva after treatment with intensity modulated radiotherapy for head and neck cancer: The role of dosimetric and clinical factors. Radiother Oncol [Internet]. 2012 Oct 1 [cited 2018 Feb 12];105(1):101–6. Available from: https://www.sciencedirect.com/science/article/pii/S016781401200117X

48. Deasy JO, Moiseenko V, Marks L, et al. Radiotherapy Dose–Volume Effects on Salivary Gland Function. Int J Radiat Oncol [Internet]. 2010 Mar 1 [cited 2018 Feb 12];76(3):S58–63. Available from: https://www.sciencedirect.com/science/article/pii/S0360301609032891

49. Dijkema T, Raaijmakers CPJ, Ten Haken RK, et al. Parotid Gland Function After Radiotherapy: The Combined Michigan and Utrecht Experience. Int J Radiat Oncol [Internet]. 2010 Oct 1 [cited 2018 Feb 12];78(2):449–53. Available from: https://www.sciencedirect.com/science/article/pii/S0360301609028156

50. Brouwer CL, Steenbakkers RJHMHM, Langendijk JA, et al. Identifying patients who may benefit from adaptive radiotherapy: Does the literature on anatomic and dosimetric changes in head and neck organs at risk during radiotherapy provide information to help? Radiother Oncol [Internet]. 2015 Jun 1 [cited 2018 Feb 12];115(3):285–94. Available from: https://www.sciencedirect.com/science/article/pii/S0167814015002728?via%3Dihub

#s0110

51. Lee C, Langen KM, Lu W, et al. Evaluation of geometric changes of parotid glands during head and neck cancer radiotherapy using daily MVCT and automatic deformable registration. Radiother Oncol [Internet]. 2008 Oct [cited 2019 Feb 2];89(1):81–8. Available from: https://linkinghub.elsevier.com/retrieve/pii/S016781400800371X

52. Castelli J, Simon A, Louvel G, et al. Impact of head and neck cancer adaptive radiotherapy to spare the parotid glands and decrease the risk of xerostomia. Radiat Oncol [Internet]. 2015 Jan 9 [cited 2019 Feb 2];10(1):6. Available from: https://ro-journal.biomedcentral.com/articles/10.1186/s13014-014-0318-z

53. Chen C, Lin X, Pan J, et al. Is it necessary to repeat CT imaging and replanning during the course of intensity-modulated radiation therapy for locoregionally advanced nasopharyngeal carcinoma? Jpn J Radiol [Internet]. 2013 Sep 9 [cited 2019 Jan 10];31(9):593–9. Available from: http://link.springer.com/10.1007/s11604-013-0225-5

54. Vásquez Osorio EM, Hoogeman MS, Al-Mamgani A, et al. Local Anatomic Changes in Parotid and Submandibular Glands During Radiotherapy for Oropharynx Cancer and Correlation With Dose, Studied in Detail With Nonrigid Registration. Int J Radiat Oncol [Internet]. 2008 Mar 1 [cited 2018 Sep 11];70(3):875–82. Available from: https://www.sciencedirect.com/science/article/pii/S0360301607044732

55. Wang Z-H, Yan C, Zhang Z-Y, et al. Radiation-induced volume changes in parotid and submandibular glands in patients with head and neck cancer receiving postoperative radiotherapy: A longitudinal study. Laryngoscope [Internet]. 2009 Oct [cited 2019 Nov 28];119(10):1966–74. Available from: http://doi.wiley.com/10.1002/lary.20601

56. Zhao L, Wan Q, Zhou Y, et al. The role of replanning in fractionated intensity

modulated radiotherapy for nasopharyngeal carcinoma. Radiother Oncol [Internet]. 2011 Jan 1 [cited 2018 Feb 12];98(1):23–7. Available from: https://www.sciencedirect.com/science/article/pii/S0167814010006043

57. Wang X, Lu J, Xiong X, et al. Anatomic and dosimetric changes during the treatment course of intensity-modulated radiotherapy for locally advanced nasopharyngeal carcinoma. Med Dosim. 2010;35(2):151–7.

58. Ahn PH, Chen C-C, Ahn AI, et al. Adaptive planning in intensity-modulated radiation therapy for head and neck cancers: single-institution experience and clinical implications. Int J Radiat Oncol Biol Phys [Internet]. 2011 Jul 1 [cited 2018 Jan 31];80(3):677–85. Available from: http://www.ncbi.nlm.nih.gov/pubmed/20619553

59. Yan D, Lockman D, Martinez A, et al. Computed tomography guided management of interfractional patient variation. Semin Radiat Oncol [Internet]. 2005 Jul [cited 2019 Jul 23];15(3):168–79. Available from: http://www.ncbi.nlm.nih.gov/pubmed/15983942

60. Schwartz DL, Garden AS, Thomas J, et al. Adaptive Radiotherapy for Head-and-Neck Cancer: Initial Clinical Outcomes From a Prospective Trial. Int J Radiat Oncol [Internet]. 2012 Jul 1 [cited 2018 Aug 29];83(3):986–93. Available from: http://www.ncbi.nlm.nih.gov/pubmed/22138459

61. O. H-V, J.J. S. ARTFORCE: Individualised treatment and prediction of response in head-neck and lung cancer patients. Radiother Oncol. 2014;111.

62. Surucu M, Shah KK, Roeske JC, et al. Adaptive Radiotherapy for Head and Neck Cancer. Technol Cancer Res Treat [Internet]. 2017 Apr [cited 2018 Jan 31];16(2):218–23. Available from: http://www.ncbi.nlm.nih.gov/pubmed/27502958

63. Zhang P, Simon A, Rigaud B, et al. Optimal adaptive IMRT strategy to spare the parotid glands in oropharyngeal cancer. Radiother Oncol [Internet]. 2016 Jul 1 [cited 2018 Mar 9];120(1):41–7. Available from:

https://www.sciencedirect.com/science/article/pii/S0167814016311562?via%3Dihub#s0085

64. Castadot P, Lee JA, Geets X, et al. Adaptive Radiotherapy of Head and Neck Cancer. Semin Radiat Oncol [Internet]. 2010 Apr 1 [cited 2018 Feb 12];20(2):84–93. Available from: https://www.sciencedirect.com/science/article/pii/S1053429609000769

65. Yang H, Hu W, Wang W, et al. Replanning During Intensity Modulated Radiation Therapy Improved Quality of Life in Patients With Nasopharyngeal Carcinoma. Int J Radiat Oncol [Internet]. 2013 Jan 1 [cited 2018 Aug 29];85(1):e47–54. Available from: http://www.ncbi.nlm.nih.gov/pubmed/23122981

66. Kataria T, Gupta D, Goyal S, et al. Clinical outcomes of adaptive radiotherapy in head and neck cancers. Br J Radiol [Internet]. 2016 Jun [cited 2019 Sep 5];89(1062):20160085. Available from: http://www.ncbi.nlm.nih.gov/pubmed/26986461

67. Kataria T, Gupta D, Bisht SS, et al. Chemoradiation in elderly patients with head and neck cancers: A single institution experience. Am J Otolaryngol - Head Neck Med Surg. 2015;

68. Geets X, Tomsej M, Lee JA, et al. Adaptive biological image-guided IMRT with anatomic and functional imaging in pharyngo-laryngeal tumors: Impact on target volume delineation and dose distribution using helical tomotherapy. Radiother Oncol [Internet]. 2007 Oct [cited 2018 Jan 31];85(1):105–15. Available from: http://www.ncbi.nlm.nih.gov/pubmed/17562346

69. Brouwer CL, Steenbakkers RJHM, van der Schaaf A, et al. Selection of head and neck cancer patients for adaptive radiotherapy to decrease xerostomia. Radiother Oncol [Internet]. 2016 Jul 1 [cited 2019 Jul 22];120(1):36–40. Available from: https://www.sciencedirect.com/science/article/pii/S0167814016311495?via%3Dihub

70. Castelli J, Simon A, Rigaud B, et al. A Nomogram to predict parotid gland overdose in head and neck IMRT. Radiat Oncol [Internet]. 2016 Jun 8 [cited 2019 Dec 10];11:79. Available from: http://www.ncbi.nlm.nih.gov/pubmed/27278960

71. Brown E, Owen R, Harden F, et al. Predicting the need for adaptive radiotherapy in head and neck cancer. Radiother Oncol [Internet]. 2015 Jul 1 [cited 2019 Jul 22];116(1):57–63. Available from: https://www.sciencedirect.com/science/article/pii/S0167814015003187?via%3Dihub#b0030

72. Surucu M, Shah KK, Mescioglu I, et al. Decision Trees Predicting Tumor Shrinkage for Head and Neck Cancer: Implications for Adaptive Radiotherapy. Technol Cancer Res Treat. 2016 Feb;15(1):139–45.

73. Dirix P, Haustermans K, Vandecaveye V. The Value of Magnetic Resonance Imaging for Radiotherapy Planning. Semin Radiat Oncol [Internet]. 2014 Jul [cited 2019 Jan 11];24(3):151–9. Available from: http://www.ncbi.nlm.nih.gov/pubmed/24931085

74. Chen AM, Li J, Beckett LA, et al. Differential response rates to irradiation among patients with human papillomavirus positive and negative oropharyngeal cancer. Laryngoscope [Internet]. 2013 Jan [cited 2019 Jan 11];123(1):152–7. Available from: http://www.ncbi.nlm.nih.gov/pubmed/23008061

75. Noel CE, Parikh PJ, Spencer CR, et al. Comparison of onboard low-field magnetic resonance imaging versus onboard computed tomography for anatomy visualization in radiotherapy. Acta Oncol [Internet]. 2015 Oct 21 [cited 2019 Jan 11];54(9):1474–82. Available from: http://www.tandfonline.com/doi/full/10.3109/0284186X.2015.1062541

76. Devic S. MRI simulation for radiotherapy treatment planning. Med Phys [Internet]. 2012 Nov 16 [cited 2019 Jan 11];39(11):6701–11. Available from:

http://doi.wiley.com/10.1118/1.4758068

77. Rasch C, Steenbakkers R, van Herk M. Target Definition in Prostate, Head, and Neck. Semin Radiat Oncol [Internet]. 2005 Jul 1 [cited 2019 Jul 16];15(3):136–45. Available from: https://www.sciencedirect.com/science/article/pii/S105342960500007X?via%3Dihub

78. Jager EA, Ligtenberg H, Caldas-Magalhaes J, et al. Validated guidelines for tumor delineation on magnetic resonance imaging for laryngeal and hypopharyngeal cancer. Acta Oncol (Madr) [Internet]. 2016 Nov 8 [cited 2018 Mar 23];55(11):1305–12. Available from: https://www.tandfonline.com/doi/full/10.1080/0284186X.2016.1219048

79. Ligtenberg H, Jager EA, Caldas-Magalhaes J, et al. Modality-specific target definition for laryngeal and hypopharyngeal cancer on FDG-PET, CT and MRI. Radiother Oncol. 2017;

80. Quon H, Brizel DM. Predictive and prognostic role of functional imaging of head and neck squamous cell carcinomas. Semin Radiat Oncol [Internet]. 2012 Jul [cited 2017 Nov 3];22(3):220–32. Available from: http://linkinghub.elsevier.com/retrieve/pii/S1053429612000264

81. Wong KH, Panek R, Welsh L, et al. The Predictive Value of Early Assessment After 1 Cycle of Induction Chemotherapy with 18F-FDG PET/CT and Diffusion-Weighted MRI for Response to Radical Chemoradiotherapy in Head and Neck Squamous Cell Carcinoma. J Nucl Med [Internet]. 2016 Dec 1 [cited 2017 Nov 2];57(12):1843–50. Available from: http://www.ncbi.nlm.nih.gov/pubmed/27417648

82. Powell C, Schmidt M, Borri M, et al. Changes in functional imaging parameters following induction chemotherapy have important implications for individualised patient-based treatment regimens for advanced head and neck cancer. Radiother Oncol [Internet]. 2013 Jan [cited 2017 Nov 2];106(1):112–7. Available from:

http://linkinghub.elsevier.com/retrieve/pii/S0167814012003842

83. Wong KH, Panek R, Dunlop A, et al. Changes in multimodality functional imaging parameters early during chemoradiation predict treatment response in patients with locally advanced head and neck cancer. Eur J Nucl Med Mol Imaging [Internet]. 2017 Nov 21 [cited 2017 Nov 23]; Available from: http://www.ncbi.nlm.nih.gov/pubmed/29164301

84. Chawla S, Kim S, Wang S, et al. Diffusion-weighted imaging in head and neck cancers. Future Oncol [Internet]. 2009 Sep [cited 2017 Nov 17];5(7):959–75. Available from: http://gateway.proquest.com/openurl?ctx_ver=Z39.88-2004&res_id=xri:pqm&req_dat=xri:pqil:pq_clntid=50352&rft_val_fmt=ori/fmt:kev:mtx:journal&genre=article&issn=1479-6694&volume=5&issue=7&spage=959

85. Vandecaveye V, de Keyzer F, Vander Poorten V, et al. Evaluation of the larynx for tumour recurrence by diffusion-weighted MRI after radiotherapy: initial experience in four cases. Br J Radiol [Internet]. 2006 Aug [cited 2017 Nov 17];79(944):681–7. Available from: http://www.birpublications.org/doi/10.1259/bjr/89661809

86. Wong KH, Panek R, Bhide SA, et al. The emerging potential of magnetic resonance imaging in personalizing radiotherapy for head and neck cancer: an oncologist's perspective. Br J Radiol [Internet]. 2017 Mar [cited 2017 Nov 14];90(1071):20160768. Available from: http://www.ncbi.nlm.nih.gov/pubmed/28256151

87. de Ridder M, Gouw ZAR, Sonke JJ, et al. Recurrent oropharyngeal cancer after organ preserving treatment: pattern of failure and survival. Eur Arch Oto-Rhino-Laryngology. 2017;

88. Chen AM, Chin R, Beron P, et al. Inadequate target volume delineation and local–regional recurrence after intensity-modulated radiotherapy for human papillomavirus-positive oropharynx cancer: Local–regional recurrence after IMRT

for HPV-positive oropharynx cancer. Radiother Oncol [Internet]. 2017 Jun 1 [cited 2018 May 2];123(3):412–8. Available from: https://www.sciencedirect.com/science/article/pii/S0167814017301561?via%3Dihub#b0075

89. De Felice F, Thomas C, Barrington S, et al. Analysis of loco-regional failures in head and neck cancer after radical radiation therapy. Oral Oncol. 2015;

90. Ding Y, Hazle JD, Mohamed ASR, et al. Intravoxel incoherent motion imaging kinetics during chemoradiotherapy for human papillomavirus-associated squamous cell carcinoma of the oropharynx: Preliminary results from a prospective pilot study. NMR Biomed. 2015;

91. Mohamed ASR, Bahig H, Aristophanous M, et al. Prospective in silico study of the feasibility and dosimetric advantages of MRI-guided dose adaptation for human papillomavirus positive oropharyngeal cancer patients compared with standard IMRT. Clin Transl Radiat Oncol [Internet]. 2018 Jun [cited 2019 May 7];11:11–8. Available from: http://www.ncbi.nlm.nih.gov/pubmed/30014042

92. Raghavan G, Kishan AU, Cao M, et al. Anatomic and dosimetric changes in patients with head and neck cancer treated with an integrated MRI-tri- ^{60}Co teletherapy device. Br J Radiol [Internet]. 2016 Nov [cited 2017 Dec 12];89(1067):20160624. Available from: http://www.ncbi.nlm.nih.gov/pubmed/27653787

93. Kamran SC, Tyagi N, Han J, et al. Weekly On-Treatment MRIs During Radiation Therapy (RT) in Head and Neck Squamous Cell Carcinoma (HNSCC) Patients to Monitor Treatment Response. Int J Radiat Oncol [Internet]. 2014 Sep 1 [cited 2019 Feb 22];90(1):S516. Available from: https://linkinghub.elsevier.com/retrieve/pii/S0360301614022317

94. Thiagarajan A, Caria N, Schöder H, et al. Target Volume Delineation in Oropharyngeal Cancer: Impact of PET, MRI, and Physical Examination. Int J Radiat

Oncol [Internet]. 2012 May 1 [cited 2018 May 8];83(1):220–7. Available from: https://www.sciencedirect.com/science/article/pii/S0360301611028070?via%3Dihub#bib6

95. Kerkmeijer LGW, Fuller CD, Verkooijen HM, et al. The MRI-linear accelerator consortium: Evidence-based clinical introduction of an innovation in radiation oncology connecting researchers, methodology, data collection, quality assurance, and technical development. Front Oncol. 2016;

96. Raaymakers BW, Jürgenliemk-Schulz IM, Bol GH, et al. First patients treated with a 1.5 T MRI-Linac: clinical proof of concept of a high-precision, high-field MRI guided radiotherapy treatment. Phys Med Biol [Internet]. 2017 Nov 14 [cited 2019 Aug 9];62(23):L41–50. Available from: http://stacks.iop.org/0031-9155/62/i=23/a=L41?key=crossref.1c8c48a76c7eafac216d1be249abc1b5

97. Chao KSC, Bhide S, Chen H, et al. Reduce in Variation and Improve Efficiency of Target Volume Delineation by a Computer-Assisted System Using a Deformable Image Registration Approach. Int J Radiat Oncol [Internet]. 2007 Aug 1 [cited 2018 Aug 8];68(5):1512–21. Available from: http://www.ncbi.nlm.nih.gov/pubmed/17674982

98. Kessler ML. Image registration and data fusion in radiation therapy. British Journal of Radiology. 2006.

99. Oh S, Kim S. Deformable image registration in radiation therapy. Radiat Oncol J [Internet]. 2017 Jun [cited 2019 Mar 12];35(2):101–11. Available from: http://www.ncbi.nlm.nih.gov/pubmed/28712282

100. Thirion JP. Image matching as a diffusion process: An analogy with Maxwell's demons. Med Image Anal. 1998;

101. Klein S, Staring M, Murphy K, et al. Elastix: A toolbox for intensity-based medical image registration. IEEE Trans Med Imaging. 2010;

102. Brock KK, Sharpe MB, Dawson LA, et al. Accuracy of finite element model-based multi-organ deformable image registration. In: Medical Physics. 2005.

103. Weistrand O, Svensson S. The ANACONDA algorithm for deformable image registration in radiotherapy. Med Phys [Internet]. 2014 Dec 16 [cited 2020 Aug 2];42(1):40–53. Available from: http://doi.wiley.com/10.1118/1.4894702

104. Gu X, Dong B, Wang J, et al. A contour-guided deformable image registration algorithm for adaptive radiotherapy. Phys Med Biol. 2013;

105. Castadot P, Lee JA, Parraga A, et al. Comparison of 12 deformable registration strategies in adaptive radiation therapy for the treatment of head and neck tumors. Radiother Oncol [Internet]. 2008 Oct 1 [cited 2018 Sep 11];89(1):1–12. Available from: https://www-sciencedirect-com.ezproxy.icr.ac.uk/science/article/pii/S0167814008002302?via%3Dihub

106. Zhang T, Chi Y, Meldolesi E, et al. Automatic delineation of on-line head-and-neck computed tomography images: toward on-line adaptive radiotherapy. Int J Radiat Oncol Biol Phys [Internet]. 2007 Jun 1 [cited 2018 Jul 10];68(2):522–30. Available from: http://linkinghub.elsevier.com/retrieve/pii/S036030160700199X

107. Hvid CA, Elstrøm U V, Jensen K, et al. Accuracy of software-assisted contour propagation from planning CT to cone beam CT in head and neck radiotherapy. Acta Oncol [Internet]. 2016 Nov 24 [cited 2018 Jun 26];55(11):1324–30. Available from: https://www.tandfonline.com/doi/full/10.1080/0284186X.2016.1185149

108. Yan D, Jaffray DA, Wong JW. A model to accumulate fractionated dose in a deforming organ. Int J Radiat Oncol Biol Phys. 1999;

109. Christensen GE, Carlson B, Chao KSC, et al. Image-based dose planning of intracavitary brachytherapy: Registration of serial-imaging studies using deformable anatomic templates. Int J Radiat Oncol Biol Phys. 2001;

110. Schaly B, Kempe JA, Bauman GS, et al. Tracking the dose distribution in radiation

therapy by accounting for variable anatomy. Phys Med Biol. 2004;

111. Velec M, Moseley JL, Eccles CL, et al. Effect of breathing motion on radiotherapy dose accumulation in the abdomen using deformable registration. Int J Radiat Oncol Biol Phys. 2011;

112. Schultheiss TE, Tome WA, Orton CG. Point/counterpoint: it is not appropriate to "deform" dose along with deformable image registration in adaptive radiotherapy. Med Phys. 2012;

113. Zhong H, Chetty IJ. Caution Must Be Exercised When Performing Deformable Dose Accumulation for Tumors Undergoing Mass Changes During Fractionated Radiation Therapy. Int J Radiat Oncol Biol Phys. 2017;

114. Qin A, Liang J, Han X, et al. Technical Note: The impact of deformable image registration methods on dose warping: The. Med Phys. 2018;

115. Qin A, Ionascu D, Liang J, et al. The evaluation of a hybrid biomechanical deformable registration method on a multistage physical phantom with reproducible deformation. Radiat Oncol. 2018;

116. Rigaud B, Simon A, Castelli J, et al. Evaluation of deformable image registration methods for dose monitoring in head and neck radiotherapy. Biomed Res Int. 2015;

117. García-Mollá R, Marco-Blancas N de, Bonaque J, et al. Validation of a deformable image registration produced by a commercial treatment planning system in head and neck. Phys Medica. 2015;

118. Kumarasiri A, Liu C, Siddiqui F, et al. Target and organ dose estimation from intensity modulated head and neck radiation therapy using 3 deformable image registration algorithms. Pract Radiat Oncol. 2015;

119. Pukala J, Johnson PB, Shah AP, et al. Benchmarking of five commercial deformable image registration algorithms for head and neck patients. J Appl Clin Med Phys.

2016;

120. Nie K, Pouliot J, Smith E, et al. Performance variations among clinically available deformable image registration tools in adaptive radiotherapy - how should we evaluate and interpret the result? J Appl Clin Med Phys [Internet]. 2016 [cited 2018 May 17];17(2):328–40. Available from: http://www.ncbi.nlm.nih.gov/pubmed/27074457

121. Zhang L, Wang Z, Shi C, et al. The impact of robustness of deformable image registration on contour propagation and dose accumulation for head and neck adaptive radiotherapy. J Appl Clin Med Phys [Internet]. 2018 Jul [cited 2019 May 31];19(4):185–94. Available from: http://www.ncbi.nlm.nih.gov/pubmed/29851267

122. Raaymakers BW, Lagendijk JJW, Overweg J, et al. Integrating a 1.5 T MRI scanner with a 6 MV accelerator: proof of concept. Phys Med Biol [Internet]. 2009 Jun 21 [cited 2019 Aug 9];54(12):N229–37. Available from: http://stacks.iop.org/0031-9155/54/i=12/a=N01?key=crossref.54089f06f82576151c8b56c369d3f175

123. Kontaxis C, Bol GH, Kerkmeijer LGW, et al. Fast online replanning for interfraction rotation correction in prostate radiotherapy. Med Phys. 2017;

124. van der Heide UA, Houweling AC, Groenendaal G, et al. Functional MRI for radiotherapy dose painting. Magn Reson Imaging. 2012;

125. Van Rossum PSN, Van Lier ALHMW, Van Vulpen M, et al. Diffusion-weighted magnetic resonance imaging for the prediction of pathologic response to neoadjuvant chemoradiotherapy in esophageal cancer. Radiother Oncol. 2015;

126. Raaijmakers AJEE, Raaymakers BW, Lagendijk JJWW. Integrating a MRI scanner with a 6 MV radiotherapy accelerator: Dose increase at tissue-air interfaces in a lateral magnetic field due to returning electrons. Phys Med Biol [Internet]. 2005 Apr 7 [cited 2019 Feb 2];50(7):1363–76. Available from: http://stacks.iop.org/0031-9155/50/i=7/a=002?key=crossref.2a1bed204f4645d5dcfb585ba97a9ae5

127. Bol GH, Lagendijk JJW, Raaymakers BW. Virtual couch shift (VCS): Accounting for patient translation and rotation by online IMRT re-optimization. Phys Med Biol. 2013 May 7;58(9):2989–3000.

128. Chuter RW, Whitehurst P, Choudhury A, et al. Technical Note: Investigating the impact of field size on patient selection for the 1.5T MR-Linac. Med Phys [Internet]. 2017 Nov 1 [cited 2019 Feb 4];44(11):5667–71. Available from: http://doi.wiley.com/10.1002/mp.12557

129. Park JM, Shin KH, Kim J, et al. Air–electron stream interactions during magnetic resonance IGRT. Strahlentherapie und Onkol. 2017;

130. Webb J, Chuter R, Mcwilliam A, et al. S1137 ESTRO 37 EP-2073 The impact of the electron return effect on radiotherapy plan quality for peripheral sarcomas. Vol. 127, ESTRO 37, April 20-24, 2018, Barcelona, Spain. 2018.

131. Nachbar M, Mönnich D, Boeke S, et al. Partial breast irradiation with the 1.5 T MR-Linac: First patient treatment and analysis of electron return and stream effects. Radiother Oncol. 2020 Apr 1;145:30–5.

132. Werensteijn-Honingh AM, Kroon PS, Winkel D, et al. Feasibility of stereotactic radiotherapy using a 1.5 T MR-linac: Multi-fraction treatment of pelvic lymph node oligometastases. Radiother Oncol. 2019;

133. Pathmanathan A, Bower L, Creasey H, et al. The PRISM Trial- First UK Experience of MRI-Guided Adaptive Radiotherapy. Int J Radiat Oncol. 2019 Sep 1;105(1):E301.

134. Ng-Cheng-Hin B, Nutting C, Newbold K, et al. The impact of restricted length of treatment field and anthropometric factors on selection of head and neck cancer patients for treatment on the MR-Linac. Br J Radiol [Internet]. 2020 May 21 [cited 2020 Jun 2];20200023. Available from: https://www.birpublications.org/doi/10.1259/bjr.20200023

135. Fast M, van de Schoot A, van de Lindt T, et al. Tumor Trailing for Liver SBRT on

the MR-Linac. Int J Radiat Oncol Biol Phys. 2019;

136. van den Wollenberg W, de Ruiter P, Nowee ME, et al. Investigating the impact of patient arm position in an MR-linac on liver SBRT treatment plans. Med Phys. 2019;

137. Cusumano D, Boldrini L, Menna S, et al. Evaluation of a simplified optimizer for MR-guided adaptive RT in case of pancreatic cancer. J Appl Clin Med Phys. 2019;

2 Chapter 2 - The evaluation of CT-based contour propagation using deformable image registration algorithm in head and neck cancers

2.1 Introduction

Radiotherapy is an organ-sparing treatment for locally advanced head and neck cancers (LAHNC). The majority of radiotherapy centres adopt a strategy of planning radiotherapy on a single pre-treatment computed tomography (CT) scan for treatment delivery. However, this single snapshot does not take into account positional and anatomical changes that arise from weight loss, tissue swelling and tumour and normal tissue shrinkage during treatment (1–3). A plan based on pre-treatment parameters may have a significant impact on the planned dosimetry with higher and lower delivered doses to organs at risk (OARs) and target volumes, respectively (4). This is particularly important in the era of intensity-modulated radiotherapy treatment (IMRT), which enables a precisely sculpted radiotherapy dose with sharp dose gradients to the tumour, albeit at the expense of increased sensitivity to geometrical errors.

Adaptive radiotherapy (ART) uses up-to-date imaging to modify the initially planned parameters, thus optimising the dose to the target volume and OARs. In LAHNC, there is non-randomised evidence that ART leads to improved quality-of-life (QoL) and treatment outcomes (5–7). However, implementing ART poses logistic and resource challenges such as repeat imaging, clinician delineation and radiotherapy planning. From a clinician's perspective, repeat delineation is time-consuming and contour propagation using deformable image registration (DIR) has been investigated as a means to facilitate this process. DIR may be used to propagate

regions of interest (ROIs) by mapping corresponding locations between the two images (8–10).

2.2 Aims

This study investigates the utility of RayStation's DIR algorithm for ROI propagation on CT during adaptive radiotherapy workflow in patients with LAHNC.

2.3 Hypothesis

DIR-based contour propagation will be geometrically accurate and more time-efficient than manual delineation.

2.4 Objectives

- To assess the geometrical agreement between DIR-propagated and manually-delineated ROIs on CT using comparison metrics.
- To assess the time taken (in minutes) to propagate ROIs from the planning scan to the repeat scan using DIR versus manual delineation.
- To assess the dosimetric impact on ROIs using DIR (unmodified versus modified delineations).

2.5 Materials and methods

2.5.1 Patients and image acquisition

Ten patients with LAHNC (7th edition American Joint Committee on Cancer Stage III to IVb), who underwent primary chemoradiotherapy, were retrospectively selected from the INSIGHT trial (CCR3926) (11) (five patients) or from non-trial patients (five patients). These patients received 6 weeks of radical radiotherapy with concurrent chemotherapy (Cisplatin (100 mg/m^2) or Carboplatin (AUC 5) on days 1 and 29). The fractionation regimen was 65 Gy in 30 fractions over 6 weeks to the high-dose planning target volume (PTV) and 54 Gy in 30 fractions over 6 weeks to the low-dose PTV. All patients consented for their images to be used for research purposes. The patients underwent pre-treatment contrast-enhanced CT in five-point thermoplastic shell immobilisation on a large-bore CT scanner (Philips Medical, Cleveland, OH, USA). A rescan planning CT with or without intravenous contrast was performed between weeks 2 to 4 of radiotherapy on the same CT scanner. Whilst the rescan planning CT was pre-planned for the patients in the INSIGHT study, these were done reactively for the other patients. Both planning and rescan CTs were acquired in 2 mm slices. As all patients had consented to have their imaging used for research purposes, institutional and ethical approval were not required.

2.5.2 Manual delineation of ROIs

ROI delineation was performed on the Research RayStation treatment planning system (version 7.0, RaySearch Laboratories, Stockholm, Sweden). I delineated the ROIs on the planning and rescan CTs using local and international guidelines (12–14). The ROIs included the parotid glands, spinal cord, brainstem, lenses, orbits,

chiasm, optic nerves, primary gross tumour volume (GTV-p), nodal gross tumour volume (GTV-n), low-dose clinical target volume (CTV) and high-dose CTV. These ROIs were chosen to assess the performance of the DIR algorithm for a range of ROIs with different volumes.

A 1 cm isotropic margin around the GTV was used to create the high-dose CTV as per local guidelines and edited off anatomical barriers to tumour spread (such as bone and air). The low-dose CTV included areas at risk of microscopic disease as per local and international guidelines (13).

2.5.3 Deformable image registration and contour propagation

ROI propagation using the DIR algorithm was processed in RayStation on a Workstation (Intel® Xeon® 3.4-GHz, 64 GB RAM, Windows 7.0, NVIDIA Quadro M6000). DIR was implemented using the ANAtomically CONstrained Deformation Algorithm (ANACONDA), allowing for intensity-based or hybrid registration (intensity plus controlling ROIs) (15). The image registration and structure mapping process involved multiple steps that were automated using a Python script. This involved an initial rigid registration of the planning CT and rescan CT followed by DIR between the two CTs. The delineated ROIs from the planning CT scan were then propagated to the rescan CT using RayStation's default intensity-based DIR settings.

I reviewed all propagated ROIs on the rescan CT and modified them if deemed necessary. To avoid recall bias, there was a minimum gap of 3 weeks between manual delineation and modification of DIR-propagated ROIs. Prior to geometric and dosimetric analysis, both manual and modified DIR-propagated ROIs were reviewed by two experienced radiation oncologists specialising in head and neck cancer (Dr Shreerang Bhide and Dr Imran Petkar) for acceptability.

2.5.4 Percentage weight change

This is expressed as a percentage (%) change of the patient weight (kilograms) at rescan to the pre-treatment weight using the following equation:

% weight change = ((pre-treatment weight - weight at rescan)/pre-treatment weight) * 100

A negative integer represents weight loss whereas a positive integer represents weight gain.

2.5.5 Time Analysis

A stopwatch was used to record the elapsed time taken:

a) to manually delineate the ROIs on the rescan CT.

b) to propagate, review and amend ROIs from the planning CT to rescan CT.

2.5.6 Geometric Analysis

Modified and unmodified DIR-propagated ROIs were compared to the manually-delineated ROIs, which were considered as the "gold standard". Geometrical agreement was measured using the dice similarity coefficient (DSC) and mean distance to agreement (MDA) calculated volume- and surface-based metrics, respectively.

DSC was defined as the volume of overlap between two structures (16):

$$DSC(A,B) = 2(A \cap B) / (A + B)$$

where A and B represented two delineated volumes of the same structure.

The MDA was defined as the mean surface distance between 2 contours on registered images and was reported in millimetres (mm).

As per the published recommendations by the American Association of Physicists in Medicine (AAPM) on the use of image registration in radiotherapy in their TG132 report (17), the minimally acceptable values of DSC and MDA were set at ≥ 0.8 and ≤ 3 mm, respectively in this study.

2.5.7 Dosimetric comparisons of the propagated plans

The dosimetric impact of the uncertainties associated with DIR structure propagation were assessed.

Planning target volume (PTV)

The high-dose and low-dose PTV were derived using a 3 mm isometric expansion margin of their respective CTVs.

IMRT plans

For this study, the IMRT plans were generated by a medical physicist (Dr Steven Court) using an identical procedure. The same objective function and number of optimisation iterations were used in each case as described below. For each patient, three plans were made, each optimised on one of the three structure sets: manually-delineated, unmodified DIR-propagated and modified DIR-propagated sets.

Plan design and objectives

The plans were generated and optimised using the collapsed cone version 5.0 algorithm in RayStation. Plans were generated using single arc, 6 MV (megavolts) volumetric-modulated arc therapy (VMAT) treatments generated in the RayStation treatment planning system.

The following planning objectives for the PTVs (Table 2-1), planning organ at risk volumes (PRVs) and OARs (Table 2-2) were used for all patients.

Table 2-1. Planning target volume (PTV) constraints for VMAT planning.

Volume (%)	Dose (%)	
	PTV65	PTV54
99	> 90	>90
98	> 95 (optimal)	>95 (optimal)
95	> 95	> 95
50	= 100	= 100
5	< 105	< 105 (optimal)
2	< 107 (optimal)	<110 (optimal)

Table 2-2 Planning target volume (PTV) constraints for organs at risk (OARs).

Structure	Constraint	Mandatory Dose constraint (Gy)	Optimal Dose constraint (Gy)
Spinal Cord	Max 1 cm^3	< 48 < 46	
Spinal Cord PRV	1 cm^3	< 48	
Brainstem	Max 1 cm^3	< 55 < 54	
Brainstem PRV	1 cm^3	< 56	
Contralateral Parotid	Mean dose	As low as possible	< 24 Gy
Ipsilateral Parotid	Mean dose	As low as possible	< 24 Gy

Abbreviation: PRV = planning organ at risk volume

Beam optimisation

Three rounds of optimisations were performed with 60 iterations each. This was followed by manual adjustments to the objectives to improve target volume coverage and reduce doses to OARs. A virtual bolus technique was used to prevent hot spots by reducing dose-boosting outside the build-up region. Once a satisfactory plan was generated, the virtual bolus was removed, and the dose recalculated to the high dose PTV.

Dosimetric Analysis

For the dosimetric comparison, dose statistics were generated by importing the dose cubes from the plans optimised on the DIR structure sets (modified and unmodified) onto the manually-delineated "ground truth" structure set. The structure sets in this analysis included the GTV node, GTV primary, parotid glands, spinal cord, brainstem, chiasm, optic nerves, lenses, globes, high-dose and low-dose CTV. The “ground truth” structure sets were manually delineated by myself and reviewed by two experienced radiation oncologists specialising in head and neck cancer (Dr Shreerang Bhide and Dr Imran Petkar) for acceptability.

2.5.8 Intra-observer and inter-observer Variability.

Intra- and inter-observer variabilities were measured as a control for comparison. As a measure of intra-observer variability, I repeated the manual delineation on a set of 3 cases (patients 2, 6 and 10) to assess the geometric differences. To avoid recall bias, there was a minimum gap of 3 weeks between the repeat delineations. To assess inter-observer variability, the ROIs delineated by another independent head and neck cancer radiation oncologist (Dr Kee Wong) were compared using the same metrics for the same 3 patients.

2.6 Statistical analysis

Statistical analysis was performed using GraphPad Prism software (Version 8.0.1; San Diego, CA). The data were tested for normality using the Shapiro-Wilk test. The paired *t*-test and the Wilcoxon matched-paired signed rank test were used to compare parametric and non-parametric data, respectively. The significance threshold was set at $p \leq 0.05$.

2.7 Results

2.7.1 Patient characteristics.

Patient characteristics are summarised in Table 2-3. The majority of patients had oropharyngeal cancers and underwent a rescan CT scan between weeks 2 to 4. The relative weight change between CT scans ranged between -14% to 0.3 %.

Table 2-3. Patient characteristics.

Patient Number	Age	Tumour Location	p16	Stage*	Timing of rescan	Intravenous contrast in rescan CT (Y/N)	Percentage weight change (%)[#]
1	60	BOT	positive	T3 N2b M0	Week 2	N	0.3
2	51	BOT	positive	T2 N2b M0	Week 2	N	-5.4
3	63	BOT	positive	T3 N2b M0	Week 2	N	1.8
4	64	Tonsil	negative	T2 N2b M0	Week 2	N	-6.1
5	52	Tonsil and BOT	positive	T2N2a M0	Week 2	N	-10.8
6	37	BOT	positive	T4 N2c M0	Week 4	Y	-1.3
7	62	BOT	positive	T1 N1 M0	Week 4	Y	-7.2
8	53	Unknown Primary	positive	T0 N3 M0	Week 4	Y	-7.3
9	57	Tonsil and BOT	positive	T2 N2a M0	Week 4	Y	-14.0
10	55	Tonsil	positive	T3 N2c M0	Week 3	Y	-11.8

Abbreviation: BOT = Base of Tongue

* 7th edition of the AJCC staging system.

[#] A negative integer represents weight loss whereas a positive integer represents weight gain.

2.7.2 Time analysis

DIR followed by ROI propagation took a mean time of 1 minute and 42 seconds. ROI propagation followed by clinician modification was consistently faster than manual delineation for every patient (Figure 2-1). The mean time to manually delineate was 83.0 minutes (SD 19.4 minutes), whereas propagating and modifying

the ROIs significantly reduced the mean time to 40.4 minutes (SD 9.9 minutes ($p=0.003$)). This translated to a mean time gain of 42.6 minutes per patient. The mean time spent to manually delineate the OAR and target volumes were 23 and 60 minutes, respectively. The corresponding mean times using DIR and modification were reduced to 18 and 24 minutes, respectively.

*Figure 2-1. Time analysis for each patient. The elapsed time for each patient is represented by 2 bars. The bar on the left represents manual delineation, whereas the bar on the right represents DIR-propagated contours. Each bar is further divided into different components. * = p<0.05.*

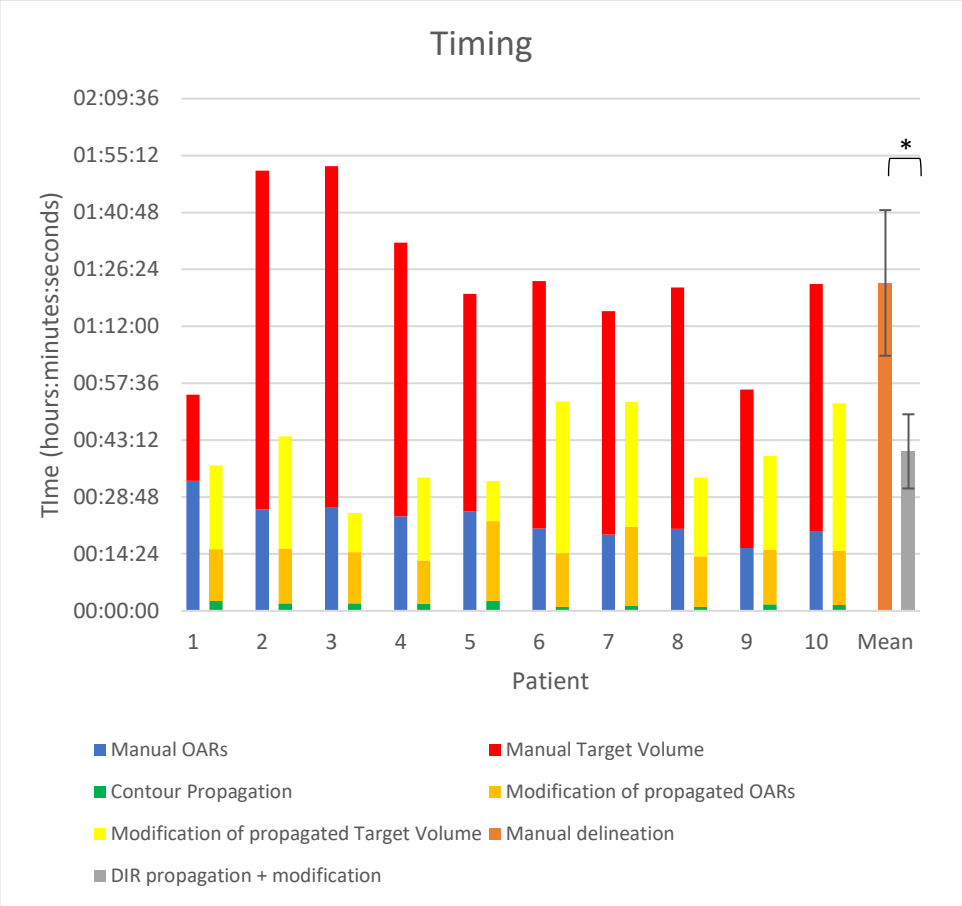

Geometric accuracy

The DSC and MDA performance varied according to the ROI (Table 2-4). Although the mean DSC for certain unmodified DIR-propagated ROIs achieved a DSC of ≥ 0.80, not all individual patient ROI scores achieved this threshold as illustrated by the SD error bars (Figure 2-2A). The unmodified DIR-propagated spinal cord,

brainstem, globes, right parotid gland, low-dose and high-dose CTV performed well with DSC of ≥ 0.80. Modification of each propagated ROI led to a higher degree of overlap with their respective manually-delineated contour. The overall mean DSCs for all patients were 0.76 (SD 0.04) and 0.82 (SD 0.03) for the unmodified and modified ROIs, respectively. However, DSC performance varied according to the ROI volume. ROIs with a median volume < 10 cm^3 such as the chiasm, optic nerves, lenses, GTV primary and GTV node achieved a poorer mean DSC compared to relatively larger ROIs with median volume ≥ 10 cm^3 such as the parotid glands, brainstem and CTVs (Table 2-4).

The mean MDAs for all structures were 1.25 mm (SD 0.33 mm) and 0.88 mm (SD 0.16 mm) for unmodified and modified DIR-propagated ROIs, respectively (Figure 2-2B). Clinician modification of propagated ROI significantly improved the MDA and DSC values (p=0.0004; p=0.0001).

Table 2-4. Comparisons of modified and unmodified DIR-propagated ROIs.

ROI	Volume			ROI Modification	DSC		MDA (mm)	
	Median (cm^3)	Minimum (cm^3)	Maximum (cm^3)		Mean	SD	Mean	SD
GTV node	3.2	0.6	113.6	Modified	0.80	0.09	1.07	0.95
				Unmodified	0.57	0.19	2.49	1.42
GTV primary*	2.9	0.8	24.2	Modified	0.74	0.07	1.32	0.41
				Unmodified	0.56	0.20	3.35	2.14
Right Parotid	23.4	12.7	34.4	Modified	0.86	0.04	1.10	0.36
				Unmodified	0.84	0.05	1.30	0.54
Left Parotid	20.8	11.6	38.2	Modified	0.85	0.05	1.10	0.44
				Unmodified	0.79	0.16	1.40	0.71
Spinal cord	21.8	14.5	31.2	Modified	0.85	0.03	0.83	0.69
				Unmodified	0.82	0.06	0.86	0.69

ROI	Volume			ROI Modification	DSC		MDA (mm)	
	Median (cm^3)	Minimum (cm^3)	Maximum (cm^3)		Mean	SD	Mean	SD
Brainstem	21.6	13.5	38.8	Modified	0.86	0.03	1.20	0.35
				Unmodified	0.83	0.05	1.30	0.24
Chiasm	1.1	0.8	2.0	Modified	0.63	0.19	0.94	0.56
				Unmodified	0.56	0.17	1.30	0.47
Right optic nerve	0.6	0.4	0.8	Modified	0.77	0.06	0.52	0.18
				Unmodified	0.71	0.09	0.68	0.29
Left Optic Nerve	0.6	0.3	0.7	Modified	0.78	0.04	0.61	0.34
				Unmodified	0.67	0.06	0.85	0.28
Right Lens	0.2	0.1	0.2	Modified	0.77	0.07	0.36	0.21
				Unmodified	0.71	0.10	0.48	0.19
Left Lens	0.2	0.1	0.2	Modified	0.75	0.14	0.42	0.27
				Unmodified	0.67	0.14	0.54	0.27
Right Globe	9.4	7.5	11.2	Modified	0.92	0.02	0.55	0.22
				Unmodified	0.91	0.03	0.64	0.24
Left Globe	8.7	8.0	11.5	Modified	0.93	0.02	0.52	0.13
				Unmodified	0.91	0.03	0.62	0.22
High-dose CTV	139.5	45.5	357.2	Modified	0.90	0.03	1.30	0.34
				Unmodified	0.88	0.05	1.50	0.52
Low-dose CTV	261.5	194.1	364.6	Modified	0.84	0.02	1.30	0.19
				Unmodified	0.81	0.04	1.60	0.42

Abbreviations: CTV: Clinical Target Volume; DSC: Dice Similarity Coefficient; GTV: Gross Tumour Volume; MDA:

Mean Distance to Agreement*;* ROI: Region of Interest*;* SD: Standard Deviation

* 9 GTVprimary were analysed as 1 patient had a carcinoma of unknown primary

Figure 2-2. Mean ROI DSC (A) and MDA(B) for 10 patients. The green-shaded area is the accepted tolerance range as per the AAPM recommendations TG132 report (17). *DSC of ≥0.8 and mean MDA ≤3 mm were used as tolerances. Inter-observer, Intra-observer and Modified ROI DSC in a subset of 3 patients (C). Error bars represent the standard deviation.*

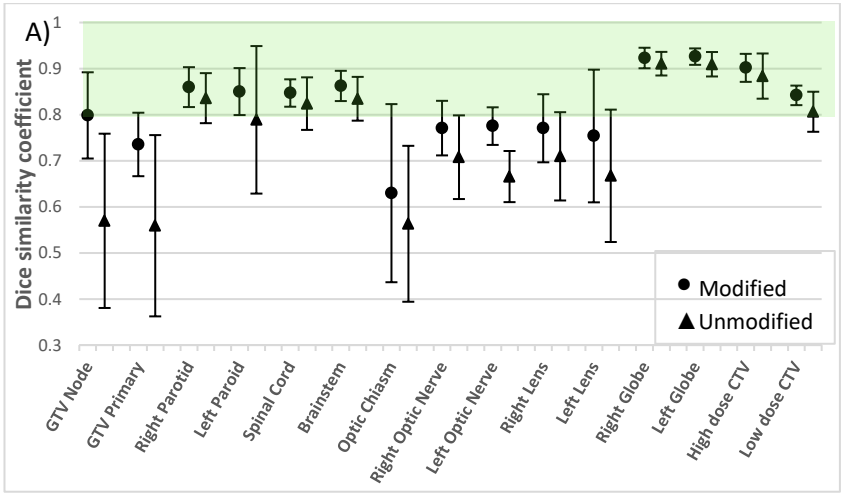

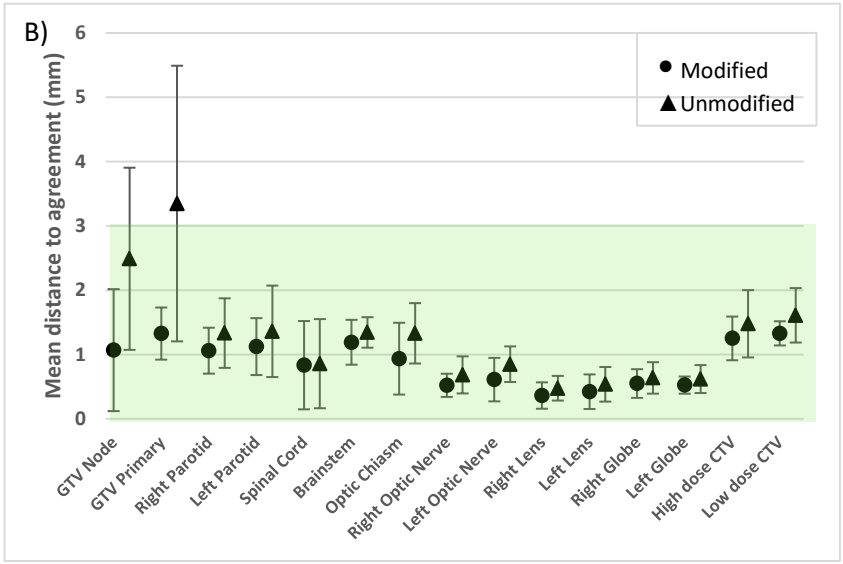

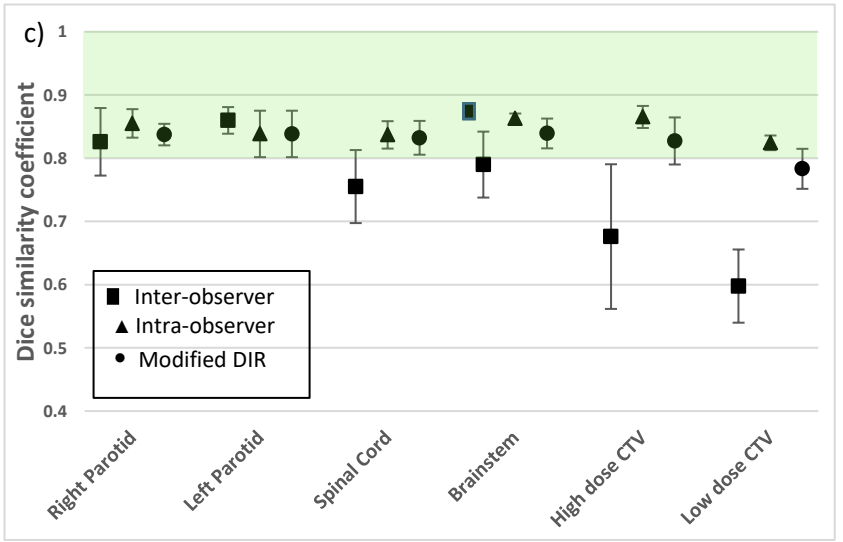

An example of the difference between manually-delineated, unmodified and modified DIR-propagated ROIs is shown in Figure 2-3 A to C.

Figure 2-3. Variability in delineation is shown for nodal GTV (A), high-dose CTV (B) and low-dose CTV (C) for patient 10. Manually-delineated ROIs (red), unmodified propagated ROIs (blue) and modified propagated ROIs (yellow) are shown.

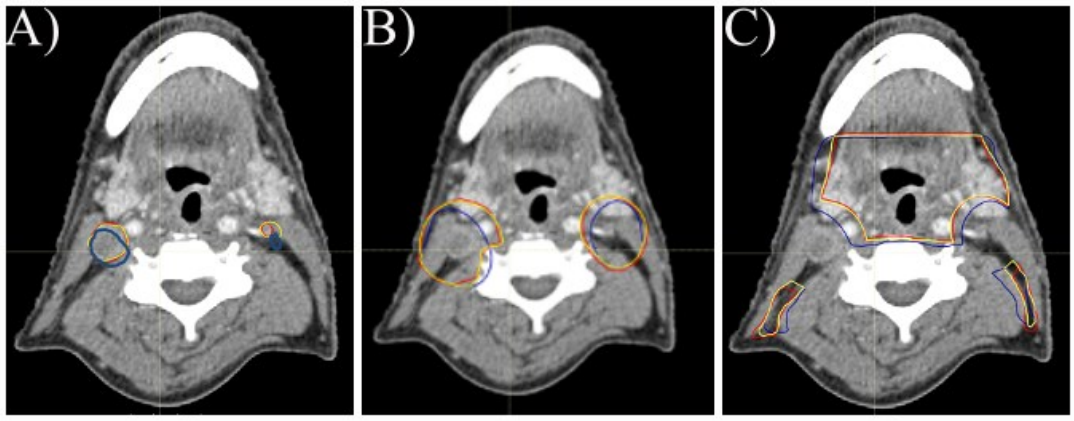

2.7.3 Correlation of weight loss with time and DSC score

There was no correlation between weight loss and the time taken to amend DIR-propagated ROIs ($r = 0.24$, $p=0.50$). There was a no significant correlation between weight loss and the geometric accuracy of the DIR-propagation (correlation between weight loss and the mean unmodified DSC score; $r = 0.25$, $p=0.06$).

2.7.4 Intra-observer and inter-observer variability

The mean inter-observer and intra-observer DSC were calculated in a subset of 3 patients (Figure 2-2C). The mean intra-observer DSC scored 0.85 (SD = 0.02), whilst the mean inter-observer DSC was 0.75 (SD = 0.11). In comparison, the mean modified DIR-propagated ROIs DSC was 0.82 for the same subset of 3 patients (SD = 0.05). ROI volume overlap between the two clinicians demonstrated a greater variability and less volumetric overlap compared to intra-clinician ROIs and modified DIR-propagated ROIs.

2.7.5 Dosimetric comparison

Table 2-5 shows the mean planned doses to the "ground truth" ROIs using plans generated from the modified and unmodified DIR-propagated ROIs. Although all OAR dose constraints were met for both plans, not all target volume coverage requirements were achieved. The mean high-dose PTV D95 (dose delivered to 95% of the volume) were 0.36 and 0.08 Gy short of achieving the clinical goal for the unmodified and modified plans, respectively. The mean low-dose PTV D95 and D99 were 0.06 and 1.36 Gy short of achieving the clinical goal for the unmodified ROIs, whilst the modified ROIs achieved their goals. Mean and range of doses to the parotid glands were similar for the three plans. Overall, the plan generated from the modified DIR-propagated ROIs was closer to meeting the ground-truth clinical target goals than the plan generated from the unmodified ROIs.

*Table 2-5. Dosimetry reflecting planned doses to the "ground truth" ROIs from plans created from manual, unmodified and modified DIR-propagated ROIs. Values not meeting the clinical goals are illustrated with an *.*

ROI	Parameter	Clinical Goal (Gy)	Plan derived from Manual ROI ± SD (Gy)	Plan derived from propagated ROI	
				Unmodified ± SD (Gy)	Modified ± SD (Gy)
High-dose PTV	D99%	58.5	62.0 ± 0.2	58.6 ± 2.9	59.0 ± 3.1
	D95%	61.8	63.0 ± 0.2	61.4 ± 1.7*	61.7 ± 1.3*
Low-dose PTV	D99%	48.6	51.1 ±0.3	47.2 ± 3.4*	49.0 ± 1.1
	D95%	51.3	52.1 ± 0.2	51.2 ± 0.5*	51.5 ± 26.9
Spinal Cord	0.1 cc	Max 46.0	42.0 ± 0.6	42.0 ± 1.0	41.9 ± 0.7
Brainstem	0.1 cc	Max 54.0	43.1 ± 3.4	44.6 ± 3.4	44.9 ± 2.8
Ipsilateral Parotid	Mean	Max 24.0	39.2 ± 9.0	39.8 ± 9.2	39.4 ± 9.3
Contralateral Parotid	Mean	Max 24.0	31.9 ± 2.0	30.9 ± 2.7	31.0 ± 2.2

Abbreviations: cc = cubic centimetre; D95% = Dose to 95% of the volume; D99% = Dose to 99% of the volume; SD = Standard Deviation; ROI = region of interest.

2.8 Discussion

This chapter evaluates the performance of RayStation's DIR algorithm for ROI propagation during adaptive radiotherapy workflow from several perspectives. In head and neck cancers (HNC), DIR-propagated ROIs have been shown to have good agreement with manually-delineated ROIs on repeat planning CTs and cone-beam CTs (18,19). Furthermore, clinician modification of DIR-propagated ROIs leads to an improved volume overlap (8,18,20).

ROI propagation using DIR was fast and this compared favourably to the literature where the same process ranges between 2 to 15 minutes (18–20). Manual delineation was time-consuming with a mean time of 83 minutes, whilst propagating and modifying ROIs halved this time and spared the clinician 43 minutes on average. Similarly, significant time-sparing using DIR propagation tools has been reported in the literature: Ramadan *et al.* (8) reported an improvement in delineation time from 67 minutes to 29 minutes with the use of a DIR propagation tool, whilst Chao *et al.* (21) reported time sparing of between 19.5 to 26.5 minutes (21). In both studies, manual delineation was faster compared to this study, taking between 44 to 67 minutes (8,21). However, fewer ROIs were delineated in both studies and in one study, time was estimated in 5 of 8 patients (8,21).

Although DIR propagation saved significant delineation time for the whole group, the individual patient data were rather variable. For example, patients 2 and 3 had a similar volume of disease, were scanned at the same time point of their treatment and demonstrated minimal weight change at the time of the rescan. Both patients were manually delineated in similar times but propagating and modifying the ROIs took 44 minutes and 25 minutes for patients 2 and 3, respectively. Longer time was spent

modifying patient 2's DIR-propagated ROIs due to a relatively poorer performance of the DIR propagation, as reflected by the lower unmodified ROI mean DSC score of 0.74 compared to patient 3's corresponding mean DSC of 0.80. Following modification, the DSC scores improved to 0.81 and 0.83 for patients 2 and 3, respectively. Patient 2 demonstrated a greater change in the shape and position of the neck and position of the shoulders between the scans than patient 3 (Figure 2-4 A and B, respectively), which could explain the difference in the performance of the DIR propagation algorithm. In addition, a change in weight can alter the head and neck anatomy but this showed no significant correlation with the time taken to modify the DIR-propagated ROIs. This suggests that a change in neck position may play a greater role than weight change and that the default DIR settings of RayStation may find it more challenging to map significant positional changes accurately.

Figure 2-4. Coronal views of the rescan CT of patients 2 (A) and 3 (B). The arrow heads indicate the displacement direction and the colour indicate the magnitude of displacement required to map from rescan CT to planning CT. Manual contours (red), unmodified propagated contours (blue) and modified propagated contours (yellow).

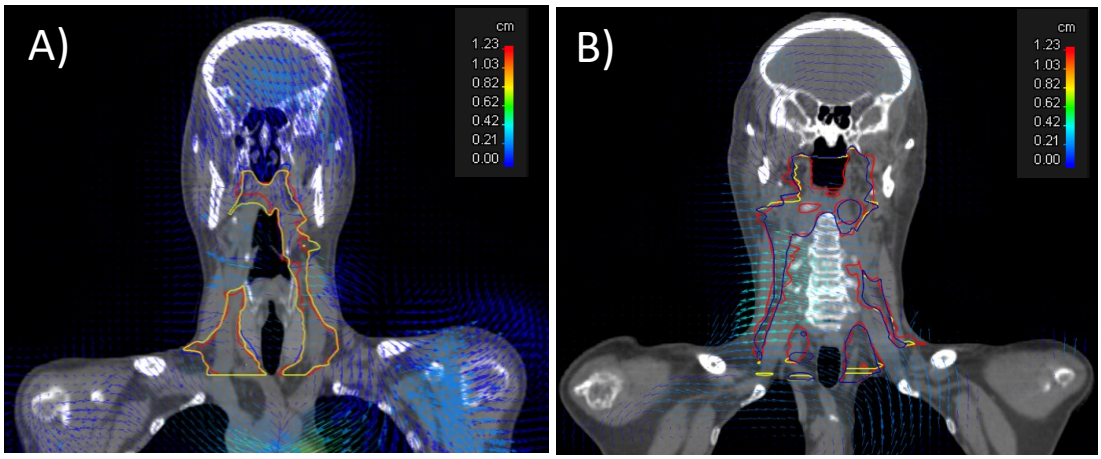

ROI delineation accuracy has been described as the weakest link in radiotherapy treatment accuracy (22) and should not be compromised as a consequence of shortening delineation time. Similar studies have reported DSC of unmodified

propagated ROIs compared to clinician ROI range between 0.64 to 0.91 (8,10). This was in keeping with this study's results that showed that unmodified ROIs had a mean DSC score of 0.76, which improved to 0.82 following clinician modification. A noteworthy finding was that DSC performance varied according to the ROI volume. ROIs with a small volume (< 10 cm^3) achieved a poorer mean DSC compared to relatively larger ROIs. A similar DSC and volume relationship has been reported (10,19). Although volumetric overlap did not perform well for small OARs and the GTV, the MDA for each structure showed a high level of agreement for all structures apart from the unmodified GTV, suggesting that DSC overestimates the errors for small structures. The difference in metric performance for small ROIs shows the importance of including multiple metrics to evaluate the degree of conformality.

Although geometric analysis indicates good agreement between two ROIs, it may be difficult to interpret and translate into clinical relevance (23). To provide clinical relevance, I investigated the dose distributions of radiotherapy plans generated from the propagated ROIs and quantified the doses received by the manually-delineated ROIs that were considered as the "gold standard". Although the results demonstrate that plans generated from both propagated ROIs failed to meet certain mandatory and optimal clinical goals, the differences were small for both plans and may be clinically acceptable if inter-observer variability is considered. Furthermore, the unmet optimal clinical goal for mean parotid glands would not have led to a rejection of the plan. In the clinical setting, it is not uncommon for different clinicians to delineate the ROIs on the baseline and rescan planning CTs for the same patient. Despite the introduction of clinical guidelines, ROI delineation may show considerable inter-observer variability; for example, the low-dose CTV and primary

tumour CTV have been reported to show a median DSC between 0.62 to 0.82 and 0.51 to 0.79, respectively (24). Interobserver variability can lead to significant dosimetric endpoint differences (25). In their study, treatment plans optimised on clinicians' contours led to a range of D98% high-dose PTV of 61.3 Gy (SD 3.7 Gy) compared to 69.2 Gy using gold-standard contours (25). In this study, the mean inter-observer DSC was 0.75, whilst modified DIR-propagated ROIs showed a mean DSC of 0.83 for the same patients. In our subset of 3 patients, there was more variability in delineated ROIs amongst two clinicians compared to the contours delineated by the same clinician, illustrating the subjective nature of delineation. This highlights the importance of delineation peer review and it is possible that the dosimetric differences generated from the DIR-propagated ROIs observed in this study could be within the realms of inter-observer variability. However, further work is required to confirm this, although that is beyond the scope of this study.

DIR propagation can play an important role in reducing the delineation workload in the era of ART. This is especially important in daily online ART workflows such as the MR-Linac where a daily plan is re-optimised. Unless dosimetric differences generated from unmodified DIR-propagated ROIs can be shown to lie within the realms of inter-observer variability, all DIR-propagated ROIs must be reviewed by the clinician to assess for acceptability and for modification.

My results suggest that DIR-propagation would perform well for propagation of the high-dose and low-dose CTV and OARs such as the brainstem, spinal cord and parotid glands. Therefore, DIR-propagation would be useful in an anatomy-adapted ART workflow where the target volume remains unchanged. On the other hand, the DIR algorithm performed poorly for GTV propagation which in effect is matching to a change in volume (i.e. shrinking target volume), as evident by the poor DSC and

MDA scores. This makes it less useful in response-adapted ART where the target volume is adapted according to treatment response. It is likely that the poor soft tissue resolution on CT scan, the lack of intravenous contrast in certain patients, and the ill-defined edges of a shrinking GTV make it difficult for the DIR algorithm. The improved soft tissue contrast of MRI may be beneficial in adapting to a shrinking target volume and this will be investigated further in Chapter 3.

This study has certain limitations. The patients were heterogenous with regards to the timing of the repeat scans and the use of intravenous contrast. The pre-setting parameters of RayStation's DIR algorithms have been reported to influence ROI propagation and dose accumulation (10). I used the default settings of the DIR algorithm to reduce the user's input and my data showed that the default settings may not map certain ROIs accurately. Adjusting the DIR algorithm settings may improve the geometric scores (10), but this would have required individual adjustments which would have contributed to significant clinician workload for each patient. The challenge of assessing DIR is the lack of an objective "gold standard" and the presence of intra- and inter-observer variabilities as demonstrated in this study. I minimised this by assessing the DIR performance with the agreed delineations amongst two other clinical oncologists. An alternative gold standard ROI could have been created by combining a multi-observer ROI set using methods such as the Simultaneous Truth and Performance Level Estimation (STAPLE) (26).

2.9 Conclusion

This study demonstrated the clinical utility of using RayStation's DIR algorithm in head and neck adaptive radiotherapy workflow to generate ROIs with acceptable geometric and dosimetric accuracy in significantly shorter time. However, the DIR-contour propagation performed less well in ROI with volume of < 10 cm^3 and in

patients with significantly altered neck position between scans. Hence, clinician modification remains an essential aspect in these circumstances.

2.10 References

1. Barker JL, Garden AS, Ang KK, et al. Quantification of volumetric and geometric changes occurring during fractionated radiotherapy for head-and-neck cancer using an integrated CT/linear accelerator system. Int J Radiat Oncol [Internet]. 2004 Jul 15 [cited 2018 Jan 12];59(4):960–70. Available from: https://www.sciencedirect.com/science/article/pii/S0360301603024544

2. Bhide SA, Davies M, Burke K, et al. Weekly volume and dosimetric changes during chemoradiotherapy with intensity-modulated radiation therapy for head and neck cancer: a prospective observational study. Int J Radiat Oncol Biol Phys. 2010 Apr;76(5):1360–8.

3. Cheng HCY, Wu VWC, Ngan RKC, et al. A prospective study on volumetric and dosimetric changes during intensity-modulated radiotherapy for nasopharyngeal carcinoma patients. Radiother Oncol [Internet]. 2012 Sep 1 [cited 2018 Feb 12];104(3):317–23. Available from: https://www.sciencedirect.com/science/article/pii/S0167814012001478

4. Hansen EK, Bucci MK, Quivey JM, et al. Repeat CT imaging and replanning during the course of IMRT for head-and-neck cancer. Int J Radiat Oncol [Internet]. 2006 Feb 1 [cited 2018 Sep 11];64(2):355–62. Available from: https://www-sciencedirect-com.ezproxy.icr.ac.uk/science/article/pii/S0360301605021449?via%3Dihub

5. Yang H, Hu W, Wang W, et al. Replanning During Intensity Modulated Radiation Therapy Improved Quality of Life in Patients With Nasopharyngeal Carcinoma. Int J Radiat Oncol [Internet]. 2013 Jan 1 [cited 2018 Aug 29];85(1):e47–54. Available from: http://www.ncbi.nlm.nih.gov/pubmed/23122981

6. Schwartz DL, Garden AS, Shah SJ, et al. Adaptive radiotherapy for head and neck cancer—Dosimetric results from a prospective clinical trial. Radiother Oncol [Internet]. 2013 Jan 1 [cited 2018 Mar 9];106(1):80–4. Available from: https://www.sciencedirect.com/science/article/pii/S0167814012004598

7. Chen AM, Daly ME, Cui J, et al. Clinical outcomes among patients with head and neck cancer treated by intensity-modulated radiotherapy with and without adaptive replanning. Head Neck. 2014 Nov;36(11):1541–6.

8. Ramadaan IS, Peick K, Hamilton DA, et al. Validation of Varian's SmartAdapt® deformable image registration algorithm for clinical application. Radiat Oncol [Internet]. 2015 Mar 31 [cited 2018 Jun 26];10(1):73. Available from: http://www.ro-journal.com/content/10/1/73

9. Hvid CA, Elstrøm U V, Jensen K, et al. Accuracy of software-assisted contour propagation from planning CT to cone beam CT in head and neck radiotherapy. Acta Oncol [Internet]. 2016 Nov 24 [cited 2018 Jun 26];55(11):1324–30. Available from: https://www.tandfonline.com/doi/full/10.1080/0284186X.2016.1185149

10. Zhang L, Wang Z, Shi C, et al. The impact of robustness of deformable image registration on contour propagation and dose accumulation for head and neck adaptive radiotherapy. J Appl Clin Med Phys [Internet]. 2018 Jul [cited 2019 May 31];19(4):185–94. Available from: http://www.ncbi.nlm.nih.gov/pubmed/29851267

11. Welsh L, R. P, D. M, et al. Prospective, longitudinal, multi-modal functional imaging for radical chemo-IMRT treatment of locally advanced head and neck cancer: the INSIGHT study. Radiat Oncol [Internet]. 2015 May 15 [cited 2017 Nov 2];10(1):112. Available from: http://www.ro-journal.com/content/10/1/112

12. Grégoire V, Evans M, Le Q-T, et al. Delineation of the primary tumour Clinical Target Volumes (CTV-P) in laryngeal, hypopharyngeal, oropharyngeal and oral cavity squamous cell carcinoma: AIRO, CACA, DAHANCA, EORTC, GEORCC, GORTEC, HKNPCSG, HNCIG, IAG-KHT, LPRHHT, NCIC CTG, NCRI, NRG Oncology, PHNS, SBRT, SOMERA, SRO, SSHNO, TROG consensus guidelines. Radiother Oncol [Internet]. 2018 Jan 1 [cited 2018 Mar 25];126(1):3–24. Available from: http://www.ncbi.nlm.nih.gov/pubmed/29180076

13. Grégoire V, Ang K, Budach W, et al. Delineation of the neck node levels for head and neck tumors: A 2013 update. DAHANCA, EORTC, HKNPCSG, NCIC CTG, NCRI, RTOG, TROG consensus guidelines. Radiother Oncol [Internet]. 2014 Jan [cited 2019 May 2];110(1):172–81. Available from: http://www.ncbi.nlm.nih.gov/pubmed/24183870

14. Brouwer CL, Steenbakkers RJHM, Bourhis J, et al. CT-based delineation of organs at risk in the head and neck region: DAHANCA, EORTC, GORTEC, HKNPCSG, NCIC CTG, NCRI, NRG Oncology and TROG consensus guidelines. Radiother Oncol [Internet]. 2015 Oct [cited

2019 May 2];117(1):83–90. Available from: https://linkinghub.elsevier.com/retrieve/pii/S0167814015004016

15. Weistrand O, Svensson S. The ANACONDA algorithm for deformable image registration in radiotherapy. Med Phys [Internet]. 2014 Dec 16 [cited 2020 Aug 2];42(1):40–53. Available from: http://doi.wiley.com/10.1118/1.4894702

16. Dice LR. Measures of the Amount of Ecologic Association Between Species. Ecology [Internet]. 1945 Jul 1 [cited 2019 Sep 16];26(3):297–302. Available from: http://doi.wiley.com/10.2307/1932409

17. Brock KK, Mutic S, McNutt TR, et al. Use of image registration and fusion algorithms and techniques in radiotherapy: Report of the AAPM Radiation Therapy Committee Task Group No. 132. Med Phys [Internet]. 2017 Jul 1 [cited 2019 Mar 25];44(7):e43–76. Available from: http://doi.wiley.com/10.1002/mp.12256

18. Hardcastle N, Tomé WA, Cannon DM, et al. A multi-institution evaluation of deformable image registration algorithms for automatic organ delineation in adaptive head and neck radiotherapy. Radiat Oncol [Internet]. 2012 Jun 15 [cited 2018 Jul 4];7(1):90. Available from: http://ro-journal.biomedcentral.com/articles/10.1186/1748-717X-7-90

19. Kumarasiri A, Siddiqui F, Liu C, et al. Deformable image registration based automatic CT-to-CT contour propagation for head and neck adaptive radiotherapy in the routine clinical setting. Med Phys [Internet]. 2014 Dec 25 [cited 2018 Jun 26];41(12):121712. Available from: http://doi.wiley.com/10.1118/1.4901409

20. Wang H, Garden AS, Zhang L, et al. Performance evaluation of automatic anatomy segmentation algorithm on repeat or four-dimensional computed tomography images using deformable image registration method. Int J Radiat Oncol Biol Phys. 2008 Sep;72(1):210–9.

21. Chao KSC, Bhide S, Chen H, et al. Reduce in Variation and Improve Efficiency of Target Volume Delineation by a Computer-Assisted System Using a Deformable Image Registration Approach. Int J Radiat Oncol [Internet]. 2007 Aug 1 [cited 2018 Aug 8];68(5):1512–21. Available from: http://www.ncbi.nlm.nih.gov/pubmed/17674982

22. Njeh CF. Tumor delineation: The weakest link in the search for accuracy in radiotherapy. J

Med Phys [Internet]. 2008 Oct [cited 2018 May 1];33(4):136–40. Available from: http://www.ncbi.nlm.nih.gov/pubmed/19893706

23. Sykes J. Reflections on the current status of commercial automated segmentation systems in clinical practice. J Med Radiat Sci [Internet]. 2014 Sep [cited 2019 May 31];61(3):131–4. Available from: http://www.ncbi.nlm.nih.gov/pubmed/26229648

24. van der Veen J, Gulyban A, Nuyts S. Interobserver variability in delineation of target volumes in head and neck cancer. Radiother Oncol [Internet]. 2019 Aug 1 [cited 2019 May 31];137:9–15. Available from: https://www.sciencedirect.com/science/article/pii/S0167814019303585?via%3Dihub

25. Lim TY, Gillespie E, Murphy J, et al. Clinically Oriented Contour Evaluation Using Dosimetric Indices Generated From Automated Knowledge-Based Planning. Int J Radiat Oncol [Internet]. 2019 Apr 1 [cited 2019 May 31];103(5):1251–60. Available from: https://www.sciencedirect.com/science/article/pii/S0360301618340458?via%3Dihub

26. Warfield SK, Zou KH, Wells WM. Simultaneous truth and performance level estimation (STAPLE): An algorithm for the validation of image segmentation. IEEE Trans Med Imaging. 2004;

3 Chapter 3 - Assessment of intra-treatment MRI changes in patients undergoing chemoradiotherapy for head and neck cancers

3.1 Introduction

Spatial shifts and regression of target volume and organs at risk (OARs) occurring during radiotherapy of head and neck cancers (HNC) have been reported in mostly computed tomography (CT)-based studies (1–5). CT imaging is limited by the lack of contrast resolution between the tumour extent and soft tissue, and in a number of these studies the analysed imaging consisted of non-contrast CT (1), cone beam CT (CBCT) and megavoltage CT (MVCT) (3), which were acquired during image-guided radiation therapy (IGRT) and were of poorer image quality.

Magnetic resonance imaging (MRI) scans provide significantly better soft tissue contrast than CT scans, particularly in defining the primary tumour but there exists few such MRI-based studies to date (6–8). Adaptive radiotherapy (ART) may be beneficial in reducing deviations from the planned radiotherapy doses by accounting for these anatomical changes (2,4,9). Prior to implementation of ART in an MRI-only workflow, it is important to assess longitudinal tumour and anatomical changes during radiotherapy on serial MRI scans. Given that ART is resource intensive, this may in turn help to inform the timepoints and frequency of plan adaptation with the most dosimetric and clinical benefit.

3.2 Aims

This study investigates the weekly MRI tumour and anatomical changes in patients with HNC undergoing radiotherapy.

3.3 Hypothesis

Sequential MRI can measure anatomical changes to the target volume and parotid glands during radical radiotherapy.

3.4 Objectives

- To evaluate the longitudinal volumetric changes of the target volumes of HNC patients undergoing radiotherapy.
- To evaluate the volumetric and positional changes of parotid glands throughout radiotherapy.

3.5 Methods and Materials

3.5.1 Patients

This was a prospective observational study of eleven patients with locally advanced head and neck cancer (LAHNC) who were recruited to the MR (Magnetic Resonance)-Library study at the Royal Marsden Hospital. This study received approvals from research review (CCR 4477) and ethical committees (16/LO/0591). Within the MR-Library study, patients were scheduled to undergo pre-treatment MRI followed by weekly MRI during the course of radiotherapy as tolerated by the patients. This sample size was considered to be representative of this tumour type based on previous studies reporting intra-treatment in HNC (3,6).

The inclusion criteria for the study were as follows:

- Patients with histologically proven squamous cell carcinoma of the head and neck or carcinoma of the skull base (American Joint Committee on Cancer

7th edition stage III-IVb) planned for primary radical chemoradiotherapy or radiotherapy.

- Age ≥18 years and able to provide consent.

The exclusion criterion for the study was as follows:

- Contra-indications to MR scans such as pacemakers and MR-incompatible metallic implants.

3.5.2 Treatment

All patients were treated according to the head and neck clinical protocol at the Royal Marsden Hospital. As this was a non-interventional study, radiotherapy delivery was not adapted during treatment.

3.5.2.1 *Radiotherapy treatment*

A single-arc volumetric-modulated arc therapy (VMAT) plan was used to deliver 65 Gy (2.17 Gy/fraction) and 54 Gy (1.8 Gy/fraction) to high-dose and low-dose planning target volume (PTV), respectively. All patients in this study received bilateral neck radiation.

3.5.2.2 *Chemotherapy*

For patients receiving concomitant chemotherapy, the regimen was either Cisplatin (100mg/m2) or Carboplatin (AUC5) on days 1 and 29. Patients with nasopharyngeal cancer also received two cycles of induction chemotherapy (3 weekly Cisplatin (75 mg/m^2) or Carboplatin (AUC 5) and 5-Fluorouracil (FU) (1000 mg/m^2/day for 4 days)) prior to chemoradiotherapy.

3.5.3 MRI acquisition protocols

Patients were scanned weekly during treatment on the same 1.5T MRI scanner (MAGNETOM Aera, Siemens Healthcare, Erlangen, Germany). A personalised 5-point thermoplastic shell covering the head, neck and shoulders was made for each patient. The same shell for radiotherapy delivery was used for immobilisation during MRI scan acquisition. Patients were immobilised in the supine position on a flat-top couch, using a foam headrest, knee and ankle supports. Foam ear plugs were used for hearing protection. Large and small flexible radiofrequency coils were used. A minimum of 2 MRI scans was needed to be eligible for assessment in this study.

The MRI sequences acquired in this study were similar to the MRI sequences on the MR-Linac to enable development of radiotherapy planning on this platform. Although the imaging quality was inferior to diagnostic MRI, all imaging were reviewed by a consultant radiologist with expertise in HNC (Dr Derfel ap Dafydd) and felt to be appropriate for the purpose of this study.

The following MRI sequences were acquired:

- T2-weighted (T2W): TE (echo time)/TR (repetition time): 184/2000 ms, 300 x 240 x 204 mm FOV, 0.8 mm isotropic voxel size.
- T1-weighted (T1W): TE/TR/TE2: 6.8/2.4/4.8 ms, 500 x 312 x307 mm FOV, 1.6 mm isotropic voxel size.

3.5.4 Image data analysis

The MR images were anonymised and analysed using Research RayStation (version 8.0, RaySearch Laboratories, Stockholm, Sweden). This radiotherapy treatment planning system enables rigid and non-rigid image co-registration and volume analysis.

3.5.5 Delineation of regions of interest.

I defined the regions of interest (ROIs) on the T2W images with reference to the co-registered T1W images. The MRI scans at each time-point were rigidly registered to the pre-treatment MRI. All ROIs were subsequently reviewed and verified by a consultant radiologist with expertise in HNC (Dr Derfel ap Dafydd).

Gross tumour volume (GTV):

The GTV was defined using clinical information, staging radiological images (CT and 18F-FDG-PET/CT, if available) and the macroscopic disease identified on the MR images. The primary tumour and the involved lymph nodes were delineated separately as the GTV-p and GTV-n, respectively. Multiple lymph nodes were delineated and labelled individually.

Parotid glands

The parotid glands were delineated on the T2W images with reference to the T1W images according to the international consensus contouring guidelines based on CT imaging (10). CT-based guidelines were used because no published consensus contouring guidelines based on MR scans have been published to date. The terms 'ipsilateral' and 'contralateral' were used to define the parotid glands that were on the same side and other side of the primary tumour, respectively.

3.5.6 Data Analysis

ROI volume measurements

The ROI volumes were measured by the treatment planning system and reported in cubic centimetre (cm^3).

The percentage reduction in volume was calculated using the following equation:

$((\text{Volume}_{\text{pre-treatment}} - \text{Volume}_{\text{week x}}) / \text{Volume}_{\text{pre-treatment}}) \times 100$

Where *x* represents the week of the scan.

Comparisons were made between the volumes on the scan at a particular time-point and the scan performed at pre-treatment.

The mean dose to the parotid glands

The mean dose to the ipsilateral and contralateral parotid glands was obtained for each patient from the delivered treatment plan on RayStation.

The positional shift of the parotid glands

The positional shifts of the parotid glands were quantified by measuring the distance between the medial or lateral surfaces of the parotid glands and the midline of the body. The latter was defined as the mid-point of the odontoid process. This measurement was made at the most cranial aspect of the odontoid process visualised on the axial T2W images (Figure 3-1). This method has previously been described by Wang *et al.* (11).

Figure 3-1. Measurement of the parotid gland shift on an axial slice of a T2W MRI scan. All measurements were made in relation to the midline at the most cranial aspect of the odontoid process. The distance between the midline and the most medial surface (vertical broken blue line) and lateral surface (vertical broken green line) of the parotid gland and the midline is indicated by the blue and green arrows, respectively. The left parotid gland (yellow), the right parotid gland (orange) and the midline (red dot) are illustrated.

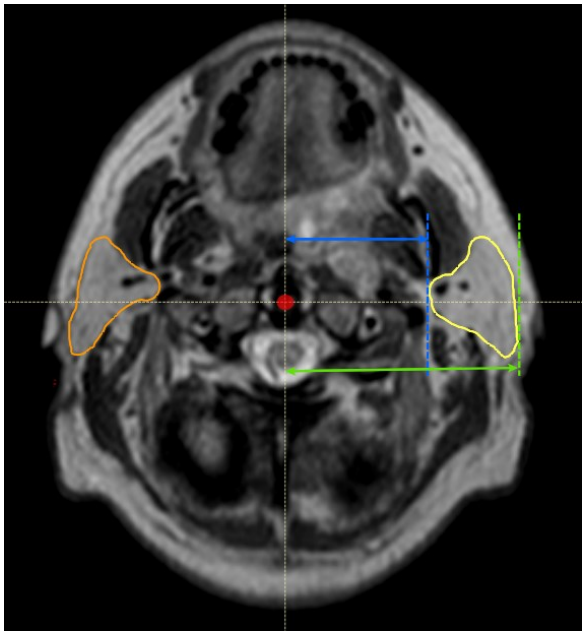

3.6 Statistical analysis

The data were analysed using GraphPad Prism software (Version 8.2.0; San Diego, CA). The data were first assessed for normal distribution using the Shapiro-Wilk test. The differences between each cohort were compared using descriptive methods such as the mean and median values for parametric and non-parametric data, respectively. The paired *t*-test and Wilcoxon matched-paired signed rank test were used to compare differences between data for parametric and non-parametric tests, respectively. Differences were defined as statistically significant at two-tailed p-values of ≤ 0.05.

3.7 Results

3.7.1 Patient characteristics

Patient characteristics are shown in Table 3-1. A total of 50 MR scans were performed. The median number of scans per patient was 5 (range, 2 to 7). The majority of patients had oropharyngeal cancer (91%) and were HPV-positive (82%). Eight patients received concurrent chemoradiotherapy only, one nasopharyngeal cancer underwent two cycles of induction chemotherapy prior to chemoradiotherapy and one patient underwent radiotherapy only.

Table 3-1. Patient characteristics. Staging according to the 7th edition of the AJCC staging system.

Characteristics	**Results**
Mean age in years (SD)	58 (8)
Sex	
Male	10
Female	1
Primary site	
Oropharynx	10
Nasopharynx	1
Tumour stage	
T1	1
T2	3
T3	2
T4	5
Nodal Stage	
N0	2
N1	1
N2a	1
N2b	4
N2c	3
p16 status	
Positive	9
Negative	1
Unknown	0
Not applicable	1
Number of MR scans per patient	
Median (range)	5 (2 to 7)

3.7.2 Target volume changes

GTV-p

Eleven GTV-p ROIs were available for analysis (Figure 3-2). During treatment, the GTV-p volume reduced in size compared to the pre-treatment volume. Compared to the pre-treatment volume, this volume reduction was statistically significant at weeks 1 (p=0.0312), 2 (p=0.0469), 3 (p=0.0039), 4 (p=0.0078) and 6 (p=0.00312). The GTV-p volume reduced by a median of 1 % (range, 0 to 13 %) by week 1, by a median of 20 % (range, 0 to 49 %) by week 2, by a median of 47% (range, 21 to 89%) by week 3, by a median of 66 % (range, 52 to 91 %) by week 4, by a median of 81 % (range, 60 to 91 %) by week 5, and by a median of 89% by week 6 of treatment (range, 69 to 99%).

Figure 3-2. Longitudinal GTV-p volume changes for individual patients (A) and whole cohort(B). In panel B, the circle and the error bars represent the median and range, respectively.

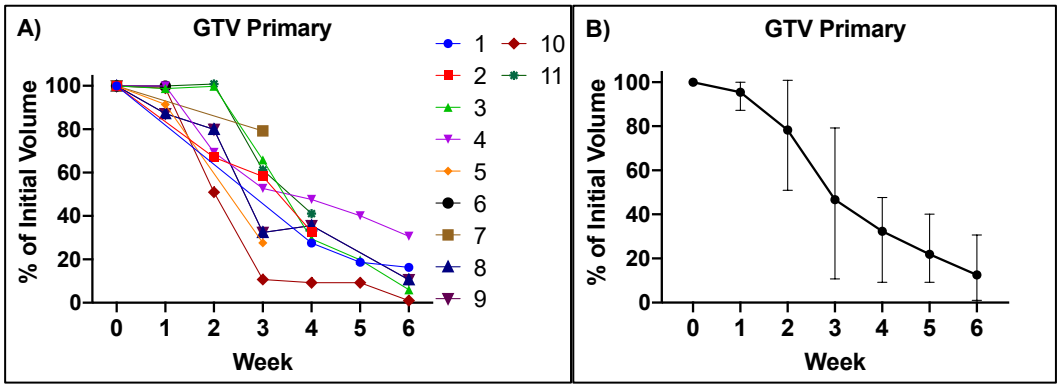

GTV-n

A total of thirteen GTV-n were analysed. During treatment, the GTV-n volume reduced in size compared to the pre-treatment volume. Compared to the pre-treatment volume, this volume reduction was statistically significant at weeks 1 (p=0.0039), 2 (p=0.0078), 3 (p=0.0039) and 4 (p=0.0078).

The GTV-n volume reduced by a median of 6 % (range, 0 to 28 %) by week 1, by a median of 44 % (range, 12 to 71 %) by week 2, by a median of 26 % (range, 0 to 79 %) by week 3, by a median of 64 % (range, 15 to 87 %) by week 4, by a median of 70 % (range, 28 to 90 %) by week 5, and by a median of 84 % by week 6 of treatment (range, 56 to 94 %).

Figure 3-3. Longitudinal GTV-n volume change for individual patients (A) and as an overall group(B). In panel B, the circle and the error bars represent the median and range, respectively.

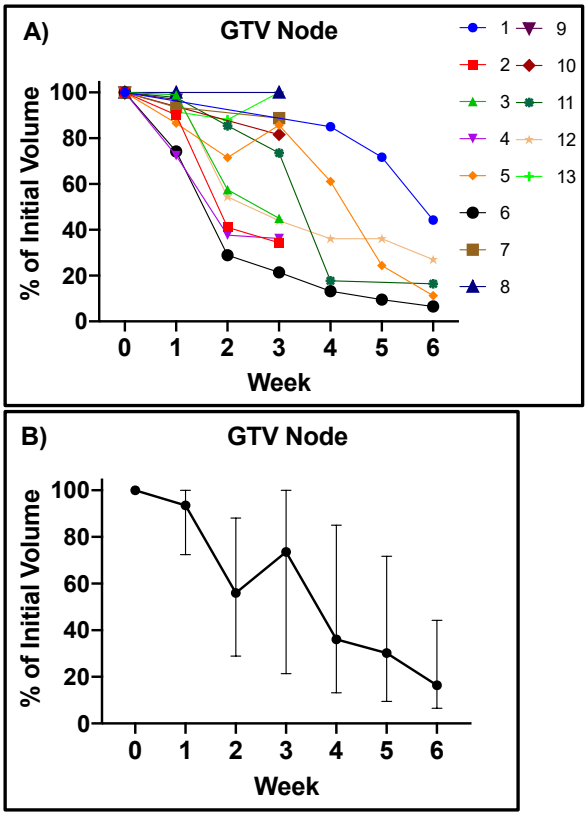

3.7.3 Parotid glands

There was a continuous reduction in the volume of the ipsilateral parotid gland throughout radiotherapy (Figure 3-4). Compared to the pre-treatment volume, there was a significant change in the ipsilateral parotid gland volume at week 1 (p=0.0156), week 2 (p=0.0312), week 3 (p=0.0039), week 4 (p=0.0312).

Figure 3-4. Longitudinal ipsilateral parotid volume change for individual patients (A) and as an overall group(B). In panel B, the circle and the error bars represent the median and range, respectively.

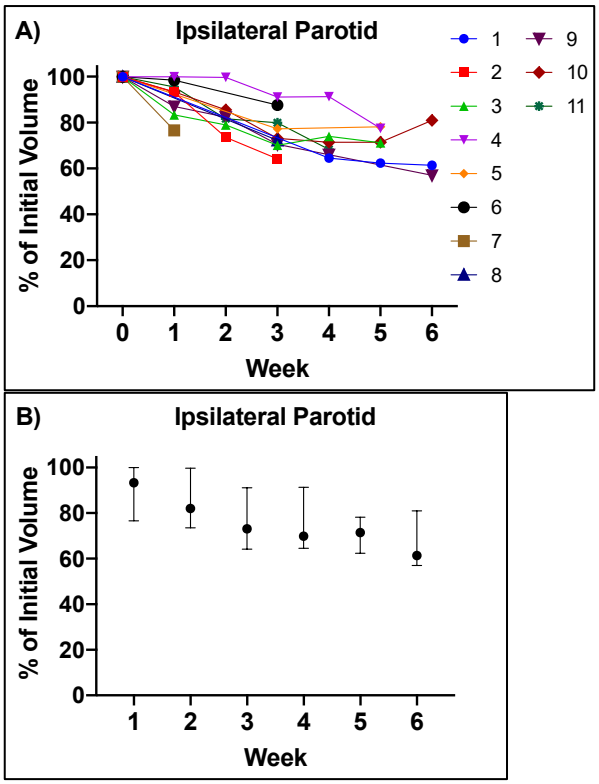

Similarly, the contralateral parotid showed a measurable reduction in volume throughout radiotherapy (Figure 3-5). Compared to the pre-treatment volume, there was a significant change in the contralateral parotid gland volume at week 2 (p=0.0312), week 3 (p=0.0039) and week 4 (p=0.0156).

Figure 3-5. Longitudinal contralateral parotid volume change for individual patients (A) and as an overall group(B). In panel B, the circle and the error bars represent the median and range, respectively.

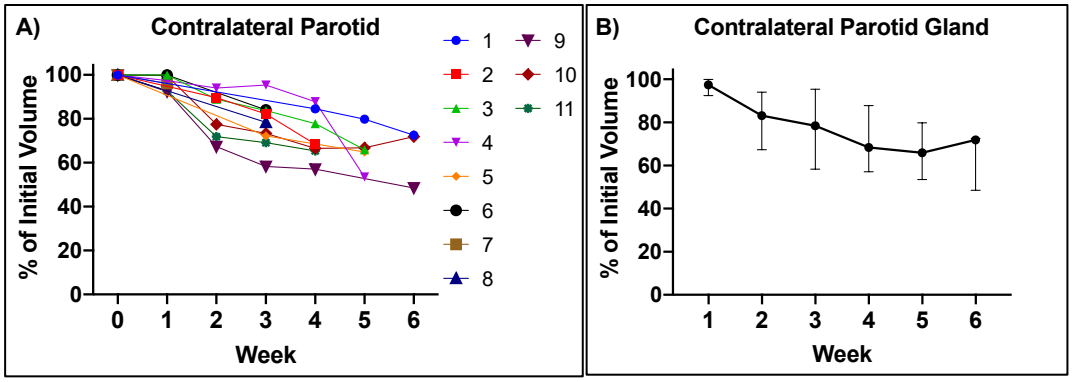

The mean parotid dose to the parotid glands were calculated to provide context for the data on parotid gland shrinkage. Analysis of radiotherapy dosimetry to the parotid glands showed no significant difference between the mean dose to the ipsilateral (mean dose, 33.9 Gy; SD, 6.6 Gy) and contralateral parotid glands (mean dose, 31.2 Gy; SD, 7.1 Gy) (p=0.05) (Figure 3-6).

Figure 3-6. Mean dose to the ipsilateral and contralateral parotid gland

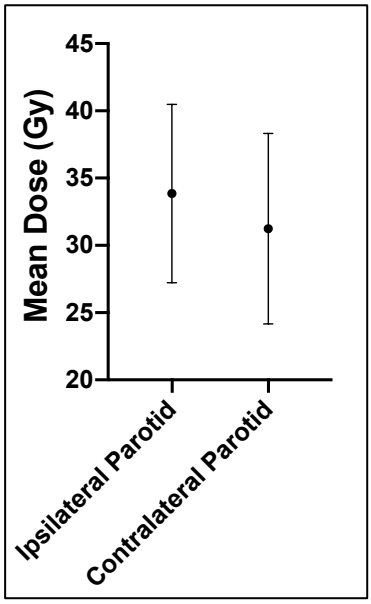

An example of longitudinal changes in parotid glands during treatment is shown in Figure 3-7.

Figure 3-7. Illustration of weekly parotid glands delineation on T2W image. Right parotid (orange) and left parotid (yellow) glands were delineated on the pre-treatment MRI (A), week 1 to 6 of treatment (B to G). The longitudinal parotid volume changes are shown in panel H for this patient.

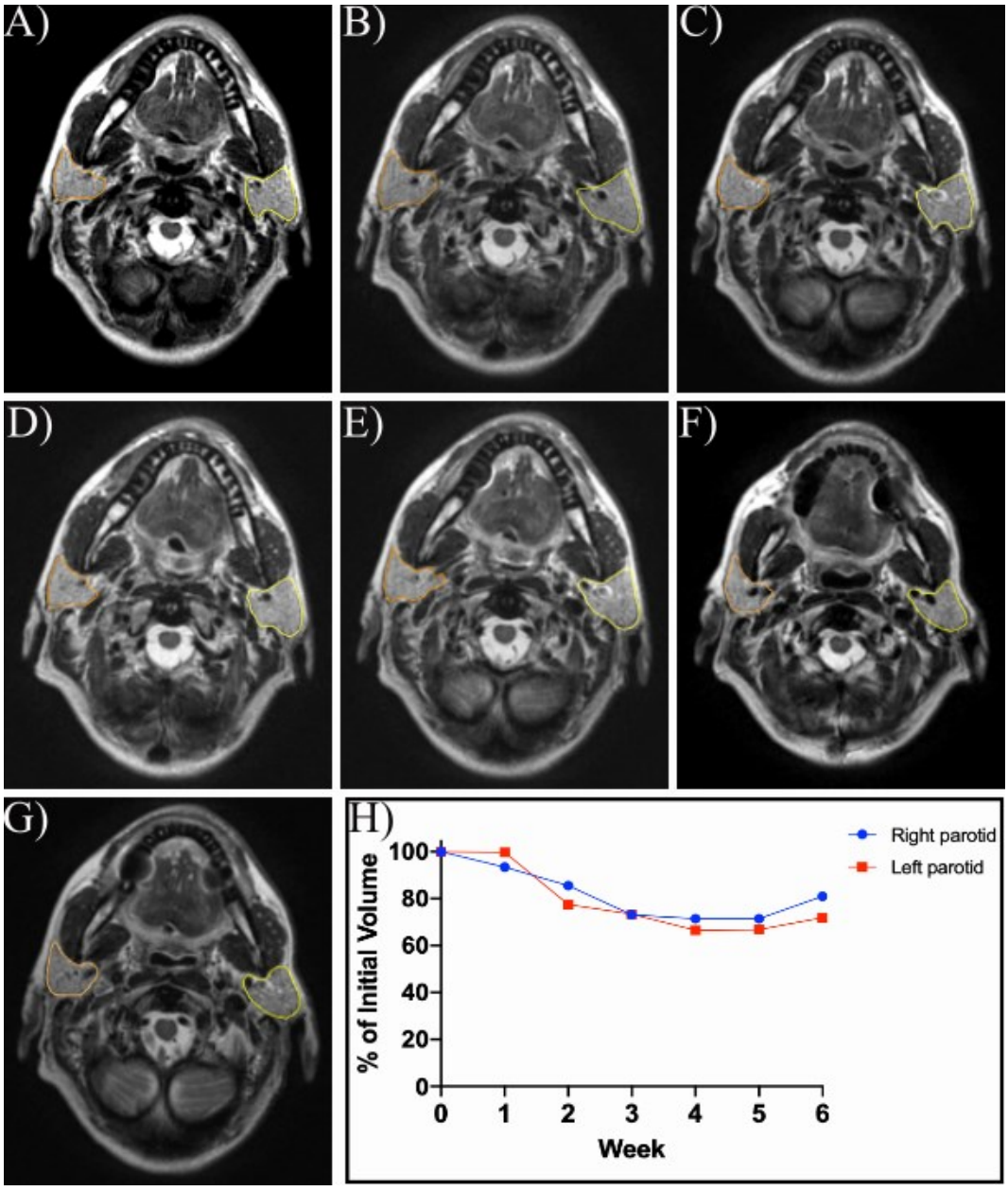

Positional change of the parotid glands

The longitudinal displacements of the borders of the parotid glands are shown in Figure 3-8. The lateral surface of both contralateral and ipsilateral parotid glands moved medially during treatment. The maximum medial movement of the lateral parotid surface was observed at week 6 of radiotherapy treatment, with a median displacement of 4.1 mm (range, -1.8 to 11 mm) and 4.3 mm (range, 0.5 to 11 mm) for the ipsilateral and contralateral parotid glands, respectively. The medial surface of the parotid gland showed smaller and less consistent movement changes during treatment. The medial surface of the contralateral parotid moved laterally between weeks 2 to 5 but ended up with a median medial shift of 1.9 mm (range, -3.3 to 4.8 mm) at week 6. The medial surface of the ipsilateral parotid gland showed minimal changes during weeks 2 to 4 and ended up with a median medial shift of -1.1 mm (range, -3.3 to 2.6 mm).

Figure 3-8. Parotid gland movement. A negative value indicates a lateral shift relative to the midline. The error bars represent the range.

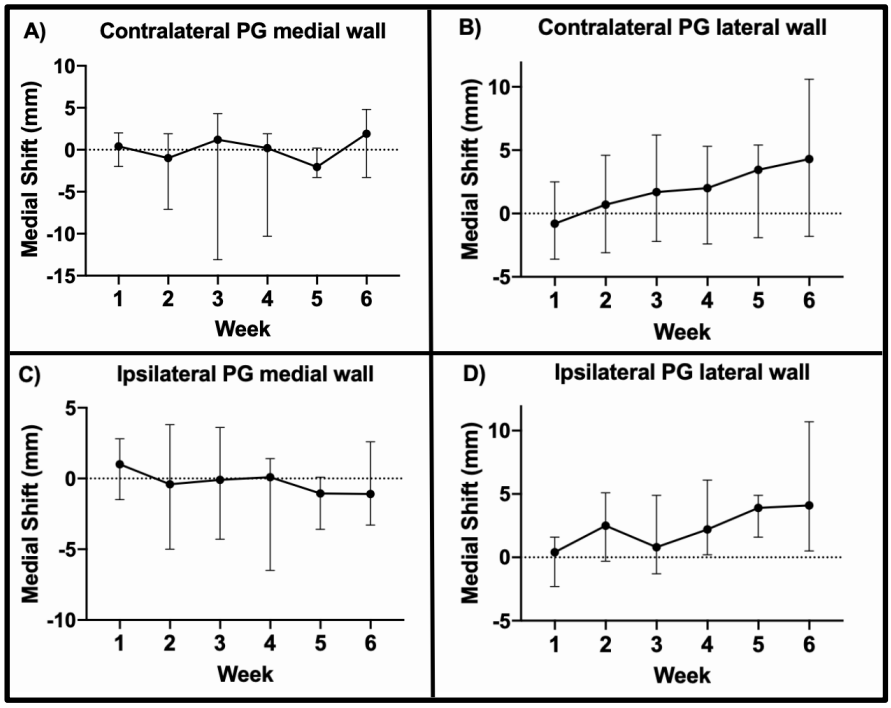

Abbreviation: PG = parotid gland

3.8 Discussion

This MRI-based study in HNC showed that anatomical changes are progressively evident during radiation therapy, even early on. The results presented are consistent with CT-based studies (1,2,4,12,13) and the few MRI-based reported studies (6–8).

In this study, the median GTV-p volumes were significantly reduced in all weeks of treatment compared to the baseline volume, except at week 5. There were only 4 data points at week 5 which would have contributed to the non-significant result that week. This reduction in GTV-p volume is consistent with two MRI-based studies (6,7). However, they reported smaller GTV-p median volume reductions of 33% (range, 17 to 75%) (6) and 38.7% (range, 29.5 to 72%) (7) by the end of treatment. This can be explained by the differences in the proportion of HPV-associated OPC as they are more radio-sensitive (14). In this study, the majority of patients had HPV-associated disease, which is in contrast to the study by Raghavan *et al.* where only 2 of 6 patients were HPV-positive. By analysing these 2 HPV-positive patients in isolation, the mean percentage reduction increased to 50.1% (7). The number of patients with HPV-associated HNC in the study by Kamran *et al.* is unclear and the authors did not report the impact of HPV status on the primary volume reduction (6). However, the authors reported that nodal change was greater for HPV-associated HNC compared to HPV-negative HNC (45% versus 22%) if cystic nodes were excluded (6). Similarly, in a CT-based study by Chen *et al.*, the HPV-associated HNSCC showed a greater reduction in GTV volume with mean percentage volume reduction of 57.5% (12). Another contributing factor to the larger reported GTV-p volume reduction in this study is the review of the target volume by a HNC radiologist. It is possible that larger reductions in volumes were more confidently identified compared to the other studies. Although GTV-p volume reduction was

reported throughout treatment, the best time-point to integrate ART to a shrinking target volume remains unclear. Bearing in mind the increased workload of ART, a pragmatic approach would be to adapt to a shrinking GTV-p once or twice during radiotherapy. With a single ART approach, GTV-p adaptation at weeks 3 or 4 would be suitable with median GTV-p volume reductions of 47 (range, 21 to 89) and 66 (range, 52 to 91), respectively. Similarly, adapting to the GTV-p volume at weeks 2 (median reduction, 20%; range, 0 to 49%) and 4 may be suitable time-points for a two ART schedule. ART at week 1 may not be beneficial as there was a very small median reduction in GTV-p volume of 1% (range, 0 to 13%). Although the GTV-p volume reduced the most at weeks 5 and 6, with median reductions of 81% (range, 60 to 91) and 89% (range, 69 to 99), respectively, ART at these time-points would not be practical due to the time required to create and adopt a new treatment plan.

Similarly, the GTV-n demonstrated a measurable decrease in volume throughout treatment. This reduction was at a slower rate than the GTV-p, which is consistent with published data by Ding *et al.* (8). The authors reported that primary tumour resolution was much faster with approximately 50% of patients showing complete response in one study compared to only 13% of lymph nodes mid-treatment (8). In this study, the percentage volume reduction was variable as indicated by the wide error bars for each treatment week. Some patients had cystic lymph nodes, which led to ‘pseudo’ enlargement mid-treatment and a slower regression of these lymph nodes (Figure 3-9 A-C). Cystic lymph nodes are a typical feature of HPV-associated disease (15,16) and may undergo a slow and prolonged resolution with complete response at up to 12 weeks after radiotherapy (17).

Figure 3-9. Nodal GTV change at baseline (A), week 3 (B) and week 6 (C) shown on axial slices of T2W MRI. Lymph nodes can show a difference in volume reduction. GTV-n1 (purple) and GTV-n2 (orange) both show reduction in size by week 6. At week 3, GTV-n2 becomes more cystic before reducing in size at the end of treatment.

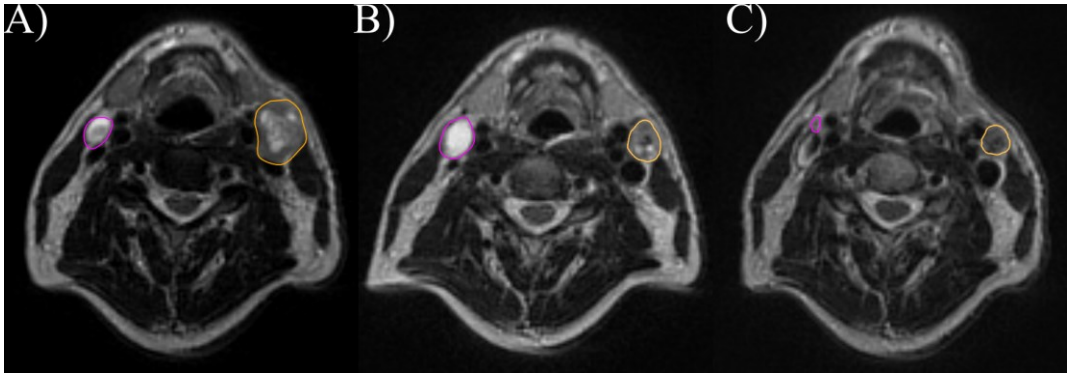

Although MR scans offer a superior soft tissue resolution, many clinical oncologists lack experience in using this modality for delineation. Furthermore, it can be difficult accurately to delineate the GTV in the context of treatment-related changes and tumour infiltration. To mitigate this, all delineations were reviewed by a consultant radiologist specialised in head and neck cancer malignancies. Although this was not used in this study, functional imaging such as diffusion-weighted (DW)-MRI can further improve tumour delineation with emerging evidence that it can be used to differentiate tumour response at an early stage in treatment (18) and can differentiate tumour from radiotherapy changes (19,20).

Both ipsilateral and contralateral parotid glands reduced in volume throughout treatment, and by the end of treatment, they had reduced in volume by a mean of 34% and 37%, respectively. Significant reduction in parotid volumes were observed as early as week 1 and week 2 for the ipsilateral and contralateral parotid glands, respectively. Compared to baseline, parotid volume reduction was not statistically significant at weeks 5 and 6 which may be explained by the smaller number data sets analysed at these time-points.

This study showed no significant difference in volume change between the ipsilateral and contralateral parotid glands which is in contrast to other studies, where the ipsilateral parotid gland shrank more than the contralateral parotid gland. For example, Loo *et al.* reported a median volume reduction of 30.2% (17.1 -55.8%) and 17.5% (16.6 – 48.5%) for the ipsilateral and contralateral parotid glands, respectively in their CT-based study (21). Similarly, the MR-based study by Raghavan *et al.* showed a median reduction of 31.1% and 21.8% for the ipsilateral and contralateral parotid glands, respectively, by end of treatment (7). In both studies, the ipsilateral parotid gland received a higher radiotherapy dose than the contralateral parotid gland due to its proximity to the high-dose PTV. In this study, there was no significant difference in mean dose to the ipsilateral and contralateral parotid glands which would explain the similar degree in parotid gland shrinkage seen. Bilateral nodal levels II were included in the low-dose PTV in all patients. This meant that the contralateral parotid gland would be within the dose fall-off of the low-dose PTV as shown in Figure 3-10. As the contralateral parotid gland dose is influenced by dose fall-off of the nodal level II contour within the low-dose PTV, it is possible that the other studies did not include the nodal level II near the contralateral parotid glands.

Figure 3-10. Coronal slice of a planning CT with the right(orange) and left (yellow) parotid glands delineated. The colour wash represents isodoses.

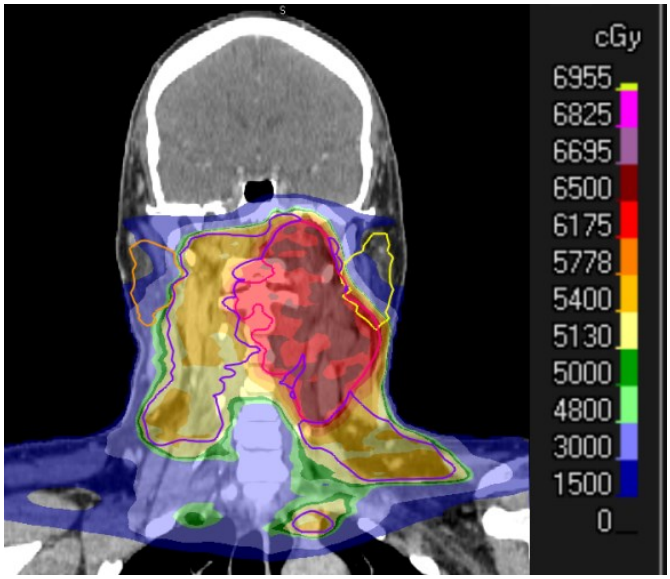

In the literature, both ipsilateral and contralateral parotid glands have been consistently shown to shift medially (1–5,7). In this study, both lateral surfaces of the contralateral and ipsilateral parotid glands shifted medially, whilst the medial surface of the parotid glands remained relatively unchanged. This is consistent with other published studies (5,22). Osorio *et al.* reported that the lateral surface of the parotid gland shifted medially by 3mm, whilst the medial surface remained in the same position (5). Robar *et al.* reported a medial shift of 0.85mm per week of the lateral aspect of the parotid gland (22).

This study has certain limitations. This study consisted of a small sample size and the MRI scans were not acquired weekly for all patients for a number of reasons. The median number of MRI scans acquired was five and weekly scans were acquired in three patients. Two patients manged two MRI scans only and declined further imaging due to worsening toxicities which led to difficulties in remaining in the treatment position for the duration of the MRI scan. With worsening radiotherapy side-effects, the patients found it more difficult to tolerate the long image acquisition

time on the MR scanner and declined to do the voluntary scans. Practical reasons also led to difficulty acquiring MRI scans. Scheduling the MRI scan to coincide with the radiotherapy treatment slot was challenging due to the capacity of the diagnostic MRI scanner. Therefore, it was not always possible to time the radiotherapy treatment and the MRI scan at similar times, so the patients declined the scans. There were also occasions of machine breakdown and servicing. Although weekly scans would have given us more accurate results, the results reported here are broadly consistent with the current literature.

3.9 Conclusion

This study reported anatomical changes on MRI scans to the target volume and parotid glands that were consistent with previously reported CT-based studies. As these changes can be demonstrated on serial MRI scans, it would be feasible to use MRI scans for future adaptive radiotherapy work as part of MRI-guidance or in an MR-only workflow.

Whilst daily adaptation would be desirable in an ART workflow, it is not feasible for daily or weekly clinician delineation of the target volume even in the context of DIR-propagation of the other structures. A pragmatic approach is to rationalise the timing for ART to a shrinking target volume when most changes are seen. Integrating two ARTs at weeks 2 and 4 may strike the balance between target volume changes and the ability to integrate a new treatment plan.

3.10 References

1. Barker JL, Garden AS, Ang KK, et al. Quantification of volumetric and geometric changes occurring during fractionated radiotherapy for head-and-neck cancer using an integrated CT/linear accelerator system. Int J Radiat Oncol [Internet]. 2004 Jul 15 [cited 2018 Jan 12];59(4):960–70. Available from: https://www.sciencedirect.com/science/article/pii/S0360301603024544

2. Bhide SA, Davies M, Burke K, et al. Weekly volume and dosimetric changes during chemoradiotherapy with intensity-modulated radiation therapy for head and neck cancer: a prospective observational study. Int J Radiat Oncol Biol Phys. 2010 Apr;76(5):1360–8.

3. Lee C, Langen KM, Lu W, et al. Evaluation of geometric changes of parotid glands during head and neck cancer radiotherapy using daily MVCT and automatic deformable registration. Radiother Oncol [Internet]. 2008 Oct [cited 2019 Feb 2];89(1):81–8. Available from: https://linkinghub.elsevier.com/retrieve/pii/S016781400800371X

4. Castadot P, Geets X, Lee JA, et al. Assessment by a deformable registration method of the volumetric and positional changes of target volumes and organs at risk in pharyngo-laryngeal tumors treated with concomitant chemo-radiation. Radiother Oncol [Internet]. 2010 May 1 [cited 2018 Jan 12];95(2):209–17. Available from: https://www.sciencedirect.com/science/article/pii/S0167814010001593

5. Vásquez Osorio EM, Hoogeman MS, Al-Mamgani A, et al. Local Anatomic Changes in Parotid and Submandibular Glands During Radiotherapy for Oropharynx Cancer and Correlation With Dose, Studied in Detail With Nonrigid Registration. Int J Radiat Oncol [Internet]. 2008 Mar 1 [cited 2018 Sep 11];70(3):875–82. Available from: https://www.sciencedirect.com/science/article/pii/S0360301607044732

6. Kamran SC, Tyagi N, Han J, et al. Weekly On-Treatment MRIs During Radiation Therapy (RT) in Head and Neck Squamous Cell Carcinoma (HNSCC) Patients to Monitor Treatment Response. Int J Radiat Oncol [Internet]. 2014 Sep 1 [cited 2019 Feb 22];90(1):S516. Available from: https://linkinghub.elsevier.com/retrieve/pii/S0360301614022317

7. Raghavan G, Kishan AU, Cao M, et al. Anatomic and dosimetric changes in patients with

head and neck cancer treated with an integrated MRI-tri- ^{60}Co teletherapy device. Br J Radiol [Internet]. 2016 Nov [cited 2017 Dec 12];89(1067):20160624. Available from: http://www.ncbi.nlm.nih.gov/pubmed/27653787

8. Ding Y, Hazle JD, Mohamed ASR, et al. Intravoxel incoherent motion imaging kinetics during chemoradiotherapy for human papillomavirus-associated squamous cell carcinoma of the oropharynx: Preliminary results from a prospective pilot study. NMR Biomed. 2015;

9. Schwartz DL, Garden AS, Shah SJ, et al. Adaptive radiotherapy for head and neck cancer—Dosimetric results from a prospective clinical trial. Radiother Oncol [Internet]. 2013 Jan 1 [cited 2018 Mar 9];106(1):80–4. Available from: https://www.sciencedirect.com/science/article/pii/S0167814012004598

10. Brouwer CL, Steenbakkers RJHM, Bourhis J, et al. CT-based delineation of organs at risk in the head and neck region: DAHANCA, EORTC, GORTEC, HKNPCSG, NCIC CTG, NCRI, NRG Oncology and TROG consensus guidelines. Radiother Oncol [Internet]. 2015 Oct [cited 2019 May 2];117(1):83–90. Available from: https://linkinghub.elsevier.com/retrieve/pii/S0167814015004016

11. Wang W, Yang H, Mi Y, et al. Rules of parotid gland dose variations and shift during intensity modulated radiation therapy for nasopharyngeal carcinoma. Radiat Oncol [Internet]. 2015 [cited 2019 Nov 13];10(1):3. Available from: http://www.ro-journal.com/content/10/1/3

12. Chen AM, Li J, Beckett LA, et al. Differential response rates to irradiation among patients with human papillomavirus positive and negative oropharyngeal cancer. Laryngoscope [Internet]. 2013 Jan [cited 2019 Jan 11];123(1):152–7. Available from: http://www.ncbi.nlm.nih.gov/pubmed/23008061

13. Marzi S, Pinnarò P, D'Alessio D, et al. Anatomical and Dose Changes of Gross Tumour Volume and Parotid Glands for Head and Neck Cancer Patients during Intensity-modulated Radiotherapy: Effect on the Probability of Xerostomia Incidence. Clin Oncol [Internet]. 2012 Apr [cited 2019 Jan 10];24(3):e54–62. Available from: http://www.ncbi.nlm.nih.gov/pubmed/22138192

14. Bhatia A, Burtness B. Human papillomavirus-associated oropharyngeal cancer: Defining risk groups and clinical trials. J Clin Oncol [Internet]. 2015 Oct 10 [cited 2017 Nov

21];33(29):3243–50. Available from: http://www.ncbi.nlm.nih.gov/pubmed/26351343

15. Goldenberg D, Begum S, Westra WH, et al. Cystic lymph node metastasis in patients with head and neck cancer: An HPV-associated phenomenon. Head Neck. 2008;

16. Mokhtari S. Mechanisms of cyst formation in metastatic lymph nodes of head and neck squamous cell carcinoma. Diagnostic Pathology. 2012.

17. Huang SH, O'Sullivan B, Xu W, et al. Temporal nodal regression and regional control after primary radiation therapy for N2-N3 head-and-neck cancer stratified by HPV status. Int J Radiat Oncol Biol Phys. 2013 Dec 1;87(5):1078–85.

18. K.H. W, A. D, D. M, et al. Changes in multimodality functional imaging parameters early during chemoradiation predict treatment response in patients with locally advanced head and neck cancer. Eur J Nucl Med Mol Imaging. 2017;1–9.

19. Chawla S, Kim S, Wang S, et al. Diffusion-weighted imaging in head and neck cancers. Future Oncol [Internet]. 2009 Sep [cited 2017 Nov 17];5(7):959–75. Available from: http://gateway.proquest.com/openurl?ctx_ver=Z39.88-2004&res_id=xri:pqm&req_dat=xri:pqil:pq_clntid=50352&rft_val_fmt=ori/fmt:kev:mtx:journal&genre=article&issn=1479-6694&volume=5&issue=7&spage=959

20. Vandecaveye V, de Keyzer F, Vander Poorten V, et al. Evaluation of the larynx for tumour recurrence by diffusion-weighted MRI after radiotherapy: initial experience in four cases. Br J Radiol [Internet]. 2006 Aug [cited 2017 Nov 17];79(944):681–7. Available from: http://www.birpublications.org/doi/10.1259/bjr/89661809

21. Loo H, Fairfoul J, Chakrabarti A, et al. Tumour shrinkage and contour change during radiotherapy increase the dose to organs at risk but not the target volumes for head and neck cancer patients treated on the TomoTherapy HiArt system. Clin Oncol. 2011 Feb;23(1):40–7.

22. Robar JL, Day A, Clancey J, et al. Spatial and Dosimetric Variability of Organs at Risk in Head-and-Neck Intensity-Modulated Radiotherapy. Int J Radiat Oncol [Internet]. 2007 Jul 15 [cited 2018 Sep 11];68(4):1121–30. Available from: https://www.sciencedirect.com/science/article/pii/S0360301607001460

4 Chapter 4 - The use of contour propagation using deformable image registration on magnetic resonance imaging

4.1 Introduction

In chapter 3, I reported that intra-treatment changes to the target volume and parotid glands can be measured on serial magnetic resonance imaging (MRI). Contour propagation using deformable image registration (DIR) facilitates repeat delineation when replanning is necessary. In Chapter 2, I have demonstrated that this method improves clinician delineation efficiency on computed tomography (CT). Few studies have investigated the application of DIR on MRI for head and neck cancers (1,2). With the intention of using adaptive radiotherapy with MRI-guidance, it is important to investigate the feasibility of using DIR algorithms to propagate contours on MRI scans.

4.2 Aim

This study assesses the feasibility and performance of the in-built RayStation DIR tool to propagate regions of interest (ROIs) between MR images acquired at different time-points.

4.3 Hypothesis

DIR will enable accurate ROI propagation from the MRI scans and produce contours that are comparable to clinician-generated contours.

4.4 Objectives

To assess the geometric accuracy of DIR-propagated ROIs compared to manually-delineated ROIs on MRI.

4.5 Materials and methods

4.5.1 Patient selection and MR acquisition.

Ten patients recruited to the MR-Library study (CCR4477) were included in this analysis. Patient selection and MR acquisition protocols were detailed in Chapter 3 Section 3.5.1. This sample size was considered to be representative of this tumour type based on previous studies reporting intra-treatment in HNC (3,4).

4.5.2 ROI delineation

The primary gross tumour volume (GTV-p), nodal gross tumour volume (GTV-n), parotid glands, optic nerves and chiasm were delineated on the T2-weighted (T2W) MR images. A limited number of ROIs was chosen in this study as the utility of DIR propagation has been demonstrated in Chapter 2 and the aim of this study was to investigate its performance for MRI. These ROIs were chosen as they represent ROIs with a range of volumes. Furthermore, as the benefit of modification of DIR-propagated ROIs has been demonstrated in Chapter 2, this was not investigated in this study.

4.5.3 Deformable Image registration and contour propagation

The DIR process has been previously explained in Chapter 2. The default setting of RayStation was used to propagate ROI contours from the pre-treatment MRI to the week 4 MRI.

4.5.4 Geometric analysis

DSC (dice similarity coefficient) and MDA (mean distance to agreement) scores were used to compare DIR-generated ROIs to clinician-generated contours. This process has been described in detail in Chapter 2. In contrast to Chapter 2, only the unmodified DIR-propagated contours were compared to the manually-delineated

contours. Values of DSC of ≥ 0.8 and mean MDA of ≤ 3 mm were deemed as acceptable (5).

4.6 Statistical analysis

The data were analysed using GraphPad Prism software (Version 8.2.0; San Diego, CA). The data were first assessed for normal distribution using the Shapiro-Wilk test. The differences between each cohort were compared using descriptive methods such as the mean and median values for parametric and non-parametric data, respectively.

4.7 Results

4.7.1 Patient characteristics

Patient characteristics are summarised in Table 4-1. The median age was 58 years (range, 47 to 70 years). The majority of patients were males (90%) and had a base of tongue tumour (60%). Eight patients underwent chemoradiotherapy and two patients underwent radical radiotherapy only.

Table 4-1. Patient characteristics. Staging according to the 7th edition of the AJCC staging system.

Characteristics	Results
Age, years	
Mean (SD)	58 (8)
Sex	
Male	9 (90%)
Female	1 (10%)
Tumour	
BOT	6 (60%)
Tonsil	3 (30%)
Nasopharynx	1 (10%)
Stage[$]	
I-II	2 (20%)
III-IV	8 (80%)

Abbreviations: BOT = base of tongue

4.7.2 ROIs

The quantitative results comparing DIR-propagated and manually-delineated ROIs are shown in Figure 4-1 and Table 4-2.

Figure 4-1. DSC (A) and MDA (B) indices calculated for the parotid glands(n=20), chiasm (n=10), brainstem (n=10), spinal cord (n=10), GTV-n (n=9) and GTV-p (n=10). The green-shaded area is the accepted tolerance range as per the AAPM recommendations TG132 report (5)*. DSC of ≥0.8 and mean MDA ≤3 mm were used as tolerances.*

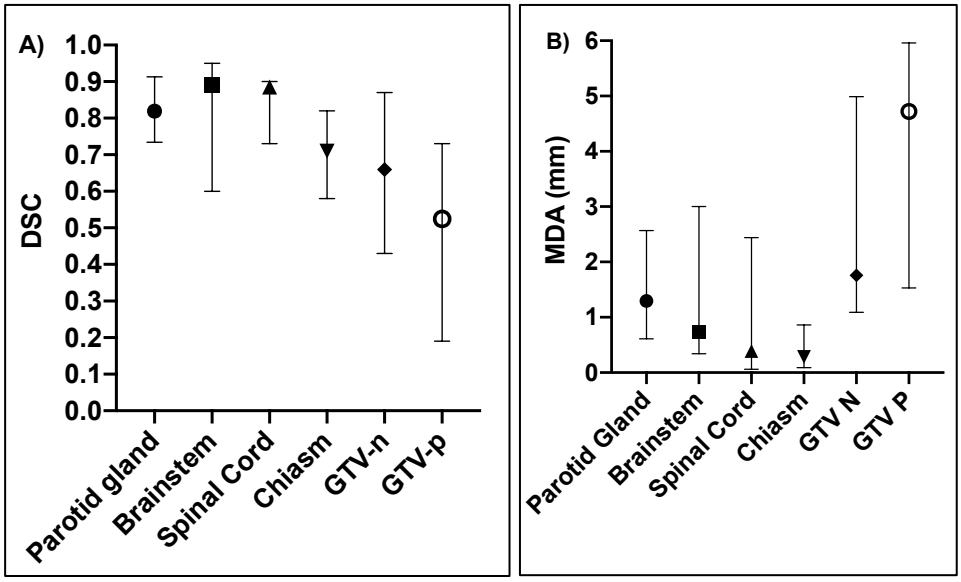

Table 4-2. DICE and MDA scores for each ROI.

ROI		DSC	MDA (mm)
Parotid	Median	0.82	1.30
	Range	0.74 to 0.91	0.61 to 2.57
Brainstem	Median	0.89	0.73
	Range	0.60 to 0.95	0.34 to 3.00
Chiasm	Median	0.71	0.28
	Range	0.58 to 0.82	0.09 to 0.86
Spinal Cord	Median	0.89	0.39
	Range	0.73 to 0.90	0.06 to 2.44
GTV-n	Median	0.66	1.76
	Range	0.43 to 0.87	1.09 to 4.99
GTV-p	Median	0.51	4.72
	Range	0.19 to 0.73	1.53 to 5.96

Abbreviations: GTV= gross tumour volume; ROI = region of interest; DSC = dice similarity coefficient; MDA = mean distance to agreement.

The performance of DIR-propagation tool was variable with particularly good overlap for the parotid gland, brainstem and spinal cord with median DSC scores of 0.82 (range, 0.74 to 0.91), 0.89 (range, 0.60 to 0.95) and 0.89 (range, 0.73 to 0.90), respectively. DIR-propagation performed less well for chiasm, GTV-n and GTV-p with median DSC scores of 0.71 (range, 0.58 to 0.82), 0.66 (range, 0.43 to 0.87) and 0.51 (range, 0.19 to 0.73), respectively. An example of this is shown in Figure 4-2A and B, where there was good overlap between the manually-delineated parotid glands, brainstem and chiasm and their respective DIR-propagated contours. Figure 4-2C shows a smaller volumetric overlap between the manual and DIR-propagated GTV-n and GTV-p.

Figure 4-2. Manual(red) and DIR-propagated ROIs(yellow) on coronal (A), sagittal (B) and axial (C) T_2W MR images.

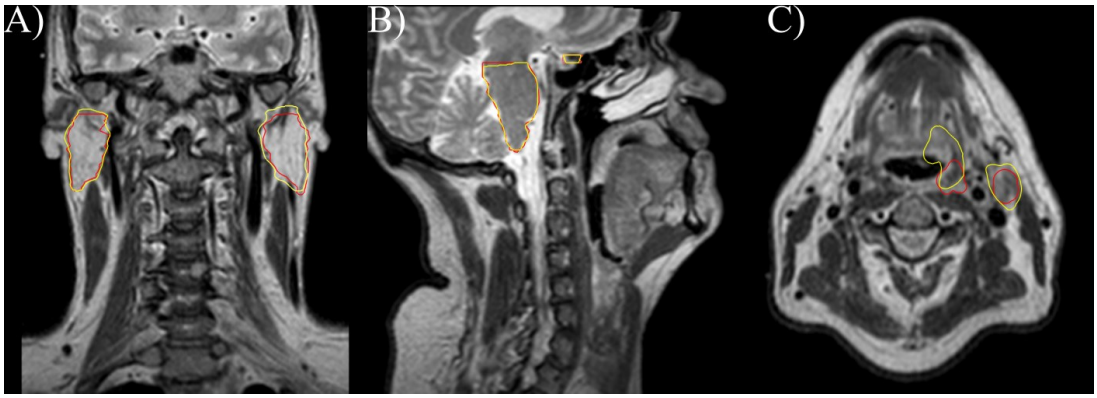

The DIR-propagated structures performed well with median MDA scores of 1.30 (range, 0.61 to 2.57) for the parotid glands, 0.73 (range 0.34 to 3.00) for the brainstem, 0.39 (range, 0.06 to 2.44) for the spinal cord, 0.28 (range, 0.09 to 0.86) for the chiasm and 1.76 (range, 1.09 to 4.99) for the GTV-n. The propagated GTV-p performed poorly with a median score of 4.72 (range, 1.53 to 5.96).

4.8 Discussion

This study has shown that it was feasible to use DIR to propagate contours between serial MRI scans. Overall, the DIR propagation tool performed well with a good agreement between the manually-delineated and the DIR-propagated OARs. Similar to the CT-based study in Chapter 2, the DIR-propagation tool performed well for the relatively large organs such as the parotid glands, spinal cord and brainstem. As discussed in Chapter 2, DSC can overestimate errors for small structures. This was the case for the chiasm where the DSC score was poor, but the MDA score was within tolerance. The DIR-propagated GTV-p and GTV-n showed poorer overlap with manually-delineated counterparts. This was due to the DIR tool struggling to adapt the volumes to large changes. Although the benefits of clinician modification of DIR-propagated ROIs was not investigated in this study, clinician modification of the DIR-propagated contours is still be required especially for ROIs such as the GTV. Few studies have evaluated the use of DIR in MRI for HNC (1,2). In keeping with the results in this study, Broggi *et al.* reported a mean parotid DSC that ranged between 0.76 to 0.81 (1).

The geometric assessments compared the unamended DIR-propagated ROIs to the manual ROIs using the default DIR settings. The DIR algorithm can be optimised and this has been shown to achieve a better contour propagation accuracy in situations where there were large deformations secondary to large changes between images (1). However, this would require significant user input for each patient. With the intention of using DIR as an adjunct rather than replacement for manual delineation, I did not investigate optimising the DIR tool.

The main limitation of this study is the small number of patients analysed. However, the sample size was comparable to the MRI-based study by Broggi *et al.* (1). As the aim of this study was to test the feasibility of using DIR propagation in MRI scans, I did not assess the effects of inter- and intra-observer variability and only assessed a limited number of ROIs.

4.9 Conclusion

DIR can be used to propagate ROIs between MRI scans, with the majority of ROIs showing a good overlap with manually-delineated ROIs. Clinician modification is still required, especially for the GTVs. However, it is feasible to use DIR for ROI propagation in MRI based workflows.

4.10 References

1. Broggi S, Scalco E, Belli ML, et al. A Comparative Evaluation of 3 Different Free-Form Deformable Image Registration and Contour Propagation Methods for Head and Neck MRI: The Case of Parotid Changes During Radiotherapy. 2017 Jun [cited 2018 Nov 15];16(3):373–81. Available from: http://www.ncbi.nlm.nih.gov/pubmed/28168934

2. Al-Mayah A, Moseley J, Hunter S, et al. Radiation dose response simulation for biomechanical-based deformable image registration of head and neck cancer treatment. Phys Med Biol. 2015 Oct 20;60(21):8481–9.

3. Lee C, Langen KM, Lu W, et al. Evaluation of geometric changes of parotid glands during head and neck cancer radiotherapy using daily MVCT and automatic deformable registration. Radiother Oncol [Internet]. 2008 Oct [cited 2019 Feb 2];89(1):81–8. Available from: https://linkinghub.elsevier.com/retrieve/pii/S016781400800371X

4. Kamran SC, Tyagi N, Han J, et al. Weekly On-Treatment MRIs During Radiation Therapy (RT) in Head and Neck Squamous Cell Carcinoma (HNSCC) Patients to Monitor Treatment Response. Int J Radiat Oncol [Internet]. 2014 Sep 1 [cited 2019 Feb 22];90(1):S516. Available from: https://linkinghub.elsevier.com/retrieve/pii/S0360301614022317

5. Brock KK, Mutic S, McNutt TR, et al. Use of image registration and fusion algorithms and techniques in radiotherapy: Report of the AAPM Radiation Therapy Committee Task Group No. 132. Med Phys [Internet]. 2017 Jul 1 [cited 2019 Mar 25];44(7):e43–76. Available from: http://doi.wiley.com/10.1002/mp.12256

5 Chapter 5 – Feasibility and dosimetric advantage of dose adaptation for oropharyngeal cancers in an MR-only workflow

5.1 Introduction

HPV-associated oropharyngeal cancers (OPC) are intrinsically more radiosensitive and this cohort demonstrates a good long-term survival (1,2). However, the long-term radiation-related morbidities from current curative treatment regimens remain substantial in this relatively younger patient group (3). Therefore, there has been considerable interest in radiotherapy de-intensification strategies to reduce doses to the organs at risk (OAR) whilst maintaining tumoricidal doses to the tumour. Radiotherapy dose adaptation in response to a responding tumour may be used to optimise the therapeutic ratio in this cohort of patients (4). Measurable intra-treatment geometric and biological tumour changes using functional imaging such as positron emission tomography with computed tomography (PET-CT) and diffusion-weighted magnetic resonance imaging (DW-MRI) (4,5) have been reported. The superior soft tissue contrast of MRI scans (6) enables accurate measurements of tumour changes with serial scans without safety concerns associated with repeated use of exogenous contrast and exposure to ionising radiation. With the development of hybrid MRI-linear accelerators, serial MR images can be readily acquired during radiotherapy. This opens the door to MR adaptive radiation therapy (ART).

5.2 Aims of the study

This study investigates the feasibility of MR-only workflow to generate adaptive radiotherapy plans and assess the potential dosimetric advantage of ART in response to tumour volume changes during treatment.

5.3 Hypothesis

It is feasible to generate adaptive radiotherapy plans using MR-only workflow and a response-adapted ART significantly reduces doses to the OARs in comparison to non-adaptive approach.

5.4 Objectives

- To assess the feasibility of generating radiotherapy plans at serial time-points using bulk-density dose assignment for an MR-only workflow.
- To assess the dosimetric impact of delivering a pre-treatment radiotherapy plan without accounting for anatomical changes.
- To evaluate the dosimetric advantage of using dose adaptation to a shrinking tumour volume.

5.5 Materials and methods

5.5.1 Patient selection

Five patients with HPV-associated OPC recruited to the MR-Library study (CCR4477) were chosen for this planning study. Only patients who had undergone repeat MRI scans at the time-points described in section 5.5.2. were selected to have a homogeneous group of patients for analysis. Therefore, this limited the sample size to five eligible patients. Patient recruitment has been defined in Chapter 3 Section 3.5.1.

5.5.2 MRI scan acquisition and radiotherapy Planning

The MRI scans were acquired in the treatment position, as described in Chapter 3 Section 3.5.3. Three radiotherapy plans were generated from MRI scans acquired at the following time-points: pre-treatment, weeks 2 and 4 (Figure 5-1).

Figure 5-1. Schema of the adaptive planning protocol.

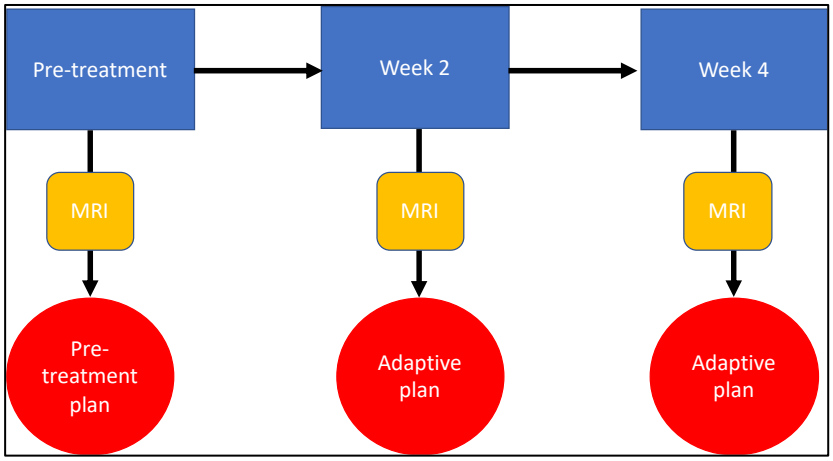

The MRI scans have a reduced craniocaudal and lateral field of view (FOV). This resulted in missing tissue at the shoulders and the cranial aspect of the brain (Figure 5-2). The planning CT and MRI scans were rigidly registered and aligned, and the external contour around the shoulders was propagated to the MRI scan. The areas

outside the MRI FOV were filled-in with water equivalent density for the synthetic CT generation as described below.

Figure 5-2. Coronal slices of the CT (A) and MRI (B) which illustrate the reduced FOV of the T2-weighted MRI scan. The planning CT scan is used to create the outline for the missing tissue around the shoulders on the MRI scan.

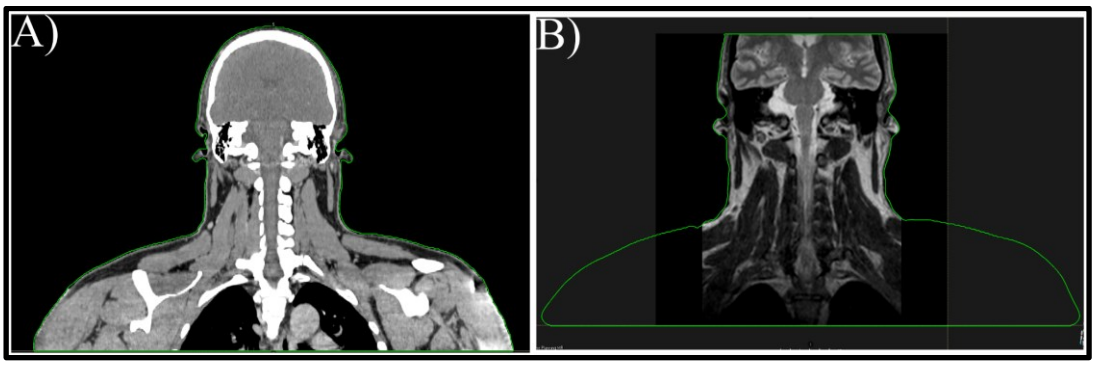

5.5.3 Target volume delineation

The MRI scans were anonymised and exported to Research RayStation (version 8.0, RaySearch Laboratories, Stockholm, Sweden) treatment planning system. I used a volumetric two dose levels approach to define the target volumes as described below.

5.5.3.1 *Gross tumour volume (GTV)*

The GTV was defined as the macroscopic primary tumour (GTV-p) and involved lymph nodes (GTV-n). The GTVs were delineated on the T2-weighted (T2W) MR images with reference to the T1-weighted (T1W) MR images. Information from the clinical notes and other imaging modalities, if available, such as the PET-CT were used to aid delineation. The GTVs were all reviewed and verified for agreement by a consultant radiologist specialising in head and neck cancers (Dr Derfel Ap-Dafydd).

5.5.3.2 *Clinical Target Volume (CTV)*

CTV65:

The GTV was expanded with a 5 mm isotropic margin to create the high-dose CTV65, which received a dose of 65.1 Gy.

CTV54:

The low-dose CTV54 received a dose of 54 Gy and included the lymph node levels at risk of microscopic involvement and a 5 mm isotropic expansion around the CTV65. Bilateral neck nodal levels II, III, IV and VIIa were included in the CTV54 in a lymph node-negative neck. Ipsilateral nodal levels Ib, V and VIIb neck nodes were also included in a lymph node-positive neck.

Both CTV54 and CTV65 were edited to exclude natural barriers to disease spread such as bone, muscle and air, unless there was radiological evidence of tumour infiltration.

Planning Target Volume (PTV)

The CTV65 and CTV54 were isometrically expanded by 3 mm to generate an uncropped PlanPTV65 and PlanPTV54, respectively. For the final dose reporting, PlanPTV65 was edited off external body contour by 5 mm to generate PTV65. Similarly, PlanPTV54 was cropped from external body contour and PTV65 to create PTV54.

5.5.3.3 *Delineation of organs at risk and regions of interest.*

The parotid glands, pharyngeal constrictor muscles (PCM), spinal cord and brainstem were delineated on the planning MRI to for radiotherapy planning optimisation and to assess the dosimetric effect of ART to these OARs. Excessive

doses to these OARs have been associated with xerostomia (7), dysphagia (8), Lhermitte's syndrome (9) and acute fatigue(10), respectively.

PCM were delineated according to the published contouring guidelines by Christianen *et al.* (11) (Table 5-1). A thickness of 3 mm was used to contour the constrictor muscles. The superior and middle pharyngeal constrictor muscle (SMPCM) were combined and the inferior pharyngeal constrictor muscle (IPCM) was defined as a separate structure.

Table 5-1. Delineation guidelines for the pharyngeal constrictor muscles (adapted from Christianen et al.(11)*)*

Organ at risk	Anatomic Borders					
	Cranial	**Caudal**	**Anterior**	**Posterior**	**Lateral**	**Medial**
Superior PCM	Caudal tip of pterygoid plates (hamulus)	Lower edge of C2	Hamulus of pterygoid plate, base of tongue, pharyngeal lumen	Prevertebral muscle	Medial pterygoid muscle	Pharyngeal lumen
Middle PCM	Upper edge of C3	Lower edge of hyoid bone	Base of tongue, hyoid bone	Prevertebral muscle	Greater horn of hyoid bone	Pharyngeal lumen
Inferior PCM	First slice caudal to lower edge of hyoid bone	Lower edge of arytenoid cartilages	Soft tissue of supraglottis/glottis	Prevertebral muscle	Superior horn of thyroid cartilage	

Abbreviations: C= cervical vertebrae; PCM = pharyngeal constrictor muscle

Bone, air and external body

To generate a synthetic CT for each patient using bulk density assignment, different tissue classes are delineated on the MRI and assigned specific physical density values. Bone and air were delineated on the MRI scans using information from the planning CT to help delineation. The external body contours were automatically contoured on the MR scans on the planning system. The rest of the body was defined to be of water equivalent density.

5.5.3.4 *Delineation on repeat MRI scans*

Deformable image registration was used to propagate the OAR and CTV contours (apart from the GTV) from the pre-treatment MRI to weeks 2 and 4 MRI for each patient as described in Chapter 4. I visually inspected the contours and amended them as necessary. For the adapted plans, the baseline CTV65 was also rigidly propagated to the repeat MRI at weeks 2 and 4. Both rigidly- and DIR-propagated CTV65 were used to ensure that any areas previously covered within the pre-treatment CTV65 were now included in the CTV54.

Adapted target volume

For the adaptive plans, a $GTV_{adapted}$ was manually delineated on the planning MRI scans at weeks 2 and 4. A $CTV65_{adapted}$ was generated using a 5 mm isotropic expansion of $GTV_{adapted}$. Any excluded volume in the baseline CTV65 was included in the $CTV54_{adapted}$, to ensure that the 'initial tumour bed' received a minimum of dose of 54 Gy over 6 weeks.

5.5.4 Planning procedure

I generated radiotherapy plans for each patient using the same process. The same objective function and number of optimisation iterations were used in each case. Dual arc, 6-MV volumetric-modulated arc therapy (VMAT) plans were generated in a research version of RayStation treatment planning system (TPS) version 8.0 (RaySearch Laboratories, Stockholm, Sweden). Each plan was reviewed and approved by an experienced radiotherapy physicist (Alex Dunlop or Dualta McQuaid).

5.5.4.1 *IMRT plans*

Plan design

The plans were generated and optimised using the collapsed cone version 5.0 algorithm in RayStation.

Beam design

Radiotherapy plans were generated using a dual-arc VMAT technique to replicate treatment delivered in the clinical setting. All the RT plans consisted of two 6 megavoltage (MV) 360º arcs with collimator angles of 3º. Each arc consisted of 180 control points with 2º control point spacing, leaf motion constraint of 0.8 cm/degree, and maximum delivery time of 90 seconds.

Beam optimisation

Non-anatomical volumes were added to guide the treatment planning system to provide an optimal plan. These included ring structures around the PTVs to increase dose conformality and homogeneity, together with the application of the dose fall-off optimising function to reduce dose to non-target tissue. This function penalises dose that exceeds the specified dose fall-off away from the target and is defined by 3 parameters: the high-dose parameter representing the high-dose within the target; the low-dose parameter representing the acceptable dose within the surrounding healthy tissue; and the distance parameter representing the distance at which the high dose will have fallen to the low-dose.

To avoid the treatment planning system boosting target tissue within the build-up region of the patient, a virtual bolus (density = 1.0 g/cm^3) was generated exterior to the body contour such that PlanPTV65 and PlanPTV54 were always at least 1 cm from either the external body contour or the virtual bolus surface (12). Once a

satisfactory plan was generated, virtual bolus was removed, the dose re-prescribed to PTV65, and the final dose was computed. The RT plan was re-evaluated to ensure optimal coverage was maintained.

Bulk density assignment

Synthetic CTs were generated from the MRI scans by using the bulk density assignment approach. In this method, different tissues were assigned specific physical density values which enables radiotherapy treatment planning (Table 5-2). These physical densities were defined according to our guidelines (13).

Table 5-2. Bulk density assignment of the different structures.

Structure	Mass density (g/cm^3)
Air	0.01
Bone	1.35
Couch	0.63
External	1.00
Lung	0.26
PTV bolus	1.00

Abbreviations: PTV = planning target volume

Planning objectives

The baseline dose-based and dose-volume based objectives were designed for the inverse planning optimisation process to satisfy the clinical planning goals (Table 2-1 and Table 5-4). Each optimisation sequence consisted of 40 automated iterations. All plans were created using an identical method, 3 optimisations of 40 iterations with a virtual bolus in place, with repeat scaling of the dose to the prescription, defined as 65.1 Gy on the full PTV between each optimisation. Finally, the bolus was removed, and the prescription applied to the reduced PTV (contracted by 5 mm

from the patient's surface) before a final dose calculation and dose rescale to match the prescription.

Table 5-3. Planning target volume (PTV) constraints for dual-arc VMAT planning.

Volume (%)	Dose (%)	
	PTV65	PTV54
99	> 90	>90
98	> 95 (optimal)	>95 (optimal)
95	> 95	> 95
50	= 100	= 100
5	< 105	< 105 (optimal)
2	< 107 (optimal)	< 107 (optimal)

Abbreviations: PTV= planning target volume.

Table 5-4. Dose constraints for organs at risk.

Structure	Constraint	Mandatory Dose constraint (Gy)	Optimal Dose constraint (Gy)
Spinal Cord	Max 1 cm^3	< 48 < 46	
Spinal Cord PRV	1 cm^3	< 48	
Brainstem	Max 1 cm^3	< 55 < 54	
Brainstem PRV	1 cm^3	< 56	
Contralateral Parotid	Mean dose Max EUD 1000cGy	As low as possible	< 24 Gy
Ipsilateral Parotid	Mean dose Max EUD 1000cGy	As low as possible	< 24 Gy

Abbreviations: EUD = equivalent uniform dose; Max = maximum; PRV = planning organ at risk volume

Dose prescription

As per the ICRU 83 (international commission on radiation units and measurements report 83), the prescription was to the median dose point on the DVH such that the prescription dose of 65.1 Gy was received by 50% of the PTV65.

5.5.5 Definitions of IMRT plans.

The following radiotherapy plans were generated for each patient:

Pre-treatment radiotherapy plan.

This plan was generated on the pre-treatment MRI scan with radiotherapy doses derived from the pre-treatment MRI ROIs.

Delivered non-ART radiotherapy plan

This non-adaptive plan was defined as the cumulative doses of delivering the pre-treatment radiotherapy plan without accounting for the anatomical changes at week 2 and 4. First, the pre-treatment MRI scan was rigidly aligned to week 2 and week 4 MRI scans using the bony anatomy. The pre-treatment plan beam configurations were applied and re-calculated on the week 2 and week 4 MRI scans. A cumulative non-ART plan was generated by deforming the dose cubes from each time-point to the pre-treatment MRI scan. Thus, the cumulative non-ART plan was the sum of the pre-treatment plan on the pre-treatment MRI for the first ten fractions, the week 2 MRI for fractions eleven to twenty and the week 4 MRI for fractions twenty-one to thirty.

Cumulative ART plan

New VMAT plans were generated using the week 2 and week 4 planning MRI scans. The dose cubes from each plan were deformed to the pre-treatment MRI scan. The cumulative ART plan was the sum of the pre-treatment, week 2 and week 4 ART plans, which accounted for ten fractions each.

5.6 Analysis

5.6.1 Target volume analysis

Dose accumulation for the delivered non-ART plan and cumulative ART plan were calculated using the deformation vector field from the DIR.

5.6.2 PCM dose analysis

This was calculated by measuring the mean dose delivered to the delineated IPCM and SMPCM that lay outside the CTV.

5.6.3 Statistical analysis

The data were analysed using Graphpad Prism software (Version 8.2.0; San Diego, CA). The Shapiro-Wilk test was used to test for normality of the data. Mean and median values were reported for parametric and non-parametric data, respectively. The paired *t*-test and Wilcoxon test were used for parametric and non-parametric data, respectively. Differences were statistically significant at two-tailed p-values of ≤ 0.05.

5.7 Results

5.7.1 Patient characteristics

The patient characteristics are summarised in Table 5-5. The median age was 62 years (range 48 to 65). Three tumours originated from the base of tongue and two in the tonsils. All patients demonstrated weight loss with a mean of 9.6% (standard deviation (SD) = 5.7%).

*Table 5-5. Patient characteristics. *TNM staging as 7th edition of the AJCC staging system. § Weight loss = the maximum weight loss as a percentage of the pre-treatment weight.*

Patient number	Age	Site	Stage*			Weight loss§ (%)
			T	N	M	
1	48	Left Tonsil	3	2b	0	17
2	51	Left BOT, tonsil and soft palate	4	2b	0	13
3	64	Left BOT	3	0	0	5
4	62	Left BOT, tonsil and soft palate	4	2b	0	10
5	65	Left tonsil	2	0	0	3

5.7.2 Dosimetric Analysis

A total of 15 radiotherapy plans were successfully generated and analysed.

Target volume

The results for the mandatory PTV dose constraints are shown in Figure 5-3 and Figure 5-4 for the pre-treatment, the delivered non-ART and cumulative ART plans. For comparison, the two ART plans at weeks 2 and 4 are also shown in Figure 5-3.

Figure 5-3. Dose constraints for the PTV65 and PTV54. The horizontal red line represents the minimum dose required for the dose constraint. Abbreviations: D95% = minimum dose delivered to 95% of the volume; D99% = minimum dose delivered to 99% of the volume; PTV = planning target volume.

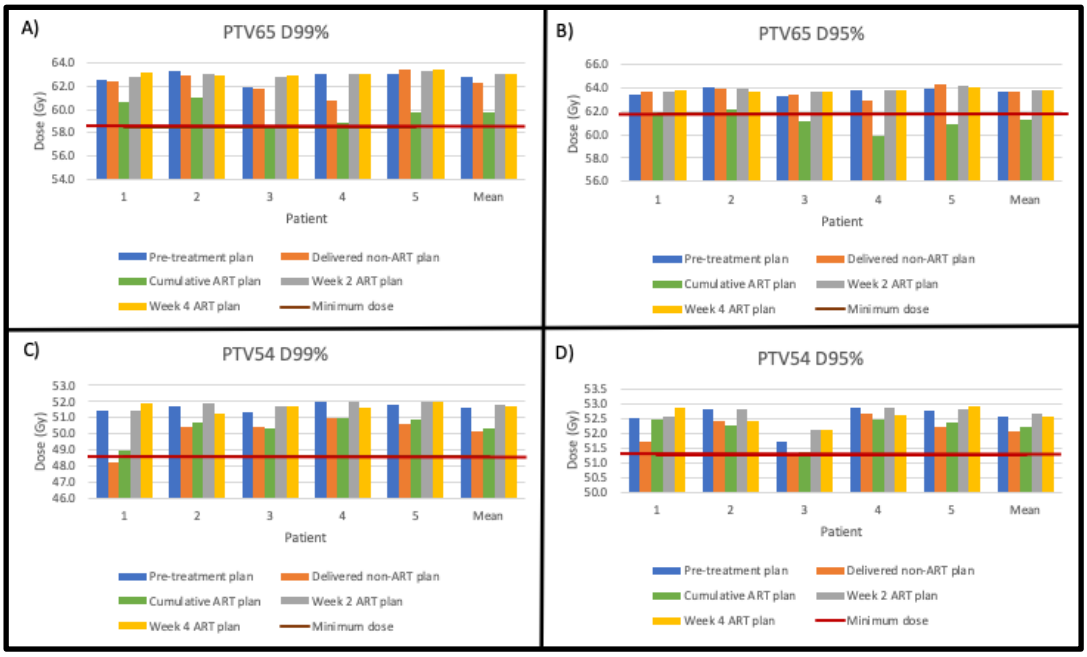

*Figure 5-4. Mandatory PTV dose constraints for the pre-treatment plan, delivered non-ART plan and cumulative ART plans. * represents statistical significance . Circle and error bars represent the mean value and standard deviation, respectively.*

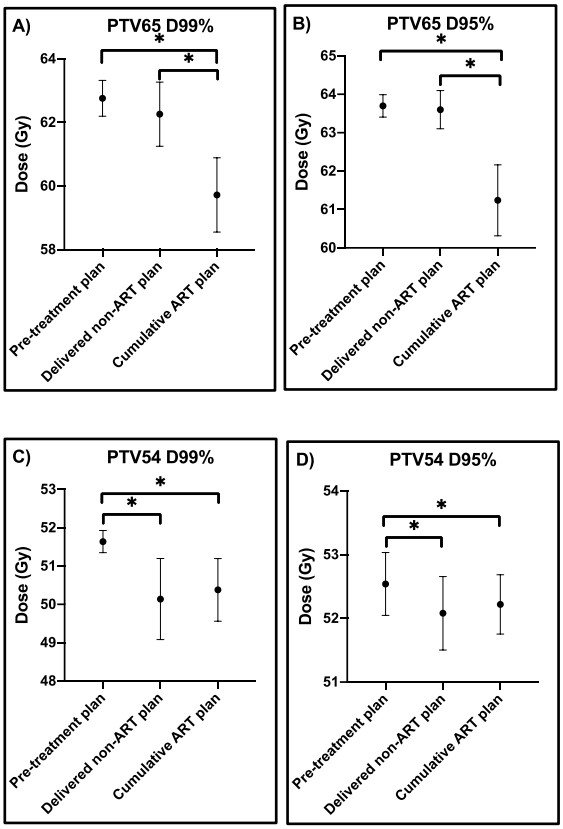

The PTV65 D99% was achieved in all patients for all plans (Figure 5-3A). However, the cumulative ART plan had a significantly smaller mean PTV65 D99% dose (mean = 59.7 Gy, SD = 1.17 Gy) compared to the pre-treatment plan (mean = 62.8 Gy, SD = 0.56 Gy, p=0.002) and the delivered non-ART plan (mean = 62.3 Gy, SD = 1.01 Gy, p=0.004) (Figure 5-4A). There was no significant difference PTV65 D99% between the pre-treatment and non-ART plans (p=0.319).

The minimum dose constraint for the PTV65 D95% was achieved for all plans, except for the cumulative ART plan in 3 of the 5 patients (Figure 5-3B). The mean PTV65 D95% dose for the cumulative ART plan (mean = 61.2 Gy, SD = 0.92 Gy) was significantly smaller compared to the pre-treatment plan (mean = 63.7 Gy, SD = 0.29 Gy, p=0.005) and the delivered non-ART plan (mean = 63.6 Gy, SD = 0.50 Gy, p=0.002) (Figure 5-4B). There was no significant difference in the PTV65 D95% between the pre-treatment and non-ART plans (p=0.658).

It is important to note that the cumulative ART doses represent the adaptation to a shrinking high-dose target volume and that the reported PTV65 dose constraints are assessed on the pre-treatment PTV65 volume. Thus, it is not surprising by adapting to a shrinking target volume in the ART plans, the cumulative dose to the pre-treatment PTV dose is significantly reduced compared to the pre-treatment and non-ART plans. An example of the smaller PTV65 D99% and D95% mean doses for the cumulative ART plans is illustrated in Figure 5-5. As both PTV65 D99% and D95% were achieved for the replans at weeks 2 and 4, this suggests that these mandatory goals were not compromised in these patients during target volume adaptation.

Figure 5-5. Effect of treatment adaptation to a shrinking volume. The pre-treatment plan (A), non-ART plan (B) and cumulative ART plan (C) are shown on the planning MRI. Pre-treatment PTV65 shown in cyan. Arrowhead (white) in Panel C show the areas of the pre-treatment PTV that receive less than the 95% isodose of the high-dose target volume in the ART plan.

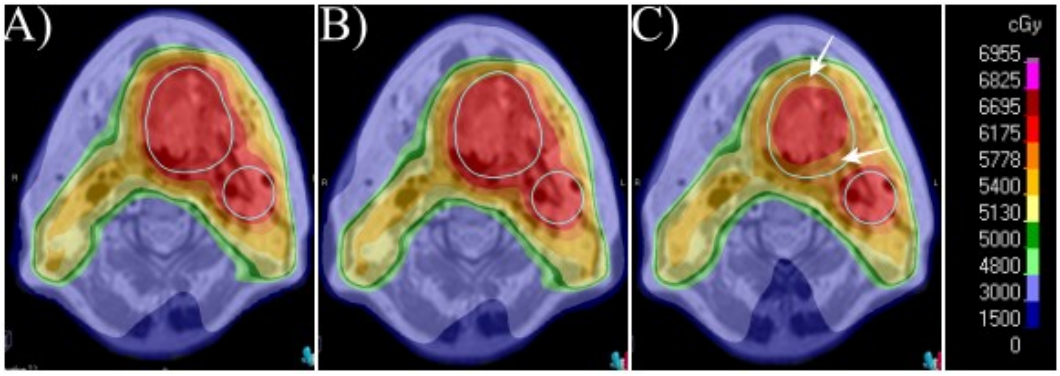

Overall, the mean PTV54 D99% and D95% were achieved for the pre-treatment, delivered non-ART and the cumulative ART plans (Figure 5-3C and D). The mandatory PTV54 D99% was not achieved in patient 1 for the non-adapted plan only (Figure 5-3C). Compared to the pre-treatment plan, the PTV54 D99% and D95% of the non-ART and cumulative ART plans were significantly smaller. The mean PTV54 D99% and PTV54 D95% for cumulative ART plan were significantly smaller than for the pre-treatment plans (50.4 Gy (SD = 0.82 Gy) *vs.* 51.6 Gy (SD = 0.29), p=0.012; 52.2 Gy (SD = 0.47 Gy) *vs.* 52.5 Gy (SD = 0.49 Gy), p=0.020, respectively). Similarly, the mean PTV54 D99% and PTV54 D95% for the non-ART plans were significantly smaller than for the pre-treatment plans (50.1 Gy (SD = 1.06 Gy) *vs.* 51.6 Gy (SD = 0.29), p=0.021; 52.1 Gy (SD = 0.58 Gy) *vs.* 52.5 Gy (SD = 0.49 Gy), p=0.013, respectively). There was no significant difference between the non-ART and ART for both PTV54 D99% and PTV54 D95% (p=0.162, p=0.488).

Although the dose constraints were met for the delivered non-ART plan, the target coverage was compromised to a varying extent on visual inspection of the radiotherapy plans in all 5 patients. Parts of the high-dose and low-dose PTV were not covered within the minimally accepted 95% isodose of their prescribed dose of

65.1 Gy and 54.0 Gy, respectively. An example of this compromise is shown in **Error! Reference source not found.**B where part of the high-dose PTVs for the primary tumour and involved node were by the 89% isodose. Similarly, the low-dose PTV was compromised at the lower aspect of the neck with coverage reduced to 89% to a proportion of the PTV as shown in **Error! Reference source not found.**D.

Delivering the pre-treatment plan without accounting for anatomical changes also led to radiotherapy dose hotspots due to soft tissue loss. An example is shown in Figure 5-6, where at week 4 an area of 61.75 Gy has appeared in the PTV54. However, there were no hotspots in the cumulative non-ART plan, which suggests that this hotspot may not be significant if the overall treatment is taken into account.

Figure 5-6. The pre-treatment plan on the planning MRI (A), the pre-treatment plan calculated on the week 2 MRI (B) and week 4 MRI (C), and cumulative non-ART plan (D) are shown. The PTV54 is represented by the purple contour. The green arrowhead shows the hotspot and white arrowhead show the compromise in target coverage.

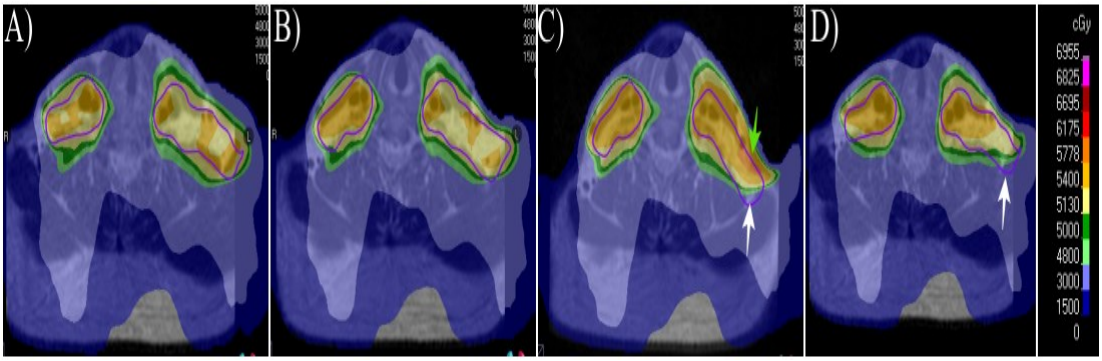

5.7.3 ROIs

Parotid gland volume

All parotid glands (n=10) decreased in volume compared to baseline (Figure 5-7 A and B), with an overall mean percentage volume loss at weeks 2 and 4 were 17.7% (SD = 5.7%) and 24.7% (SD = 10.0%), respectively. The ipsilateral mean percentage volume loss at weeks 2 and 4 were 19.3% (SD=5.5%) and 25.9% (SD=11.0%),

respectively. The contralateral parotid gland showed a smaller loss with a mean percentage volume loss at weeks 2 and 4 were 16.1% (SD=6.2%) and 23.4% (SD=10.0%), respectively.

Figure 5-7. Parotid gland volume change as percentage volume of the pre-treatment parotid volume.

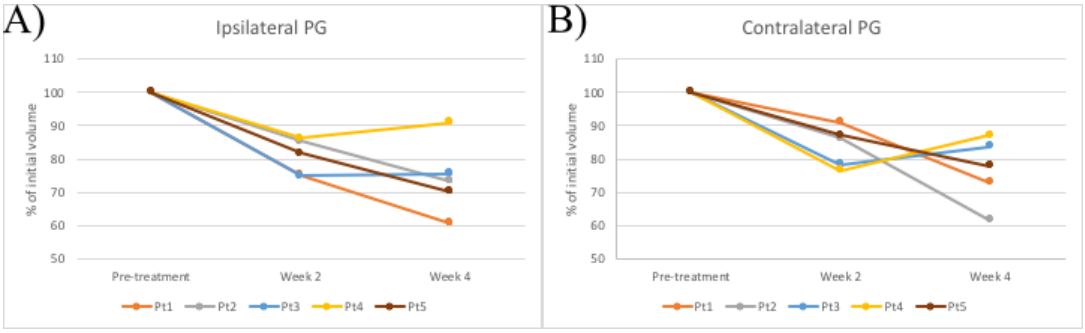

Abbreviations: Pt = patient

5.7.3.1 *Dosimetry*

The mandatory Dmax (1 cm^3) dose constraints for the spinal cord, brainstem and their respective PRVs were met for the pre-treatment, delivered non-ART and the ART plans (Figure 5-8 C-F). There was no significant difference in the mean doses to these OARs for the three plans (Figure 5-9 C-F).

There was no significant difference in mean dose to the ipsilateral and contralateral parotid glands between all plans (Figure 5-9A and B).

Figure 5-8. Dose constraints for the organs at risk. The horizontal red line represents the dose constraint.

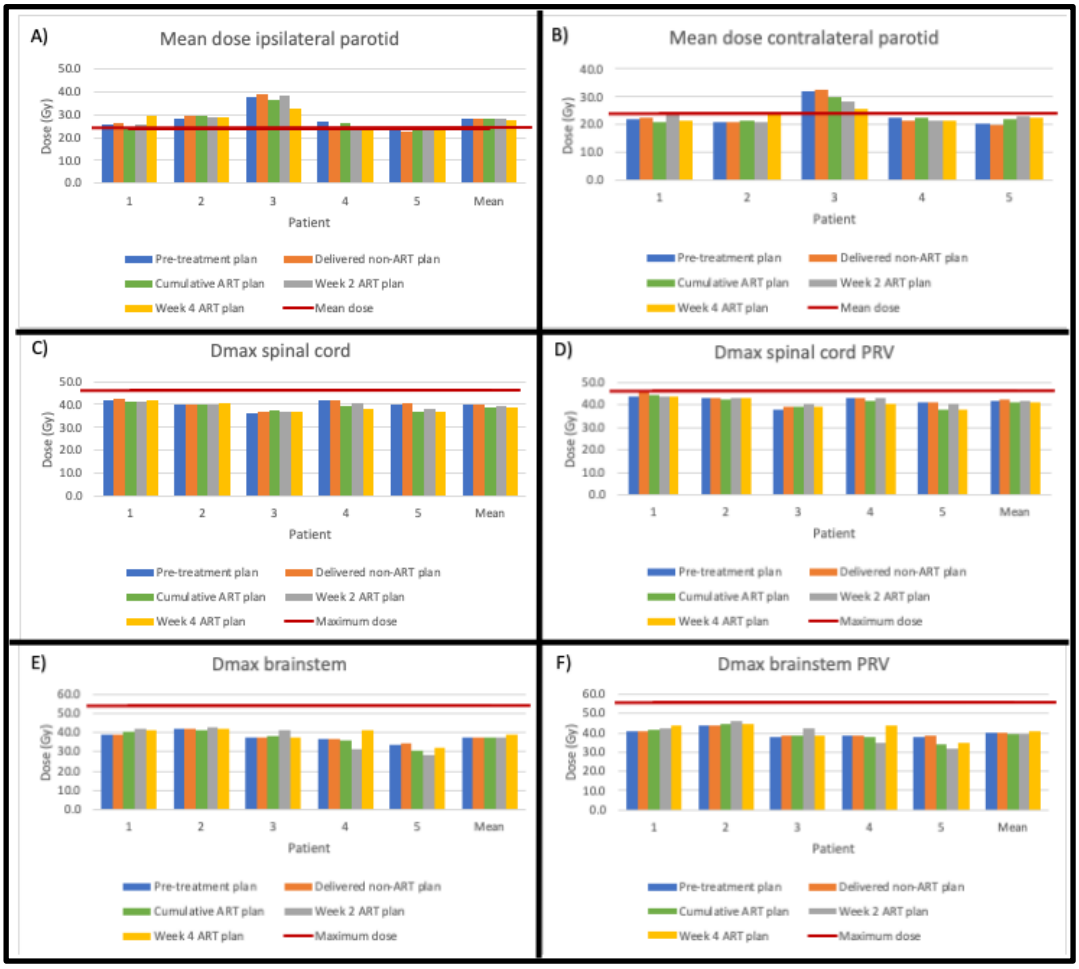

*Figure 5-9. OAR dose constraints for the pre-treatment plan, delivered non-ART plan and cumulative ART plans. * represents statistical significance. Circle and error bars represent the mean and standard deviations, respectively.*

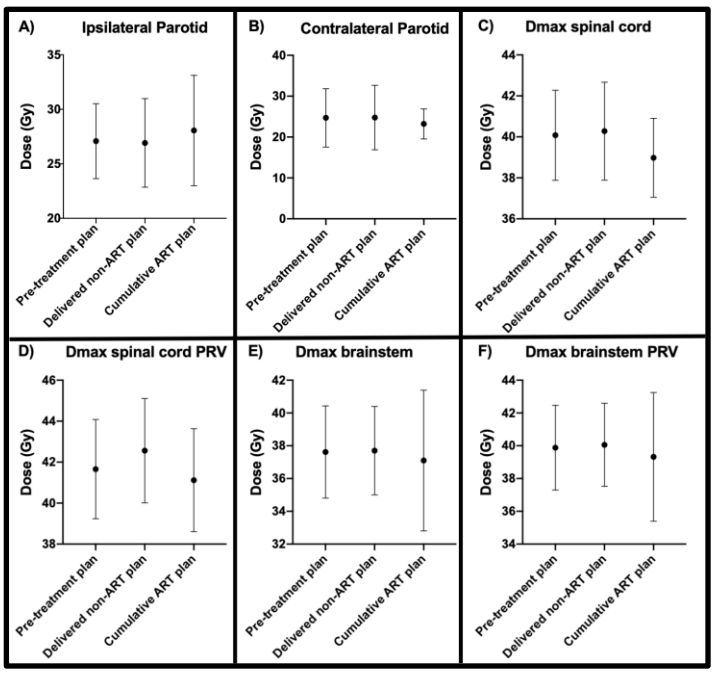

5.7.3.2 *Parotid dose without ART.*

Compared with the pre-treatment plan, delivering a delivered non-ART plan led to greater than planned parotid dose in 3 of the 5 patients (Figure 5-10), with the parotid gland increase in dose ranging between 0.1 and 1.4 Gy. This dose difference is small, and the clinical significance is uncertain.

Figure 5-10. Greater than planned parotid dose without ART. A positive value indicates that the parotid glands in the delivered non-ART plan receive a higher mean dose compared with the pre-treatment plan.

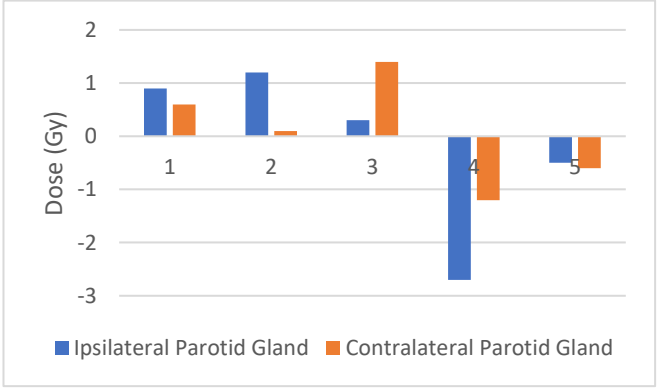

Conversely, the parotid glands of patients 4 and 5 received a lower mean dose (range, 0.5 to 2.7 Gy) than initially planned on the pre-treatment plan.

5.7.3.3 *Parotid dose with ART*

On the other hand, the cumulative ART plan led to a reduction in parotid gland dose in 2 of the 5 patients (range, 1.7 to 2.7) (Figure 5-11) compared with a delivered non-ART plan. However, ART led to an increase in radiotherapy dose to the parotid glands (range, 1.1 to 2.1 Gy) in 2 patients. Patient 3 showed minimal changes to the parotid glands, with ART leading to an increase of 0.1 and 0.2 Gy to the ipsilateral and contralateral parotid glands, respectively.

Figure 5-11. Parotid gland dose reduction using ART compared with no ART. A positive value indicates a reduction in the mean parotid gland dose using ART compared with the non-ART plan.

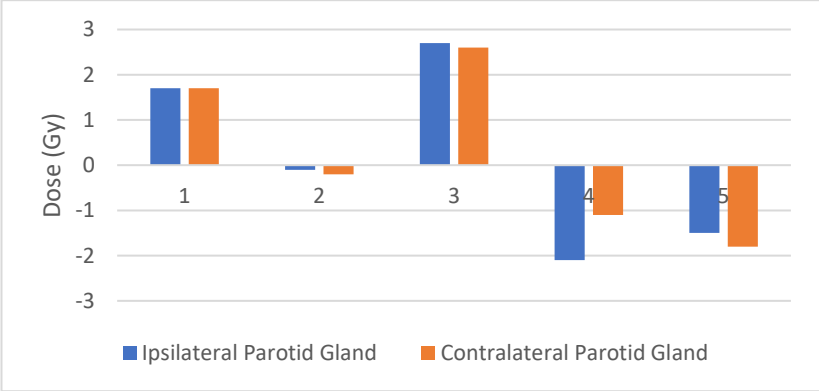

5.7.3.4 *Dose to the pharyngeal constrictor muscles*

The cumulative ART plan showed a significantly smaller mean dose to the SMPCM than the delivered non-ART plan (mean, 54.3 Gy *vs.* 55.6 Gy, respectively; p<0.001) and the pre-treatment plan (mean, 54.3 Gy *vs.* 55.2 Gy; p=0.0222) (Figure 5-12A). However, these dose differences to the SMPCM are small and clinical significance is uncertain.

There were no significant differences in the mean dose to the IPCM between the cumulative ART plan and the delivered non-ART plan (mean, 45.2 Gy *vs.* 47.3 Gy, respectively; p=0.221) and between the cumulative ART plan and the pre-treatment plan (mean, 45.2 Gy *vs.* 45.6 Gy, p=0.518) (Figure 5-12B).

*Figure 5-12. The mean dose received by the SMPCM and the IPCM. Circle symbol and the error bars represent the mean and standard deviation, respectively. * represent statistical significance with an adjusted p-value.*

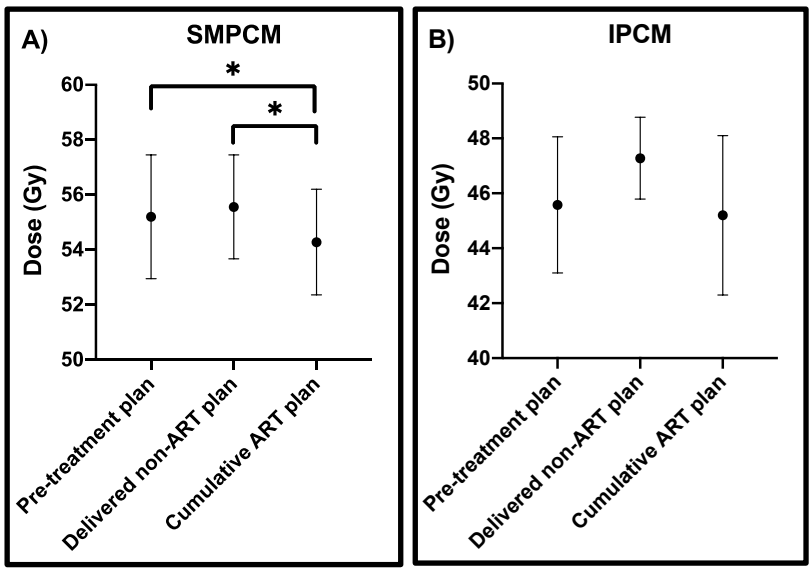

An example of the effect of ART and no ART on the volume of SMPCM within the high-dose target volume is shown in Figure 5-13.

Figure 5-13. Axial slices of the pre-treatment plan (A), non-ART plan (B) and cumulative ART plan(C) on the pre-treatment MRI. PCM is delineated in yellow outside high-dose CTV and in green inside the high-dose CTV. The high-dose CTV is delineated in blue.

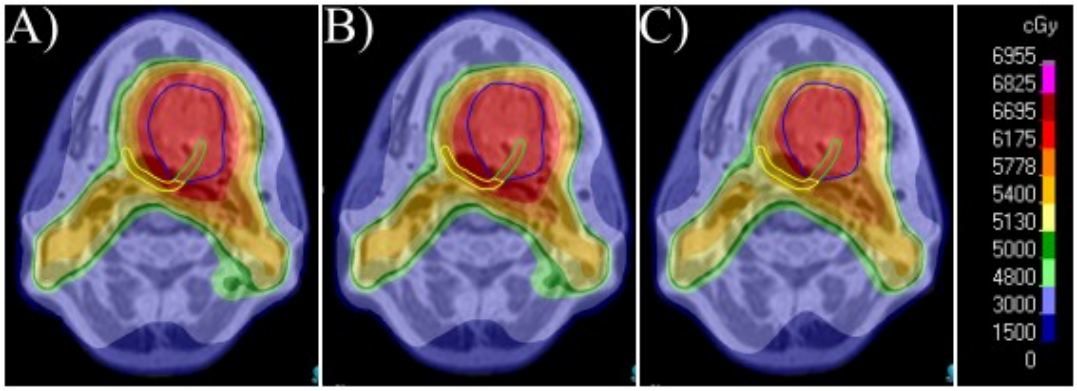

5.8 Discussion

In this small study, I have demonstrated that radiotherapy adaptation based on tumour response using an MR-only workflow is possible and that response-adapted ART maintains target volume coverage and reduces dose to the SMPCM. However, it is important to note the small sample size and that the magnitude of dose reduction was small to the SMPCM with ART with uncertain clinical significance.

Despite delivering a non-adapted plan, all PTV and OAR mandatory dose constraints were met in all but one patient. The latter's non-adapted plan did not meet the PTV54 D99% dose constraint. This patient lost 17% of his pre-treatment weight loss and thus, had a greater change in body contour around the neck and shoulders. This translated to a poorer coverage of the PTV54 in these areas. Nonetheless, a review of the non-adapted radiotherapy plans showed that the target volume coverage (PTV54 and/or PTV65) was compromised in all patients. This is in keeping with the literature, which suggests that unaccounted intra-treatment changes may have a significant impact on the planned dosimetry with a lower delivered dose to target volumes (14).

In this study, ART to a shrinking target volume led to a reduction in the mean dose to 95% of the initial PTV volume from 63.7 Gy (SD, 0.3 Gy) to 61.2 Gy (SD, 0.9 Gy). There are limited published data on the use of MRI-guided dose adaptation. A CT-planned MRI-guided ART study by Mohamed et al. investigated the dosimetric advantage of shrinking the target volume according to tumour response with the use of MRI-guidance. They reported that by shrinking the visible target volume, ART led to a reduction in mean dose to 95% of the initial PTV volume from 70.7 Gy (SD,

0.3) to 58.5 Gy (SD, 2.0) for the adaptive plans for five patients (4). Target volume coverage and dosimetric parameter assessments were not reported.

Although dose adaptation according to tumour response inherently selects responders, this is not standard practice outside of a clinical trial. One particular concern of dose adaptation is the possibility of undertreating potential microscopic disease left in the original high dose volume. A study by Hamming-Vrieze *et al.* reported that tumours may shrink asymmetrically in relation to their surrounding tissues (15). The authors reported that the GTV surface showed a larger displacement than fiducial markers placed at the tumour surface, suggesting that part of the GTV was dissolving rather than shrinking. This concern was addressed in this study by ensuring that any areas previously encompassed by the high-dose CTV in the pre-treatment plan remained within a low-dose CTV following a tumour response. This would ensure that any areas previously in the high-dose CTV would receive a minimum dose of 57.7 Gy. This concept of dose adaptation is being investigated in two prospective studies; the INSIGHT II (Optimising Radiation Therapy in Head and Neck Cancers Using Functional Image-Guided Radiotherapy and novel biomarkers) (CCR4934) (16) and MR-ADAPTOR trials (Magnetic Resonance-based Response Assessment and Dose Adaptation in Human Papilloma Virus Positive Tumours of the Oropharynx treated with Radiotherapy: An R-IDEAL stage 2a-2b/Bayesian phase II trial) (17). Current evidence suggests that reducing the radiotherapy dose to under 70 Gy for HPV-associated OPC is safe with excellent locoregional control (18,19). Chera *et al.* reported two such de-escalation studies. In their first study, treatment was de-escalated in 44 favourable risk HPV-associated OPC patients using a reduced cisplatin dose (30mg/m^2 weekly) and 60 Gy in 30 fractions to the high-dose target volume and 54 Gy to the low-dose target volume.

The 3-year local control, regional control and distant metastasis-free survival were 100% and overall survival was 95% (18). In a second similar study of 114 patients, the 2-year progression-free survival was 86%, loco-regional control 95% and overall survival of 95% (19).

Radiotherapy dose to the PCM influences the risk of persistent dysphagia following chemoradiotherapy for head and neck cancers (8). Dysphagia remains a distressing symptom with nearly 50% reporting this one year after treatment completion (20). Persistent dysphagia leads to aspiration risks, prolonged feeding tube dependence and poor quality of life (21). Therefore, I investigated the impact of ART on the dose received by the PCM and found that ART led to a non-significant reduction in mean dose to the SMPCM and IPCM compared to the pre-treatment plan. This study shows that there was a significant reduction in dose to the SMPCM, even with only fortnightly replan compared to the non-ART plan. This dose reduction was small and is of uncertain clinical significance. In contrast, there was no change in dose to the IPCM. This is similar to the findings of Mohamed et al. who reported that ART led to dose reductions to the pharyngeal constrictor muscles compared to standard IMRT. In their study, ART reduced the mean dose to superior PCM to 58.1 Gy (SD 5.0 Gy) compared to 62.8 Gy (SD 6.7 Gy) for a non-ART plan. Doses to the middle and inferior PCM with ART were 48.4 Gy (SD 12.5 Gy) and 32.0 Gy (SD 18.6 Gy), respectively, compared to 51.6 Gy (SD 16.4 Gy) and 34.7 Gy (SD 23.3 Gy), respectively. This study showed a smaller reduction in dose reduction to the PCM which may be related to the more advanced nature of the primary tumours in this study. All five patients in Mohamed *et al.*'s study had T2 tumours compared to the four patients having at least T3 in this study. Reducing dose to the PCM using dysphagia-optimised IMRT (Do-IMRT) with mandatory mean dose constraints to

PCM outside the high-dose CTV has been reported to improve patient-reported swallowing function compared to standard IMRT (22) and this may become standard of care.

The parotid glands received a higher dose than initially planned in three of the five patients whilst the remaining two patients received a lower dose than planned. ART led to an increase in mean dose to the parotid glands in three patients, whilst improving doses in two patients only. In these two patients, the parotid glands migrated away from the midline and the low-dose PTV (Figure 5-14A and B, and Figure 5-15). In comparison, the study by Mohamed *et al.* reported that ART reduced doses to both contralateral and ipsilateral parotid glands compared to no ART (4). The doses to the contralateral and ipsilateral parotid glands were 16.5 Gy (SD 8.4 Gy) and 26.9 Gy (SD 8.3 Gy) with ART, respectively. In comparison, the non-ART plan led to mean doses of 17.4 Gy (SD 8.6 Gy) and 30.2 Gy (SD 11.3 Gy), respectively. This could be explained by differences in patient characteristics (all their patients had T2 tonsil or BOT primary). This study suggests that although parotid gland dosimetry may not be improved with ART, the actual benefits of ART comes with the fact that the target volume coverage is improved. Another potential benefit of ART is the potential dose reduction to the oral cavity and mandible dose, which are associated with the risk of mucositis (23) and osteoradionecrosis (24–26), respectively.

Figure 5-14. Deformation vector illustrated on coronal T2W images of the planning MR of patient 4(A), patient 5(B) and patient 2(C). The arrowheads indicate the direction of deformation of the planning MR to week 4 imaging. Colourwash represents the distance moved and the size of the arrow represents the amount of movement and direction Orange and yellow contours represent the right and left parotid glands, respectively.

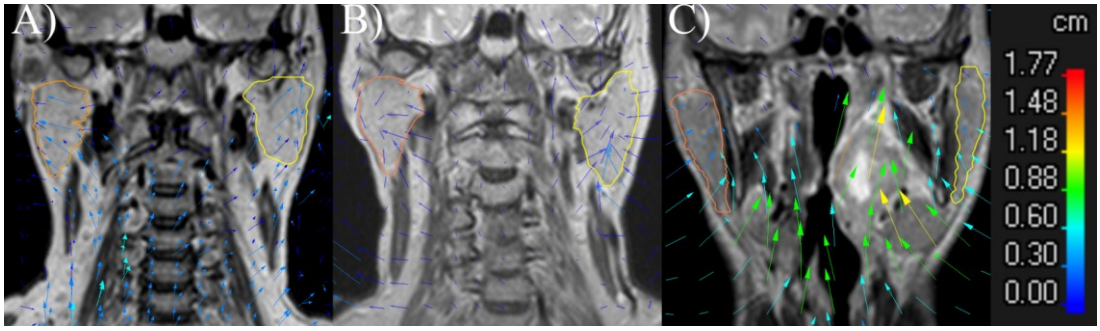

Figure 5-15. Axial slices of the radiotherapy plan on the pre-treatment MRI (A), Week 2 MRI (B) and Week 4 MRI (C). Parotid glands delineated in orange and pink. (Patient 4)

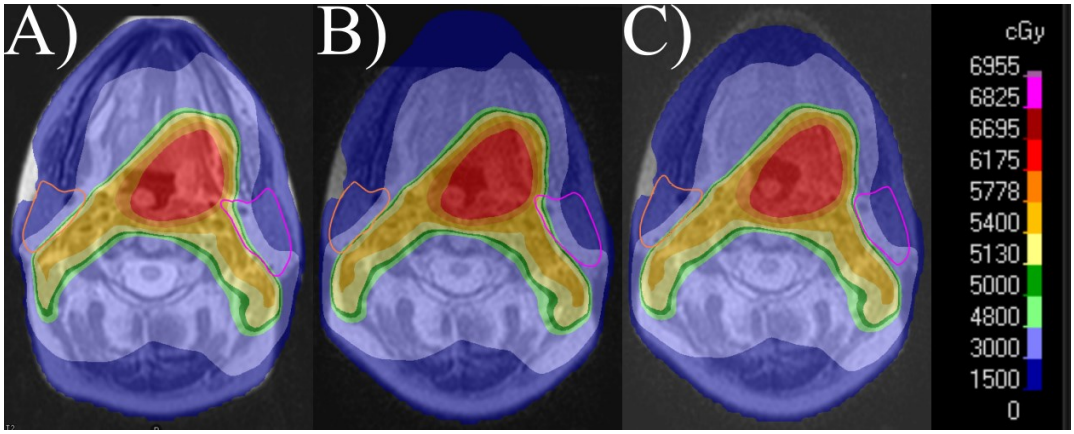

An MRI-only radiotherapy treatment planning workflow requires the creation of a synthetic CT for dose calculation. In this study, I used a bulk density assignment approach to assign electron density values to the tissues (air, bone and soft tissue). Although the dosimetry was not compared to the current gold standard CT-based plans, synthetic CTs derived from bulk density assignment have been shown to be accurate with mean dose differences less than 1% for the PTV and OARs compared to a CT-based plan (27). Therefore, the results reported in this study would represent accurate clinical dose calculations.

Although the results of this study were limited by the small sample size, the sample size was the same as the MRI-guided ART study reported by Mohamed *et al.* (4).

Dose accumulation for the delivered non-ART plan was recalculated on the two intra-treatment MRI scans. Dose accumulation could have been recalculated on weekly scans, but this would have limited the number of patients that could be analysed. Patients with MRI scans at weeks 2 and 4 were analysed as these time-points have been reported to demonstrate the most anatomical changes (28). Another limitation is the small FOV of the MRI scans which did not include the patient shoulders. However, this was accounted for by extrapolating the shoulder contours from the patient's CT scan. Nonetheless, the shoulder positions were estimated and may not represent their true position.

5.9 Conclusion

This planning study has shown that a response-adapted ART is possible using an MR-only workflow and advantageous in reducing doses to certain OARs such as the superior and middle pharyngeal constrictor muscles whilst maintaining target volume dose. However, the magnitude of dose reduction to these OARs were small and of uncertain clinical significance. Confirmation of these findings should be done with a bigger sample size.

5.10 References

1. Gillison ML, Chaturvedi AK, Anderson WF, et al. Epidemiology of human papillomavirus-positive head and neck squamous cell carcinoma. Journal of Clinical Oncology. 2015.

2. Bhatia A, Burtness B. Human papillomavirus-associated oropharyngeal cancer: Defining risk groups and clinical trials. J Clin Oncol [Internet]. 2015 Oct 10 [cited 2017 Nov 21];33(29):3243–50. Available from: http://www.ncbi.nlm.nih.gov/pubmed/26351343

3. Simcock R, Simo R. Follow-up and Survivorship in Head and Neck Cancer. Clin Oncol. 2016;

4. Mohamed ASR, Bahig H, Aristophanous M, et al. Prospective in silico study of the feasibility and dosimetric advantages of MRI-guided dose adaptation for human papillomavirus positive oropharyngeal cancer patients compared with standard IMRT. Clin Transl Radiat Oncol [Internet]. 2018 Jun [cited 2019 May 7];11:11–8. Available from: http://www.ncbi.nlm.nih.gov/pubmed/30014042

5. Wong KH, Panek R, Dunlop A, et al. Changes in multimodality functional imaging parameters early during chemoradiation predict treatment response in patients with locally advanced head and neck cancer. Eur J Nucl Med Mol Imaging [Internet]. 2017 Nov 21 [cited 2017 Nov 23]; Available from: http://www.ncbi.nlm.nih.gov/pubmed/29164301

6. Wippold FJ. Head and neck imaging: The role of CT and MRI [Internet]. Journal of Magnetic Resonance Imaging Wiley Subscription Services, Inc., A Wiley Company; Mar 1, 2007 p. 453–65. Available from: http://doi.wiley.com/10.1002/jmri.20838

7. Nutting CM, Morden JP, Harrington KJ, et al. Parotid-sparing intensity modulated versus conventional radiotherapy in head and neck cancer (PARSPORT): A phase 3 multicentre randomised controlled trial. Lancet Oncol. 2011 Feb;12(2):127–36.

8. Eisbruch A, Schwartz M, Rasch C, et al. Dysphagia and aspiration after chemoradiotherapy for head-and-neck cancer: Which anatomic structures are affected and can they be spared by IMRT? Int J Radiat Oncol Biol Phys. 2004;

9. Pak D, Vineberg K, Feng F, et al. Lhermitte's Syndrome After Chemo-IMRT of Head and Neck Cancer: Incidence, Doses, and Potential Mechanisms. Int J Radiat Oncol Biol Phys

[Internet]. 2012 Aug 1 [cited 2021 Aug 26];83(5):1528. Available from: /pmc/articles/PMC3481166/

10. Gulliford SL, Miah AB, Brennan S, et al. Dosimetric explanations of fatigue in head and neck radiotherapy: An analysis from the PARSPORT Phase III trial. Radiother Oncol. 2012;

11. Christianen MEMC, Langendijk JA, Westerlaan HE, et al. Delineation of organs at risk involved in swallowing for radiotherapy treatment planning. Radiother Oncol. 2011;

12. Thilmann C, Grosser KH, Rhein B, et al. Virtual bolus for inversion radiotherapy planning in intensity-modulated radiotherapy of breast carcinoma within the scope of adjuvant therapy. Strahlentherapie und Onkol. 2002;178(3):139–46.

13. Dunlop A, Mitchell A. Recommended methods for bulk density assignments for pelvic and head and neck treatment sites for MR linac-based treatment planning using the Monaco TPS.

14. Hansen EK, Bucci MK, Quivey JM, et al. Repeat CT imaging and replanning during the course of IMRT for head-and-neck cancer. Int J Radiat Oncol [Internet]. 2006 Feb 1 [cited 2018 Sep 11];64(2):355–62. Available from: https://www-sciencedirect-com.ezproxy.icr.ac.uk/science/article/pii/S0360301605021449?via%3Dihub

15. Hamming-Vrieze O, van Kranen SR, Heemsbergen WD, et al. Analysis of GTV reduction during radiotherapy for oropharyngeal cancer: Implications for adaptive radiotherapy. Radiother Oncol [Internet]. 2017 Feb 1 [cited 2017 Dec 12];122(2):224–8. Available from: http://www.ncbi.nlm.nih.gov/pubmed/27866848

16. Optimising Radiation Therapy in Head and Neck Cancers Using Functional Image-Guided Radiotherapy and Novel Biomarkers - Full Text View - ClinicalTrials.gov [Internet]. [cited 2021 Feb 7]. Available from: https://clinicaltrials.gov/ct2/show/NCT04242459

17. Bahig H, Yuan Y, Mohamed ASR, et al. Magnetic Resonance-based Response Assessment and Dose Adaptation in Human Papilloma Virus Positive Tumors of the Oropharynx treated with Radiotherapy (MR-ADAPTOR): An R-IDEAL stage 2a-2b/Bayesian phase II trial. Clin Transl Radiat Oncol [Internet]. 2018 Aug 24 [cited 2018 Aug 29]; Available from: https://www.sciencedirect.com/science/article/pii/S240563081830048X

18. Chera BS, Amdur RJ, Tepper JE, et al. Mature results of a prospective study of deintensified

chemoradiotherapy for low-risk human papillomavirus-associated oropharyngeal squamous cell carcinoma. Cancer [Internet]. 2018 Jun 1 [cited 2018 Jul 10];124(11):2347–54. Available from: http://doi.wiley.com/10.1002/cncr.31338

19. Chera BS, Amdur RJ, Green R, et al. Phase II trial of de-intensified chemoradiotherapy for human papillomavirus–associated oropharyngeal squamous cell carcinoma. J Clin Oncol. 2019;

20. Roe JWG, Drinnan MJ, Carding PN, et al. Patient-reported outcomes following parotid-sparing intensity-modulated radiotherapy for head and neck cancer. How important is dysphagia? Oral Oncol. 2014;

21. Petkar I, Bhide S, Newbold K, et al. Dysphagia-optimised Intensity-modulated Radiotherapy Techniques in Pharyngeal Cancers: Is Anyone Going to Swallow it? Clin Oncol. 2017;

22. Nutting C, Rooney K, Foran B, et al. Results of a randomized phase III study of dysphagia-optimized intensity modulated radiotherapy (Do-IMRT) versus standard IMRT (S-IMRT) in head and neck cancer. J Clin Oncol. 2020 May 20;38(15_suppl):6508–6508.

23. Eisbruch A, Harris J, Garden AS, et al. Multi-Institutional Trial of Accelerated Hypofractionated Intensity-Modulated Radiation Therapy for Early-Stage Oropharyngeal Cancer (RTOG 00-22). Int J Radiat Oncol Biol Phys. 2010 Apr;76(5):1333–8.

24. Gomez DR, Estilo CL, Wolden SL, et al. Correlation of osteoradionecrosis and dental events with dosimetric parameters in intensity-modulated radiation therapy for head-and-neck cancer. Int J Radiat Oncol Biol Phys. 2011;

25. Mohamed ASR, Hobbs BP, Hutcheson KA, et al. Dose-volume correlates of mandibular osteoradionecrosis in Oropharynx cancer patients receiving intensity-modulated radiotherapy: Results from a case-matched comparison. Radiother Oncol. 2017 Aug 1;124(2):232–9.

26. Aarup-Kristensen S, Hansen CR, Forner L, et al. Osteoradionecrosis of the mandible after radiotherapy for head and neck cancer: risk factors and dose-volume correlations. Acta Oncol (Madr) [Internet]. 2019 Oct 3 [cited 2020 Mar 19];58(10):1373–7. Available from: https://www.tandfonline.com/doi/full/10.1080/0284186X.2019.1643037

27. Guerreiro F, Burgos N, Dunlop A, et al. Evaluation of a multi-atlas CT synthesis approach for

MRI-only radiotherapy treatment planning. Phys Medica. 2017 Mar 1;35:7–17.

28. Bhide SA, Davies M, Burke K, et al. Weekly volume and dosimetric changes during chemoradiotherapy with intensity-modulated radiation therapy for head and neck cancer: a prospective observational study. Int J Radiat Oncol Biol Phys. 2010 Apr;76(5):1360–8.

6 Chapter 6 -The impact of restricted length of treatment field and anthropometric factors on selection of head and neck cancer patients for treatment on the MR-Linac

6.1 Introduction

As described in Chapter 6, the MR-Linac bears important differences to a conventional linac. The MR-linac has a shorter radiation window in the craniocaudal (CC) direction, which is of relevance to head and neck cancer (HNC) treatment. A 1 cm margin in all directions to correct patient set-up errors and daily plan adaptation restricts the maximum CC radiation field length to 20 cm in this direction. This may influence the selection and the absolute number of HNC patients who can be treated on the MR-Linac using a single isocentre technique.

6.2 Aims

This study first assesses the effect of a restricted CC field length on the suitability and selection of HNC patients who can be treated on the MR-Linac using a single isocentre technique.

This study then assesses the association between CC field length and anthropometric factors such as patient height, hyo-sternal neck length and neck treatment position.

6.3 Hypotheses

A restricted CC field length of <20 cm on the MR-Linac will reduce the number of HNC cancer patients suitable for treatment on the MR-Linac.

In most oropharyngeal cancer cases, the CC field length is determined by the length of the neck nodal chain. Therefore, the CC field length will be longer in cases that

increase the length of the neck nodal chain such as an extended neck position and a taller stature.

6.4 Objectives

- To determine the proportion of HNC patients undergoing radiotherapy treatment at the Royal Marsden Hospital (Sutton Branch) with a CC field length of <20 cm.
- To investigate the relationship between patient anthropometric factors and neck position with the CC field length.

6.5 Materials and methods

6.5.1 Patient selection

This retrospective study analysed patients with HNC who underwent either radical primary or adjuvant (chemo)radiotherapy at the Royal Marsden Hospital (Sutton branch) between January 2018 and June 2019. All patients consented to have their imaging used for research purposes.

To investigate the two aims set out in Section 6.2, two HNC populations were defined as below:

- Assessment of the proportion of HNC patients with a CC field length <20 cm.

A total of 110 HNC patients were analysed. The HNC subsites included oropharynx, nasopharynx, hypopharynx, larynx, paranasal sinus, parotid, oral cavity and unknown primary.

- Relationship between the anthropometric factors and neck treatment position with the CC field length.

To investigate the influence of the neck position on CC field length, 23 patients with oral cavity cancer and 51 patients with oropharyngeal cancer were selected to represent the neutral and extended neck cohorts, respectively. To investigate the "worst-case" scenario, only patients with a radiation field encompassing both primary site and neck nodal levels were included.

6.5.2 Radiotherapy planning image acquisition

Patients were immobilised with a custom-made five-point thermoplastic mask and scanned in the supine position on a large-bore CT scanner (Philips Medical,

Cleveland, OH, USA). Scans were acquired in 2 mm slices. At the Royal Marsden hospital, patients with pharyngeal and laryngeal HNC were scanned and treated in an extended neck position. This originates from the PARSPORT trial where the neck was comfortably extended to help reduce the radiotherapy dose to the oral cavity whilst also sparing the parotid glands (1,2). Other HNC sites, such as the oral cavity and paranasal sinuses, were scanned and treated in a neutral neck position. The difference in neck positions is illustrated in Figure 6-1.

Figure 6-1. Patient set-up illustrated for extended neck (A) and neutral neck (B) positions on a sagittal CT scan slice. Neck position is altered using a combination of a headrest (green), shoulder wedge (yellow) and wedge (grey).

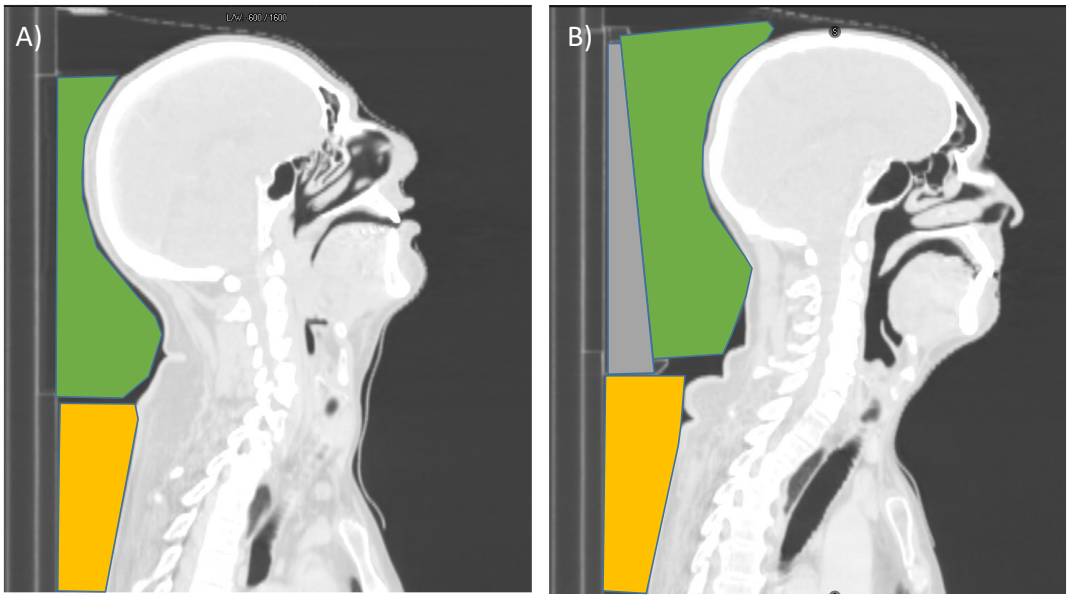

6.5.3 Target volume delineation

Target volume delineation for each aim (Section 6.2) is described below:

- Assessment of the proportion of HNC patients with a CC field length <20 cm.

For this cohort, each CC field length was derived from the target volumes that had been used to plan and deliver the patient's radiotherapy treatment. The target volume had been delineated using local and international guidelines (3,4) for their respective

tumour sites by clinical oncology consultants specialised in HNC. There were three dose levels for clinical target volume (CTV): high, intermediate low dose CTVs corresponded to 65.1 Gy, 60 Gy and 54 Gy in 30 fractions delivered over 42 days. The planning target volume (PTV) was generated using 3 mm isometric expansion of clinical target volume (CTV) as per our institution's protocol. I reviewed these target volumes on a clinical version of RayStation (Version 8.0, RaySearch Laboratories, Stockholm, Sweden) and derived the CC field length by measuring the absolute distance between the most cranial and caudal aspects of the PTV for each patient.

- Relationship between the anthropometric factors and neck treatment position with the CC field length.

For this cohort, I simulated the longest treatment field for a lymph node-positive HNC by delineating standardised CTVs that extended cranially to the skull base to include level VIIb nodes and caudally to level IVa. I delineated the CTV which was independently checked by a consultant clinical oncologist specialised in HNC (Dr Kee Wong) for agreement. As per our institution's protocol, the CTV was expanded by 3mm isometrically to form the PTV.

For this study, the hyo-sternal neck length was defined as the absolute distance (cm) between the superior surface of hyoid to sternal notch measured in the midline on the coronal reconstruction of the radiotherapy planning CT scan (Figure 6-2).

Figure 6-2. An example of neck length measurement on a coronal CT slice. The neck length is illustrated by the double ended arrow in red.

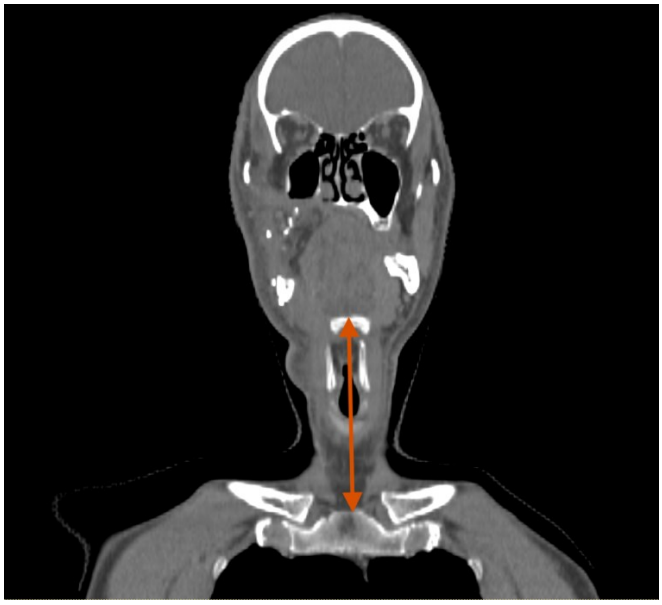

6.6 Statistical Analysis

I analysed the data using Graphpad Prism software (Version 8.2.0; San Diego, CA). The Shapiro-Wilk test was used to test for normality of the data. Mean and median values were reported for parametric and non-parametric data, respectively. The independent *t*-tests and Mann-Whitney were used as parametric and non-parametric tests, respectively. Pearson correlation was used to measure statistical relationships. The strength of the correlation was defined using the following absolute values of r: 0 to 0.19 as very weak, 0.20 to 0.39 as weak, 0.40 to 0.59 as moderate, 0.6 to 0.79 as strong and 0.8 to 1 as very strong correlation (5). Simple linear regression was used to analyse the correlation between CC field length and factors such as patient neck length and height. For this test, logarithmic transformation was used to convert non-parametric data. Differences were statistically significant at two-tailed p-values of ≤0.05.

6.7 Results

6.7.1 Patient characteristics

Patient and tumour characteristics are summarised in Table 6-1.

Table 6-1. Patient and tumour characteristics of patients undergoing radical or adjuvant (chemo)radiotherapy. Staging according to American Joint Committee on Cancer (AJCC) 7th edition.

Mean age (years)	63 (Range 31 - 85)			
Tumour Site (n = 110)	**Number of patients**	**Craniocaudal field length (cm)**		
		Median	**Minimum**	**Maximum**
Oropharynx	51	17.6	11.2	20.0
Nasopharynx	3	20.6	18.8	23.0
Hypopharynx	7	15.2	11.8	18.0
Paranasal sinus	3	20.3	20.0	24.6
Unknown Primary	9	17.0	15.2	19.0
Oral Cavity	23	16.8	13.4	19.0
Larynx	13	13.6	11.2	17.8
Parotid	1	18.4	18.4	18.4
Tumour Stage				
T0	9			
T1	18			
T2	37			
T3	25			
T4	21			
Nodal Stage				
N0	37			
N1	18			
N2	53			
N3	2			

6.7.2 CC treatment field length distribution in the overall HNC population.

Overall, 95% of the HNC patients demonstrated a CC field length <20 cm, with the majority (75%) ranging between 15 to 19.9 cm (Figure 6-3 A and B). Patients with nasopharyngeal and paranasal HNC had the longest maximum CC field lengths at 23.0 cm and 24.6 cm, respectively (Table 6-1).

Figure 6-3. A) Histogram and B) Cumulative distribution plot illustrating the frequencies of craniocaudal field length in head and neck cancers. n = 110.

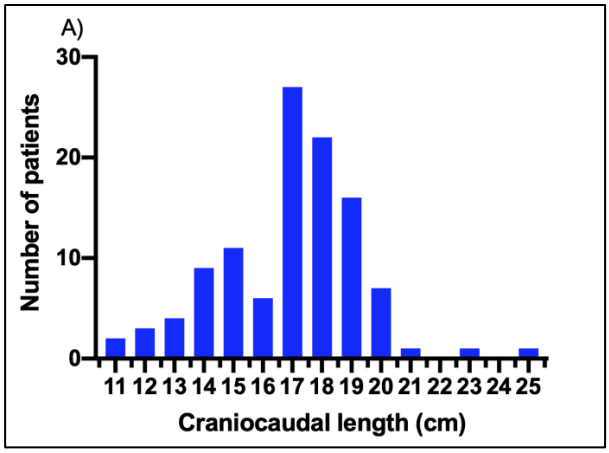

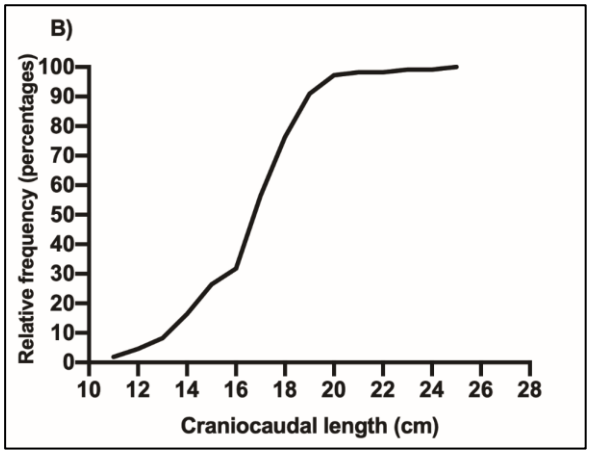

Six patients had a CC field length of ≥20 cm (Table 6-2). Their primary sites were nasopharynx (two patients), oropharynx (one patient) and paranasal sinus (three patients). The majority of the patients were male and were taller on average than the overall population (mean height, 177 cm (SD=5.9 cm) versus 173 cm (SD=8.6 cm)). The median neck length was 13.3 cm (range 10.6 to 14.6 cm).

Table 6-2. Patient characteristics with a craniocaudal length of ≥ 20.0 cm. Staging according to American Joint Committee on Cancer (AJCC) 7th edition.

Patient	TNM staging	Primary site	Craniocaudal length (cm)	Gender	Height (cm)	Neck Length (cm)	Neck position
1	T1 N2b M0	Oropharynx	20.0	M	185	14.6	Extended
2	T4b N1 M0	Paranasal	24.6	M	178	12.6	Neutral
3	T3 N0 M0	Paranasal	20.3	F	173	13.0	Neutral
4	T4a N0 M0	Paranasal	20.0	F	168	10.6	Neutral
5	T2 N0 M0	Nasopharyngeal cancer	20.6	M	180	13.6	Extended
6	T1 N1 M0	Nasopharyngeal cancer	23.0	M	179	14.4	Extended

Abbreviations: M = Male, F= Female

6.7.3 Effect of gender on the CC field length in the extended neck position

Female patients had a significantly shorter mean height of 165.0 cm (SD = 7.9 cm) compared with a mean height of 177.0 cm (SD = 5.5cm) for male patients (p=0.0001). Female patients also showed a significantly shorter median CC field length of 17.0 cm (range, 11.0 to 19.0 cm) compared to 18.0 cm (range, 16.0 to 20.0 cm) for the male patients (p=0.0003).

6.7.4 Effect of neck position on the CC field length.

The comparison between neutral and extended neck cohorts is shown in Table 6-3. Patients scanned in a neutral neck position had a significantly shorter median CC field length of 15.8 cm (range, 14.8 to 19.2 cm) compared to 17.6 cm (range, 13.6 to 20.0 cm) in the extended neck (p=0.0119). There was no statistical difference in height between the two cohorts (p=0.051), indicating that neck position independently influences the CC field length.

Table 6-3. Comparison of the craniocaudal field length, neck length and patient height for patients scanned in a neutral and extended neck positions.

	Craniocaudal field length (cm)			Neck length (cm)			Patient height (cm)	
	Median (cm)	**Minimum (cm)**	**Maximum (cm)**	**Median (cm)**	**Minimum (cm)**	**Maximum (cm)**	**Mean (cm)**	**SD (cm)**
Neutral neck (n=23)	15.8	14.8	19.2	10.6	9.2	13.6	171	8.9
Extended neck (n=51)	17.6	11.0	20.0	12.0	8.4	15	175	1.6

Abbreviation: SD = standard deviation.

Patient height showed moderate correlation with CC field length in both neutral and extended neck positions ($r = 0.55$, $p=0.0070$ and $r = 0.65$, $p<0.0001$, respectively) (Figure 6-4A and Figure 6-5A, respectively).

Figure 6-4. Patients scanned in the neutral neck position, n = 23. A) Correlation between patient height and craniocaudal field length. B) Correlation between patient neck length and craniocaudal field length

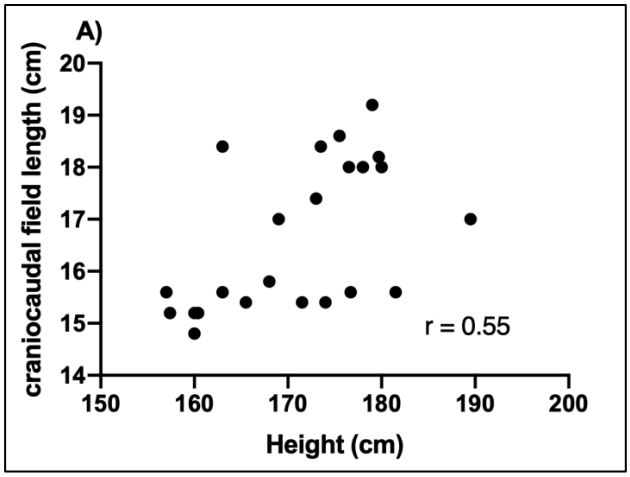

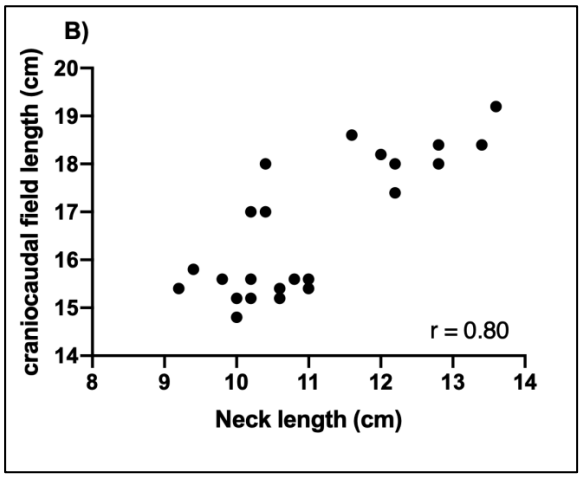

Figure 6-5. Patients scanned in the extended neck position, n = 51. A) Correlation between patient height and craniocaudal field length. B) Correlation between patient neck length and craniocaudal field length

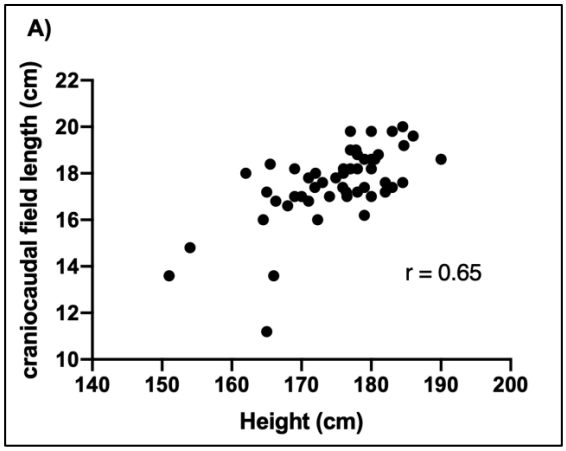

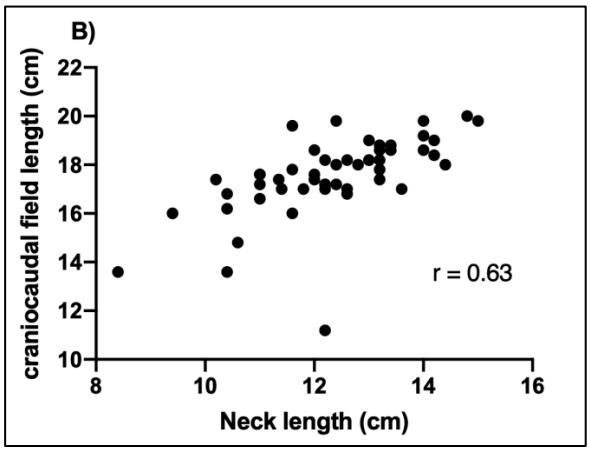

Similarly, neck length also showed a statistically significant strongly positive correlation with CC field length in both neutral neck position ($r = 0.80$, $p<0.0001$, Figure 6-4B) and extended neck position ($r = 0.63$, $p<0.0001$, Figure 6-5B). As expected, this suggested that the CC length increased with an increase in patient's height and neck length.

Amongst all anthropometric factors, the hyo-sternal neck length showed the strongest positive correlation with CC field length in the neutral neck position, making it the most clinically relevant predictive factor for patient selection suitable for MR-Linac treatment.

6.7.5 Proposed height and neck length cut-off values in the neutral neck position.

Using simple linear regression, the relationship between neck length (x) and $\log_{(10)}$ CC field length (y) was predicted with the following equation:

$y = 0.02305 *x + 0.9651$

This equates to a patient neck length of 14.6 cm predicting a CC field length of 20 cm in the neutral neck position.

Similarly, the relationship between patient height (x) and $\log_{(10)}$ CC field length (y) was predicted with the following equation:

$y = 0.002298*x + 0.8271$

This equates to a patient height of 206 cm predicting a craniocaudal field length of 20 cm in the neutral neck position.

6.8 Discussion

The MR-Linac has the potential to deliver truly a personalised adaptive radiotherapy for HNC. However, the CC field restriction imposed by a modified MR coil means that not all HNC patients will be suitable for treatment using a single isocentre. First, this analysis shows that the majority of the HNC patients treated at the Royal Marsden Hospital would have a treatment field deliverable by the MR-Linac using a single isocentre, irrespective of the treatment neck position. However, cancers originating from certain subsites such as the nasopharynx and paranasal sinus may not be suitable due to the additional cranial extension of target volumes. For example, the inferior half of the sphenoid sinus needs to be included in the low dose CTV for T1-2 nasopharyngeal cancer and the whole sphenoid sinus if T3-4 (4). In this study, no paranasal cancer patients and only one of three nasopharyngeal cancer patients had a treatment field length of <20 cm. Recent international delineation guidelines for nasopharyngeal cancer suggest that the lymph nodal levels IV and Vb can be omitted from the low-dose CTV in patients with lymph node-negative neck. Using these guidelines, the lymph node-negative nasopharyngeal cancer patient (patient 5 from Table 6-2) would have a craniocaudal field length of 16.4 cm and have a treatment field size suitable for treatment in the MR-Linac. However, this differs from our local institution delineation guideline as the level IVa lymph nodes are included in this group of patients. Therefore, the use of these consensus guidelines may make it is possible to treat early-stage nasopharyngeal cancers (T1-2 N0 M0) on the MR-L using a single isocentre. A single oropharyngeal cancer patient had a treatment field length of 20 cm. Review of the treatment field showed no delineation deviations. A likely explanation is that this patient's extended neck position contributed to a longer treatment field, as indicated by my results.

In this study, the lower neck levels IVb (medial supraclavicular) and Vc (lateral supraclavicular lymph nodes) were not included. Nodal level IVb would extend the CC field length caudally to the cranial edge of the sternal manubrium. Including nodal level Vc would not change the CC field length the caudal border of level Vc corresponds to the caudal border of IVa. These nodal levels would be included if involved or at high-risk of harbouring metastatic disease in cases such as nasopharyngeal, hypopharyngeal, sub-glottic laryngeal and thyroid cancers. Thus, any lower neck treatment requiring level IVb treatment would increase the treatment field size and be difficult to treat on the MR-Linac using a single-isocentre.

The result of this study is based on a maximum CC size of 20 cm due to an isotropic margin of 1 cm. This is a conservative margin which may be reduced further with more clinical experience on the MR-Linac. Reducing the margin would increase the treatable CC field size and increase the number of eligible patients. In fact, a margin reduction to 5mm has been reported to increase the number of eligible patients by 10% (6). However, this remains a topic for further research.

Second, I investigated the impact of anthropometric factors such as height, neck length and position on CC field length that simulated the treatment field of node-positive HNC. I demonstrated that the neck length showed a very strong correlation with CC field length in the neutral neck position and was the best predictor of field length in this group. Patient's height showed a weaker correlation with craniocaudal field length and this could be explained by a change in patient height not being in proportion to a change in the patient's neck length. Other clinically measurable anthropometric factors such as the percutaneous lengths of the ulna (7) and tibia (8) have been reported to be predictors of a patient's stature. However, these

measurements were not readily available for correlation with the CC field length and this analysis was beyond the scope of this study.

I showed that female patients had a significantly shorter CC treatment field length compared to male patients, irrespective of neck position and this may be explained by their overall shorter stature. In keeping with this, Vasavada *et al.* demonstrated that females necks are 9 to 16% smaller than their male counterparts (9). Although gender may influence treatment field length, this may not be as influential in tumours that extend cranially. This is illustrated by the two female patients with paranasal cancers had CC treatment field lengths that exceeded the MR-Linac treatment length.

Third, this study suggests that the neck position influences the CC field length. Patients scanned in the neutral neck position demonstrated a smaller median CC field length compared to patients scanned in the extended neck position. Each treatment session on the MR-Linac will last up to 40 to 50 minutes, in line with treatment of other sites such as prostate cancer (10). Therefore, a neutral neck position may be preferable to maximise the number of patients eligible for treatment on the MR-Linac and, from experience, help with comfort and tolerance of treatment. With increased IMRT planning experience, an extended neck position is no longer crucial in reducing doses to the oral cavity. Techniques such as using specific dose constraints to the oral cavity may be used (11) in the neutral neck position and this will be investigated in Chapter 8.

As we intend to treat patients in the neutral neck position, I derived cut-offs for neck length and patient height to act as surrogate markers for patient selection. These cut-offs were not tested in the overall HNC cohort as these patients consisted of a combination of patients scanned in the extended and neutral neck positions. The

upper limits of a neck length of 14.6 cm and a height of 206 cm should be validated in larger studies.

This study has a few limitations. Some sub-types of HNC in this study were under-represented with only a small number of patients which prevents concrete conclusions to be made on their suitability. However, patients with nasopharyngeal and paranasal cancers will usually need a longer treatment field that encompasses a target beyond the nodal levels cranially. This means that it is likely that these subtypes will have a treatment field that is not currently treatable on the MR-Linac. This is likely to change with the development of dual isocentre treatment techniques. The lack of matched-controls and a relatively small number of female patients in our analysis means that there may be unaccounted confounding factors that may have affected some of our results. For the neck position analysis, I considered using the diagnostic CT of the patients treated in the extended neck position as this are acquired in a "neutral neck" position. However, I felt that the radiotherapy CT scans of oral cavity patients would be more representative of a "neutral neck" treatment position because of the immobilisation equipment used.

Despite these limitations, the results of this study reflect those of a study by Chuter *et al.,* who reported that the majority (86%) of their HNC patients would be treatable with a 1 cm adaptive CC margin (6). The authors concluded that 75% of their oropharyngeal cancers and 30% of their nasopharyngeal cancer patients would be treatable (6). I have reported a larger proportion of patients eligible for treatment on the MR-Linac and the differences may be related to differences in delineation protocols. My results reflect target delineation according to international guidelines and are, therefore, likely to apply to other institutions. To my knowledge, this is the first study to demonstrate a very strong correlation between patient neck length with

the CC field length. Currently, a patient is assessed for MR-Linac treatment suitability, including likely field length, following review of the radiotherapy planning CT and MR scans. These planning scans must be acquired on a special table overlay to enable reproducible positioning of the RF coil and patient set-up using specific couch index points on the MR-Linac. These are not required for treatment on a conventional linac and therefore, patient selection using neck length at an earlier stage of the planning process would prevent these unnecessary steps for MR-linac ineligible patients.

6.9 Conclusion

This study shows that the majority of head and neck cancers at the Royal Marsden Hospital have a treatment field that is achievable on the MR-Linac using a single isocentre technique. Primary tumour sites such as nasopharyngeal cancers with significant intracranial extension or paranasal cancers requiring nodal irradiation may not be suitable for treatment on MR-Linac. This study proposes that a hyo-sternal neck length cut-off of 14.6 cm in the neutral neck position could be used as a surrogate marker for suitability of treatment on MR-Linac and patients at the Royal Marsden Hospital will be treated in a neutral neck position unless there is significant dose distribution benefit from neck extension.

6.10 References

1. Nutting CM, Morden JP, Harrington KJ, et al. Parotid-sparing intensity modulated versus conventional radiotherapy in head and neck cancer (PARSPORT): A phase 3 multicentre randomised controlled trial. Lancet Oncol. 2011 Feb;12(2):127–36.

2. Clark CH, Miles EA, Guerrero Urbano MT, et al. Pre-trial quality assurance processes for an intensity-modulated radiation therapy (IMRT) trial: PARSPORT, a UK multicentre Phase III trial comparing conventional radiotherapy and parotid-sparing IMRT for locally advanced head and neck cancer. Br J Radiol [Internet]. 2009 Jul [cited 2019 Nov 26];82(979):585–94. Available from: http://www.birpublications.org/doi/10.1259/bjr/31966505

3. Grégoire V, Ang K, Budach W, et al. Delineation of the neck node levels for head and neck tumors: A 2013 update. DAHANCA, EORTC, HKNPCSG, NCIC CTG, NCRI, RTOG, TROG consensus guidelines. Radiother Oncol [Internet]. 2014 Jan [cited 2019 May 2];110(1):172–81. Available from: http://www.ncbi.nlm.nih.gov/pubmed/24183870

4. Lee AW, Ng WT, Pan JJ, et al. International guideline for the delineation of the clinical target volumes (CTV) for nasopharyngeal carcinoma. Radiother Oncol [Internet]. 2017 Nov 15 [cited 2018 Jan 19]; Available from: http://www.sciencedirect.com/science/article/pii/S0167814017326865?via%3Dihub

5. 11. Correlation and regression | The BMJ [Internet]. [cited 2019 Dec 19]. Available from: https://www.bmj.com/about-bmj/resources-readers/publications/statistics-square-one/11-correlation-and-regression

6. Chuter RW, Whitehurst P, Choudhury A, et al. Technical Note: Investigating the impact of field size on patient selection for the 1.5T MR-Linac. Med Phys [Internet]. 2017 Nov 1 [cited 2019 Feb 4];44(11):5667–71. Available from: http://doi.wiley.com/10.1002/mp.12557

7. Gul H, Mansor Nizami S, Khan MA. Estimation of Body Stature Using the Percutaneous Length of Ulna of an Individual. Cureus. 2020 Jan 8;12(1).

8. Gualdi-Russo E, Bramanti B, Rinaldo N. Stature estimation from tibia percutaneous length: New equations derived from a Mediterranean population. Sci Justice. 2018 Nov 1;58(6):441–6.

9. Vasavada AN, Danaraj J, Siegmund GP. Head and neck anthropometry, vertebral geometry and neck strength in height-matched men and women. J Biomech [Internet]. 2008 Jan 1 [cited 2019 Aug 7];41(1):114–21. Available from: https://www.sciencedirect.com/science/article/pii/S002192900700317X?via%3Dihub

10. Murray J, Tree AC. Prostate cancer – Advantages and disadvantages of MR-guided RT. Clin Transl Radiat Oncol [Internet]. 2019 Sep 1 [cited 2019 Oct 4];18:68–73. Available from: https://www.sciencedirect.com/science/article/pii/S2405630819300527

11. McQuaid D, Dunlop A, Nill S, et al. Evaluation of radiotherapy techniques for radical treatment of lateralised oropharyngeal cancers: Dosimetry and NTCP. Strahlentherapie und Onkol. 2016;

7 Chapter 7 - The dosimetric effect of neck positioning during head and neck radiotherapy treatment

7.1 Introduction

Since the implementation of intensity-modulated radiation therapy (IMRT) at the Royal Marsden Hospital, all patients with laryngeal and pharyngeal head and neck cancers (HNC) requiring nodal irradiation have been immobilized and treated in an extended neck position. This treatment position stems from the PARSPORT trial where a comfortably extended neck was used to reduce the delivered radiotherapy dose to the oral cavity and parotid glands (1,2). Following the transition to volumetric-modulated arc therapy (VMAT), the same extended neck treatment position has been kept. However, a neutral neck position is a more natural and comfortable position for most patients and many centres treat HNC patients in this immobilisation position. Furthermore, published international HNC contouring guidelines of neck nodal levels (3) and primary tumours (4) are based on patients scanned in a neutral neck position. Immobilisation and treatment of HNC in this position may be better tolerated, particularly on the MR-Linac where each fraction time is expected to be lengthier than conventional treatment. Each HNC radiotherapy treatment session is estimated to last between 40 to 50 minutes, similar to the reported time for prostate cancer treatment on the MR-Linac (5). This is in contrast to a conventional linac where HNC IMRT and VMAT can be delivered in under 7 minutes (6). Therefore, patients must remain as comfortable as possible to tolerate and complete the 30 treatment fractions on the MR-Linac. This may be more achievable in the neutral neck position. However, there are no formal reports that

compare the dosimetric differences of treatment delivery in an extended versus neutral neck position to surrounding head and neck structures.

7.2 Aims

This study first investigates the impact of the neck treatment position on the radiotherapy doses delivered to the oral cavity, posterior cranial fossa, parotid glands and mandible. These regions of interest (ROIs) are chosen as excessive doses have been associated with acute mucositis (7), acute fatigue(8), xerostomia (1) and osteoradionecrosis (9), respectively.

The impact of the neck treatment position on dosimetry is investigated in both node-negative and node-positive oropharyngeal cancers (OPC). A node-positive OPC cohort is included as this group of patients required a larger nodal irradiation volume (including level Ib and often level VIIb). Therefore, this will evaluate the effect of radiotherapy volume on the dosimetry to the ROIs in both neck positions.

If a difference in ROI dosimetry between the two neck positions is identified, the effectiveness of re-optimising the radiotherapy plans to reduce ROI doses will be investigated.

7.3 Hypotheses

Radiotherapy treatment in a neutral neck position will lead to increased radiation dose delivered to the oral cavity, parotid glands, posterior fossa and mandible compared to extended neck position, irrespective of the nodal irradiation volumes. Optimising the radiotherapy treatment plans with an oral cavity dose constraint will reduce radiotherapy doses to the ROIs.

7.4 Objectives

- To assess the dosimetric differences (mean dose and/or dose-volume assessments) to the oral cavity, mandible, parotid glands and posterior cranial fossa in the node-positive and node-negative neck in both neck positions.
- To optimise the radiotherapy plans using a dose constraint to the oral cavity and to assess the dosimetric differences (mean dose and/or dose-volume assessments) to the oral cavity, mandible, parotid glands and posterior cranial fossa in the node-positive and node-negative neck in both neck positions.

7.5 Materials and methods

7.5.1 Study design

This was a retrospective radiotherapy planning study that used the radiotherapy CT data of patients treated at the Sutton branch of Royal Marsden Hospital. All patients had consented to their CT imaging being analysed for research purposes. A total of twenty patients with HNC were retrospectively identified with 1:1 ratio in the neutral and extended neck positions. The CT scans in these positions were obtained from patients with oral or nasal cavity cancers, and oropharyngeal cancers, respectively.

As OPC HNC patients were treated in an extended neck position at the Royal Marsden Hospital, there were no comparable OPC patients treated in a neutral neck position. To enable comparison between both groups of patients, I simulated a base of tongue primary cancer, irrespective of the patient's treated primary tumour site. A base of tongue cancer was chosen as this tumour requires bilateral neck irradiation and commonly has level II nodal involvement. For each patient, I generated two radiotherapy plans: one for a node-negative neck and a second simulating a node-positive neck.

7.5.2 Radiotherapy treatment

7.5.2.1 *Planning CT Image acquisition*

The patients were immobilised in a custom-made five-point thermoplastic immobilisation shell and underwent a contrast-enhanced planning CT on a large-bore CT scanner (Philips Medical, Cleveland, OH, USA). The images were acquired in 2 mm slice thickness.

7.5.2.2 *Target volume delineation*

Primary Gross tumour volume (GTV-p)

A GTV-p representing a central base of tongue was simulated in both cohorts, irrespective of the patient's primary tumour site. I used an identical method to generate this GTV-p in all patients. The GTV-p was simulated by creating a 1 cm radius sphere centred in the midline. The GTV-p was translated so that the caudal border was situated at the level of the vallecula as shown in Figure 7-1.

Figure 7-1. Delineation of the GTV-p (orange) using a sphere with a 1 cm radius. Sagittal CT slices of a patient in a neutral neck position (A) and extended neck position (B) are shown.

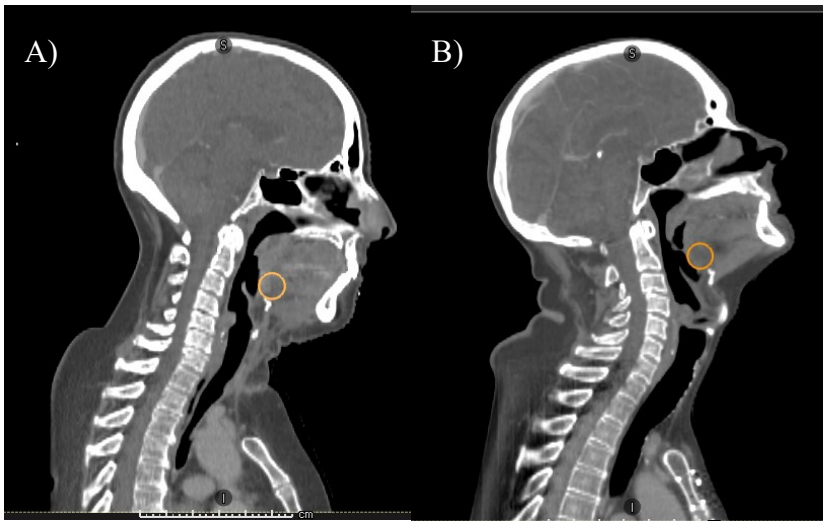

7.5.2.3 *Clinical Target Volume (CTV)*

A volumetric 2-dose level approach to define the target volumes.

CTV65:

The GTV was expanded with a 5 mm isotropic margin to create the high-dose CTV65 as per international guidelines (4). In the neck node-positive cases, level II lymph node chains were included in the CTV65. I edited the CTV to exclude natural barriers to disease spread such as bone, muscle and air unless there was radiological evidence of tumour infiltration.

CTV54:

The low-dose CTV54 included a 5 mm isotropic expansion around the CTV65 and the lymph node chains at risk of microscopic metastases. In the node-negative neck, bilateral levels II, III, IV and VIIa were included. In the node-positive neck, bilateral levels Ib, III, IV, V, VIIa and VIIb neck lymph nodes were included.

Planning Target Volume (PTV)

The CTV65 and CTV54 were grown isotropically by 3 mm to generate uncropped PlanPTV65 and PlanPTV54 respectively. For the final dose reporting, PlanPTV65 was edited off external body contour by 5 mm to generate PTV65, which received a dose of 65.1 Gy. Similarly, PlanPTV54 was cropped from eternal body contour, and PTV65 to create PTV54, which received a dose of 54 Gy.

7.5.2.4 ***OARs (organs at risk) and ROIs delineation***

OARs

I delineated the parotid glands, spinal cord and brainstem on the planning CT using local and international guidelines (10). The mandible was delineated automatically by the treatment planning system, which I edited if needed.

Oral Cavity

For this study, the oral cavity volume included the extrinsic tongue muscles (hyoglossus, genioglossus, geniohyoid) but edited off any overlapping high-dose and low-dose PTVs. By excluding the PTVs, the doses received by the untreated oral cavity can be reported. The borders of the oral cavity were defined as per Table 7-1.

Table 7-1. Anatomical borders of the oral cavity.

Border	Anatomical site
Anterior	Mandible
Posterior	Hard Palate
Lateral	Mandible
Superior	Air or hard palate
Inferior	Mylohyoid muscle

7.5.3 Planning procedure

I generated radiotherapy plans on a research version of RayStation treatment planning system (version 8.0, RaySearch Laboratories, Stockholm, Sweden) for each patient using an identical procedure. The same objective function and number of optimisation iterations were used in each case. Plans were dual-arc, 6-MV (megavolts) VMAT treatments. Each generated plan was reviewed and approved by an experienced radiotherapy physicist (Dualta McQuaid).

7.5.3.1 *IMRT plans*

Plan design

The plans were generated and optimised using the collapsed cone version 5.0 algorithm in RayStation.

Beam design

A dual-arc VMAT was selected to generate the RT plans to replicate treatment delivered in the clinical setting. All the RT plans consisted of two 6-MV 360º arcs with collimator angles of 3º. Each arc consisted of 180 control points with 2º control point spacing, leaf motion constraint of 0.8 cm/degree, and a maximum delivery time of 90 seconds.

Beam optimisation

Non-anatomical volumes were added to guide the treatment planning system to provide an optimal plan. These included ring structures around the PTVs to increase dose conformality and homogeneity, together with the application of the dose fall-off optimising function to reduce dose to non-target tissue. This function penalises dose that exceeds the specified dose fall-off away from the target and is defined by 3 parameters: the high-dose parameter representing the high-dose within the target; the low-dose parameter representing the acceptable dose within the surrounding healthy tissue; and the distance parameter representing the distance at which the high dose will have fallen to the low dose.

To avoid the treatment planning system from boosting target tissue within the build-up region of the patient, a virtual bolus (density = 1.0 g/cm^3) was generated exterior to the body contour such that PlanPTV65 and PlanPTV54 were always at least 1 cm from either the external body contour or the virtual bolus surface (11). Once a satisfactory plan was generated, virtual bolus was removed, the dose re-prescribed to PTV65, and the final dose was computed. The radiotherapy plan was re-evaluated to ensure optimal coverage was maintained.

Planning objectives

The baseline dose-based and dose-volume-based objectives were designed for the inverse planning optimisation process, in order to satisfy the clinical planning goals (Table 7-2 and Table 7-3). Each optimisation sequence consisted of 40 automated iterations. All plans were created using an identical method, 3 optimisations of 40 iterations with a virtual bolus in place, with repeat scaling the dose to the prescription, defined as 65.1 Gy on the full PTV between each optimisation. Finally, the bolus was removed, and the prescription applied to the reduced PTV (contracted by 5 mm from the patient's surface) before a final dose calculation and dose rescale to match the prescription.

Table 7-2. Planning target volume (PTV) constraints for VMAT planning.

Volume (%)	Dose (%)	
	PTV65	PTV54
99	> 90	>90
98	> 95 (optimal)	>95 (optimal)
95	> 95	> 95
50	= 100	= 100
5	< 105	< 105 (optimal)
2	< 107 (optimal)	<110 (optimal)

Abbreviation: PTV = planning target volume

Table 7-3. Dose constraints for organs at risk (OARs).

Structure	Constraint	Mandatory Dose constraint (Gy)	Optimal Dose constraint (Gy)
Spinal Cord	Max 1 cm^3	< 48 < 46	
Spinal Cord PRV	1 cm^3	< 48	
Brainstem	Max 1 cm^3	< 55 < 54	
Brainstem PRV	1 cm^3	< 56	
Contralateral Parotid	Mean dose	As low as possible	< 24 Gy
Ipsilateral Parotid	Mean dose	As low as possible	< 24 Gy

Abbreviation: PRV = planning organ at risk volume

Dose prescription

In accordance with ICRU 83, the prescription was to the median dose point on the DVH such that the prescription dose of 65.1 Gy was received by 50% of the PTV65.

Dose delivered to OARs

The mean dose delivered to the oral cavity, mandible, parotid glands were tabulated and analysed. The dose-volume histograms (DVH) parameters were also analysed and were defined as below:

Vx (%) which was defined as the percentage volume of the ROI receiving a dose of x Gy.

The clinical goals were also reviewed and analysed for each plan to assess for suitability of treatment delivery.

Optimised dose constraint to the oral cavity

The plans were optimised using a constraint of equivalent uniform dose (EUD) 10 Gy to the untreated oral cavity with a weighting of 0.02. EUD is a generalised biologically equivalent dose that, if given uniformly, will lead to the same cell kill as

the non-uniform dose distribution. Objective functions using EUD have been used to optimise IMRT and VMAT plans (12).

No planning objectives were made for the posterior cranial fossa in this study.

7.6 Statistical Analysis

The data were analysed using GraphPad Prism software (Version 8.2.0; San Diego, CA). Data were collected from the DVHs and were tabulated for each patient for each cohort. The data of interests were first assessed for normal distribution using the Shapiro-Wilk test. The differences between each cohort were compared using descriptive methods such as the mean and median values for parametric and non-parametric data, respectively. The independent *t*-tests and Mann-Whitney were used to compare the differences between data for parametric and non-parametric tests for unpaired data, respectively. The paired t-test and Wilcoxon test were used to compare the differences between data for parametric and non-parametric tests for paired data, respectively. Differences were defined as statistically significant at two-tailed p-values of ≤0.05.

7.7 Results

7.7.1 Lymph node-negative neck

*Table 7-4. Doses delivered to the oral cavity, mandible, parotid glands and posterior cranial fossa in node-negative patient cohorts. * indicates statistically significant, p<0.05.*

	Oral Cavity				Mandible				Parotid Glands				Posterior Cranial Fossa	
	Mean dose (Gy)		Volume (cm^3)		Mean dose (Gy)		Volume (cm^3)		Mean dose (Gy)		Volume (cm^3)		Mean dose (Gy)	
	Neutral	Extended	Neutral	Extended	Neutral	Extended	Neutral	Extended	Neutral	Extended	Neutral	Extended	Neutral	Extended
Mean	32.3	28.2	45.2	58.7	27.4	23.4	56.5	59.7	21.7	21.0			6.9	10.2
Standard deviation	3.0	3.6	7.4	12.0	3.0	4.5	12	7.1	1.3	1.7			3.2	3.8
Median											24.1	25.5		
Range											18.7 – 34.7	19.8 – 47.4		
p-value	0.0131*		0.0058*		0.0328*		0.4713		0.1909		0.3372		0.0480*	

Doses to the oral cavity

The oral cavity volumes and mean radiotherapy doses are summarised in Table 7-4. The mean oral cavity volume was significantly smaller in the neutral neck position at 45.2 cm^3 (standard deviation (SD)=7.4 cm^3) compared to 58.7 cm^3 (SD=12.0 cm^3) in the extended neck position (p=0.0058). The mean dose to the oral cavity in the neutral neck position (32.3 Gy, SD=3.0 Gy) was significantly larger than in the extended neck position (28.2 Gy, SD=3.6 Gy; p=0.0131). On average, a patient treated in the neutral neck position would receive 4.1 Gy (Standard error of mean 1.5 Gy) more than in the extended neck position.

Statistically significant differences were noted for the radiotherapy dose-volume assessments (Figure 7-2); the neutral neck position showed a significantly larger percentage oral cavity volume in the low-dose radiotherapy areas (V10 median=100%, range 87 to 100%; V20 median=87.5%, range 71 to 100%) compared to patients in the extended neck position (V10 median=91.5%, range 68 to 100%; V20 median=71%, range 50 to 97%; p=0.0105 and p=0.0241, respectively). There was no significant difference for the intermediate and high dose radiotherapy areas of V30, V40 and V50 (p=0.1095, p=0.4017 and p=0.1119, respectively).

*Figure 7-2. Dose-Volume assessment to the oral cavity in node-negative patient cohorts. Symbols represent the median values and the error bars represent the range. * indicates statistically significant, p≤0.05.*

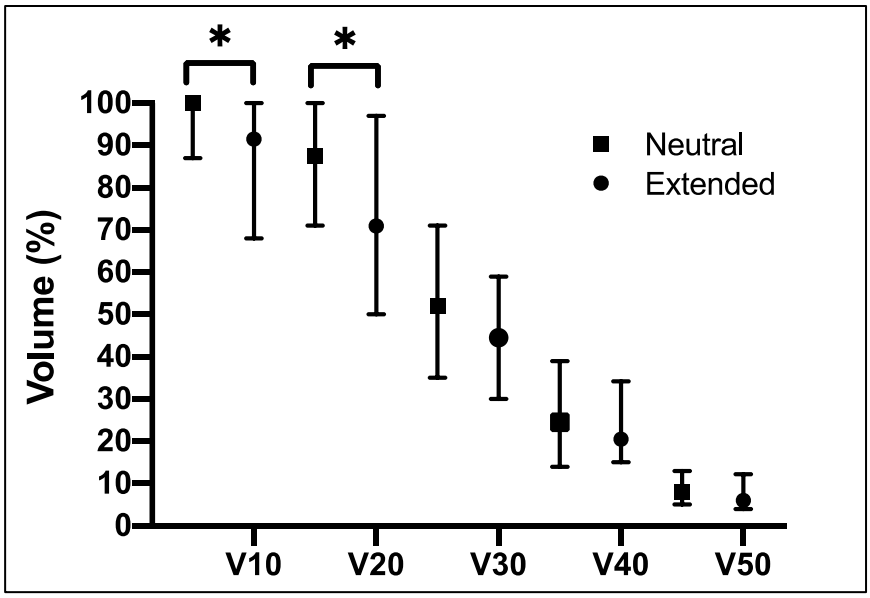

An example of the difference in dose distribution is illustrated in Figure 7-3, where a larger proportion of the oral cavity lies within the 20 Gy isodoses in the neutral neck position (A) compared to the extended neck position (B).

Figure 7-3. Sagittal view of radiotherapy planning CT and dosimetry plan for a node-negative patient with a neutral(A) and extended (B) neck position, respectively. The colourwash represents the isodoses. The green, green and yellow contours represent the oral cavity, posterior cranial fossa and the mandible, respectively.

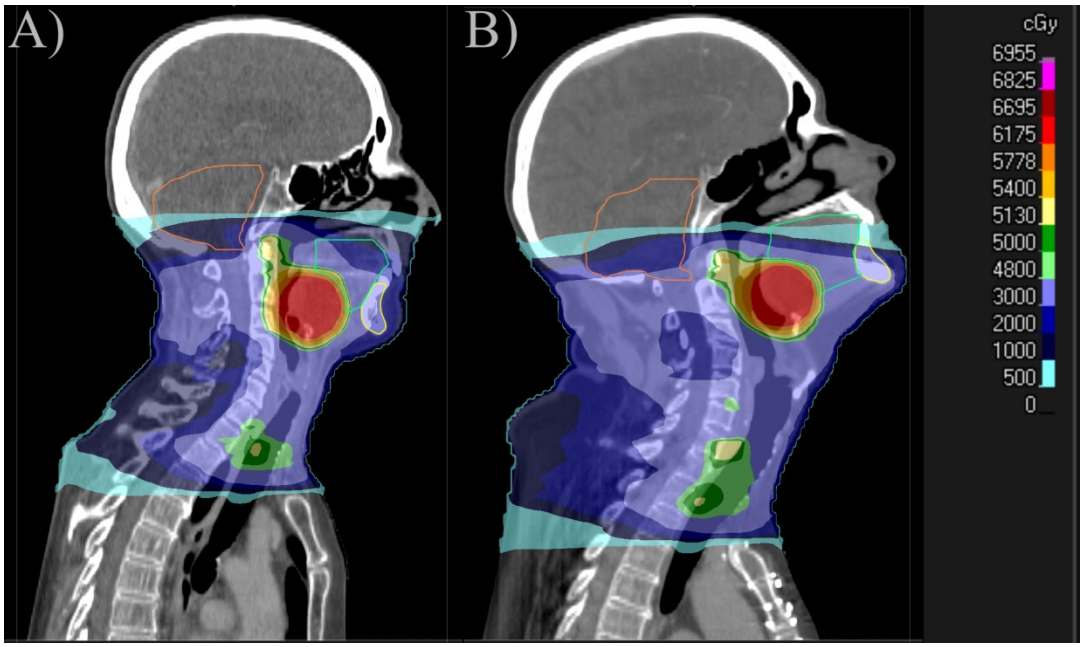

Doses to the mandible

The mandible volume and mean mandible dose are summarised in Table 7-4. There was no significant mandible volume difference between the two groups (p=0.4713). The mean dose to the mandible was significantly higher in the neutral neck at 27.4 Gy (SD=3.0 Gy) compared to an extended neck at 23.4 Gy (SD=4.5 Gy) (p=0.0328).

A statistically significant difference was noted for the radiotherapy dose-volume assessments (Figure 7-4); the neutral neck position showed a significantly larger percentage mandible volume in the low to intermediate dose radiotherapy areas (V10 median=88%, range 85 to 95%; V30 median=52%, range 24 to 77%) compared to patients in the extended neck position (V10, median=85%, range 52 to 90%; V30, median=36%, range 6 to 52%; p=0.0107 and p=0.0175, respectively). There was no significant difference for the V20 and V40 between the two groups (p=0.1092 and p=0.2666, respectively). An example of this difference is shown in Figure 7-3. In this example, a smaller volume of the mandible is located in the 30 Gy isodose in the extended neck position compared to the neutral neck position.

*Figure 7-4. Dose-Volume assessment to the mandible in node-negative patient cohorts. Symbols represent the median values and the error bars represent the range. * indicates statistically significant, p≤0.05.*

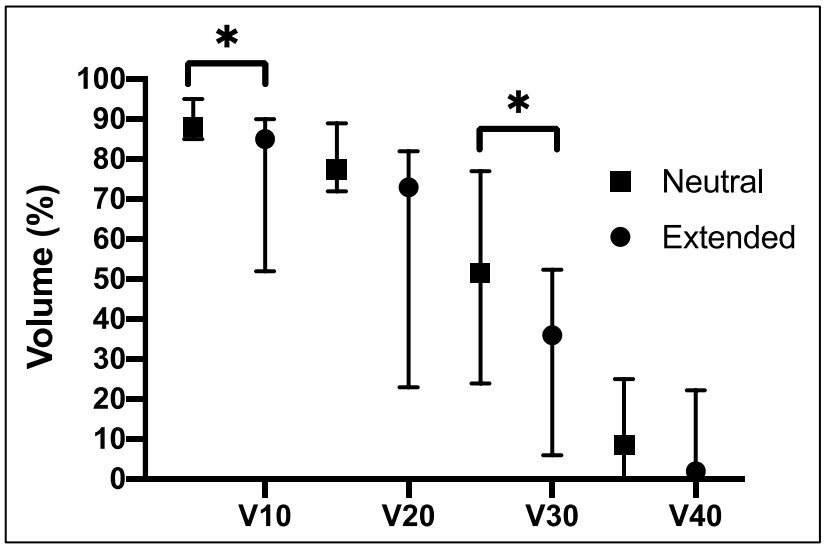

Doses to the parotid glands

There was no significant difference between the parotid volumes (p=0.3372) and mean parotid gland doses (p=0.1909) in the extended and neutral neck positions (Table 7-4).

Doses to the posterior cranial fossa

As summarised in Table 7-4, the mean posterior cranial fossa dose was significantly smaller in the neutral neck position 6.9 Gy (SD=3.2 Gy) compared to 10.2 Gy (SD=3.8 Gy) in the extended neck position (p=0.0480)

7.7.2 Lymph node-positive neck

*Table 7-5. Doses delivered to the oral cavity, mandible, parotid glands and posterior cranial fossa in node-positive patient cohorts. * indicates statistically significant, p≤0.05. The volumes are the same as in Table 8-4 and are not shown in this table.*

	Oral Cavity		Mandible		Parotid Glands		Posterior Cranial Fossa	
	Mean dose (Gy)		Mean dose (Gy)		Mean dose (Gy)		Mean dose (Gy)	
	Neutral	Extended	Neutral	Extended	Neutral	Extended	Neutral	Extended
Mean	36.3	31.3	36.2	31.4	22.8	22.8	14.2	18.6
Standard deviation	2.7	3.4	2.7	4.0	1.4	1.2	3.05	3.18
p-value	0.0018*		0.0054*		0.9610		0.0057*	

Doses to the oral cavity

The mean dose to the oral cavity was significantly larger in the neutral neck position with a mean dose of 36.3 Gy (SD=2.7 Gy) compared to 31.3 Gy (SD=3.4 Gy) in the extended neck position (p=0.0018) (Table 7-5). On average, a patient treated in the neutral neck position would receive 5.4 Gy (standard error of mean 1.4 Gy) more than a patient scanned in the extended neck position.

A statistically significant difference was noted for the radiotherapy dose-volume assessments (Figure 7-5); the neutral neck position showed a significantly larger percentage oral cavity volume in the low to intermediate radiotherapy dose areas (V20 median=99.5 % , range 89.0 to 100%; V30 median=74.5%, range=46.0 to 91.0%) compared to patients in the extended neck position (V20 median=78.0%, range 64.0 to 98.0 %; V30 median=45.5%, range=30.0 to 64.0%; p=0.0009 and p=0.0002, respectively). There was no significant difference for the percentage oral cavity volume receiving the higher doses of 40 Gy and 50 Gy (p=0.1933 and p=0.8669, respectively) or the low dose of 10 Gy (p=0.4737).

*Figure 7-5. Dose-Volume assessment to the oral cavity in node-positive patient cohorts. Symbols represent the median values and the error bars represent the range. * indicates statistically significant, p≤0.05.*

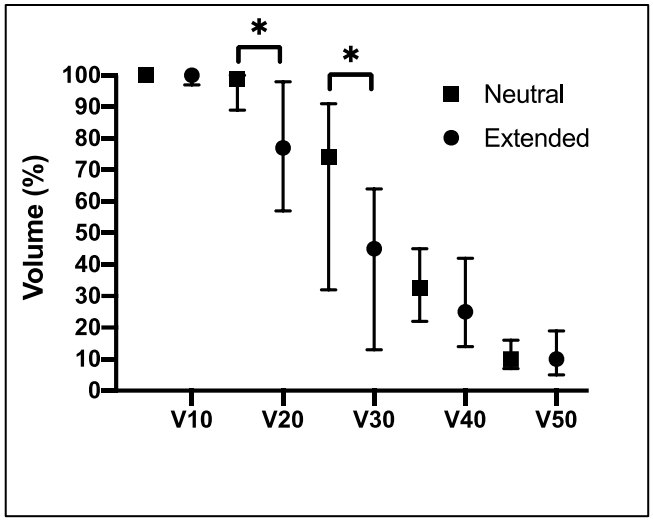

An example is illustrated in Figure 7-6 where the oral cavity receives a greater proportion of the 20 Gy and 30 Gy isodoses in the neutral neck position compared to the extended neck position.

Figure 7-6. Sagittal view of radiotherapy planning CT and dosimetry plan for a node-positive patient with a neutral(A) and extended (B) neck position, respectively. The colourwash represents the isodoses. The green, red and yellow contours represent the oral cavity, combined PTV65 and PTV54, and the mandible, respectively.

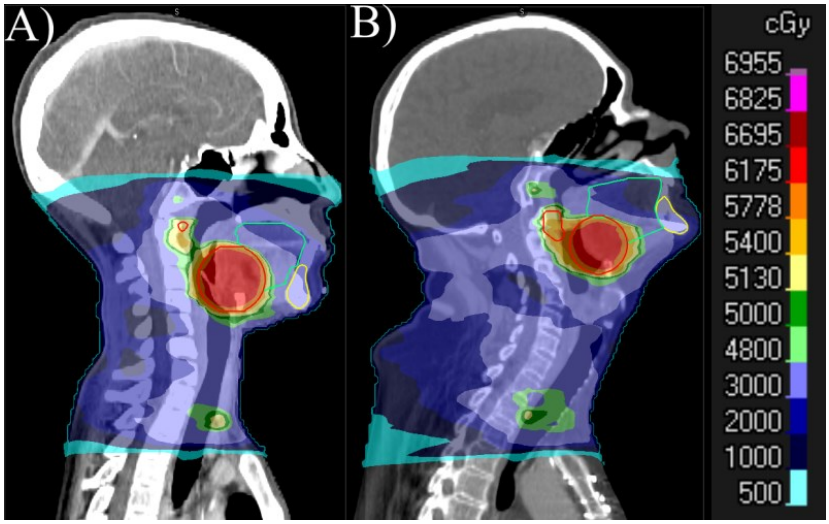

Doses to the mandible

The mean mandible dose was significantly higher in the neutral neck position compared to the extended neck position (36.2 Gy (SD=2.7 Gy) *vs.* 31.4 Gy (SD=4.0 Gy), p=0.0054) (Table 7-5). A statistically significant difference was noted for the radiotherapy dose-volume assessments (

Figure 7-7); the neutral neck position showed a significantly larger percentage mandible volume in the intermediate to high dose radiotherapy areas (V30 median=89.0%, range 84.0 to 95.0%; V40 median=75.5%, range 58.0 to 87.0%) compared to patients in the extended neck position (V30 median=79.5%, range 62.0 to 92.0%; V40 median=52.0%, range %; p=0.0026 and p=0.0014, respectively). There was no significant difference between the two groups for V10 (p=0.4086), V20 (p=0.1614) and V50 (p=0.059).

*Figure 7-7. Dose-Volume assessment to the mandible in node-positive patient cohorts. Symbols represent the median values and the error bars represent the range. * indicates statistically significant, p≤0.05.*

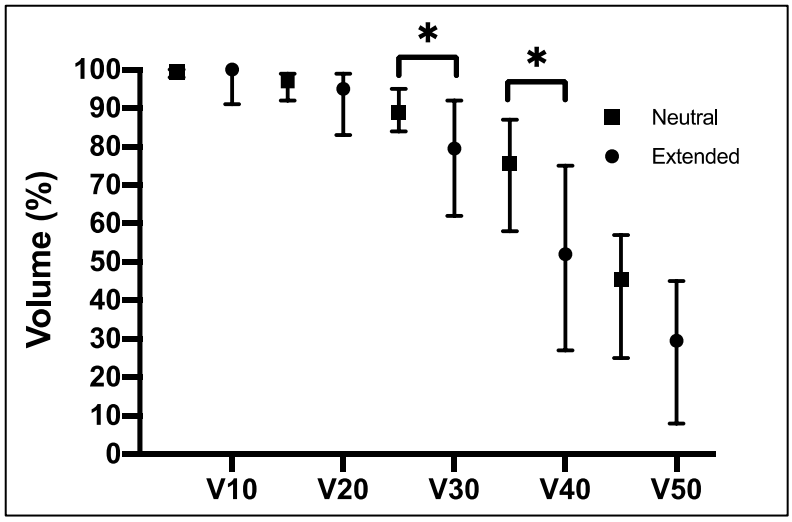

Doses to the parotid gland

Patient neck position did not lead to any significant differences to the doses delivered to the parotid glands (p=0.9610) (Table 7-5).

Doses to the posterior cranial fossa

A neutral neck position led to a significantly smaller mean dose to the posterior cranial fossa (14.2 Gy (SD=3.05 Gy)) compared to the extended neck position (18.6 Gy (SD=3.18 Gy); p=0.0057) (Table 7-5).

7.7.3 Dosimetry using an oral cavity dose constraint

Doses to the oral cavity

As expected, optimising the treatment plan with an oral cavity dose constraint led to a reduction of the mean oral cavity dose, irrespective of the neck position and neck node status (Figure 7-8). In the node-negative neck, the mean oral cavity dose was significantly smaller with an oral cavity dose constraint compared to standard treatment in the neutral (22.9 Gy (SD=1.6 Gy) *vs.* 32.3 Gy (SD=3.0 Gy), $p<0.0001$) and extended neck positions (21.0 Gy (SD=2.0 Gy) *vs.* 28.2 Gy (SD=3.6 Gy), $p<0.0001$). Similarly, in the node-positive neck, the mean oral cavity dose was significantly smaller with an oral cavity dose constraint compared to standard treatment in the neutral (26.4 Gy (SD=1.6 Gy) *vs.* 35.3 Gy (SD=2.7 Gy), $p<0.0001$) and extended neck positions (25.0 Gy (SD=2.9 Gy) *vs.* 31.3 (SD=3.4 Gy), $p<0.0001$).

*Figure 7-8. Mean oral cavity dose with and without the use of an oral cavity dose constraint. Symbols represent the mean values and the error bars represent the standard deviation. * indicates statistically significant, p≤0.05.*

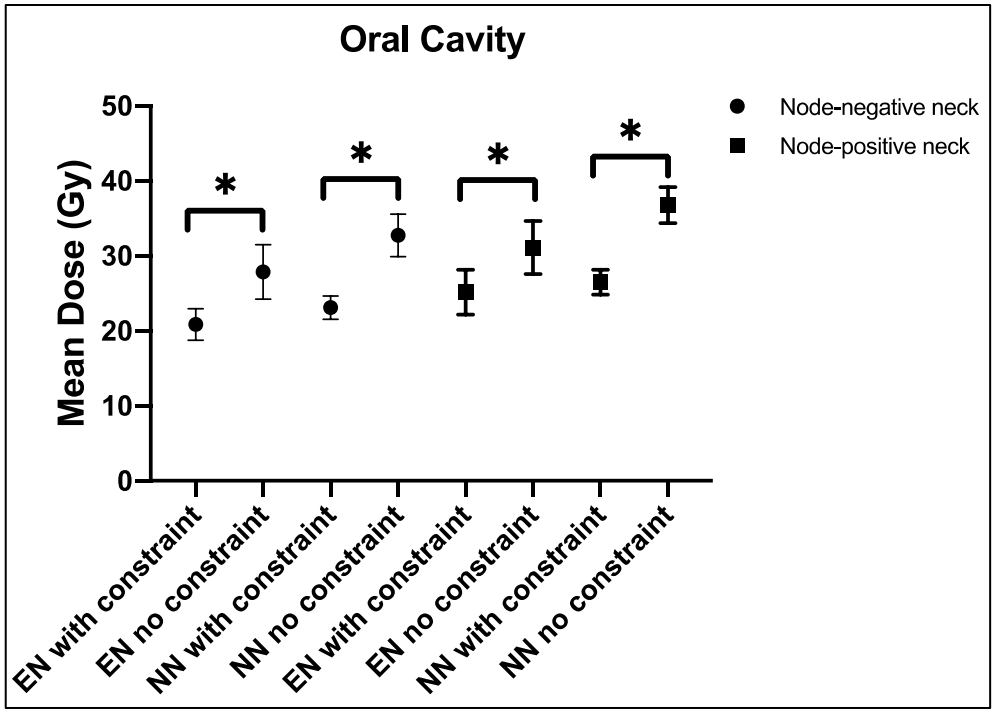

Abbreviations: EN = Extended neck; NN = neutral neck.

Doses to the mandible

By introducing a dose constraint to the oral cavity, the mean mandible dose was reduced, irrespective of the neck position and neck node status (Figure 7-9). In the node-negative neck, the mean mandible dose was significantly smaller with an oral cavity dose constraint compared to standard planning in the neutral (26.5 Gy (SD=3.0 Gy) versus 27.4 Gy (SD=3.0 Gy), p<0.0024) and extended neck positions (21.9 Gy (SD=4.5 Gy) versus 23.4 (SD=4.5 Gy), p=0.0002). Similarly, in the node-positive neck, the mean mandible dose was significantly smaller with an oral cavity dose constraint compared to standard planning in the neutral (35.5 Gy (SD=3.0 Gy) versus 36.2 Gy (SD=2.7 Gy), p=0.0495) and extended neck positions (30.1 Gy (SD=4.2 Gy) versus 31.4 (SD=4.0 Gy), p<0.0001).

*Figure 7-9. Mean mandible dose with or without the use of an oral cavity dose constraint. Symbols represent the mean values and the error bars represent the standard deviation. * indicates statistically significant, p≤0.05.*

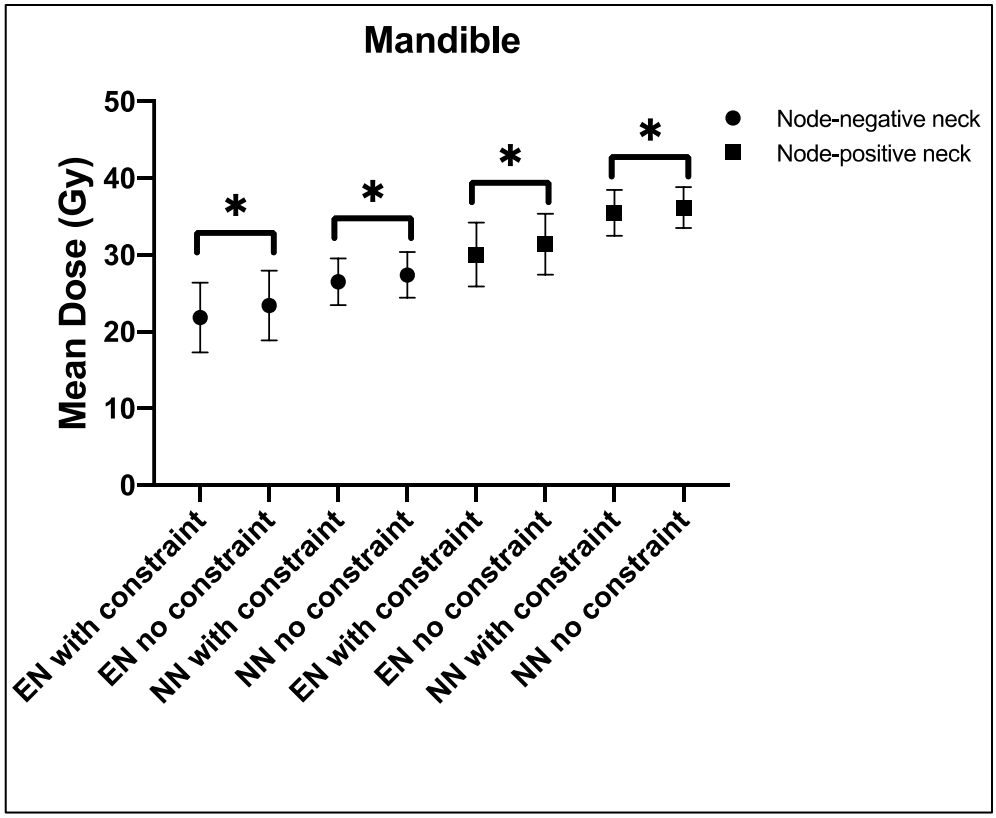

Abbreviations: EN = Extended neck; NN = neutral neck.

Doses to the parotid glands

There was no significant difference in mean parotid gland dose between the oral cavity optimised radiotherapy plans and the standard plan, irrespective of the neck position and neck nodal status (Figure 7-10). In the node-negative extended neck, the mean parotid gland dose was 21.0 Gy (SD=1.8 Gy) and 21.0 Gy (SD=1.7 Gy) for the oral cavity optimised and standard plans, respectively, (p=0.9905). In the node-negative neutral neck, the mean parotid gland dose was 22.4 Gy (SD=1.1 Gy) and 21.7 Gy (SD=1.3Gy) for the oral cavity optimised and standard plans, respectively (p=0.1076). In the node-positive extended neck, the mean parotid gland dose was 22.4 Gy (SD=1.0 Gy) and 22.9 Gy (SD=1.3 Gy) for the oral cavity optimised and standard plans, respectively (p=0.1866). In the node-positive neutral neck, the

mean parotid gland dose was 22.9 Gy (SD=1.3 Gy) and 22.8 Gy (SD=1.4Gy) for the oral cavity optimised and standard plans, respectively (p=0.7306).

*Figure 7-10. Mean parotid gland dose with or without the use of an oral cavity dose constraint. Symbols represent the mean values and the error bars represent the standard deviation. * indicates statistically significant, p≤0.05.*

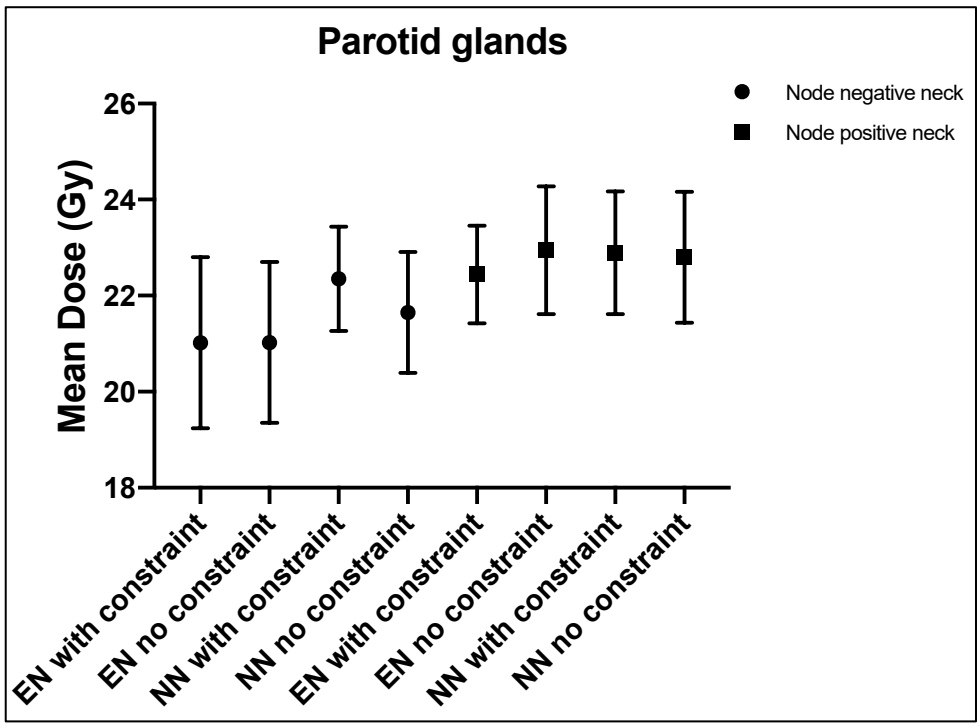

Abbreviation: EN = Extended neck; NN = neutral neck.

Doses to the posterior cranial fossa

In the node-negative neck, optimising the treatment plan with an oral cavity dose constraint led to a significant reduction in the mean posterior cranial fossa radiotherapy doses compared to standard treatment for both extended (9.5 Gy (SD=3.6 Gy) *vs.* 10.2 Gy (SD=3.8 Gy), p<0.0001) and neutral (6.4 Gy (SD=3.1 Gy) *vs.* 6.9 Gy (SD=3.2 Gy), p<0.0009) neck positions (Figure 7-11). In the node-positive neck, an oral cavity dose constraint did not lead to any significant difference in the extended (18.6 Gy (SD=3.2 Gy) *vs.* 18.5 Gy (SD=2.7 Gy), p=0.7934) and neutral neck positions (14.0 Gy (SD=3.2 Gy) *vs.* 14.2 Gy (SD=3.1 Gy), p=0.2266).

*Figure 7-11. Mean posterior cranial fossa dose with and without the use of an oral cavity dose constraint. Symbols represent the mean values and the error bars represent the standard deviation. * indicates statistically significant, p≤0.05.*

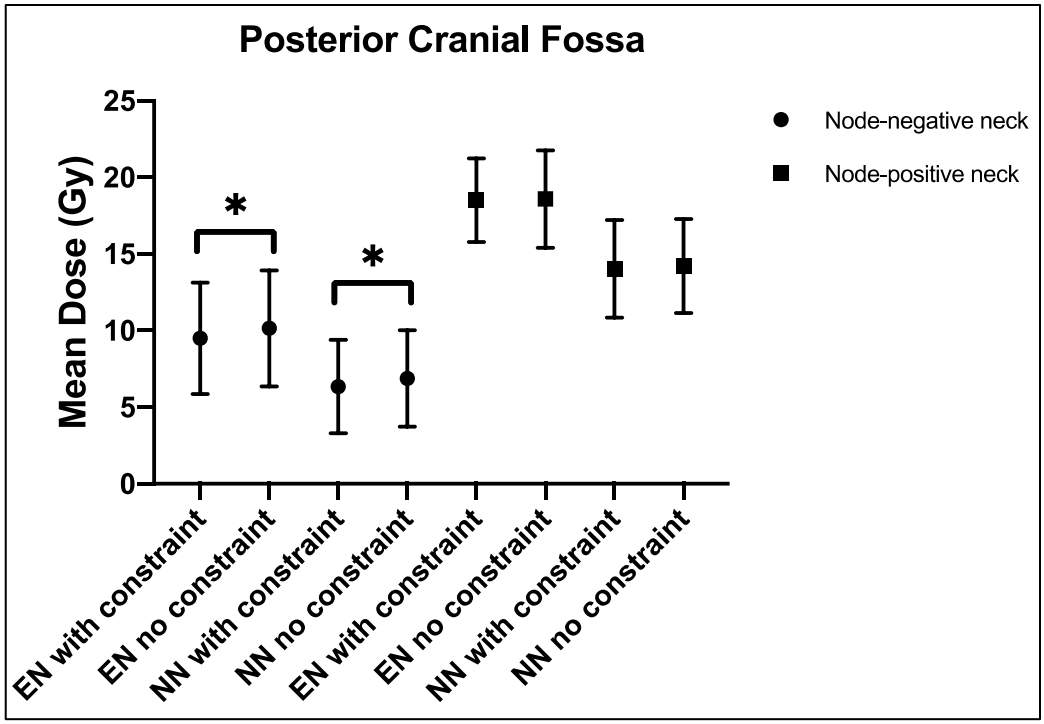

Abbreviation: EN = Extended neck; NN = neutral neck.

7.8 Discussion

In this study, I demonstrated that radiotherapy treatment neck position influenced the mean doses delivered to the oral cavity, mandible and posterior cranial fossa but not to the parotid glands.

A neutral neck position significantly increased the mean radiotherapy doses to the oral cavity and mandible compared to an extended neck position, irrespective of the extent of the lymph node target volumes. In the neutral neck position, a significantly larger percentage volume of the oral cavity received a low dose (10 to 20 Gy) and low to intermediate dose (20 to 30 Gy) in the node-negative neck and node-positive neck, respectively, compared to the extended neck position. Neck extension led to the stretching of the oral cavity which was reflected by a significantly larger volume compared to the neutral neck position. This larger volume may have contributed to the smaller mean dose to the oral cavity in the extended neck position. Compared to an extended neck position, a neutral neck position led to a significantly larger percentage volume of the mandible receiving a low to intermediate dose (10 and 30 Gy) and intermediate to high dose (30 to 40 Gy) in the node-negative neck and node-positive neck, respectively. Conversely, the mean posterior cranial fossa dose was significantly reduced in the neutral neck position compared to an extended neck position, irrespective of the extent of the lymph node target volumes.

As the deposited doses are a combination of dose build-up and scattered dose, these dosimetric differences can be explained by the position of these structures relative to the treatment fields; neck extension led to a proportion of the mandible and oral cavity to move out of the radiotherapy treatment field, whilst moving a greater proportion of the posterior fossa into the treatment field (Figure 7-12). The higher ROI doses observed in a node-positive neck may be explained by the addition of levels Ib and VIIb in the low dose CTV

and the inclusion of level II nodes in the high dose CTV, which led to a higher 'dose bath' to these structures.

Figure 7-12. Sagittal views of the radiotherapy CT plan of patients with node-negative and extended neck (A), node-negative and neutral neck(B), node-positive and extended neck (C) and node-positive and neutral neck (D). Yellow line illustrates the beam edge of one of the anterior VMAT beams. The oral cavity, mandible and posterior fossa are delineated in green, yellow and orange, respectively. The colourwash represent the isodoses.

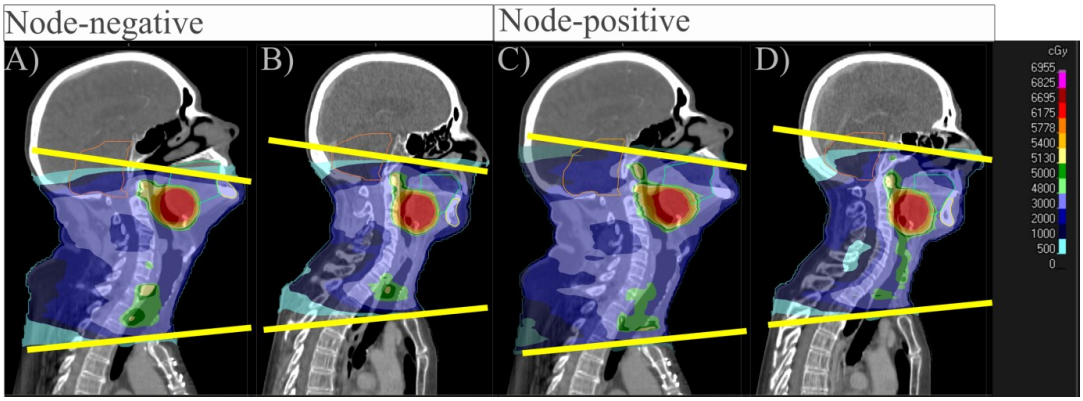

To put these dosimetric differences into clinical context, excessive dose to the oral cavity, mandible and posterior fossa have been associated with acute oral mucositis (7), osteoradionecrosis (13) and acute fatigue (8), respectively.

Oral mucositis is a common and self-limiting side-effect of HNC radiotherapy, but it is associated with pain, impaired nutrition, decreased quality of life and may hinder treatment completion in severe cases (14). Although radiotherapy dose constraint for acute oral mucositis has not been defined, the risk and grade of acute mucositis may be related to a cumulative dose threshold (15) and dose-volume relationship (7,16), respectively. A mean dose smaller than 32 Gy has been associated with minimal acute mucositis (15) and this was exceeded in the neutral neck position in both node-positive and node-negative patients. Shogan *et al.* reported that a V15 of 69%, V30 of 61%, V40 of 30% and V45 of 10% significantly correlated with the grade of acute mucositis (7). In this study, the V30 and V40 exceeded this threshold in the node-positive neutral neck only, suggesting that these patients may be at higher risk of high-grade mucositis. Overall, the results in this study suggested that a neutral neck position would increase the risk of acute oral mucositis, irrespective of

neck nodal status. However, it is important to note that these studies had important differences to this study. First, the oral mucosa was defined as the upper aerodigestive tract mucosa (oral cavity, oropharynx and hypopharynx) (7,17) and second, it was unclear from their study what extent of lymph nodes and neck position that the patients were treated in (7,15).

Osteoradionecrosis of the mandible is a debilitating radiotherapy treatment sequelae (9) that can negatively impact on a patient's quality of life (18). However, osteoradionecrosis is uncommon in the modern era of IMRT, with an incidence of less than 5% (13,19,20). The mean radiotherapy dose threshold associated with a significant risk of osteoradionecrosis is based on several retrospective and single-centre studies and is estimated to range between 40 to 60 Gy (13,21,22). Although a neutral neck position was associated with a higher mean mandible dose, the mean doses were smaller than this threshold of 40 to 60 Gy and would not place the patient at higher risk of osteoradionecrosis. Other studies have suggested that the risk of osteoradionecrosis may instead be related to the mandible volume within the high 'dose bath' of 40 to 60 Gy (22,23). In a retrospective case-control study by Mohamed et al., the mandible V44 ≥ 42% and V58 ≥ 25% were associated with osteoradionecrosis (22). In this study, this dose was exceeded in the node-positive neck only, with mean V40 of 73.5 % (SD 9.3 %) and 50.5 % (SD 17.0 %) in the neutral and extended neck positions, respectively. Reducing these doses may be difficult without compromising target coverage as this increased dose resulted from the inclusion of the nodal levels Ib and VIIb, and II in the low- and high-dose PTVs, respectively.

In this study, a neutral neck position led to a smaller mean dose to the posterior fossa in both neck node-negative and positive groups. The mean dose observed in the node-positive group was higher due to the inclusion of the level VIIb lymph nodes. In the phase III parotid sparing study (PARSPORT study) (1), patients in the IMRT treatment arm suffered from

increased rates of acute fatigue compared to the conventional radiotherapy arm. This was due to an increased dose to brain structures such as the posterior fossa (8). In their study, the mean posterior fossa doses in the IMRT arm was 25 Gy (8). This was higher than the mean doses observed in this study, which could be secondary to differences in defining the low-dose and high-dose target volumes. There was no significant difference to the mean parotid gland dose. This was not surprising as both parotids were given dose constraints to which the radiotherapy planning system adhered to.

Optimising the treatment plan with an oral cavity dose constraint led to a significant reduction in mean dose to the oral cavity in both neutral and extended neck positions, irrespective of neck node status. This led to a reduction below the 32 Gy threshold in the previously exceeded neutral neck, and a further reduction in dose in the extended neck position. This optimisation method also led to a significant reduction in the mean doses to the mandible in both extended and neutral neck positions, irrespective of neck node status. For the posterior cranial fossa, there was only significant reduction in mean dose for the node-negative cohort only. In the node-positive cohorts, treatment of the level VIIb lymph nodes led to increased dose to the posterior cranial fossa. Optimising the plan using posterior cranial fossa dose constraint in addition to an oral cavity dose constraint was no investigated in this study. Although it may be tempting to spare the oral cavity as much as possible, stringent dose objectives can lead to an increase in radiotherapy doses deposited the other important surrounding OARs (17). An example of this is shown in Figure 7-13. A smaller proportion of the oral cavity is covered by the 15 Gy isodose (panels A, D, G, J) compared to a normal plan (panels B, E, H, K). The differences in isodoses in those particular axial CT slices are shown in panels C, F, I and L. The addition of an oral cavity dose constraint led to extra doses being deposited (green arrows) and posteriorly (red arrows). This is more pronounced in the neutral neck position compared to the extended neck position where up to an extra mean dose of 3.3

Gy is deposited anteriorly in the masseter muscles (Figure 7-13I and L). Increased dose to the masseter muscles could lead to long-term side effects such as trismus.

Figure 7-13. Oral cavity optimised plans (A, D, G, J) and normal plans (B, E, H, K). Difference between optimised and normal plans (C, F, I and L). The additional dosse deposited anteriorly and posteriorly using the oral cavity dose constraint are indicated by the green and red arrows, respectively. The oral cavity (cyan), left parotid (yellow), right parotid (orange), PTV 54 (purple) are the delineated ROIs. The different isodoses are indicated by the respective colourwash.

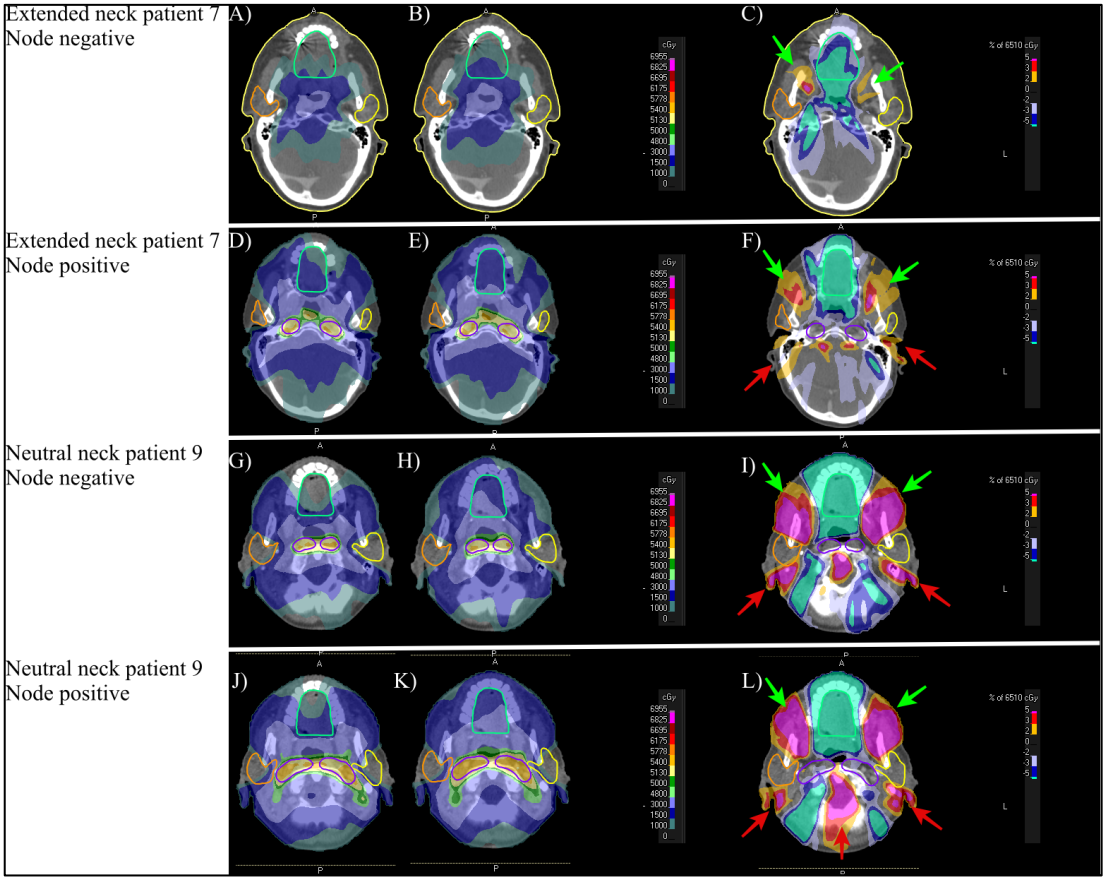

This study has certain limitations. The patients in both groups were not paired. Therefore, the dosimetric differences reported in this study may be due to unaccounted confounding factors. Without clinical guidelines to define the neutral or extended neck position during the immobilisation process, the degree of head and neck extension or flexion was driven by a combination of patient comfort and experience by the mould room technicians. Thus, the head and neck positions were variable in both cohorts. An OPC tumour was stimulated in both cohorts as there were no OPC patients scanned in the neutral neck position. A BOT tumour was simulated as it was centrally located and not immediately posterior to the oral

cavity. Therefore, it offered the ‘best case scenario’ to assess the oral cavity sparing achieved for OPC using different neck positions.

In summary, irrespective of the neck nodal status, oropharyngeal cancer treatment in a neutral neck position led to an increase in mean dose to the oral cavity and mandible, and a decreased mean dose to the posterior fossa compared to treatment in an extended neck position. An oral cavity dose constraint can be used to optimise the treatment plan to reduce doses to the organs. This benefit was seen in all but the node-positive neck for the posterior fossa.

7.9 Conclusion

Head and neck cancer treatment in a neutral neck position can be delivered without significant increased toxicities if an oral cavity dose constraint is used. This is particularly relevant for treatment on the MR-Linac where this treatment position will reduce the craniocaudal field length, increase the number of eligible patients and improve patient comfort and tolerance.

7.10 References

1. Nutting CM, Morden JP, Harrington KJ, et al. Parotid-sparing intensity modulated versus conventional radiotherapy in head and neck cancer (PARSPORT): A phase 3 multicentre randomised controlled trial. Lancet Oncol. 2011 Feb;12(2):127–36.

2. Clark CH, Miles EA, Guerrero Urbano MT, et al. Pre-trial quality assurance processes for an intensity-modulated radiation therapy (IMRT) trial: PARSPORT, a UK multicentre Phase III trial comparing conventional radiotherapy and parotid-sparing IMRT for locally advanced head and neck cancer. Br J Radiol [Internet]. 2009 Jul [cited 2019 Nov 26];82(979):585–94. Available from: http://www.birpublications.org/doi/10.1259/bjr/31966505

3. Grégoire V, Ang K, Budach W, et al. Delineation of the neck node levels for head and neck tumors: A 2013 update. DAHANCA, EORTC, HKNPCSG, NCIC CTG, NCRI, RTOG, TROG consensus guidelines. Radiother Oncol [Internet]. 2014 Jan [cited 2019 May 2];110(1):172–81. Available from: http://www.ncbi.nlm.nih.gov/pubmed/24183870

4. Grégoire V, Evans M, Le Q-T, et al. Delineation of the primary tumour Clinical Target Volumes (CTV-P) in laryngeal, hypopharyngeal, oropharyngeal and oral cavity squamous cell carcinoma: AIRO, CACA, DAHANCA, EORTC, GEORCC, GORTEC, HKNPCSG, HNCIG, IAG-KHT, LPRHHT, NCIC CTG, NCRI, NRG Oncology, PHNS, SBRT, SOMERA, SRO, SSHNO, TROG consensus guidelines. Radiother Oncol [Internet]. 2018 Jan 1 [cited 2018 Mar 25];126(1):3–24. Available from: http://www.ncbi.nlm.nih.gov/pubmed/29180076

5. Murray J, Tree AC. Prostate cancer – Advantages and disadvantages of MR-guided RT. Clin Transl Radiat Oncol [Internet]. 2019 Sep 1 [cited 2019 Oct 4];18:68–73. Available from: https://www.sciencedirect.com/science/article/pii/S2405630819300527

6. Van Gestel D, van Vliet-Vroegindeweij C, Van den Heuvel F, et al. RapidArc, SmartArc and TomoHD compared with classical step and shoot and sliding window intensity modulated radiotherapy in an oropharyngeal cancer treatment plan comparison. Radiat Oncol. 2013;

7. Shogan JE, Bhatnagar AK, Heron DE, et al. Dosimetric Correlation of Oral Cavity Dose with Acute Mucositis in Patients Treated with Intensity Modulated Radiation Therapy (IMRT) and Chemotherapy. Int J Radiat Oncol. 2005 Oct;63:S74–5.

8. Gulliford SL, Miah AB, Brennan S, et al. Dosimetric explanations of fatigue in head and neck radiotherapy: An analysis from the PARSPORT Phase III trial. Radiother Oncol. 2012;

9. Thorn JJ, Hansen HS, Specht L, et al. Osteoradionecrosis of the jaws: Clinical characteristics and relation to the field of irradiation. J Oral Maxillofac Surg. 2000 Oct 1;58(10):1088–93.

10. Brouwer CL, Steenbakkers RJHM, Bourhis J, et al. CT-based delineation of organs at risk in the head and neck region: DAHANCA, EORTC, GORTEC, HKNPCSG, NCIC CTG, NCRI, NRG Oncology and TROG consensus guidelines. Radiother Oncol [Internet]. 2015 Oct [cited 2019 May 2];117(1):83–90. Available from: https://linkinghub.elsevier.com/retrieve/pii/S0167814015004016

11. Thilmann C, Grosser KH, Rhein B, et al. Virtual bolus for inversion radiotherapy planning in intensity-modulated radiotherapy of breast carcinoma within the scope of adjuvant therapy. Strahlentherapie und Onkol. 2002;178(3):139–46.

12. Wu Q, Mohan R, Niemierko A, et al. Optimization of intensity-modulated radiotherapy plans based on the equivalent uniform dose. Int J Radiat Oncol Biol Phys [Internet]. 2002 Jan 1 [cited 2020 Jun 21];52(1):224–35. Available from: http://www.redjournal.org/article/S0360301601025858/fulltext

13. Aarup-Kristensen S, Hansen CR, Forner L, et al. Osteoradionecrosis of the mandible after radiotherapy for head and neck cancer: risk factors and dose-volume correlations. Acta Oncol (Madr) [Internet]. 2019 Oct 3 [cited 2020 Mar 19];58(10):1373–7. Available from: https://www.tandfonline.com/doi/full/10.1080/0284186X.2019.1643037

14. Trotti A, Bellm LA, Epstein JB, et al. Mucositis incidence, severity and associated outcomes in patients with head and neck cancer receiving radiotherapy with or without chemotherapy: A systematic literature review. Vol. 66, Radiotherapy and Oncology. Elsevier Ireland Ltd; 2003. p. 253–62.

15. Eisbruch A, Harris J, Garden AS, et al. Multi-Institutional Trial of Accelerated Hypofractionated Intensity-Modulated Radiation Therapy for Early-Stage Oropharyngeal Cancer (RTOG 00-22). Int J Radiat Oncol Biol Phys. 2010 Apr;76(5):1333–8.

16. Dean JA, Wong KH, Welsh LC, et al. Normal tissue complication probability (NTCP) modelling using spatial dose metrics and machine learning methods for severe acute oral mucositis resulting from head and neck radiotherapy. Radiother Oncol. 2016;

17. Sanguineti G, Endres EJ, Gunn BG, et al. Is there a “mucosa-sparing” benefit of IMRT for head-and-

neck cancer? Int J Radiat Oncol Biol Phys. 2006 Nov 1;66(3):931–8.

18. Rogers SN, D'Souza JJ, Lowe D, et al. Longitudinal evaluation of health-related quality of life after osteoradionecrosis of the mandible. Br J Oral Maxillofac Surg. 2015 Nov 1;53(9):854–7.

19. Moon DH, Moon SH, Wang K, et al. Incidence of, and risk factors for, mandibular osteoradionecrosis in patients with oral cavity and oropharynx cancers. Oral Oncol. 2017 Sep 1;72:98–103.

20. Caparrotti F, Huang SH, Lu L, et al. Osteoradionecrosis of the mandible in patients with oropharyngeal carcinoma treated with intensity-modulated radiotherapy. Cancer [Internet]. 2017 Oct 1 [cited 2020 Mar 19];123(19):3691–700. Available from: http://doi.wiley.com/10.1002/cncr.30803

21. Gomez DR, Estilo CL, Wolden SL, et al. Correlation of osteoradionecrosis and dental events with dosimetric parameters in intensity-modulated radiation therapy for head-and-neck cancer. Int J Radiat Oncol Biol Phys. 2011;

22. Mohamed ASR, Hobbs BP, Hutcheson KA, et al. Dose-volume correlates of mandibular osteoradionecrosis in Oropharynx cancer patients receiving intensity-modulated radiotherapy: Results from a case-matched comparison. Radiother Oncol. 2017 Aug 1;124(2):232–9.

23. Tsai CJ, Hofstede TM, Sturgis EM, et al. Osteoradionecrosis and radiation dose to the mandible in patients with oropharyngeal cancer. Int J Radiat Oncol Biol Phys. 2013;

8 Chapter 8 – Feasibility of daily MR-guided adaptive radiotherapy head and neck cancer treatment delivered on the MR-Linac

8.1 Introduction

Whilst treatment of oligometastatic, pelvic and breast cancers have been reported on the MR-Linac (1–4), head and neck cancer (HNC) treatment remains under evaluation.

At the Royal Marsden Hospital, HNC treatment will be delivered on the MR-Linac within the **P**rospective **E**valuation of **R**adiotherapy using **M**agnetic Resonance **I**mage-Guided **T**reatment (PERMIT) trial (CCR 4841) (5). This prospective trial enables delivery of standard-of-care radiotherapy on the MR-Linac and ongoing data collection to accelerate the technical and clinical development of MR-guided radiotherapy (MRgRT).

An adaptive MRgRT treatment can be delivered at each radiotherapy session on the MR-Linac. A summary of this workflow is shown in Figure 8-1. Before each fraction delivery, a MRI (session MRI) is first acquired. Following image co-registration with the baseline planning CT or MRI scan, the pre-treatment contours are propagated, manually inspected and amended (if needed). The treatment plan is adapted, evaluated and checked on a verification MRI scan before treatment delivery (Figure 8-1).

Figure 8-1. Summary of online treatment workflow on MR-Linac.

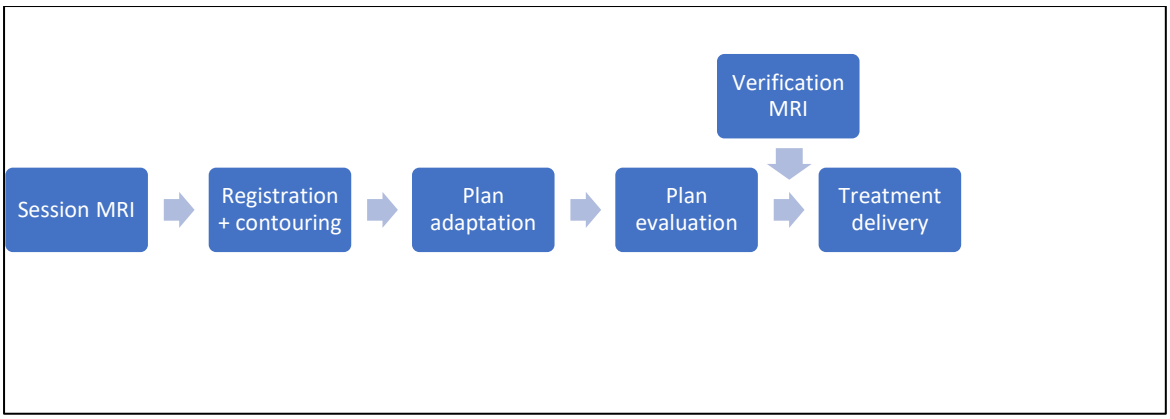

8.2 Aim

This chapter describes the treatment of the first HNC patient on the 1.5T unity Elekta Unity MR-Linac at the Royal Marsden Hospital. This chapter reports the feasibility, performance and dosimetric results of a daily online adaptive radiotherapy (ART) workflow.

8.3 Objective

- To assess the dosimetric differences to the target volume and organs at risk (OARs) between the adapted, non-adapted and the reference plans.

8.4 Hypothesis

ART will ensure that the target volume coverage and OARs doses do not deviate significantly from the planned doses and improve dosimetry compared to a non-adapted plan.

8.5 Methodology

8.5.1 Study design and patient selection

This is a single centre case report of the first HNC patient undergoing radiotherapy treatment on the MR-Linac at the Royal Marsden Hospital (Sutton Branch) within the PERMIT trial.

To be eligible for HNC treatment on the MR-linac, the following inclusion criteria were required:

- A craniocaudal PTV length of <20 cm due to field size constraint **(6)**.
- A visible tumour on the MR scan

Exclusion criteria:

- Claustrophobia
- Contra-indications to MRI such as a non-MRI compatible pacemaker.

8.5.2 Patient set-up

Acoustic noise protection

Double ear protection was used on the MR-Linac for acoustic noise reduction as per the imaging department's safety guidance. This consisted of foam earplugs and a pair of MR-compatible over-ear headphone. The earplugs were placed at the entrance of the ear canal (Figure 8-2A) whilst the headphone was placed over the thermoplastic shell (Figure 8-2F).

Radiotherapy thermoplastic shell

A five-point thermoplastic immobilisation shell was custom made in the mould room as per the standard procedure. This shell was used for the planning CT scan, planning MR scan and for treatment delivery.

Planning scans

Both CT and MR planning scans were acquired on the same day with the same immobilisation devices to enable accurate rigid registration.

A contrast-enhanced planning CT was acquired on a large-bore CT scanner (Philips Medical, Cleveland, OH, USA) in 2 mm slices. The patient was immobilised with the thermoplastic shell in the supine position on a head and neck board, with a foam headrest, black mattress, knee rest and the acoustic ear protection. A special table overlay was used to facilitate

reproducible positioning of the radiofrequency coil and approximate patient set-up using specific couch index points (Figure 8-2 B and C).

The planning MRI was acquired on the MR-Linac in the same position as the planning CT. In addition, an anterior flex coil and a posterior non-flex coil were used (Figure 8-2 E and F). A non-conducting foam material was placed between any radiofrequency coil component to reduce the risk of MRI-related radiofrequency burns (Figure 8-2 E) in areas that were in direct contact with the patient's skin. During the treatment delivery, a 1 cm sheet of wax bolus was placed over the chest to reduce the electron streaming effect (shown on a volunteer in Figure 8-2 D).

A T2-weighted sequence (Echo time/Repetition time, 90/2100 ms; 1.2 mm isotropic voxel size; field size 520 by 297 by 249 mm; 6 minutes) and a T2-weighted sequence (Echo time/Repetition time, 90/1535 ms; 1.5 mm isotropic voxel size; field size 400 by 400 by 300 mm; 2 minutes), and a 2D balanced fast field echo in three orthogonal directions for motion estimation were acquired. The MR imaging acquired on the MR-Linac was reviewed by a consultant radiologist with expertise in HNC (Dr Derfel ap Dafydd) and felt to be appropriate for the purpose of this study.

Figure 8-2. Patient set-up for the MR-Linac. Foam earplugs inserted in the ear canal(A); patient positioning on a table overlay (B and C); 1 cm bolus placed over areas at-risk of dose deposition from the electron stream effect (D); non-conducting foam material between the anterior radiofrequency coil and patient's skin (E); MRI-compatible headphones placed over the thermoplastic shell (F).

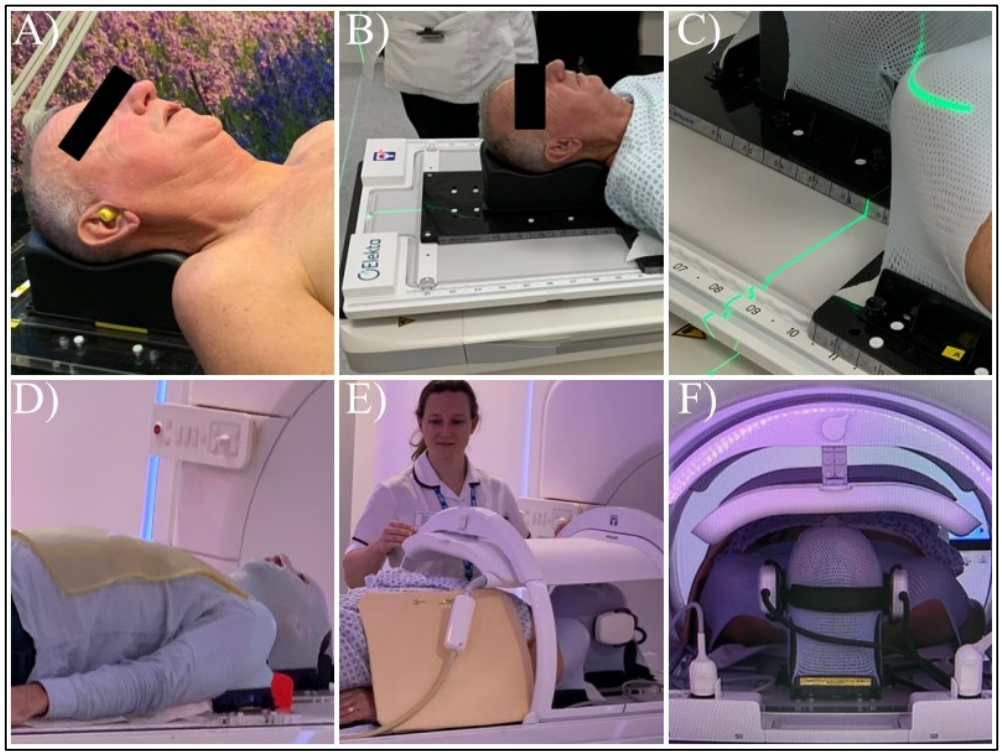

8.5.3 Radiotherapy treatment planning

The planning CT was used to generate both the 'back-up' plan and the MR-Linac reference plan. The CT and T2-weighted MR scans were rigidly co-registered to aid target volumes and OARs delineation.

8.5.3.1 *Target volume delineation*

Gross tumour volume (GTV)

I delineated the primary GTV (GTV-p) and nodal GTV (GTV-n) on the planning CT scan with reference to a registered T2-weighted planning MRI scan.

Clinical Target Volume (CTV)

A volumetric 2-dose level approach to define the target volumes which has been described in Chapter 8 Section 8.5.2.

Planning Target Volume (PTV)

The low-dose PTV (PTV54) and high-dose PTV (PTV65) were isometrically grown from their respective CTVs using an isotropic 3mm margin.

Organs at risk (OAR) delineation

I delineated the parotid glands, spinal cord and brainstem on the planning CT using local and international guidelines (7).

Before treatment planning, the target volumes and OARs were reviewed and approved by two consultants specialised in HNC (Dr Shreerang Bhide and Dr Kee Howe Wong).

8.5.4 Treatment plans

A 'backup' plan and a reference plan were created and optimised by medical physicists (Dr Dualta McQuaid and Dr Ian Hanson) to be delivered on the conventional linac and the MR-Linac, respectively.

Conventional linac radiotherapy 'backup' treatment plan

The 'backup' plan was created using the clinical version of RayStation version 9.0 (RaySearch Laboratories, Stockholm, Sweden). The purpose of this dual-arc volumetric-modulated arc therapy (VMAT) plan was to deliver treatment on a conventional linac if treatment could not be delivered on MR-Linac for a particular fraction e.g. linac breakdown, planned gap days and patient intolerance. Since this plan was created as per standard clinical practice, it also served to derive a priori information that can be used to optimise the reference MR-Linac plan.

Reference MR-Linac plan

The MR-linac treatment was planned on the clinical version of Monaco treatment planning system (TPS) (Version 5.4, Elekta AB, Stockholm, Sweden). The plan was generated using

step and shoot IMRT with a 15-beam arrangement (angles 0º, 28º, 45º, 62º,79º, 96º, 144º, 168º, 192º, 216º, 264º, 281º, 298º, 315º, 332º) which enabled a closer replication of the dose distribution of the VMAT 'backup' plan. Since the gantry rotation speed was fast, the total number of beams did not significantly lengthen the overall treatment time.

Dose prescription

In accordance with ICRU 83, the prescription was to the median dose point on the DVH such that the prescription dose of 65.1 Gy was received by 50% of the PTV65.

8.5.5 MR-Linac HNC online adaptive workflow

The online ART workflow has been described in detail by Winkel *et al.* (8). A simplified version is summarised in the next section.

Online treatment adaptation

The treatment is then adapted using either an "adapt to position" (ATP) or "adapt to shape" (ATS) workflow.

- ATP workflow

The ATP workflow is equivalent to the daily image guidance and couch shifts performed on a conventional linac. The session MRI scan is rigidly co-registered with the reference CT or MRI scan. An isocentre shift is made to translate the reference plan isocentre to the equivalent position on the newly acquired MR scan and this is followed by dose recalculation and re-optimisation. The delineations are not amended in this workflow and the online plan recalculation is made on the reference image. This is similar to treatment on a conventional linear accelerator with daily image guidance and couch shifts.

- ATS workflow

In this workflow, the adapted plan is fully re-optimised on the patient's new anatomy using the session MRI (8). The reference image and session MRI scan are rigidly co-registered, and the delineations are propagated to the session MRI scan. The delineations are reviewed and edited as necessary. A synthetic CT is generated from the MRI scan and a plan is recalculated and optimised. The optimisation in ATP workflow is performed based on the pre-treatment planning objectives but based on the new anatomy.

- The simplified ATS workflow

Due to the complexity of HNC treatment plans, the ATP workflow does not reproducibly recover the required dose distribution for the target volumes unless patient alignment differences between the reference and session images are small (9). Thus, the ATP workflow leads to inferior target coverage and dose distribution. For HNC, a daily online ATS workflow is not feasible given the number of structures that would need to be delineated. Thus, a 'simplified' ATS workflow is proposed to treat HNC on the MR-Linac. Online clinician contouring is not required as all ROIs (except the external body contour) are rigidly propagated. The external body contour will be deformably propagated. Thus, none of the propagated ROIs were manually amended. This approach has the advantage of delivering an adapted plan to the patient's external contour without the need for daily clinician contour. The simplified ATS workflow is summarised in Figure 8-3. A session MRI scan is first acquired and rigidly co-registered with the planning scan. Translation errors are corrected and the isocentre shift is assessed. The simplified ATS workflow is then triggered to create an adaptive plan. The ROIs are propagated and reviewed, the PTV is grown and a new plan is derived using the same objectives used to generate the reference plan. The adapt shape and segment approach (equivalent to a full repeat plan) is used to derive a new treatment plan.

The plan is reviewed and compared to the derived off-line plan, and treatment is then delivered after the relevant checks are done by the physicists.

Figure 8-3. The simplified ATS workflow for head and neck cancer treatment on the MR-Linac.

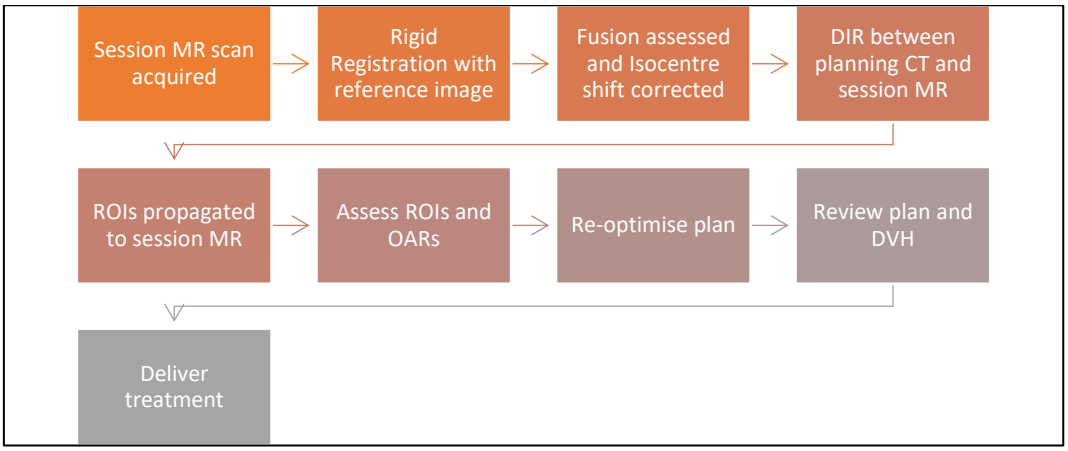

Abbreviations: ATS, adapt to shape; CT, computed tomography; DVH, dose-volume assessment; MR, Magnetic resonance; OARs, organs at risk; PTV, planning target volume; ROIs, regions of interest.

If clinically indicated, an offline repeat plan to update the reference plan will be performed as per the Royal Marsden standard departmental protocol.

Recalculation and re-optimisation methods

Intensity-modulated radiation therapy (IMRT) uses multiple beams to deliver the radiotherapy treatment. The intensity of each IMRT beam is divided into small segments and modulated by the multi-leaf collimator (MLC). A full explanation of the reoptimisation and recalculation methods are beyond the scope of this thesis and explained in detail in an article by Winkel *et al.* (8). In summary, this can be divided into 'original segments', 'adapt segments', 'optimise weights' and 'optimise weights and shapes' (8). In this study, a full re-optimisation was performed used 'optimise weights and shapes' which is equivalent to a full repeat plan.

Bulk electron density assignment

Bulk-density override can provide sufficient accuracy for radiotherapy dose calculations for HNC treatment when compared to the ground-truth of a Hounsfield unit-to-density look-up-table (LUT) based computation (10,11). Bulk density assignment for HNC was evaluated for MR-linac-based treatment planning using Monaco TPS in the commissioning report for bulk density approach (12). The authors showed that acceptable dose calculation accuracy is achieved when comparing to the ground truth (calculated using LUT). As part of quality assurance, all plans are calculated with LUT-based calculations and with density overrides for comparison. In this study, the bulk density override method uses patient-specific overrides and electron densities (ED) assigned per structure based on the average ED value of the corresponding contour on the pre-treatment CT.

8.5.6 Plan assessments

Dose accumulation was carried out on Research RayStation (Version 8.0, RaySearch Laboratories, Stockholm, Sweden). To assess the daily plan generated by the simplified ATS workflow, the reference plan was compared to the cumulative dose of the adaptive plans.

Deformable image registration (DIR) was used to accumulate the daily adaptive plans on the initial planning scan. Only the MR-Linac plans were accounted for in the dosimetric analyses. If treatment fractions were delivered on the conventional linac, the last delivered plan on the MR-Linac was scaled for the number of fractions delivered on the conventional linac. For example, if the patient received fractions 16 to 20 on the conventional linac, the adapted radiotherapy plan delivered on the MR-linac on fraction 15 was used to calculate dose for fractions 16 to 20.

The non-adapted cumulative dose was defined as the cumulative dose delivered using the reference plan. The reference plan was calculated on the daily acquired MRI anatomy and the dose cubes were then deformed to the planning MRI scan to enable dose accumulation.

Both plans were evaluated using the standard dosimetric constraints. I visually assessed the 95% dose distribution of the PTV65 and PTV54 and position of any hotspots > 105% using the dose colour wash. The dose constraints were assessed using the dose-volume histograms (DVHs).

The adapted and non-adapted plans were compared to the reference plan by calculating the percentage difference.

Percentage difference (%) = $(D_x - D_{ref})/D_{ref}$ x 100

Where x represents the adapted or non-adapted plan and ref represents the reference plan.

8.5.7 Treatment times

Treatment times were measured using a stopwatch by recording various checkpoints (setup and plan reoptimisation, beam delivery, total treatment time). This was measured by the radiographers during each treatment session.

8.6 Statistical analysis

The data were analysed using Graphpad Prism software (Version 8.2.0; San Diego, CA). The Shapiro-Wilk test was used to test for normality of the data. Mean and median values were reported for parametric and non-parametric data, respectively.

8.7 Results

8.7.1 Patient characteristics

Table 8-1. Summary of patient characteristics and treatment.

Gender	Male
Age	70 years old
Tumour site	Tongue base
HPV	positive
Sterno-hyoid neck length	12 cm
Craniocaudal PTV length	18 cm
Stage (AJCC 7th edition)	
T	3
N	2c
M	0
Radiotherapy details	
Total number of fractions	30
Fractions delivered on MR-linac	23
Fractions delivered on conventional linac	7
High-dose CTV	65.1 Gy
Low-dose CTV	54 Gy
Chemotherapy details	
Cisplatin Day 1 (100mg/m^2)	209 mg
Cisplatin Day 29 (100mg/m^2)	209 mg

Abbreviations: AJCC = American joint committee on cancer; CTV = clinical target volume; PTV = planning target volume.

A summary of the patient's details and treatment are shown in Table 8-1. The majority of treatment (23 out of 30 fractions) was delivered on the MR-Linac. Of the seven radiotherapy fractions delivered on the conventional linac, one fraction was pre-planned to account for the gap day treatment over a bank holiday. In week 5 of radiotherapy, the patient developed aspiration pneumonia following displaced nasogastric tube and required a prolonged intensive care unit stay. A clinical decision was made to deliver the remaining six radiotherapy fractions (fractions 25 to 30) on the conventional linac as the patient could not tolerate extended periods immobilised in the treatment position. However, an MRI scan in the

treatment position was acquired on the MR-linac on the last day of treatment to enable dose accumulation calculations. The sterno-hyoid neck length measured 12 cm in the craniocaudal direction and the predicted craniocaudal PTV length was 17.5 cm using the equation derived from Chapter 8. The actual measure PTV craniocaudal length was 18 cm.

Despite dietetic input, the patient lost up to 12% of their initial weight by the end of treatment (Table 8-2).

Table 8-2. Measured intra-treatment weight changes. Percentage weight loss was calculated from the baseline weight.

	Baseline	**Week 1**	**Week 2**	**Week 3**	**Week 4**	**Week 5**	**Week 6**
Weight (Kg)	77.8	81.1	77.9	74	68.0	68.5	68.6
% weight change		4.2	0.1	-4.9	-12.6	-12.0	-11.8

8.7.2 Morphological changes

Similar to the findings in Chapter 3A, changes to the GTV could be accurately visualised on serial MRI scans acquired on the MR-Linac (Figure 8-4). By the end of treatment, the GTVs were difficult to visualise on the T2-weighted MRI scans.

Figure 8-4. Axial slices of T2-Weighted MRI scans at fractions 1, 6, 11, 16, 21 and 30 in panels A, B, C, D, E, F, respectively. GTV delineated in orange.

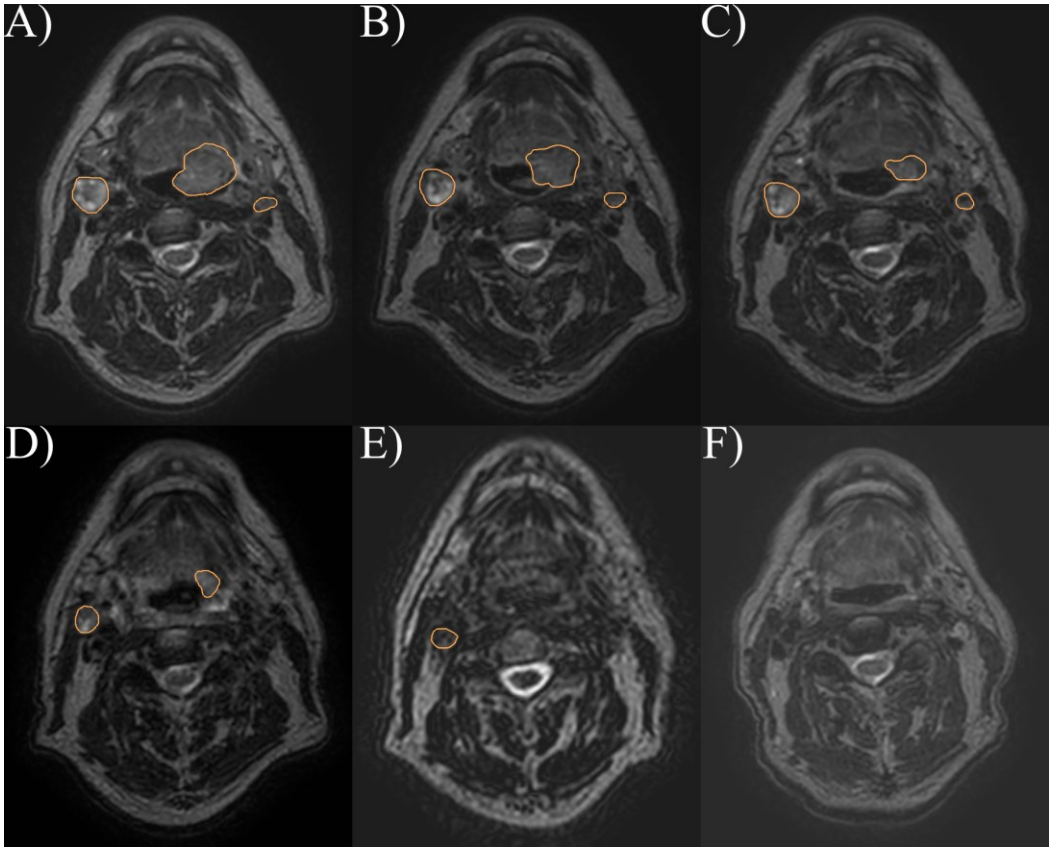

8.7.3 Treatment time

The patient spent a mean time of 43 minutes (SD (standard deviation) = 5.2 minutes) on the treatment bed. This included patient set-up (mean = 5 minutes; SD = 1 minute), session image acquisition (mean = 6 minutes; SD = 1.4 minute), registration and contour propagation (mean = 9 minutes; SD = 1.6 minute), treatment planning and checking (mean = 13 minutes; SD = 4 minute) and treatment delivery (mean = 10 minutes; SD = 0.8 minute).

Table 8-3. Mean and standard deviation of the total treatment time and the components of the workflow for a total of 23 fractions.

	Patient set-up	Image acquisition	Registration & contour propagation	Planning & checking	Treatment delivery	Total time
Mean time (minutes)	5.0	6.0	9.0	13.0	10.0	43.0
Standard Deviation (minutes)	1.0	1.4	1.6	4.0	0.8	5.2

8.7.4 Comparisons of the adapted, non-adapted and reference plans.

Target Volume

All mandatory PTV planning objectives were met for the reference, adapted and non-adapted plans (Table 8-4). Compared to the reference plan, the adapted plans received lower doses to 95% and 99% of the PTV65 (-1.9% and -2.2%, respectively) and PTV54 (-2.8% and -5.4%, respectively) (Table 8-4). Similarly, the non-adapted plan received lower doses to 95% and 99% of the PTV65 (-0.5% and -2.1%, respectively) and PTV54 (-2.8% and -6.1%, respectively).

Differences between the adapted and non-adapted plans were smaller. Compared to the non-adapted plan, the adapted plans received lower doses to 50%, 95% and 99% of the PTV65 (-0.3%, -0.9% and -0.2%, respectively) and to the 50% of the PTV54 (-0.9%) (Table 8-4). The D5% PTV65 and D99% of the PTV54 of the adapted plans were larger than for the non-adapted plan (1.1 and 0.8%, respectively).

Table 8-4. Comparison of the objective parameters for the adapted, non-adapted and reference plans.

	Objective	Dose Constraint (Gy)	Reference plan (Gy)	Adapted Plan			Non-adapted Plan	
				Gy	% difference to reference plan	% difference to non-adapted plan	Gy	% difference to reference plan
PTV65	D99%	> 58.50	63.0	61.6	-2.2	-0.2	61.7	-2.1
	D95%	> 61.75	63.4	63.0	-1.9	-0.9	63.6	0.5
	D50%	> 64.35	65.1	65.4	0.5	-0.3	65.6	0.8
	D5%	< 68.25	66.3	67.0	1.4	1.1	66.3	0.3
PTV54	D99%	>48.60	52.1	49.3	-5.4	0.8	48.9	-6.1
	D95%	>51.30	52.9	51.4	-2.8	0.0	51.4	-2.8
	D50%	>53.46	54.2	53.9	-0.6	-0.9	54.4	0.4

Abbreviations: PTV = planning target volume; Dx = dose to x% of the volume.

Although both adapted and non-adapted plans satisfied the planning objectives, visual inspection of the PTV coverage showed that the PTV54 was compromised in small areas where the PTV was not covered by the 95% isodose in the non-adapted plan. An example of this is shown in Figure 8-5. The PTV65 was not compromised in this patient.

Figure 8-5. Adapted (A) versus non-adapted (B) plans. The PTV65 (red) and PTV54(purple) are shown in the axial MR scan. The arrowheads (white) point to compromised areas of PTV that are not covered by the 95% prescribed isodose.

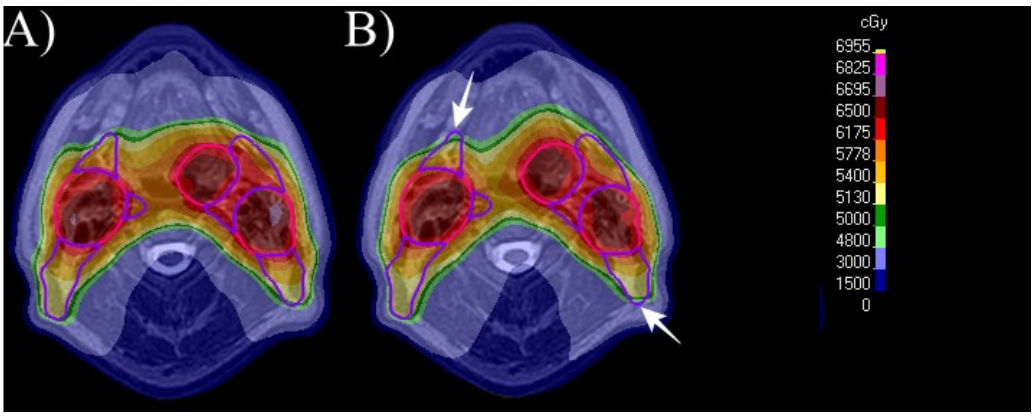

Although no hotspots were observed in either radiotherapy plans, the PTV of the non-adapted plan received a relatively higher dose than the adapted plan PTV. For example, in the non-adapted plan (Figure 8-6 C and D), a greater proportion of PTV54 and PTV65 of the non-

adapted plan was within the 100% isodose of their respective prescribed dose whilst in the adapted plan a greater proportion was within the 95% isodose of their respective prescribed dose (Figure 8-6 A and B).

Figure 8-6. Adapted (A and B) vs non-adapted (C and D) axial slices of radiotherapy MR plan. PTV65 (red), PTV54 (purple), spinal cord (green), right parotid gland (yellow) and left parotid gland (orange).

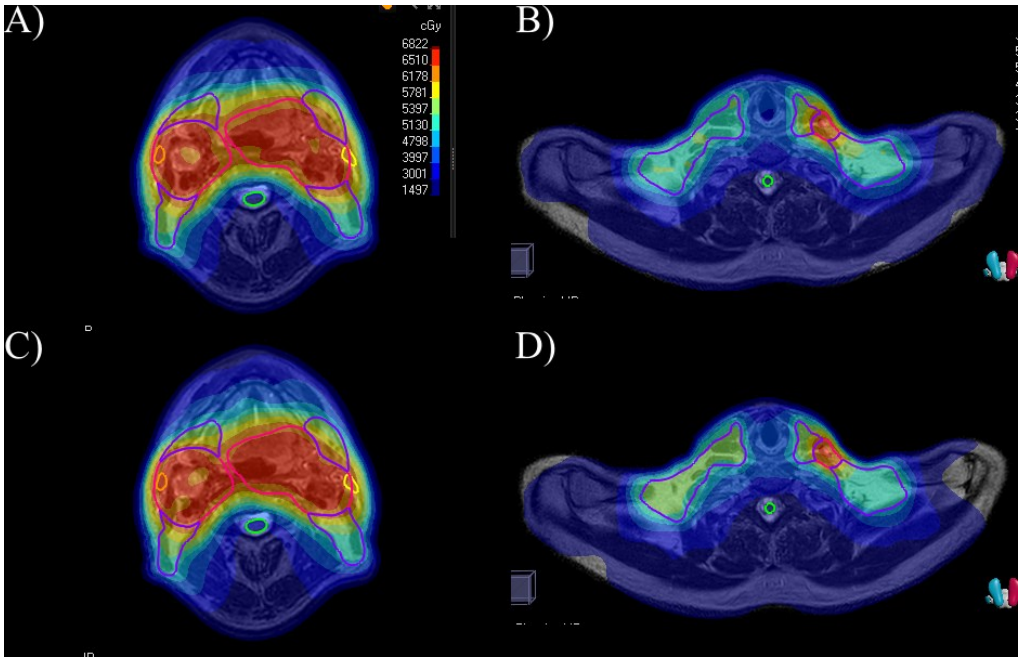

OAR dose constraints

Treatment plan adaptation led to a reduction in the maximum dose (D_{max}) to the spinal cord, spinal cord PRV, brainstem and brainstem PRV compared to a non-adapted plan (-10.6%, -9.2%, -13.5%, -15.7%)

Table 8-5). Treatment plan adaptation also led to a reduction in D_{max} to the spinal cord, spinal cord PRV, brainstem and brainstem PRV compared to the reference plan (-3%, -1%, -18% and -19%, respectively) and compared to a non-adapted plan (-10.6%, -9.2%, -13.5% and -15.7%, respectively). In contrast, a non-adapted plan led to increases of 8 and 9% to the spinal cord and spinal cord PRV, respectively, compared to the reference plan. Doses to the brainstem and brainstem PRV were reduced by 6% and 4%, respectively, compared to the reference plan. However, both adapted and non-adapted plans led to increases in dose to the

contralateral and ipsilateral parotid glands compared to the reference plan, with a greater increase found in the non-adapted plans. A non-adapted plan led to an increase of 8% and 13% to the contralateral and ipsilateral parotid glands, respectively, compared to an increase of 1% and 6% in the adapted plan, respectively.

Table 8-5. Comparison of organs at risk dose parameters for the adapted plan, non-adapted plan and reference plan.

Structure	Constraint	Reference plan (Gy)	Adapted Plan			Non-adapted Plan	
			Gy	% difference to reference plan	% difference to non-adapted plan	Gy	% difference to reference plan
Spinal Cord	**D_{max} to 1cm^3**	36.7	35.6	-3.0	-10.6	39.8	8.4
	D_{max} to PRV 1cm^3	40.0	39.6	-1.0	-9.2	43.6	9.0
Brainstem	**D_{max} to 1cm^3**	39.3	32.1	-18.3	-13.5	37.1	-5.6
	D_{max} to PRV 1cm^3	41.7	33.9	-18.7	-15.7	40.2	-3.6
Contralateral Parotid	**Mean dose**	23.7	24.0	1.3	-6.3	25.6	8.0
Ipsilateral Parotid	**Mean dose**	24.3	25.8	6.2	-6.2	27.5	13.2

Abbreviations: D_{max} = maximum dose; Gy = gray; PRV = planning organ at risk volume.

8.8 Discussion

The introduction of the MR-linac in clinical practice has made daily ART for HNC a real possibility. This chapter reports the clinical experience of the first HNC patient undergoing treatment on the Elekta Unity MR-linac within the PERMIT trial at the Royal Marsden Hospital.

The aim of ART was to maintain the pre-treatment dose constraints of the target volume and OARs. In this online adaptive workflow, no changes were made to the target volume or OARs and thus, the reported dosimetry reflected adaptation to a change in body contour only. Although significant intra-treatment changes to the target volume were observed, adapting to a shrinking target volume remains beyond the standard of care and as such could not be acted on within the PERMIT trial which required delivery of 'standard' treatment. Nonetheless, this conservative ART approach demonstrated the feasibility and safety of the simplified ATS online adaptive workflow.

Doses were compared between the reference plan, adapted and non-adapted plans which represent the planned delivered dose on a single snapshot of the patient's anatomy, the cumulative dose adapted to a changing body contour and the doses delivered without adapting to body contour changes, respectively.

In this study, I have shown that online treatment adaptation using a simplified ATS workflow is feasible. Radiotherapy treatment was adapted according to changes in body contour and this led to an improved PTV coverage whilst fulfilling the target volume dose constraints compared to a non-adapted plan. The differences between the adapted plan and reference plan were small for the PTV, with differences ranging between -5.4% and 1.4%. Similarly, differences between the non-adapted plan and the reference plans were small and ranged between -6.1% and 0.8%. In this case, the non-adapted plan had no significant compromise

of the high-dose PTV and small deficiencies in low-dose PTV at the extremities of the PTV which may be of less clinical consequence.

Treatment adaptation led to reduction in the maximum doses to the spinal cord, brainstem, and their respective PRVs compared to both the planned doses and non-adapted doses. Treatment adaptation also reduced the mean parotid gland doses compared to the non-adapted plan, but not compared to planned doses. Generally, the non-adapted plan was 'hotter' than the adapted plan as demonstrated by the PTV and OAR doses being higher. A likely explanation is that tissue loss due to weight loss resulted in increased dose deposit in the non-adapted plan whilst adapting to body contour changes accounted for this in the adapted plan. By week 4, the patient had lost 12% of baseline weight but remained stable for the rest of treatment. This could explain the lesser differences in dosimetry observed than anticipated despite no adaptation. A poorer set-up associated with greater weight loss could have led to worse dosimetry in a non-adapted plan. Treatment adaptation also reduced the maximum doses to the spinal cord, brainstem and their respective PRVs compared to the reference plan and the non-adapted plan. On the other hand, the adapted plan had larger mean parotid gland doses than the reference plan, but smaller compared to the non-adapted plan. This is consistent with the results from Chapter 3. The parotids glands shrink in volume and move medially towards the high-dose target volume. This would explain the increase dose to the parotid glands compared to the planned doses for both ART and non-ART plans. This could be explained by the treatment planning system stopping further dose optimisations due to time constraints in the online setting. Overall, this suggests that ART leads to improved PTV coverage and reduced doses to certain OARs compared to a non-adapted plan.

The mean treatment time for each MR-Linac fraction was over 40 minutes and longer than conventional linac treatment due to the extra steps required before treatment delivery, such as MR image acquisition, image registration, contour propagation, treatment planning and

checking. This is in keeping with the reported mean treatment time of prostate cancer on the MR-Linac (mean of 45 minutes per fraction) at the Royal Marsden Hospital (13). The workflow may be hastened by using the 2-minute MRI scan during image acquisition rather than the 6-minute scan. However, this would be at the expense of image quality and may not be appropriate if in ART techniques such as a shrinking target volume, where accurate target volume delineation is needed. Treatment times are likely to remain greater than 35 minutes and therefore careful selection of patients should be considered. Therefore, I would propose to use the 2-minute scan on a daily basis for online-adaptation, whilst reserving the 6-minute scan when adapting to a shrinking target volume is required. This can be done during treatment delivery.

This study has certain limitations. The results reported represent a single patient experience and therefore, more patients should be recruited to assess the benefits of MR-guided daily ART. It is also important to note the potential drawbacks of the dosimetric assessment due to a) the extrapolation of the missed treatment fractions and b) the intrinsic dose uncertainties associated with DIR.

8.9 Conclusion

This chapter describes the first HNC patient undergoing treatment on the MR-Linac in the UK using a simplified ATS workflow. Daily MR-guided ART is feasible on the MR-linac and may lead to improved dosimetry compared with a non-adapted plan. The simplified ATS workflow offers the groundwork required to open the door to more complex ART approaches such as shrinking target volume.

8.10 References

1. Raaymakers BW, Jürgenliemk-Schulz IM, Bol GH, et al. First patients treated with a 1.5 T MRI-Linac: clinical proof of concept of a high-precision, high-field MRI guided radiotherapy treatment. Phys Med Biol [Internet]. 2017 Nov 14 [cited 2019 Aug 9];62(23):L41–50. Available from: http://stacks.iop.org/0031-9155/62/i=23/a=L41?key=crossref.1c8c48a76c7eafac216d1be249abc1b5

2. Nachbar M, Mönnich D, Boeke S, et al. Partial breast irradiation with the 1.5 T MR-Linac: First patient treatment and analysis of electron return and stream effects. Radiother Oncol. 2020 Apr 1;145:30–5.

3. Werensteijn-Honingh AM, Kroon PS, Winkel D, et al. Feasibility of stereotactic radiotherapy using a 1.5 T MR-linac: Multi-fraction treatment of pelvic lymph node oligometastases. Radiother Oncol. 2019;

4. Bertelsen AS, Schytte T, Møller PK, et al. First clinical experiences with a high field 1.5 T MR linac. Acta Oncol (Madr). 2019;

5. Prospective Evaluation of Radiotherapy Using Magnetic Resonance Image Guided Treatment - Full Text View - ClinicalTrials.gov [Internet]. [cited 2021 Feb 7]. Available from: https://clinicaltrials.gov/ct2/show/NCT03727698

6. Ng-Cheng-Hin B, Nutting C, Newbold K, et al. The impact of restricted length of treatment field and anthropometric factors on selection of head and neck cancer patients for treatment on the MR-Linac. Br J Radiol [Internet]. 2020 May 21 [cited 2020 Jun 2];20200023. Available from: https://www.birpublications.org/doi/10.1259/bjr.20200023

7. Brouwer CL, Steenbakkers RJHM, Bourhis J, et al. CT-based delineation of organs at risk in the head and neck region: DAHANCA, EORTC, GORTEC, HKNPCSG, NCIC CTG, NCRI, NRG Oncology and TROG consensus guidelines. Radiother Oncol [Internet]. 2015 Oct [cited 2019 May 2];117(1):83–90. Available from: https://linkinghub.elsevier.com/retrieve/pii/S0167814015004016

8. Winkel D, Bol GH, Kroon PS, et al. Adaptive radiotherapy: The Elekta Unity MR-linac concept. Clin Transl Radiat Oncol. 2019;

9. Dunlop A. Adapt-to-position simulation for H&N on the MR linac. Sutton; 2019.

10. Fotina I, Hopfgartner J, Stock M, et al. Feasibility of CBCT-based dose calculation: Comparative analysis of HU adjustment techniques. Radiother Oncol. 2012;

11. Dunlop A, McQuaid D, Nill S, et al. Comparison of CT number calibration techniques for CBCT-based dose calculation. Strahlentherapie und Onkol. 2015;

12. Dunlop A, Mitchell A. Recommended methods for bulk density assignments for pelvic and head and neck treatment sites for MR linac-based treatment planning using the Monaco TPS.

13. Dunlop A, Mitchell A, Tree A, et al. Daily adaptive radiotherapy for patients with prostate cancer using a high field MR-linac: Initial clinical experiences and assessment of delivered doses compared to a C-arm linac. Clin Transl Radiat Oncol [Internet]. 2020 Jul 1 [cited 2020 Sep 21];23:35–42. Available from: /pmc/articles/PMC7210377/?report=abstract

9 Chapter 9 – Thesis summary and future directions

This chapter summarises the findings of my thesis chapters on adaptive radiotherapy (ART) in head and neck cancers (HNC).

9.1 The utility of DIR for contour propagation

A major limitation of integrating ART into routine clinical practice is the associated increased workload in a busy radiotherapy department. Although previous studies have reported a benefit in using deformable image registration (DIR) for contour propagation, the DIR algorithms and treatment planning systems used were heterogeneous. Therefore, I assessed the inbuilt DIR algorithm of the treatment planning system in use at the Royal Marsden Hospital in Sutton. The results presented in Chapter 2 and 4 demonstrated the value of using DIR for contour propagation in ART which is applicable for both CT and MRI scans. I have shown that DIR-contour propagation can improve workflow efficiency by significantly reducing the clinician delineation time if repeat planning is required in the context of ART. Contour propagation using DIR was fast and significantly reduces clinician workload even when manual modifications of the regions-of-interest (ROIs) were taken into account. In particular, the DIR algorithm propagated ROIs with volumes >10cm^3 with good agreement to manually-delineated ROIs. This geometric overlap improved further with manual modification. Compared to manually-delineated ROIs, the dosimetric differences of using DIR-propagated ROIs were small and could be within the inter-observer variabilities. Nonetheless, clinician modification of DIR-propagated ROIs remains essential, especially for small volume ROIs, for the Gross tumour volume (GTV) and in patients who undergo significant positional changes between scans.

9.2 MR-guided adaptive radiotherapy

The improved soft tissue contrast using MRI unlocks the potential of adapting to a shrinking target volume. Prior to the clinical introduction of MR-guided ART, the intra-treatment changes reported in the CT-based studies should be replicated on MR-based studies. Chapter 3 reported that both the target volumes and the parotid glands volumes reduce throughout treatment and that the parotid glands migrate medially as described in CT-based studies.

Whilst adapting to the weekly observed changes was possible, it would be neither practical nor feasible for weekly ART. A pragmatic approach would be to implement ART at weeks 2 and 4, where significant changes to the target volume and parotid glands are observed as reported in Chapter 3. Practically this would also enable enough time to create and deliver the new adapted plans in a timely manner.

The results in Chapter 5 described the feasibility and advantage of using a response-adapted ART using an MR-only workflow. By adapting to both a shrinking target volume and a changing anatomy, the high-dose target volume dose was shrunk whilst maintaining the low-dose target volume distribution. This led to a reduction in dose deposited to a number of OARs, but this was most significant for the superior and middle pharyngeal constrictor muscles. This is especially important in the context of dysphagia-optimised IMRT which may become the standard of care in the future.

9.3 HNC treatment on the MR-Linac

With the introduction of the MR-Linac at the Royal Marsden Hospital, daily MR-guided ART for HNC has become possible. HNC treatment planning is complex and the patient selection for treatment is crucial due to the innate characteristics of the MR-Linac. Although the results in Chapter 7 suggests that the majority of HNC treated at the Royal Marsden Hospital will have a treatment field suitable for treatment on the MR-Linac, certain tumour

subsites such as the nasopharynx with significant intracranial extension or paranasal sinus requiring nodal irradiation may not be suitable for treatment on MR-Linac. My results also demonstrate that patients immobilised in a neutral neck position have a smaller craniocaudal treatment field compared to patients immobilised in an extended neck position. Thus, treating patients in a neutral neck position increases the number of eligible patients and is a more natural and comfortable position. Improving patient tolerance is pivotal as each radiotherapy fraction can last up to 40 minutes. A hyo-sternal neck length of less than 14.6 cm in a neutral neck position can be used as a surrogate to identify patients with a suitable craniocaudal field length. This is important to avoid the extra steps needed for treatment on the MR-Linac.

Whilst treatment in the neutral neck position is advantageous on the MR-linac, radiotherapy of certain HNC sub-sites at the Royal Marsden Hospital have been traditionally treated in an extended neck position to reduce the oral cavity dose. However, the results in Chapter 8 demonstrate that the additional oral cavity dose in the neutral neck position can be mitigated by using oral cavity dose constraints.

This groundwork led to the treatment of the first HNC patient on the MR-Linac as described in Chapter 9. This chapter reported an improved dosimetry to the target volume and to the OARs in a single patient using a simplified online adaptive strategy compared to a non-adapted plan. Despite the limitations associated with a single patient report, a simplified anatomy-adapted ART to body contour changes led to a reduction in the maximum doses delivered to the OARs and to an improvement in the PTV dosimetry.

9.4 Future work

This thesis has demonstrated that personalised MR-guided dose adaptation to a shrinking target volume is feasible and can lead to reduced doses delivered to the OARs, which may translate to a reduction in long-term toxicities. This is particularly important in HPV-

associated oropharyngeal cancers (OPC), which typically affect younger patients and have excellent outcomes. Prospective validation is required before adopting response-adapted ART into clinical practice to ensure that locoregional control is not compromised at the expense of reducing toxicities. There are two MR-guided phase II trials which are investigating this in HPV-associated oropharyngeal cancer patients. The MR-ADAPTOR trial (NCT03224000) is a two-stage Bayesian phase II trial assessing the non-inferiority of MR-guided radiotherapy (MRgRT) dose adaptation for patients with HPV-associated OPC compared to standard IMRT treatment with a primary endpoint of locoregional control. In the first phase of this study, locoregional control will be compared to historical data. The second phase will randomise 60 patients to either MRgRT or standard IMRT. These patients will undergo weekly response-adapted ART based on GTV response. Similarly, the INSIGHT II study (CCR 4934/IRAS 245340) is a phase I/II study at the Royal Marsden Hospital which will use MRgRT at two time-points (weeks 2 and 4) to adapt the high-dose PTV based on GTV response in HPV-positive oropharyngeal cancer. This trial will be assessing the dosimetric advantage to the OARs, loco-regional control, acute and long-term toxicities.

Treatment on the MR-Linac enables the collection of an enormous amount of daily anatomic and functional imaging, which can be used to optimise and improve the treatment workflow. This data can be used to assess the best timing of these offline response-adapted ARTs and on the benefits of using functional imaging to predict tumour response. However, functional imaging remains investigative at this stage on the MR-Linac and the sequences require optimisation. The simplified adapt to shape treatment workflow on the MR-Linac has just tapped into the potential of the MR-Linac. Daily online response-adapted ART is unlikely to be feasible due to the time-constraints associated with an online-flow and the uncertain benefits of adapting to daily target volume changes. With this in mind, a proposed HNC workflow would be to deliver a simplified ATS workflow on a daily basis and using a

manageable offline response-adapted ART at two time-points such as weeks 2 and 4. This would combine the benefits of adapting to both body contours and to a responding target volume.

9.5 Conclusion

The work presented in this thesis has demonstrated the feasibility of using DIR for contour propagation to aid ART and the benefit of response-adapted ART using MR-guidance in reducing OAR dose. This thesis has also investigated the practical differences of treating patients on the MR-Linac and laid the groundwork for the first HNC patient to be treated on the MR-Linac.